



NATIONAL CENTER FOR TRANSPORTATION SYSTEMS PRODUCTIVITY AND MANAGEMENT

# Innovative Modular High Performance Lightweight Decks for Accelerated Bridge Construction

Contract # DTRT12GUTC12 with USDOT Office of the Assistant Secretary for Research and Technology (OST-R)

Final Report

December 2015

Principal Investigator: Amir Mirmiran, Ph.D.



## National Center for Transportation Systems Productivity and Management

O. Lamar Allen Sustainable Education Building  
788 Atlantic Drive, Atlanta, GA 30332-0355  
P: 404-894-2236 F: 404-894-2278  
nctspm@ce.gatech.edu nctspm.gatech.edu



*DISCLAIMER*

*The contents of this report reflect the views of the authors, who are responsible for the facts and the accuracy of the information presented herein. This document is disseminated under the sponsorship of the U.S. Department of Transportation's University Transportation Centers Program, in the interest of information exchange. The U.S. Government assumes no liability for the contents or use thereof.*

## **ACKNOWLEDGEMENTS**

The authors would like to thank the University Transportation Center (UTC) for providing the necessary funding for this project. Special thanks are also due to the project manager, Dr. Michael Hunter, Director of the National Center for Transportation Systems Productivity and Management (NCTSPM) at the Georgia Institute of Technology (GTU) for his continued support of the project.

The authors would also like to acknowledge the matching support received from the Florida Department of Transportation (FDOT) and the Alabama Department of Transportation (ALDOT). Of particular, the FDOT's Accelerated Pavement Testing (APT) facility at the State Materials and Research Park in Gainesville, FL, and the FDOT's Marcus H. Ansley Structures Research Center at the Innovation Park in Tallahassee, FL supported the unique testing of the proposed waffle deck system under repeated wheel loading of the Heavy Vehicle Simulator (HVS). Sincere thanks are also due to the MMFX Technologies of Irvine, CA, for providing its high-strength steel MMFX reinforcement, and the Lafarge North America for providing its Ductal<sup>®</sup>, the ultra-high performance concrete (UHPC), for this project.

## TABLE OF CONTENTS

1 Introduction	11
1.1 Problem Statement	11
1.2 Research Objectives	11
1.3 Research Approach	12
1.4 Report Outline	12
2 Literature Review	13
2.1 Background on Current State of Bridges in the U.S.	13
2.2 Accelerated Bridge Construction (ABC)	16
2.2.1 Overview of ABC	16
2.2.2 Superstructure Systems for ABC	17
2.2.3 Common ABC Tools and Technologies	22
2.2.4 U.S. Bridges Constructed Using ABC Tools	24
2.2.5 International Bridges Constructed Using ABC Tools	28
2.3 Department of Transportation Surveys	30
2.4 Synthesis of National Bridge Inventory Data	35
2.5 Proposed Lightweight Bridge Deck Systems	37
2.5.1 Advanced Materials for Bridge Decks	37
2.5.1.1 Ultra-High Performance Concrete (UHPC)	37
2.5.1.2 Fiber Reinforced Polymer (FRP)	39
2.5.1.3 High-Strength Steel (HSS)	41
2.5.2 UHPC Waffle Deck	42
2.5.2.1 FRP Reinforcement	46
2.5.2.2 HSS Reinforcement	47
2.5.3 Hybrid Full-Depth UHPC-FRP Deck System	49
2.6 Summary and Conclusions	53
3 Hybrid UHPC-FRP Deck System	56
3.1 Introduction	56
3.2 Literature Review	57
3.3 Hybrid UHPC-FRP Deck	59
3.3.1 Material Properties	59
3.3.2 Specimen Preparation and Test Setup	60
3.3 Experimental Results	65
3.3.1 First Set Specimens	65
3.3.2 Second Set Specimens	69
3.3.3 Comparison of Test Results	72
3.4 Bonding of FRP Laminates to UHPC	74
3.4.1 Background	74
3.4.2 Literature Review	75
3.4.3 Specimen Preparation	77
3.4.3.1 Double Lap Shear Test	77
3.4.3.2 Single Lap Shear Test	79

3.4.4 Test Setup and Measurement	81
3.4.4.1 Double Lap Test	81
3.4.4.2 Single Lap Test	81
3.4.5 Test Results	83
3.5 Conclusions	94
4 Waffle UHPC Deck System	95
4.1 Introduction	95
4.2 Assessment of UHPC-HSS Deck System	97
4.2.1 Experimental Work	97
4.2.2 Test Matrix	97
4.2.3 Specimen Preparation and Material Properties	100
4.2.4 Test Setup and Instrumentation	101
4.2.5 Test Results and Discussion	102
4.2.5.1 Panel Action	105
4.2.5.2 Punching Shear Behavior	107
4.2.5.3 Continuity Effects	108
4.2.6 Summary of Findings from UHPC-HSS Deck Tests	111
4.3 Assessment of UHPC-CFRP Deck System	111
4.3.1 Test Matrix and Specimen Preparation	111
4.3.2 Test Setup and Instrumentation	117
4.3.3 Test Results and Discussion	118
4.3.3.1 Anchorage of CFRP Bars	120
4.3.3.2 Flexural Behavior	120
4.3.3.3 Panel Action	122
4.3.3.4 Punching Shear	124
4.3.3.5 Continuity Effect	125
4.3.4 Summary of Findings from UHPC-CFRP Deck Tests	127
4.4 Accelerated Pavement Testing	128
4.4.1 Preparatory Lab Tests	128
4.4.2 Heavy Vehicle Simulator Tests	143
4.5 Finite Element Modeling	161
5 Conclusions and Recommendations	182
5.1 UHPC-FRP Hybrid Bridge Deck System	182
5.2 UHPC Waffle Deck System	182
References	184

## LIST OF TABLES

Table 2.1 Comparison of Benefits among Three ABC Tools Promoted by EDC-2	23
Table 2.2 List of Surveyed State DOTs	32
Table 2.3 Summary of DOT Survey Results	33
Table 2.4 NBI List of Structurally Deficient and Functionally Obsolete Bridges by State	35
Table 2.5 Deficient Bridge Decks in Region 2 by State from the NBI Data	36
Table 3.1 Sample of FRP Bridges in the U.S.	59
Table 3.2 Material Properties from Coupon Tests	59
Table 3.3 Test Matrix	78
Table 3.4 Test Results for Double Lap Test	84
Table 3.5 Test Results for Single Lap Test	85
Table 3.6 Fiber Properties from Coupon Tests	85
Table 4.1 Test Matrix	99
Table 4.2 Summary of the Test	103
Table 4.3 Test Matrix	112
Table 4.4 Geometric and Material Properties of CFRP Bars	115
Table 4.5 Summary of Test Results	119
Table 4.6 Test Matrix	129
Table 4.7 Summary of Test Results	130

## LIST OF FIGURES

Figure 2.1 U.S. Map of Bridges Rated Structurally Deficient	13
Figure 2.2 U.S. Map of Bridges Rated Functionally Obsolete	14
Figure 2.3 Early Age Cracking (Note: Cell Phone 4.5 x 2 in. for Size Comparison)	14
Figure 2.4 Crew Working on Exodermic Deck of South Grand Island Bridge	18
Figure 2.5 NYSDOT Bulb-Tee Girders with Shear Pocket Ready for UHPC Pour	18
Figure 2.6 Detail of UHPC Shear Key Pocket	18
Figure 2.7 Transverse U-Bar Joint Section: (a) Plan View (b) Elevation View	19
Figure 2.8 Shear Key Used to Contain Grout in Joining Prefabricated Elements	20
Figure 2.9 Headed studs Extending out of Deck Panel	21
Figure 2.10 Cross-section of Shear Key Used to Enclose Headed Studs	21
Figure 2.11 Moving Prefabricated Bridge Element into Place at Construction Site	22
Figure 2.12 Rendering of Bridge Spans Laterally Sliding into Place	23
Figure 2.13 Bridge Span Being Moved with SPMTs	24
Figure 2.14 Completed Parkview Avenue Bridge	25
Figure 2.15 Estimated Cost Savings for ABC vs Conventional Construction	26
Figure 2.16 Sam White Bridge in Utah Being Moved into Place Using SPMTs	27
Figure 2.17 Map Showing Planned Move of Wellesley Bridge	28
Figure 2.18 Prefabricated VFT Girder	29
Figure 2.19 Friedberg Bridge Lifted into Place	29
Figure 2.20 Measured and Recommended Design Stress-Strain of UHPC in Compression	39
Figure 2.21 Measured and Recommended Design Stress-Strain of UHPC in Tension	39
Figure 2.22 FHWA's UHPC Waffle Deck System	43
Figure 2.23 Details of the Replacement Bridge with a UHPC Waffle Deck System	44
Figure 2.24 Shear Pocket Connection	45
Figure 2.25 Longitudinal Connection	45
Figure 2.26 Transverse Connection	45
Figure 2.27 Cross-Section of Hybrid Beams Used in Experiments by Keller et al.	50
Figure 2.28 ODOT Sample Deck Tests: (a) Reinforced Concrete (b) Creative Pultrusions (c) Composite Deck Solutions (d) Hardcore Composites (e) Infrastructure Composites International	52
Figure 3.1 Details of the New Hybrid Deck	57
Figure 3.2 Construction Stages of Hybrid System	61
Figure 3.3 Details of First Set of Decks	62
Figure 3.4 Details of the Second Set of Decks	63
Figure 3.5 Test Setup for the First Set	63
Figure 3.6 Instrumentation Plan for the First Set	64
Figure 3.7 Test Setup for the Second Set	64
Figure 3.8 Instrumentation Plan for the Second Set	65
Figure 3.9 End of the Specimen after Grouting	65
Figure 3.10 Load-Displacement Responses for the First Set	66
Figure 3.11 The FRP Cloth after Demolding	67
Figure 3.12 Failure Mode near the End of the Grouted Region	67

Figure 3.13 The Bond between the UHPC and Top FRP	68
Figure 3.14 The Failure Mode near the End of the Grouted Region	68
Figure 3.15 Strain at Top UHPC Plate for the First Set	69
Figure 3.16 Strain at Bottom FRP for the First Set	69
Figure 3.17 Load-Displacement Responses for the Second Set	70
Figure 3.18 Number of Grooves in the Second Group of the Second Set	71
Figure 3.19 Strain at Top UHPC Plate for the Second Set	71
Figure 3.20 Strain at Bottom FRP for the Second Set	72
Figure 3.21 Scaled Moment - Scaled Displacement for the First and Second Set	73
Figure 3.22 Scaled Load - Scaled Displacement for the First and Second Set	73
Figure 3.23 Different Test Setup for FRP Bond	75
Figure 3.24 Specimen Preparation Showing the Plywood Position	77
Figure 3.25 Installation and Distribution of High Strength Nuts	77
Figure 3.26 Specimen's Identification	78
Figure 3.27 The Carbon Specimens under Atmosphere Pressure	79
Figure 3.28 Details of bonding Length	79
Figure 3.29 Details of bonding length in single lap test	80
Figure 3.30 Details of grooves mesh	80
Figure 3.31 Location of plastic bolts	81
Figure 3.32 Strain Gage Distribution	82
Figure 3.33 Double Lap Specimen Arrangement during the Test	82
Figure 3.34 Single Lap Specimen Arrangement during the Test	83
Figure 3.35 FRP Coupons	83
Figure 3.36 Failure Modes of Specimens in Double Lap Test	86
Figure 3.37 Failure Modes of Specimens in Single Lap Test	87
Figure 3.38 Strain Profile for G-SP1-S-1	87
Figure 3.39 Strain Profile for G-SP2-S-2	88
Figure 3.40 Strain Profile for G-SP2-S-2	88
Figure 3.41 Strain Profile for C-SP4-S-1	89
Figure 3.42 Strain Profile for C-SP4-S-1	89
Figure 3.43 Strain Profile for C-SP5-S-1	90
Figure 3.44 Strain Profile for G-SP7-B-1	90
Figure 3.45 Strain Profile for G-SP8-B-1	91
Figure 3.46 Strain Profile for Grid-SP1	91
Figure 3.47 Strain Profile for Grid-SP2	92
Figure 3.48 Strain Profile for Grid-SP3	92
Figure 3.49 Strain Profile for Bolt-SP1	93
Figure 3.50 Strain Profile for Bolt-SP2	93
Figure 3.51 Strain Profile for Bolt-SP3	94
Figure 4.1 Schematics of the Proposed UHPC Waffle Deck System	97
Figure 4.2 Schematics of Single-Rib, Simple-Span, or Two-Span Specimens	98
Figure 4.3 Schematics of Multi-Rib Simple-Span Specimen	100
Figure 4.4 Specimen Preparation: (a) Formwork, and (b) Casting	101
Figure 4.5 Flexure Tests of Specimens 1T1S: (a) Test Setup, (b) Failure Mode, and (c) Load-Deflection Responses (Note: Curves 1T1S-5#1 and #2 from Saleem 2011)	104

Figure 4.6 Load-Strain Response of Rebars in Specimens 1T1S	105
Figure 4.7 Tests of Specimens 4T1S: (a) Test Setup, (b) Failure Mode, and (c) Load-Deflection Responses (Note: Curves 4T1S-127-D1, D2, and D3 from Saleem 2011)	106
Figure 4.8 Load-Strain Response of Rebars in Specimen 4T1S	107
Figure 4.9 Punching Shear Test of Specimen 4T1S: (a) Test Setup, (b) Failure Mode, and (c) Load-Deflection Responses	108
Figure 4.10 Flexure Tests of Specimen 1T2S: (a) Test Setup, (b) Deflected Shape, and (c) Failure Mode	109
Figure 4.11 Load-Deflection Responses of Specimens 1T2S (Note: Curves 1T2S-127-D1 & D2 from Saleem 2011)	110
Figure 4.12 Load-Deflection Responses of Specimens 1T2S (Note: Curves 1T2S-127-D1 & D2 from Saleem 2011)	110
Figure 4.13 Schematics Single-Rib Specimens in Simple-Span or Two-Span Configurations: (a) Plan View, and (b) Section	113
Figure 4.14 Schematics of Multi-Rib Simple-Span Specimen: (a) Plan View, and (b) and (c) Sections	114
Figure 4.15 Specimen Preparation: (a) & (b) Formwork, and (c) & (d) Casting	115
Figure 4.16 Simple End Anchorage System for CFRP Bars in Phase 1: (a) Grinded End, and (b) Slippage of CFRP Bar	116
Figure 4.17 Anchorage System for CFRP Bars in Phase 2: (a) Casting of Expansive Grout, (b) Close-up View, (c) Ancillary Test Setup, and (d) Failure of CFRP Bar	117
Figure 4.18 Setup for Flexure Tests of (a) Specimen 1T1S, (b) Specimen 1T2S, (c) Specimen 4T1S, and (d) Punching Shear Test of Specimen 4T1S	118
Figure 4.19 Flexure Test and Failure Mode of Specimens 1T1S, (a) Deflected Shape of Specimen 1T1S, (b) Close of View of Beam Shear Crack, and (c) Shear Crack at the Edge of the Loading Pad	120
Figure 4.20 Load-Deflection Responses of Specimens 1T1S	121
Figure 4.21 Load-Strain Responses of CFRP Bars in Specimens 1T1S	122
Figure 4.22 Failure Modes in Specimen 4T1S: (a) Top View, (b) Bottom View, (c) Load-Deflection Responses under Each Rib of Specimen 4T1S	123
Figure 4.23 Load-Strain Responses of CFRP Bars in Each Rib of Specimen 4T1S	124
Figure 4.24 Punching Shear Test and Failure Mode in Specimens 4T1S	124
Figure 4.25 Load-Deflection Responses of Specimen 4T1S in Punching Shear	125
Figure 4.26 Failure Mode of Specimen 1T2S: (a) Deflected Shape, and (b) Shear Crack	126
Figure 4.27 Load-Deflection Responses of Specimens 1T2S	126
Figure 4.28 Load-Strain Responses of CFRP Bar in Specimen 1T2S	127
Figure 4.29 Flexure Test and Failure Mode of Specimens 1T1S-HSS, (a) Deflected Shape of Specimen 1T1S, and (b) Beam Shear Crack	131
Figure 4.30 Flexure Test and Failure Mode of Specimens 1T1S-CFRP, (a) Deflected Shape of Specimen 1T1S, and (b) Beam Shear Crack	131
Figure 4.31 Load-Deflection Responses of all Specimens 1T1S	132
Figure 4.32 Strain Responses of HSS Bars in Specimens 1T1S	132
Figure 4.33 Strain Responses of CFRP Bars in Specimens 1T1S	133
Figure 4.34 Flexure Test and Failure Mode of Specimens 4T1S-HSS, (a) Test Setup, (b) Beam Shear Crack, (c) Cracks on the Slab, and (d) Cracks on the Top Slab	134

Figure 4.35 Flexure Test and Failure Mode of Specimens 4T1S-CFRP, (a) Test Setup, (b) Beam Shear Crack, and (c) Cracks on the Top of the Slab	134
Figure 4.36 Load-Deflection Responses of all Specimens 4T1S	135
Figure 4.37 Load-Strain Responses of all Specimens 4T1S-HSS	136
Figure 4.38 Load-Strain Responses of all Specimens 4T1S-CFRP	136
Figure 4.39 Punching Shear Test of Specimen 4T1S: (a) Test Setup, (b) Beam Shear Crack, and (c) Cracks on the Top of the Slab	137
Figure 4.40 Load-Deflection Responses of Specimen 4T1S-HSS	137
Figure 4.41 Punching Shear Test of Specimen 4T1S: (a) Test Setup, (b) Beam Shear Crack, and (c) Cracks on the Top of the Slab	138
Figure 4.42 Load-Deflection Responses of Specimen 4T1S-CFRP	139
Figure 4.43 Flexure Tests of Specimen 1T2S-HSS: (a) Test Setup, (b) Deflected Shape, and (c) Failure Mode	140
Figure 4.44 Flexure Tests of Specimen 1T2S-CFRP: (a) Test Setup, (b) Deflected Shape, (c) Failure Mode (Beam Shear Crack), and (d) Flexural Crack on the Interior Support	140
Figure 4.45 Load-Strain Responses of All Specimens 1T2S	141
Figure 4.46 Load-Strain Responses of All Specimens 1T2S-HSS	142
Figure 4.47 Load-Strain Responses of All Specimens 1T2S-CFRP	142
Figure 4.48 Panels Layout	144
Figure 4.49 Panel 1 (UHPC-HSS)	145
Figure 4.50 Detail of Panel 1 (UHPC-HSS)	146
Figure 4.51 Panel 2 (UHPC-HSS)	147
Figure 4.52 Detail of Panel 2 (UHPC-HSS)	148
Figure 4.53 Panel 3 (UHPC-CFRP)	149
Figure 4.54 Detail of Panel 3 (UHPC-CFRP)	150
Figure 4.55 Panel 4 (UHPC-CFRP)	151
Figure 4.56 Detail of Panel 4 (UHPC-CFRP)	152
Figure 4.57 Detail of Connections	153
Figure 4.58 Loading Plan	154
Figure 4.59 Location of Blockouts	154
Figure 4.60 Wheel Path Dimensions	155
Figure 4.61 Instrumentation Plan (String Pots)	155
Figure 4.62 Instrumentation Plan (Strain Gauge)	156
Figure 4.63 Strain Responses of HSS Bars vs. the Number of Truck Passages	157
Figure 4.64 Strain Responses of CFRP Bars vs. the Number of Truck Passages	158
Figure 4.65 Deflections of Panels vs. the Number of Truck Passages	158
Figure 4.66 Relative Deflections of Panels vs. the Number of Truck Passages	159
Figure 4.67 Deck Status after the APT, (a) Deck Overview, (b) Cracks on the Connection Parts, (c) Cracks on the top of Panel 2 (d) Close up view of the Cracks on Panel 2	160
Figure 4.68 Stress-Strain Behavior of UHPC	161
Figure 4.69 Stress-Strain Behavior of HSS (MMFX)	162
Figure 4.70 Geometry and Mesh of Specimen 1T1S-HSS	163
Figure 4.71 Boundary Conditions of Specimen 1T1S-HSS	163
Figure 4.72 Failure Modes and Deflected shape of the Specimen 1T1S-HSS, (a) FE	164

Modeling, and (b) Failure Mode in Experimental Test	
Figure 4.73 Load-Deflection Response of Model 1T1S-HSS	165
Figure 4.74 Finite Element Model of Specimen 1T2S-HSS	165
Figure 4.75 Failure Modes and Deflected shape of the Specimen 1T2S-HSS, (a) FE Modeling, and (b) Failure Modes in Experimental Test	166
Figure 4.76 Top View of the Deformed Model	167
Figure 4.77 Side View of the Deformed Model	167
Figure 4.78 Load-Deflection Response of Specimen 1T2S-HSS	168
Figure 4.79 Finite Element Modeling of Specimen 4T1S-HSS, (a) Geometry and Mesh, and (b) Modeling of the Main and Transverse Ribs	169
Figure 4.80 Failure Modes and Deflected shape of the Specimen 4T1S-HSS, (a) FE Modeling, and (b) Failure Modes in Experimental Test	170
Figure 4.81 Beam Shear Cracks on the Main Ribs, (a) FE Modeling, and (b) Experimental Test	171
Figure 4.82 Beam Shear Cracks on the Transverse Ribs, (a) FE Modeling, and (b) Experimental Test	172
Figure 4.83 Load-Deflection Response of Specimen 4T1S	173
Figure 4.84 Failure Modes and Deflected shape of the Specimen 1T1S-CFRP, (a) FE Modeling, and (b) Failure Mode in Experimental Test	174
Figure 4.85 Load-Deflection Response of Model 1T1S-CFRP	174
Figure 4.86 Failure Modes and Deflected shape of the Specimen 1T2S-CFRP, (a) FE Modeling, (b) Crack on the Slab, and (c) Shear Cracks on the Web	175
Figure 4.87 Top View of the Deformed Model	176
Figure 4.88 Side View of the Deformed Model	176
Figure 4.89 Load-Deflection Response of Specimen 1T2S-CFRP	177
Figure 4.90 Failure Modes and Deflected shape of the Specimen 4T1S-CFRP, (a) FE Modeling, and (b) Failure Modes in Experimental Test	178
Figure 4.91 Beam Shear Cracks on the Main Ribs, (a) FE Modeling, and (b) Experimental Test	179
Figure 4.92 Beam Shear Cracks on the Transverse Ribs, (a) FE Modeling, and (b) Experimental Test	180
Figure 4.93 Load-Deflection Response of Specimen 4T1S-CFRP	181

# Chapter-1

---

## Introduction

### 1.1 Problem Statement

Of the over 605,000 bridges in the U.S., about 12% are structurally deficient and another 16% are functionally obsolete (FHWA 2012). Three out of four structurally deficient bridges have major problems with their decks. For example, the most recent case of the collapsed bridge on I-5 in Washington is reported to have been on the state's structurally deficient bridge list for its deck problems. In addition to structural deficiency, the deck weight and geometry often limit both the load rating and functionality of the bridge. It is commonly accepted that service life of bridges could be extended by replacing their decks. However, traditional construction methods and deck systems often lead to lengthy construction and major traffic delays, and limit states' ability and interest in replacing or widening of bridge decks, especially in urban areas.

### 1.2 Research Objectives

The primary objective of the proposed research was to develop innovative modular high performance lightweight deck options that lend themselves to accelerated bridge construction (ABC). Such bridge decks would allow an increase in the load rating of existing bridges and accordingly improve their functionality and service life. The lightweight bridge deck would also allow widening of existing bridges without placing additional dead weight on their substructure.

Given the primary objective of the NCTSPM (i.e., to improve the productivity and management of the U.S. Transportation System in an accountable and measurable way), and the fact that constrained resources are the greatest barrier to achieving this objective, the proposed research addresses two of the fundamental three questions of the 2014-15 solicitation; *How do we get most out of the existing transportation systems?* And *how should we build for the future?* The proposed bridge deck systems improve the state of good repair in bridge infrastructure throughout the U.S., thereby improving public safety on their daily commute. This will lead to the next generation transportation infrastructure, which is the first defined NCTSPM research area, as these systems address the fundamental issue of maintenance of existing bridge decks, an ongoing challenge with almost every transportation agency in the U.S. The proposed deck options also address durability of deteriorating infrastructure in constant need of rehabilitation. The innovative lightweight bridge decks will be modularized and prefabricated with highest quality control and quality assurance during the manufacturing process. The systems would integrate advanced construction materials, including ultra-high performance concrete (UHPC), high-strength steel (HSS), and fiber reinforced polymer (FRP), as appropriate. The systems would also provide options for different arrangements of superstructure, including different spacing of girders or stringers.

The Research Team at FIU-UCF has been working with the Florida Department of Transportation on two such lightweight bridge deck options for movable bridges. However, with the inclusion of a partner from UAB, tremendous opportunity developed to expand this work to have national impact on accelerated construction of all high-traffic and urban bridges that require lightweight deck replacement and/or widening. The experience of the Research Team at UAB with the development of novel high performance precast concrete components, which were used in the construction of highway bridges in Alabama, also helped enhance the impact of this research project.

### **1.3 Research Approach**

The FIU/UCF/UAB Research Team proposed to develop innovative modular high performance lightweight deck systems that lend themselves to accelerated bridge construction (ABC). The new systems will allow easy and rapid deck replacement, partial rehabilitation, and bridge widening. They will enhance service life of the bridge, and help remove them from the list of structurally deficient or functionally obsolete bridges. The proposed research will also allow the integration of advanced materials in a new design paradigm that combines the benefits of different materials in a performance-based design approach that will ultimately make highway bridges more sustainable. The following tasks were identified in the proposed work plan:

**Task 1. Literature Review:** This task includes an intense review and synthesis of available literature as well as DOT surveys on construction methods and advanced materials used in bridge decks, current state of bridge decks across the United States and the world, current girder/stringer spacing, and potential retrofit needs including deck replacement and bridge widening.

**Task 2. Preliminary Design and Optimization:** This task includes a preliminary analysis and design optimization of two specific deck systems, i.e., hybrid FRP-UHPC deck, and the waffle UHPC deck with either HSS or CFRP reinforcement.

**Task 3. Bond and Interface Investigations:** This task includes interface bond assessment between FRP and UHPC for the hybrid FRP-UHPC deck system.

**Task 4. Experimental Work on Connections and Precast Modules:** This task includes laboratory tests as well as heavy vehicle simulation (HVS) testing of the proposed deck systems.

**Task 5. Design Guidelines and Implementation Plan:** This task identifies necessary aspects of design guides and implementation plans for the proposed deck systems.

### **1.4 Report Outline**

This report is comprised of five chapters. This first chapter serves as an introduction, mainly describing the problem statement, research objectives, and research approach. Chapter 2 covers the literature review. Chapter 3 presents experimental work related to the Hybrid UHPC-FRP Deck System. Chapter 4 focuses on the experimental work and analytical simulation of the UHPC waffle decks with two types of reinforcement (i.e., HSS and CFRP). Chapter 5 includes summary and conclusions for the project, as well as recommendations for future research.

# Chapter-2

## Literature Review

### 2.1 Background on Current State of Bridges in the U.S.

According to the Federal Highway Administration (FHWA), as of 2012 there were more than 605,000 bridges in the United States (see Figures 2.1 and 2.2). About 12% of those bridges are structurally deficient and another 16% are functionally obsolete. A bridge is considered structurally deficient if the condition of important load carrying elements in the superstructure or substructure is found to be lacking due to damage or deterioration. A bridge is considered functionally obsolete if the deck geometry, clearance, or capacity are out of date and no longer meet current specifications for its purpose (Ahmad, 2011).

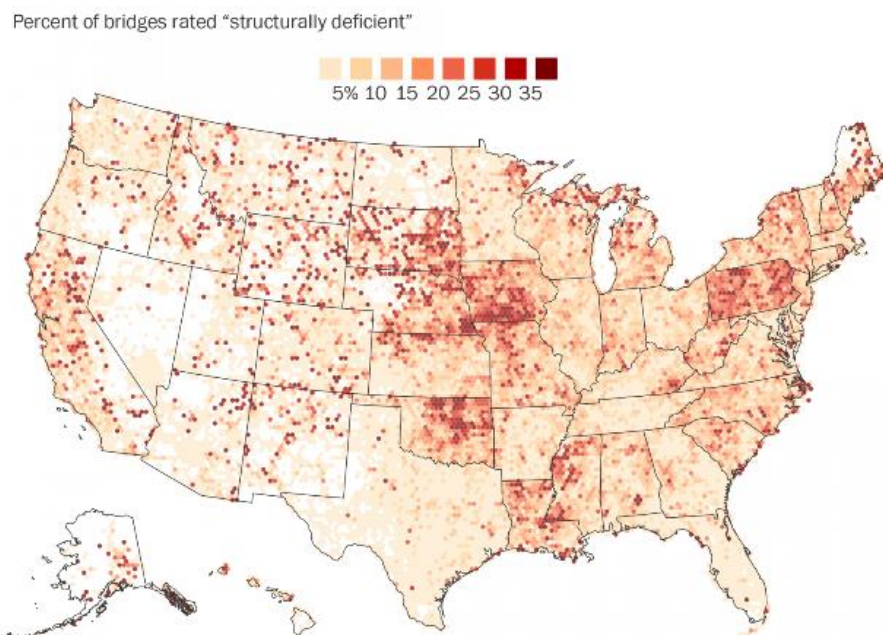


Figure 2.1 U.S. Map of Bridges Rated Structurally Deficient

Infrastructure in the United States is ageing, and a large portion of bridges are in need of some level of rehabilitation, repair, or replacement. The issue is made worse by increased levels of traffic, limited funding, and rising costs of labor and materials, which limit the amount of work performed on bridges each year. The FHWA released a manual entitled *Bridge Preservation Guide* in an attempt to prevent the issue from worsening. The manual provides an outline for a preventative maintenance program, which the author states must be a combination of preservation and replacement. "Focusing only on replacing deficient bridges while ignoring preservation needs will be inefficient and cost-prohibitive in the long term" (Ahmad, 2011).

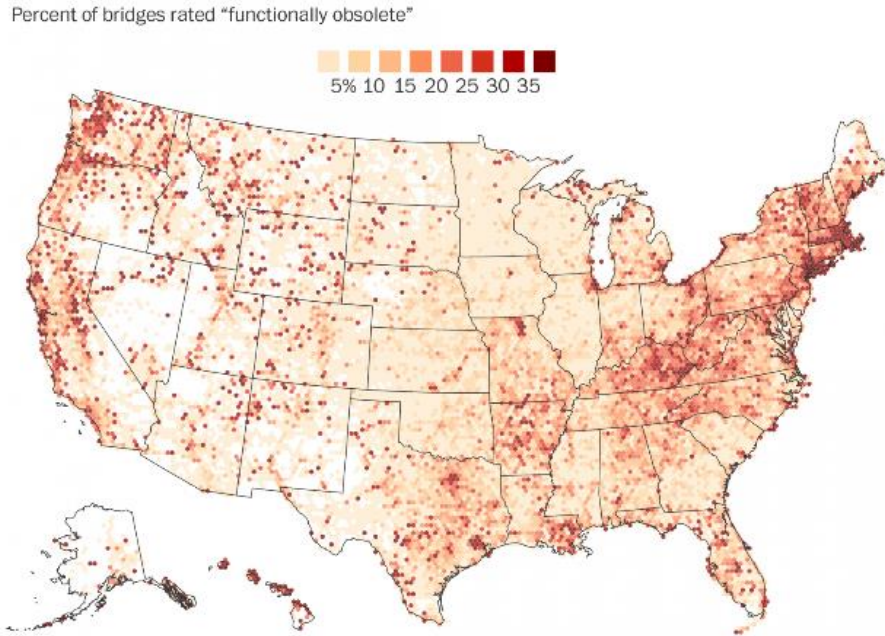


Figure 2.2 U.S. Map of Bridges Rated Functionally Obsolete

The state DOTs are working to rehabilitate and replace the insufficient bridge structures, but they are now facing an issue that is inhibiting this work: early age cracking on newly constructed and rehabilitated bridge decks. Many state DOTs have reported a problem with transverse early age cracking in newly constructed bridge decks, but Wright et al. determined that there was not much research about the causes of longitudinal cracking in new repair sections, shown in Figure 2.3. The purpose of their research is to identify the causes of longitudinal early age cracking in concrete deck sections adjacent to newly repaired bridge deck expansion joints (Wright, Rajabipour, Laman, & Radlińska, 2013).

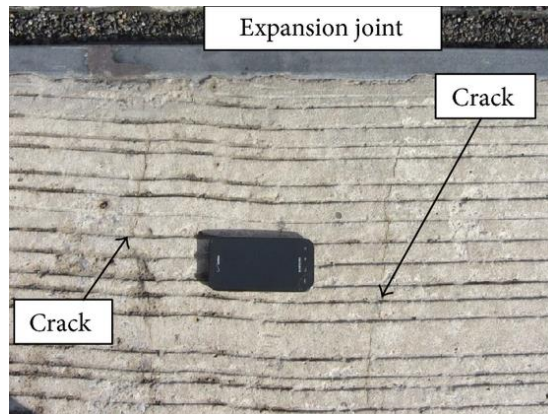


Figure 2.3 Early Age Cracking (Note: Cell Phone 4.5 x 2 in. for Size Comparison.)

In order to identify the causes, Wright et al. visited eleven past bridge deck expansion rehabilitation sites and two active deck dam rehabilitation projects in Pennsylvania to gather information about the concrete mixture proportions and properties, the construction and curing practices, and the structural design factors (2013). After gaining field data from the past and

current rehabilitation projects, Wright et al. performed laboratory tests to determine cracking risks with two concrete mixtures typically used for bridge deck rehabilitation (2013). They made the following conclusions:

- The observed early age cracking is likely caused by inadequate moist curing practices and a failure to properly eliminate the risk of plastic shrinkage cracking during construction.
- The 28-day compressive strength of the placed concrete exceeded the design required strength by up to 43% and the measured slumps were in excess of 200 mm. These high compressive strengths and slump values increase the risk of early age cracking. The maximum allowable compressive strength and slump for the concrete should be included in the construction specifications.
- A lower cement paste content, lower coefficient of thermal expansion, lower drying shrinkage, and lower compressive strengths were factors that improved the performance of one of the tested mixtures.
- A review of the structural design of the decks and reinforcing bars suggests that the early age cracking is caused by material issues, not structural design factors (Wright, Rajabipour, Laman, & Radlińska, 2013).

Another study was performed in Colorado to determine the cause behind concrete cracking in newly constructed bridge decks around the state. In order to identify the cause behind the cracking, the Colorado Department of Transportation (CDOT) construction practices were compared with the bridge deck construction practices of the Nevada DOT, Kansas DOT, and Utah DOT. After comparing construction practices, a database analysis on reports of deterioration and cracking problems provided by CDOT's Bridge Inspection Unit was performed to determine the extent of early bridge deck cracking in Colorado. According to this database analysis, as of 2002, only 18% of Colorado's bridge decks had no problems while 82% had issues ranging from spalling/delamination to unsealed cracks with moderate size and/or density. These results were then verified with field inspections of several bridges, which included photos, crack mapping (to determine the length, width, shape, and location of the cracks), sounding tests by chain-dragging to detect concrete delamination, ultrasonic tests for evaluating the concrete quality and possible internal damage and cracks, and concrete coring to determine chloride permeability (Xi, et al., 2003). Xi et al. provided a list of recommendations for material, design, and construction changes that will help reduce the severe deck cracking problem in Colorado. These recommendations include:

1. Material changes:

- Use Type I or II Portland cement and avoid fine ground cement
- Limit cement content to a maximum of 470 lb/yd<sup>3</sup>
- Use a water/cement ratio of around 0.40
- Limit silica flume to 5% by weight of cement to reduce permeability
- Given the high early shrinkage strain, the rate of strength gain should be specified at curing days 1, 3, 7, 28, and 56 instead of only 28-days (Xi, et al., 2003)

2. Design changes:

- Consider post-tensioning the slab in the transverse direction with unbonded tendons to enhance the shear transfer between girders and reduce longitudinal shrinkage cracks in the slab for decks with adjacent girders
  - Use smaller reinforcement bars in areas that have negative moments
  - Reduce longitudinal restraint on bridge decks when possible because restrained ends cause more cracking
  - Consider thicker decks ( >8.6 inches) – thin decks tend to crack more often (Xi, et al., 2003)
3. Construction changes:
- Do not cast concrete decks when ambient temperatures are lower than 45°F or higher than 80°F. Also avoid large temperature variations during concrete placement
  - For concrete with silica fume and or/fly ash, adopt a 7-day continuous moist curing to reduce early age cracking
  - Seal all cracks that develop within the first year of casting
  - Apply surface finishing and texture as soon as possible to allow final curing of the deck (Xi, et al., 2003)

The problem of early age cracking noted in these bridge deck examples are not limited to a state or region, but rather the entire U.S., albeit to varying degrees.

## **2.2 Accelerated Bridge Construction (ABC)**

### **2.2.1 Overview of ABC**

In 2009, the Federal Highway Administration (FHWA) collaborated with the American Association of State and Highway Transportation Officials (AASHTO) to create a program called Every Day Counts (EDC). This program was created to combat the long duration of highway projects as well as budget constraints. The goal of Every Day Counts is to instill proven but underused ideas to decrease project times as well as enhance highway safety, lessen traffic congestion, and improve environmental sustainability at the state level. State and local transportation agencies and industry stakeholders create innovative methods of achieving these goals. During a two-year period, the stakeholders generate specifications, best practices, lessons learned, and relevant data so that the ideas can be quickly implemented nation-wide (Wolf, 2015).

Accelerated bridge construction was one of the innovations in “EDC-2”, which was published in 2012. Accelerated Bridge Construction (ABC) uses “innovative planning, design, materials and construction methods in a safe and cost-effective manner to reduce the onsite construction time that occurs when building new bridges, or replacing and rehabilitating existing bridges” (Accelerated Bridge Construction, n.d.). ABC is becoming increasingly popular as technology advances and the need for prompt, efficient replacement of existing bridges with minimal interruption of traffic flow. This concept is not only here in the United States, but Germany, France, the United Kingdom and other European countries have made developments in pre-fabricated composite girders, welded joints, and dry connections utilizing no grout (Hällmark, White, & Collin, 2012).

While conventional construction methods are typically less expensive at the onset of a project, they cause lengthy traffic delays and can be very labor intensive, which adds to the overall cost. A fundamental difference between conventional bridge construction and accelerated bridge construction is the use of cast-in-place concrete structures versus precast concrete elements and other prefabricated systems. Because the majority of the concrete placement work is done onsite, installation of the substructure and superstructure forms must also be completed onsite. Once the forms are installed, they are filled with reinforcing steel and concrete (Mercer, 2012). Cast-in-place concrete requires a great deal of field labor and time must be allotted for the concrete to cure. Conventional construction methods are also dependent upon weather, where precast elements can be constructed in a closed facility away from the jobsite, regardless of weather conditions, and moved into position when required. Although there are advantages to using conventional construction methods such as lower initial costs and fewer joints required because the members can be cast-in-place into continuous spans, there are several significant advantages to using ABC, especially for bridges where there is a large volume of traffic. ABC reduces traffic disruption by reducing road closures. Structures are often prefabricated off-site and moved into place, allowing time for better quality control. The quickness of the construction period increases crew safety because workers are not required to be present at the job site for an extended length of time, which also reduces the environmental impact of the jobsite (Sivakumar, 2012).

### **2.2.2 Superstructure Systems for ABC**

There are several bridge superstructure systems that can be prefabricated for ABC. Some of these systems include full-depth precast deck panels with or without post-tensioning, fiber reinforced polymer deck panels, steel grids, orthotropic decks, adjacent deck bulb-T beams, adjacent inverted-T beams, adjacent box beams, voided slabs, modular beams with decks, and full-width beam span with decks (Mercer, 2012).

Steel grids may be used as part of an Exodermic bridge deck system, which consists of a reinforced concrete slab on top of and composite with an unfilled steel grid. The combination creates a deck system that is lightweight and strong, typically only reaching weights 50-65% as heavy as standard reinforced concrete decks (Shahawy, 2003). The northbound structure of the South Grand Island Bridges in Grand Island, New York is an example of bridge rehabilitation where the existing deck was replaced with an Exodermic deck system. To minimize traffic impact, deck replacement was performed at night, replacing an average of 2000 square feet of deck each night (Representative Exodermic® Bridge Deck Projects: South Grand Island Bridges, Grand Island NY, 2015).



Figure 2.4 Crew Working on Exodermic Deck of South Grand Island Bridge

New York State Department of Transportation (NYSDOT) investigated and implemented the use of a field-cast ultra-high performance concrete (UHPC) joint fill system for side-by-side bulb-tee girders (See Figures 2.5 and 2.6).



Figure 2.5 NYSDOT Bulb-Tee Girders with Shear Pocket Ready for UHPC Pour

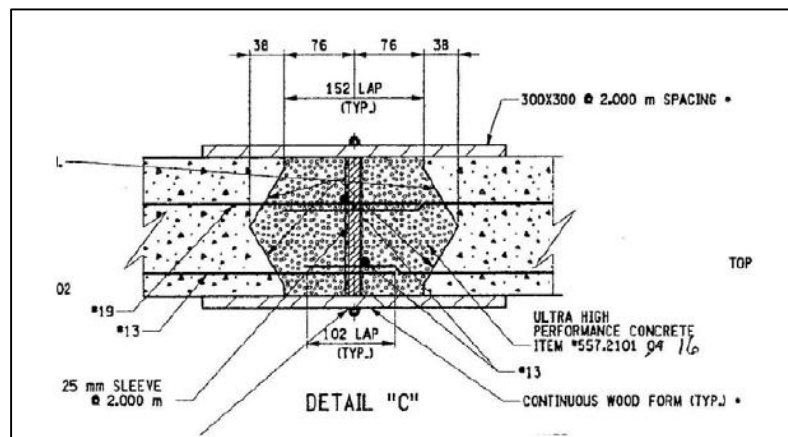


Figure 2.6 Detail of UHPC Shear Key Pocket

This system consisted of precast bulb-tee girders connected longitudinally with shear pocket filled with UHPC. This joint provided very small shrinkage, low permeability, high strength, and excellent bonding for the bridge panels (Perry & Royce, 2010). Research by Harris also states that UHPC has very low permeability, making it very resistant to chloride penetration and a very good protector of any reinforcement in the concrete (Harris, 2004).

Zhu et al. investigated the fatigue and tension stress capacity of transverse U-bar joints. These joints consist of U-shaped, transverse reinforcement bars cast into either double Bulb-Tees or precast decks. These U-bars are then aligned and a headed lacer bar is passed through U-bars of the elements being connected as shown in Figure 2.7.

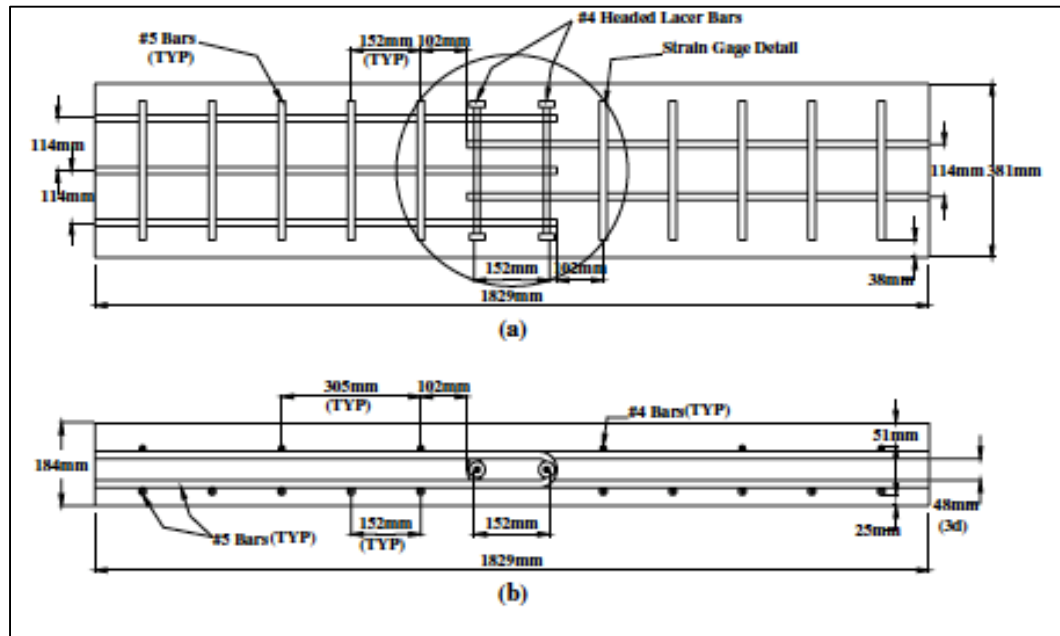


Figure 2.7 Transverse U-Bar Joint Section: (a) Plan View (b) Elevation View

After the elements are connected with the lacer bars, they are sealed with grout contained within a shear key as shown in Figure 2.8.

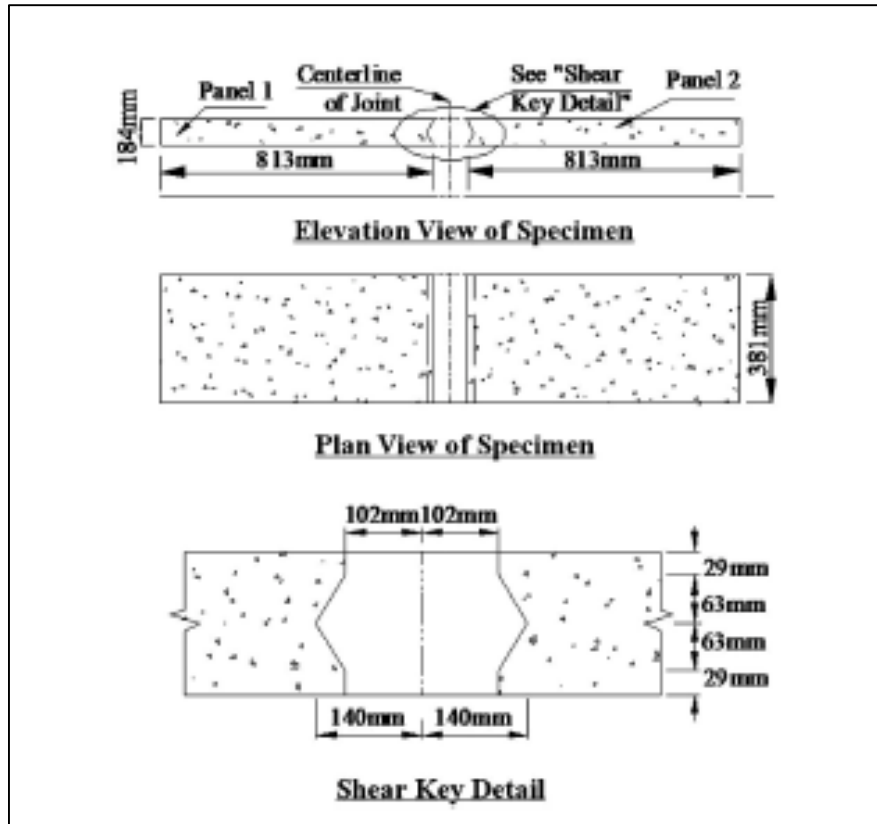


Figure 2.8 Shear Key Used to Contain Grout in Joining Prefabricated Elements

This study used two types of grout, namely, an overnight cure grout and a seven-day cure grout. The joint was tested first in tension and cyclical fatigue loading. Important findings were the following:

1. Lacer bars provided a joint that when loaded to failure behaved in a ductile manner through failure.
2. The overnight grout had a lower compressive strength and thus a lower overall capacity for the joint.
3. Moisture loss during the first 3 hours of grout curing is critical (Zhu, John Ma, Cao, & French, 2012).

The Florida Department of Transportation (FDOT) has also used a U-Bar lap joint for panel-to-panel connections similar to that shown in Figure 2.7. Tom Andres, currently the Assistant Structures Design Engineer for FDOT, also emphasizes that moisture control is critical for successful closure pours of precast components. He states the following:

Dry concrete substrate has the tendency to draw water out of a grout or concrete mixture causing a weak bond to develop at the interfacing surface. The concrete substrate should be wetted to a SSD [Saturated Surface Dry] condition prior to grout or concrete in-fill application, usually requiring continuous pre-soaking the area for five hours or more. Consult grout manufacturer's printed recommendations to obtain SSD at the interfaced surface and provide presoaking times for SSD condition for concrete in-fills.

Epoxy bonding agents have a tack-free time of between 4 and 8 hours which may not be appropriate for certain applications depending on precast component(s) placement, leveling and form sealing timeframes. Epoxy bonding agents which have cured prior to casting grout or concrete will have significant adverse effects on the bond of the interfacing surfaces (Andres, 2014).

NYSDOT used UHPC as a transverse shear connector in bulb-tee girders. The design consisted of epoxy-coated reinforcement bars extending from the top flange of the bulb-tee girder and being grouted with field mixed and cast ultra-high performance concrete (Shutt, 2010).

Another type of longitudinal bulb-tee girder connection similar to the one used by NYSDOT consists of headed studs extending from the deck of the bulb-tee. These headed studs are then enclosed in a shear key with a quick set grout, appropriate for accelerated bridge construction (See Figures 2.9 and 2.10).



Figure 2.9 Headed studs Extending out of Deck Panel

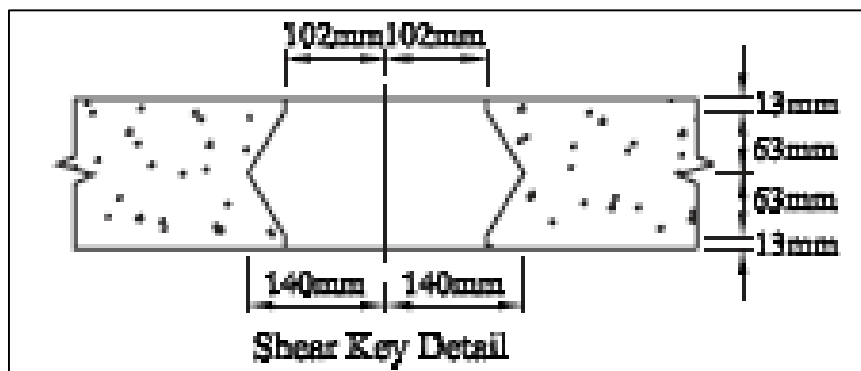


Figure 2.10 Cross-section of Shear Key Used to Enclose Headed Studs

Ultimately, flexural and shear fatigue tests show that this connections is “...a viable connection system to transfer the forces between adjacent [deck bulb-tee] girders” (Li, Ma, & Oesterle, 2010).

One important resource that contains multiple connection details, connection prototypes, and general connection information is “Connection Details for Prefabricated Bridge Elements and Systems” published by the Federal Highway Administration (Culmo, Connecticut Details for

Prefabricated Bridge Elements and Systems, 2009). Not only does this connection guidelines but also experiences and recommendations with connections that have been actually implemented.

### 2.2.3 Common ABC Tools and Technologies

There are three main ABC tools promoted by the “Every Day Counts” initiative “EDC-2”: prefabricated bridge elements and systems (PBES), slide-in bridge construction, and geosynthetic reinforced soil – integrated bridge systems (GRS-IBS) (Accelerated Bridge Construction, 2012). PBES is the most commonly used method of accelerated bridge construction. Structural bridge members are constructed offsite and are later moved into position through various means including self-propelled modular transports and lateral sliding (Sivakumar, 2012).



Figure 2.11 Moving Prefabricated Bridge Element into Place at Construction Site

Common prefabricated elements for bridge construction include I-beams, box beams, hollow and solid slabs, and deck panels. Although typically more expensive at the project offset, there are several advantages to using prefabricated bridge elements that can offset the initial cost, especially in areas that experience heavy traffic. Using members that can be mass-produced offsite reduces labor and forming costs and minimizes the road closure durations (Shahawy, 2003). The main goal of using prefabricated elements is to lessen traffic disruptions by moving construction activities that have long durations, such as casting concrete, offsite (Sivakumar, 2012). Using concrete PBES results in many benefits including shorter construction times, improved safety to the public, work crews, and inspection teams, lessen environmental impacts, lower initial and life-cycle project costs, and improved quality of the finished product due to more time for quality control and lowered weather impact (Lwin & Triandafilou, 2011).

Slide-in bridge construction is a cost-effective method of implementing prefabricated bridge elements and systems. When a bridge is no longer serviceable and needs replacement, the new bridge is constructed on temporary supports adjacent to the existing structure. Once construction for the new bridge is complete, the existing bridge is demolished and the new bridge is slid into place and paved within 48-72 hours (Accelerated Bridge Construction, 2012).



Figure 2.12 Rendering of Bridge Spans Laterally Sliding into Place

A geosynthetic reinforced soil – integrated bridge system can be used once the new bridge deck is built and moved into place. GRS-IBS is a method of construction that creates a new composite material by combining geosynthetic reinforcement and granular soils. This new material is used to create abutments and embankments that have a lower probability of settling and causing bumps at the ends of bridges (Accelerated Bridge Construction, 2012). The Federal Highway Administration compiled a list of the benefits of each of these accelerated bridge construction tools:

Table 2.1 Comparison of Benefits among Three ABC Tools Promoted by EDC-2

<b>Benefits</b>	<b>Slide-In Construction</b>	<b>PBES</b>	<b>GRS-IBS</b>
Enhances Safety	Yes	Yes	Yes
Can Lower Construction Costs	Yes	Yes	Yes
Reduces Mobility Impacts	Yes	Yes	Yes
Shortens Onsite Construction Time	Yes	Yes	Yes
Reduces Environmental Impacts	Yes	Yes	Yes
Can Improve Quality	Yes	Yes	Yes
Increases Constructability	Yes	Yes	Yes
Eliminates “Bump at the Bridge”	No	No	Yes
Accommodates On-Site Modifications	No	No	Yes

Depending on the size of the prefabricated elements, there are three main placement methods that can accelerate bridge projects, including self-propelled modular transporters (SPMTs), longitudinal launching, and transverse sliding (Lwin & Triandafilou, 2011). Self-propelled modular transporters are large, multi-axle platforms operated by computers and able to pivot 360 degrees (Sivakumar, 2012). They are able to lift loads weighing up to several thousand tons, such as bridge systems, and move them with precision within a fraction of an inch (Accelerated Bridge Construction, n.d.).



Figure 2.13 Bridge Span Being Moved with SPMTs

According to the FHWA, the initial cost of using SPMTs can range from \$50,000 to \$500,000, depending on the locations and requirements of individual jobs. However, those costs are also offset because less construction time is lost due to manpower switching shifts, few hours are needed for off-duty police officers to control traffic and roadblocks, there is not a need to build and maintain detours or temporary structures that would be required for long-term road closures, and because smaller contractors and workforces can be used to construct the prefabricated elements that would not be able to handle the workload of a full bridge replacement (Beerman & Garcia, 2007).

While more state DOTs are experimenting with ABC and are seeing the potential benefits, it is not currently a construction method that is utilized by everyone. Many have cited not only the increased initial costs when compared to conventional construction methods, but also the risks associated with custom engineering each project. Bala Sivakumar, the director of special bridge projects with HNTB Corporation, had a large role in the development of the ABC Toolkit which is essentially a manual for accelerated bridge construction that developed a standardized approach to design and constructing complete bridge systems using ABC techniques (A Toolkit for Accelerated Bridge Construction, 2015). Sivakumar has stated that the toolkit will “bring about greater familiarity about ABC technologies and concepts and also foster more widespread use of prefabricated elements”. As of January 2014, the ABC Toolkit was used in two field demonstrations. The first was two spans across I-84 in Putnam County, New York and the second was in Vermont to repair damage to three bridges after Tropical Storm Irene. The bridge spans in New York were demolished and replaced in 20 hours using the toolkit’s guidance for lateral-slide design and construction techniques (Cho & Parsons, ABC Tool Kit Crafter Spreads The Word, 2014). The toolkit contains ABC standard concepts, ABC sample design calculations, recommended ABC design specifications, and recommended ABC construction specifications. The toolkit is not intended as a complete manual on accelerated bridge construction methods and techniques, but instead is a guide for engineers and contractors new to ABC. The standards that are in the toolkit were deemed most useful on a large scale, and include precast modular abutment systems, precast complete pier systems, modular superstructure systems, and ABC bridge erection systems (A Toolkit for Accelerated Bridge Construction, 2015).

#### **2.2.4 U.S. Bridges Constructed Using ABC Tools**

Several state Departments of Transportation are experimenting with ABC techniques. The Ohio Department of Transportation (ODOT) employed ABC methods to replace a Quaker City Bridge in 2003. The existing structure was a two-span continuous reinforced concrete slab with a

reinforced concrete substructure and was built in the 1950 (Salem, et al., 2006). Salem et al. states that the closure of the bridge would result in a 20 mile detour for cars and a 40 mile detour for trucks and busses, including school busses (2006). In order to mitigate traffic interruptions, ABC was utilized to replace the bridge deck with precast, post-tensioned, full-depth slabs onto the existing substructure (Salem, et al., 2006). From this project important lessons were learned, as follows:

1. Because of the fast track nature of ABC, reasonable contingencies such as equipment malfunction or an unavailable material need to be considered in the planning stage of the project. Along with this, very close communication needs to be maintained between the contractor and the project engineer to both monitor progress and address issues that arise. A one-day delay in an accelerated bridge construction project is a significant loss.
2. This project experienced problems with obtaining the type of grout specified in the plans. The type of grout the contractor intended to use on the project was not on an approved list of ODOT grouts. Because of this, a type of grout that took significantly longer to cure was used. A possible solution is to specify a performance based material rather than a particular type. Ultimately, in ABC the cure time is of equal importance as the strength.
3. Although a mockup of the bridge was done off-site, the slope of the bridge location was not accounted for in the mockup. Because of this, post-tensioning ducts did not align properly and needed adjusting in the field. Close quality control and tight tolerances are essential in accelerated bridge construction because of the rigorous schedule of these projects (Salem, et al., 2006).

Salem et al. states that due to the problems experienced during construction, the original 16-day window that the Ohio Department of Transportation (ODOT) gave to the construction crews was extended by three days (2006).

The Michigan Department of Transportation (MDOT) completed its first ABC project in 2008 - the repair of the deficient Parkview Avenue Bridge overpassing U.S. Route 131.



Figure 2.14 Completed Parkview Avenue Bridge

The allotted construction time for this project was 12 weeks (Attanayake, Abudayyeh, Cooper, Mohammed, & Aktan, 2014). Important considerations that were noted during this project include:

1. Post tensioning duct alignment was not accurate due to a miscalculation of the skew.

2. As the panels were being placed on the girders, shear pockets on the precast panels were misaligned. The pre-stressed girders had flared coil inserts to establish the composite action between the girder and the deck. This misalignment was caused by sweep which can be caused by eccentricity in pre-stressing, improper storage, or uneven bearing.
3. Challenges in grouting resulted in recommending a leak-proof formwork for grouting haunches. Leveling screws and flexible formwork is recommended (Attanayake, Abudayyeh, Cooper, Mohammed, & Aktan, 2014).

The allotted construction time for this project was 12 weeks, but the problems encountered delayed the bridge opening by 2 months. Cost savings information was provided for the original schedule to determine if the time-savings would outweigh the higher initial costs of accelerated bridge construction. The project costs were estimated at \$2.85 million with ABC and \$2.30 million with conventional construction, however, the estimated time-savings of 45 days would result in a savings of \$972,000 due to the reduced construction duration, causing ABC to be the more economical route (Attanayake, Abudayyeh, Cooper, Mohammed, & Aktan, 2014). These results are shown graphically in Figure 2.15.

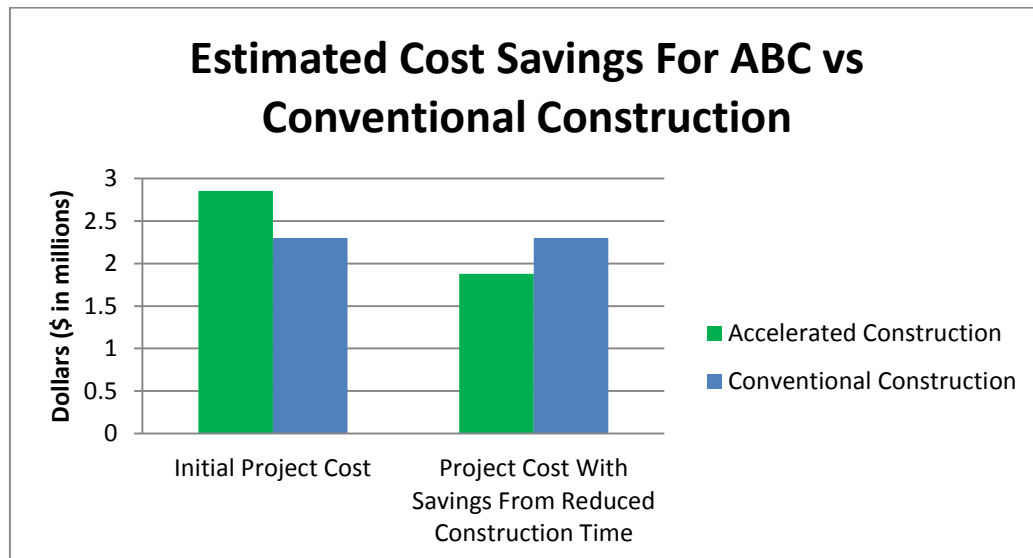


Figure 2.15 Estimated Cost Savings for ABC vs Conventional Construction

In 2010, the Iowa Department of Transportation was involved in a research study with the Transportation Research Board's Strategic Highway Research Program 2 (SHRP2). The goal of the study was to develop standardized accelerated bridge construction systems for nationwide use, and Iowa DOT was selected because of their role as a leader in ultra-high performance concrete bridge applications (U.S. 6 Bridge Over Keg Creek, n.d.). The site selected for the project was the U.S. 6 Bridge over Keg Creek, a three-span steel and precast concrete modular bridge with a length of 210 feet and a width of 47 feet. The estimated cost of this structure with accelerated bridge construction techniques was approximately 30% higher than the cost with conventional construction, however the bridge would only be closed to traffic for two weeks as opposed to several months (U.S. 6 Bridge Over Keg Creek, n.d.). Mr. Abu-Hawash of the Office of Bridges and Structures said that a concrete overlay is typically used with precast deck panels to protect the joints between the panels, but the overlay would add weeks to the construction

duration. Instead, Iowa DOT decided to use ultra-high performance concrete to create more durable joints with the added benefits of low permeability and high strength (U.S. 6 Bridge Over Keg Creek, n.d.).

As of 2011, eight states had deployed self-propelled modular transport (SPMT) technology: Florida, Illinois, Louisiana, Massachusetts, New York, Rhode Island, Utah, and Washington. In 2011, the Utah Department of Transportation completed the feat of installing the longest two-span bridge moved by self-propelled modular transporters in the Western Hemisphere (O'Donoghue, Page, & McCord, 2011). The Sam White Bridge in Utah measured 345 feet long, 76.8 feet wide, and had a 10-inch thick lightweight concrete deck with six steel plate girders spaced at 13.5 feet (Farris, n.d.). The bridge was moved into place with two sets of self-propelled modular transporters over a 6.5 hour time period (National Steel Bridge Alliance 2012 Prize Bridge Awards, 2012). The Sam White Bridge was Utah DOT's 23<sup>rd</sup> bridge move using accelerated bridge construction techniques (O'Donoghue, Page, & McCord, 2011).



Figure 2.16 Sam White Bridge in Utah Being Moved into Place Using SPMTs

In 2015, Massachusetts Department of Transportation (MassDOT) replaced an existing bridge on Cedar Street in Wellesley using accelerated bridge construction methods. MassDOT wanted to ensure the least possible impact to the motoring public and the surrounding community. The cast-in-place high performance concrete replacement bridge was constructed adjacent to the existing bridge (Wellesley "Heavy Lift" Project Accelerated Bridge Replacement, 2015). Once the replacement bridge was completed, the roads were closed and the existing bridge was demolished. The replacement bridge was then moved into place using self-propelled modular transports and major road impacts were limited to 60 hours, which was 13 hours ahead of schedule (Kelleher, n.d.).

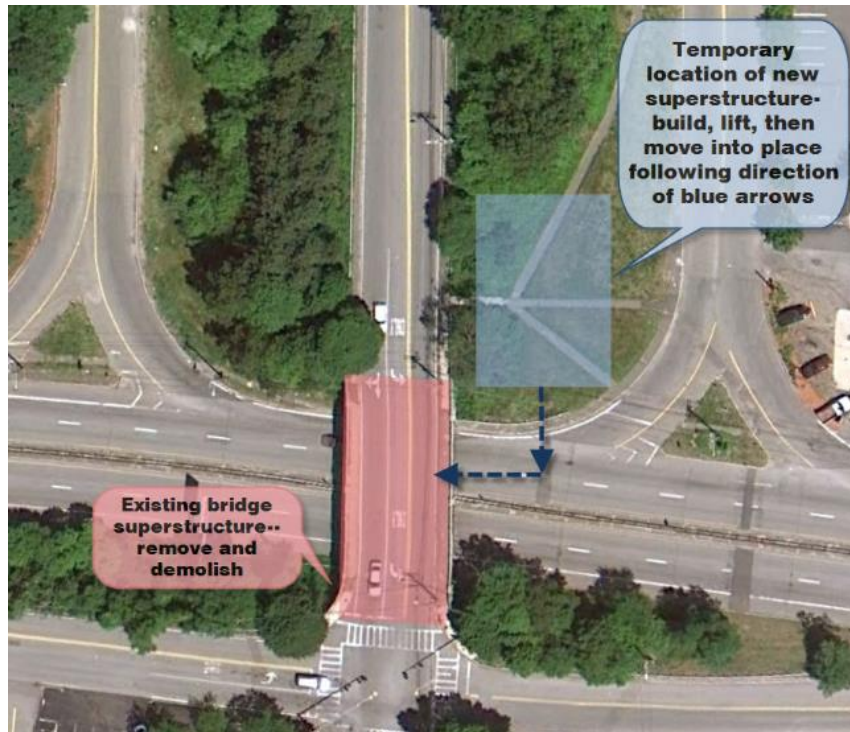


Figure 2.17 Map Showing Planned Move of Wellesley Bridge

### 2.2.5 International Bridges Constructed Using ABC Tools

Accelerated bridge construction techniques are gaining popularity within the United States and internationally. Methods such as self-propelled modular transports for bridge placement have been used in Europe for more than 30 years (WisDOT Bridge Manual, 2015). Accelerated bridge construction is currently used in several countries outside of the United States including Germany, France, and United Kingdom, Finland, Sweden, and Japan.

As of 2009, prefabricated deck systems were not common in Germany. However, prefabricated composite girders are gaining popularity, especially with the construction method Verbundfertigträger (VFT), which has been developed to achieve a high level of prefabrication and shorten construction times (Hällmark, White, & Collin, 2012). Hällmark, White, and Collin state that the VFT method, which was created in Germany and tested on railway overpass bridges in Austria, is used for composite steel girders prefabricated with precast partial depth slabs (2012).



Figure 2.18 Prefabricated VFT Girder

The Bahretal viaduct in Germany is an example of a prefabricated full-depth slab. It is made of a steel box girder with cantilevered cross beams every 13.1 feet (4 meters). Precast concrete deck slabs are placed in the cantilever section and concrete is poured between the precast elements in the longitudinal direction of the bridge (Hällmark, White, & Collin, 2012).

In 2008, the first mainland European fiber reinforced polymer bridge was constructed near Frankfurt, Germany. The Friedberg Bridge is a hybrid fiber reinforced polymer system consisting of two steel girders covered by a pultruded multi cellular deck with both elements clad with a polymer concrete material to resist weathering (Friedberg Bridge, Friedberg, Germany, 2015). The bridge is lightweight and was constructed adjacent to the highway before being moved into position so that traffic disruption would be minimized.



Figure 2.19 Friedberg Bridge Lifted into Place

Unlike Germany, France has been using prefabricated elements in bridge construction for many years. There are two kinds of transverse joints that France has used to accelerate their construction: match-cast joints and reinforced joints. In the past, France used a technique where

elements are assembled with carefully filled keys in the joint faces that are then glued to one another (Hällmark, White, & Collin, 2012). Inspections of these joints showed no sign of cross-cracking and they seemed to perform well. A more recent technique uses high-strength concrete and the steps for assembly are:

1. Steel girders and match-cast deck elements are prefabricated off-site.
2. Elements are placed onto the girder.
3. The precast concrete elements are pre-stressed together, without connection to the steel.
4. Shear studs are welded to the steel beam through holes in the concrete.
5. The holes are filled with fresh concrete, creating composite action between the deck and girder (Hällmark, White, & Collin, 2012).

Prefabricated systems have become so common in France that companies are creating pre-designed and prefabricated steel bridge systems. Eiffage Construction Metallique and Matière, two companies who specialize in steel bridge construction and precast concrete products/permanent steel bridges respectively have merged to create a product called Unibridge®. Unibridge® is a pre-designed and prefabricated modular steel bridge system that can be used for single or multi-lane bridges, can accommodate a wide range of live loads, is designed for a 100-year lifespan, is capable of accommodating oversized and overweight vehicles, and does not require additional reinforcement members in most cases (Unibridge Product Info, 2012). According to the Unibridge® Trading website, the bridges are constructed from prefabricated girders and are connected with pins or bolts so there are no specialist tools or welding needed onsite (2012).

Finland's Steel Bridges Development Group of the Constructional Steelwork Association (TRY) developed a new type of cantilever composite steel-concrete bridge (Hällmark, White, & Collin, 2012). According to Hällmark et al., the goals of the study were to develop a composite bridge that had the shortest possible installation time, was simple to construct even in unfavorable conditions, and that utilized three-dimensional design tools (2012). The result of this study was the Laisentianjoki Bridge, which consists of two steel girders and four cross beams. The installation of the girders and cross beams took about six hours, and the bridge deck was constructed of prefabricated concrete elements (Hällmark, White, & Collin, 2012).

### **2.3 Department of Transportation Surveys**

As part of this project, Departments of Transportation (DOT) in AASHTO Region 2 (Southeastern Region) were contacted to gather two main categories of information. First, in order to better develop a bridge deck that could be applied to current retrofit needs, information was gathered about basic bridge types and geometries. Second, any data or information on experiences with accelerated bridge construction (ABC) was gathered. All information was gathered from independent interviews with state DOTs. The survey included the following questions:

1. Generally, what percentage of bridges are composed of steel girders, reinforced concrete girder, and pre-stressed concrete girders? What would be the preferred type for new bridge construction?

2. Do the majority of bridges have composite deck slabs? If not, what types of bridges *do not* have composite deck slabs?
3. What is the range of bridge spans in this state (maximum/minimum)? Can a general span *range* be classified as a “typical” bridge span for this state?
4. What is the range of girder spacing in this state (maximum/minimum)? Can a general girder spacing *range* be classified as a “typical” girder spacing for this state?
5. Has this state utilized Ultra-High Performance Concrete (UHPC), Fiber-Reinforced Polymer (FRP), or High Strength Steel (HSS) in bridge deck construction? If so, how?
6. Has this state utilized the process of Accelerated Bridge Construction? If so, how?
7. If prefabricated deck panels have been used, what type of connection was used in construction?
8. Are there any plans to use Accelerated Bridge Construction for bridge construction/rehabilitation in this state?
9. What is the largest size load (weight and dimensions) that can be transported in this state without requiring a permit?

Table 2.2 lists the parties contacted with their respective position in each state DOT that completed the survey. Table 2.3 summarizes the survey results. Information marked “Unspecified” was not provided by the interviewee. Some data on maximum load and size requirement were obtained independent of the survey.

The following conclusions may be drawn from the DOT survey:

- Many older bridge systems have steel girders, but the preferred girder for new bridges is pre-stressed concrete.
- Bridge spans can be up to 300 ft, but are typically in the range of 40-130 ft.
- Girder spacing typically ranges from 6 to 10 ft, but could be as high as 13 ft.
- While use is limited, several states are implementing UHPC, FRP, and HSS in actual projects or in some cases research and demonstration projects.
- Most states have used or have plans to use ABC in various ways including precast deck panels, emergency repairs, and lateral slide elements.
- Eight of the twelve states have some experience with precast panels or are using them in test projects.
- Weight and size requirements do exist, but special permits are available for oversized loads.

Table 2.1 List of Surveyed State DOTs

<b>State</b>	<b>Contact</b>	<b>Position</b>
AL	John (Buddy) Black	State Bridge Engineer
AR	Rick Ellis	Division Head – Bridge
FL	Thomas Andres	Assistant State Structures Design Engineer
GA	Clayton Bennett	GDOT State Bridge Engineer
KY	Kevin Sandefur	Bridge Design & Maintenance Branch Manager
LA	Paul Fossier Jr.(Fossier, 2014)	Bridge Design Engineer Administrator
MS	Scott Westerfield	Deputy Director of Structures
NC	Brian Hanks	Unspecified
SC	David Rister	Bridge Construction Engineer
TN	Wayne Seger	Director of Structures Division
VA	Kendal Walus	State Structure and Bridge Engineer
WV	Ahmed Mongi	QA/QC Unit Leader, Engineering Division

Table 2.3 Summary of DOT Survey Results

State	Primary Existing Girder System	Preferred New Girder System	Typical Bridge Span (ft)	Typical Girder Spacing (ft)	Has State Utilized UHPC, HSS, or FRP	Has State Utilized ABC	Has State Used Prefabricated Deck Panels	Maximum Shipping Weight without Permit (lb)	Maximum Shipping Dimensions without Permit (ft)
AL	Unspecified	Pretensioned concrete	34-140	7-8	No	No	No. Currently do not allow prefabricated decks only stay-in-place forms.	80,000	13.5 Height 8.5 Wide
AR	Steel Girder	Pretensioned concrete	45-90	7.5-9.5	No	No. But are considering its use	No	80,000	13.5 Height 8.5 Wide
FL	Pretensioned concrete	Pretensioned concrete	<300	<12	FRP in test projects	Yes	Yes, full-depth panels have been utilized	80,000	13.5 Height 8.5 Wide
GA	Steel Girder/ Pretensioned concrete	Pretensioned concrete	30-150	5-10	No	Precast Decks	Yes	80,000	13.5 Height 8.5 Wide 100 Long
KY	Unspecified	Pretensioned concrete	75-100	8	Experimented with FRP	Yes	Yes	80,000	13.5 Height 8.5 Wide
LA	Unspecified	Unspecified	20-130	4-11	No	Yes	Full-depth concrete decks in pilot projects	88,000	Unspecified
MS	Pretensioned concrete	Pretensioned concrete	40-125	7-8.5	No	Limited. Voided slab bridge spans and emergency repair	No	80,000	13.5 Height 8.5 Wide
NC	Steel	Unspecified	40-140	1-12	HSS used in flanges at interior bent	Yes. Sub- and super-structure	Unspecified	80,000	Unspecified

					locations for continuous girders	elements			
SC	Steel Girder	Pretensioned Concrete	40-180	6-10	No	Precast slabs, caps, and slide-in-place elements	Very Limited	Unspecified	Unspecified
TN	Pretensioned concrete	Unspecified	<100	7-10	No	Yes	Yes Full depth pretensioned precast deck panels	80,000	13.5 Tall 8.5 Wide 65 Long
VA	Steel	Unspecified	60-80	6-12	UHPC: joint elimination FRP: joint elimination and bridge decks HSS: reinforcement	Yes	Yes	80,000	13.5 Tall 8.5 Wide 53 Long
WV	Steel/ Pretensioned Girders	Pretensioned Concrete	20-200	6-13	FRP reinforcement and FRP deck panels; UHPC and HSS in bridge deck	Yes. Prefab. bridge deck elements, lateral slide, and geosynthetic refor.	Yes	110,000	14 Wide 97 Long

## 2.4 Synthesis of National Bridge Inventory Data

The National Bridge Inventory (NBI) collects and records data for the U.S. bridge system. Table 2.4 shows percentages of structurally deficient (SD) or functionally obsolete (FO) bridges (and the total deficient bridges) for each state. AASHTO Region 2 states are highlighted in yellow.

Table 2.4 NBI List of Structurally Deficient and Functionally Obsolete Bridges by State

State	# Bridges	# SD	% SD	# FO	% FO	# Def	% Def
AL	16,078	1,405	8.7%	2,203	13.7%	3,608	22.4%
AK	1,196	133	11.1%	157	13.1%	290	24.2%
AZ	7,862	238	3.0%	716	9.1%	954	12.1%
AR	12,748	880	6.9%	2,014	15.8%	2,894	22.7%
CA	24,955	2,769	11.1%	4,184	16.8%	6,953	27.9%
CO	8,612	536	6.2%	902	10.5%	1,438	16.7%
CT	4,218	413	9.8%	1,059	25.1%	1,472	34.9%
DE	864	56	6.5%	121	14.0%	177	20.5%
DC	252	21	8.3%	159	63.1%	180	71.4%
FL	12,070	259	2.1%	1,785	14.8%	2,044	16.9%
GA	14,769	835	5.7%	1,765	12.0%	2,600	17.6%
HI	1,125	144	12.8%	350	31.1%	494	43.9%
ID	4,232	406	9.6%	453	10.7%	859	20.3%
IL	26,621	2,275	8.5%	1,971	7.4%	4,246	15.9%
IN	18,953	1,944	10.3%	2,224	11.7%	4,168	22.0%
IA	24,398	5,043	20.7%	1,228	5.0%	6,271	25.7%
KS	25,171	2,554	10.1%	1,911	7.6%	4,465	17.7%
KY	14,116	1,234	8.7%	3,202	22.7%	4,436	31.4%
LA	13,050	1,827	14.0%	1,963	15.0%	3,790	29.0%
ME	2,402	366	15.2%	425	17.7%	791	32.9%
MD	5,291	333	6.3%	1,085	20.5%	1,418	26.8%
MA	5,136	487	9.5%	2,207	43.0%	2,694	52.5%
MI	11,022	1,298	11.8%	1,720	15.6%	3,018	27.4%
MN	13,137	1,086	8.3%	427	3.3%	1,513	11.5%
MS	17,044	2,274	13.3%	1,362	8.0%	3,636	21.3%
MO	24,350	3,357	13.8%	3,276	13.5%	6,633	27.2%
MT	5,126	376	7.3%	506	9.9%	882	17.2%
NE	15,370	2,739	17.8%	1,026	6.7%	3,765	24.5%
NV	1,853	36	1.9%	217	11.7%	253	13.7%
NH	2,438	355	14.6%	435	17.8%	790	32.4%
NJ	6,566	624	9.5%	1,710	26.0%	2,334	35.5%
NM	3,935	298	7.6%	356	9.0%	654	16.6%
NY	17,442	2,078	11.9%	4,697	26.9%	6,775	38.8%
NC	18,168	2,308	12.7%	3,226	17.8%	5,534	30.5%
ND	4,439	726	16.4%	240	5.4%	966	21.8%
OH	27,015	2,242	8.3%	4,405	16.3%	6,647	24.6%
OK	22,912	4,227	18.4%	1,601	7.0%	5,828	25.4%
OR	7,656	431	5.6%	1,323	17.3%	1,754	22.9%
PA	22,660	5,218	23.0%	4,343	19.2%	9,561	42.2%
RI	766	167	21.8%	266	34.7%	433	56.5%

SC	9,275	1,048	11.3%	872	9.4%	1,920	20.7%
SD	5,875	1,210	20.6%	249	4.2%	1,459	24.8%
TN	20,058	1,157	5.8%	2,645	13.2%	3,802	19.0%
TX	52,561	1,283	2.4%	8,715	16.6%	9,998	19.0%
UT	2,974	117	3.9%	320	10.8%	437	14.7%
VT	2,731	251	9.2%	652	23.9%	903	33.1%
VA	13,765	1,186	8.6%	2,402	17.5%	3,588	26.1%
WA	7,902	372	4.7%	1,694	21.4%	2,066	26.1%
WV	7,125	944	13.2%	1,570	22.0%	2,514	35.3%
WI	14,088	1,198	8.5%	772	5.5%	1,970	14.0%
WY	3,099	443	14.3%	280	9.0%	723	23.3%
PR	2,280	315	13.8%	957	42.0%	1,272	55.8%
Sum	607,751	63,522	10.5%	84,348	13.9%	147,870	24.3%

While the above table shows the overall totals of deficient and obsolete bridges, more detailed information about the influence of bridge decks in this data was desired. Detailed data about all bridges in each state is placed in a code assembled by the National Bridge Inventory (NBI). Data was obtained on the number of structurally deficient bridges due to decks by state. The NBI classifies bridges deck condition based on a 0 to 10 rating with 0 being a failed condition and 10 being an excellent condition. Bridges with a condition rating of less than or equal to 4 are classified as structurally deficient. Table 2.5 was constructed based on this rating system.

Table 2.5 Deficient Bridge Decks in Region 2 by State from the NBI Data

State	Total Number of Bridges	Total Number of Deficient Bridges	Percent with Structurally Deficient Element	Number of Bridges with Structurally Deficient Decks	Percent of Structurally Deficient Bridges With Deficient Decks
AL	16,078	1,405	8.7%	247	17.6%
AR	12,748	880	6.9%	59	6.7%
FL	12,070	259	2.1%	40	15.4%
GA	14,769	835	5.7%	141	16.9%
KY	14,116	1,234	8.7%	409	33.1%
LA	13,050	1,827	14.0%	574	31.4%
MS	17,044	2,274	13.3%	433	19.0%
NC	18,168	2,308	12.7%	406	17.6%
SC	9,275	1,048	11.3%	186	17.7%
TN	20,058	1,157	5.8%	299	25.8%
VA	13,765	1,186	8.6%	299	25.2%
WV	7,125	944	13.2%	411	43.5%
Sum	168,266	15,357	9.1%	3,504	22.8%
Average	14,022	1,280	9.3%	292	22.5%
Std. Dev.	3,619	599	3.7%	164	9.9%

\*Data obtained from the 2013 National Bridge Inventory.

The following conclusions may be drawn from the above two tables:

- Of the more than 168,266 bridges listed in the NBI database for the 12 states in Region 2, a total of 15,357 or 9.1% are classified as structurally deficient.
- Of these, 3,504 or approximately 2% of the entire 168,266 bridge population in these 12 states have deficient bridge decks.
- Of the 15,357 bridges that are rated as structurally deficient, 3,504 or 22.8% have deficient bridge decks.
- On average, 22.5% of each state deficient bridges is due at least in part to deficient bridge decks.

This data indicates that deficient bridge decks are a substantial contributor to those bridges classified as structurally deficient. While about 9% of these states' bridge populations are rated as structurally deficient, about 22% of that 9% includes structurally deficient decks. It should also be noted that while 22% of these bridges have deficient decks, this does not mean that deficiency is exclusively related to the deck and there could be additional deficiencies in the substructure that are not accounted for in this data. It is concluded from this data that the development of a lightweight bridge deck is an important endeavor with potential to meet current bridge deck needs in the U.S.

## **2.5 Proposed Lightweight Bridge Deck Systems**

### **2.5.1 Advanced Materials for Bridge Decks**

#### **2.5.1.1 Ultra-High Performance Concrete (UHPC)**

Ultra-high performance concrete (UHPC) is a highly engineered material composed of portland cement, high water reducers, and fine aggregate made of sand, silica fume, crushed quartz, steel fibers, and super plasticizers (Aaleti, Petersen, & Sritharan, 2013). This material differs from conventional concrete and high performance concrete because it contains little or no coarse aggregate, a low water-cement ratio, and the addition of reinforcement fibers that give the concrete non-negligible tension capacity and the capability of resisting tensile forces after cracking. Ultra-high performance concrete is characterized with a compressive strength of 22 ksi or greater and a post-cracked tensile capacity of 0.72 ksi or greater (Garcia, 2007).

The inclusion of the steel reinforcing fibers may allow for the elimination of conventional mild steel reinforcement in some cases. A company called LaFarge North American produces a product called Ductal®, which is a form of UHPC with steel fibers that achieves compressive strengths between 24 and 30 ksi. As of 2010, Ductal® has been used for beams, girders, decks, piles, and joint fill for precast deck systems on bridges in France, Canada, the United States of America, Australia, New Zealand, Japan, and South-Korea (Ductal® Bridge Solutions: Gaining Acceptance in North America, 2010). During an interview for the Ductal® Solutions newsletter, Ben Graybeal discusses four obstacles the Federal Highway Administration has identified regarding widespread ultra-high performance concrete usage by state departments of transportation. These four obstacles are the high manufacturing costs associated with UHPC, the lack of design code provisions for the specific properties displayed by UHPC, the limited experience with inspections, maintenance, and repair of UHPC structures due to the current lack of aforementioned structures, and the higher cost of the materials needed to make UHPC increases the per-unit volume costs higher than normal strength concrete or high performance concrete materials costs (2010).

Although there are multiple reasons why bridge industry has not adopted UHPC as a regularly used material, there are also several advantages gained when using UHPC. The material contains super plasticizers which cause a “self-consolidating/self-leveling behavior”. This means that the concrete can be cast in plant or field conditions at a lower construction cost due to the lack of vibration needed to level the mixture (Aaleti, Petersen, & Sritharan, 2013). According to Aaleti et al., the high compressive strength of the material allows engineers to select smaller members for their designs, which decreases the dead load while improving efficiency and costs.

Ultra-high performance concrete may be substituted in any application where conventional or high performance concrete is used, but UHPC can also have special applications including overlays, claddings, and shells (Graybeal B. , 2011). Research by Noshiravani and Brühwiler found that by applying a thin two to four-inch overlay on a standard reinforced concrete beam, the stiffness and ultimate resistance were increased by up to 2.77 times that of a normal reinforced concrete beam (2013). UHPC can also be used as an overlay on bridge decks that serves to protect damaged or exposed elements, replace deteriorated reinforcing bars, and increase ultimate resistance of the bridge elements. This increased stiffness delays crack formation and, according to Habal et al, is the most efficient way to increase stiffness to a concrete element (2006). One of the most common uses for UHPC is as a grout in field-cast connections between bridge elements. Russel and Graybeal state that it can be used effectively as a shear connector in both longitudinal and transverse connecting joints (2013).

In their report, Aaleti, Petersen, and Sritharan created a list of design recommendations for ultra-high performance concrete based on material properties and testing. The recommendations span from determining the compressive strength based on the curing conditions to the Poisson’s ratio for ultra-high performance concrete. A selection of the recommendations are listed below:

- The conservative compressive strength of UHPC shall be taken as 24 ksi for steam-cured conditions and 18 ksi when air-cured for 28 days.
- For design purposes when test data is not available, the maximum compressive strain shall not exceed 0.0032, shown in Figure 2.20b.
- The stress-strain behavior of ultra-high performance concrete in tension shall be assumed as a bilinear curve, shown in Figure 2.21b.
- The elastic modulus of UHPC can be calculated with the equation  $46,200\sqrt{f'_c}$  (psi) or assumed as 7,500 ksi if the exact concrete strength is not available.
- The unit weight of ultra-high performance concrete shall be taken as 157 lb/ft<sup>3</sup> for dead load estimations.
- The coefficient of thermal expansion should be taken as  $8.2 \times 10^{-6}/^{\circ}\text{F}$  when thermally treated.
- For precast concrete panels, the chloride penetration resistance (determines how rapidly the concrete degradation from chloride ions found in deicing agents will occur) can be assumed negligible.
- The minimum concrete cover for unprotected mild reinforcement in ultra-high performance concrete shall be 0.75 inches.

- Although the current AASHTO requirements state that decks exposed to tire studs of chain wear need increased cover, there is no need to increase the cover for decks using UHPC because the abrasion resistance of the material is significantly higher than that of normal strength concrete.
- The Poisson's ratio for ultra-high performance concrete shall be taken as 0.20.

These recommendations could be used as a foundation for future design code provisions for ultra-high performance concrete, which was one of the obstacles facing the usage of UHPC by the Departments of Transportation.

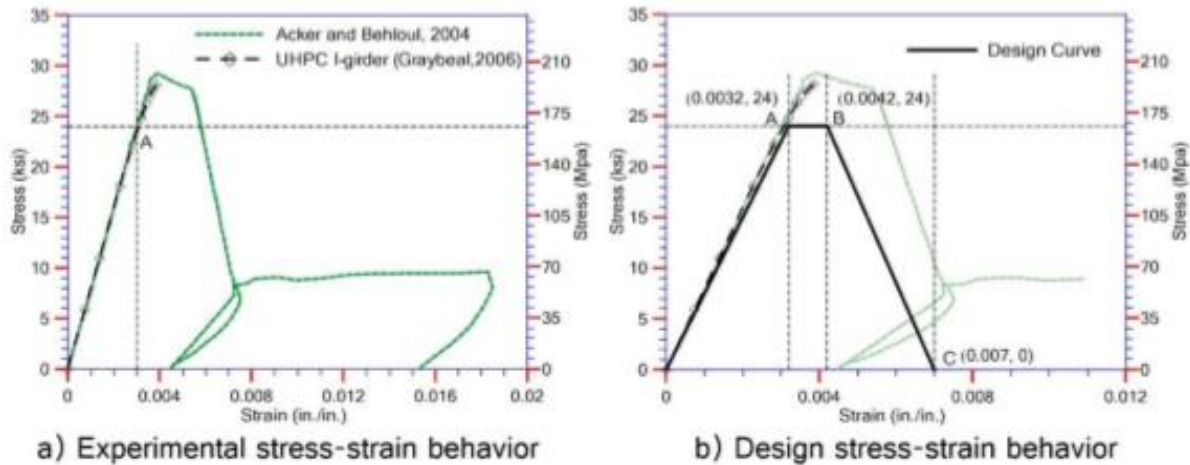


Figure 2.20 Measured and Recommended Design Stress-Strain of UHPC in Compression

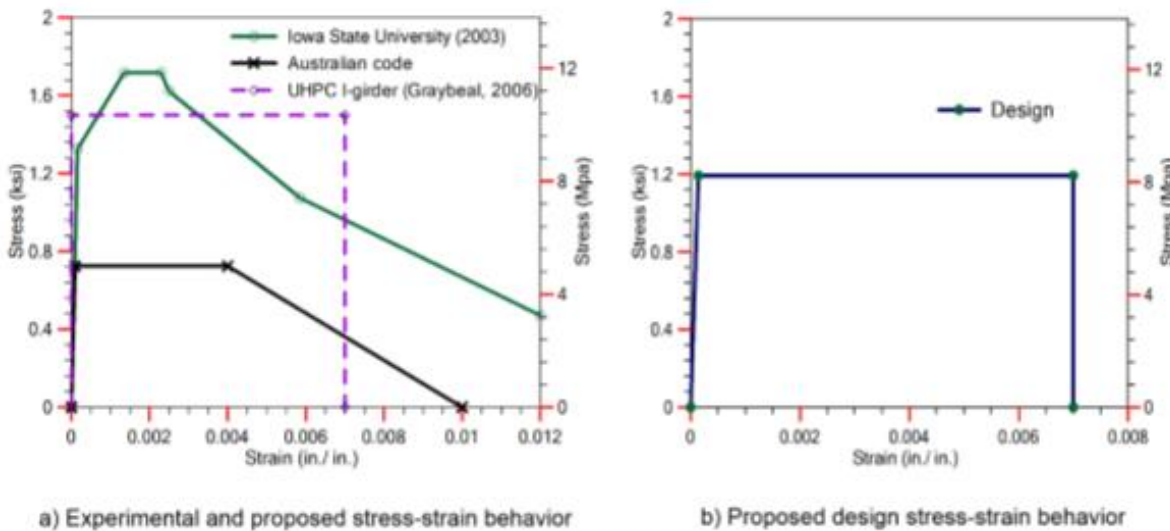


Figure 2.21 Measured and Recommended Design Stress-Strain of UHPC in Tension

### 2.5.1.2 Fiber Reinforced Polymer (FRP)

Fiber-reinforced polymer (FRP) is a composite material characterized as a combination of a polymer (plastic) matrix, reinforcing material, fillers, additives, and core materials (Sahirman, Creese, & Setyawati, 2003). Sahirman et al. elaborates on the polymer matrix stating that it can

be either a thermoplastic or a thermoset resin, such as polyester, vinyl ester, or epoxy and the reinforcing material is typically made of glass, carbon, or any other material that creates a sufficient length to thickness ratio (2003). FRP has desirable characteristics including a very low weight, an excellent strength to weight ratio, a tolerance for exposure to severe environments, a high tensile strength, and a high resistance to fatigue. Use of FRP can help reduce project delivery time due to the ease of manufacturing, handling, and construction of this material (Sahirman, Creese, & Setyawati, 2003). Despite these benefits, FRP is rather expensive and is a material with which many bridge designers are unfamiliar because of no standardized specifications for its use. Additional challenges to FRP in bridge applications include no guardrail specifications, inadequate durability of the wearing surface, and challenges in connecting FRP components together and to other bridge components (Mertz, et al., 2003).

Despite some concerns, FRP can be utilized in various bridge elements including beams, stringers, and full-depth deck panels. Many states have had success with implementing FRP components in bridge systems (Culmo, Connecticut Details for Prefabricated Bridge Elements and Systems, 2009). The first highway bridge containing composite reinforcement was built in Germany in 1986. The first FRP reinforced concrete bridge deck in the United States was built in 1996 in McKinleyville, West Virginia due to a need for high corrosion resistance and a long lifespan for the bridge (Sahirman, Creese, & Setyawati, 2003). As of February 2010, almost 100 bridges in the United States and more than 200 worldwide have been rehabilitated using composites (Reeve, 2010). FRP is receiving more recognition for its usefulness in replacement projects. The article written by Scott Reeve entitled “FRP Bridge Decking – 14 Years and Counting” provides details about the different advantages of FRP, which could help owners decide where fiber reinforced polymer materials would be best suited to bring the most value.

The first advantage discussed is the lightweight nature of fiber reinforced polymer. Reeve states that FRP bridge decks tend to weigh only 10-20% as much as a structurally equivalent reinforced concrete deck (2010). This weight reduction results in lowered dead loads, which can help reduce the load rating of structures and keep ageing structures in service longer (Reeve, 2010). Reeve notes that the lower dead loads can also mean cost savings in new construction due to smaller structural members and foundations (2010). The lighter weight also means that less expensive construction equipment can be used to move the panels into place. Backhoes and excavators that are already onsite are typically sufficient, therefore cranes are not required. This reduces installation costs and can avoid complications with overhead power lines that limit crane usage (Reeve, 2010).

The second advantage discussed is fiber reinforced polymer’s resistance to corrosion from de-icing salts. This is a very large problem for steel reinforced concrete structures, where the steel corrodes and leads to a premature deterioration of the concrete (Reeve, 2010). He states that durability tests have been performed on FRP materials in corrosive chemical environments and that the FRP materials have survived for 50 years without degradation. This lends support to the theory that FRP decks can have an expected lifespan of 75-100 years (Reeve, 2010). Reeves also highlights the advantages of quick installation time, high strength, and lower life cycle costs (2010).

There is a significant potential for fiber reinforced polymer as a replacement for steel reinforced concrete in bridge decks, but the initial FRP costs must be lowered to become competitive with the cost of steel reinforced concrete decks before this can happen. It is important to note that the increased material cost is not the only factor causing FRP to not be competitive with conventional reinforced concrete; fiber reinforced polymer deck systems require intense design changes to ensure that the decks meet specifications (Sahirman, Creese, & Setyawati, 2003). Although FRP has higher initial costs, its long lifespan and low maintenance requirements suggest that it will have a lower life cycle cost than steel reinforced concrete, even offsetting its own initial cost (Reeve, 2010). However, the fiber reinforced polymer bridge decks have not been in service long enough to determine the full cost-savings benefits.

### **2.5.1.3 High-Strength Steel (HSS)**

High strength steels (HSS) are designed to provide better mechanical properties and higher resistance to corrosion than conventional carbon steels (High-Strength Low-Alloy Steels, 2001). ASTM A1035 reinforcing bars are low carbon, low chromium steel bars characterized by high tensile strength and a stress-strain relationship having no yield plateau (Shahrooz, Miller, Harries, & Russell, 2011). According to Shahrooz et al., these bars are reported to have excellent corrosion resistance compared to standard steel and designers have specified that A1035 reinforcing bars are acceptable as a one-to-one replacement for conventional reinforcing steel as an alternative to expensive stainless steel or epoxy-coated bars (2011). Although the A1035 reinforcing bars have very high yield strengths, the American Concrete Institute regulates that yield strength for steel reinforcement may not exceed 80 ksi (Shahrooz, Miller, Harries, & Russell, 2011). A1035 steel may be used as a reinforcing material, but its full yield strength cannot be utilized by the design. Shahrooz et al. reported the mechanical properties of the A1035 steel which include:

- The average ultimate strength was 163 ksi
- The average rupture strain exceeded 0.10
- The average yield strength was 129 ksi
- Yield and ultimate strength values remained mostly unaffected by bar size
- The condition  $f_u > 1.25f_y$  remained true for all test cases
- Calculated values for the modulus of elasticity averaged 28,137 ksi
- All bars tested demonstrated linear behavior through stress levels of at least 70 ksi (2011)

The purpose of the research performed by Shahrooz et al. was to determine recommended changes to the existing AASHTO *LRFD Bridge Design Specifications* as they pertain to A1035 reinforcing steel and other high strength steels with no yield plateau (Shahrooz, Miller, Harries, & Russell, 2011).

As of 2011, MMFX Inc. is the only supplier of A1035 reinforcing steel in the United States (Shahrooz, Miller, Harries, & Russell, 2011). MMFX Steel® has the potential to resist corrosion while maintaining an efficient initial cost (Kahl S. , 2007). According to Kahl, the mechanical, chemical, and corrosion properties of MMFX were investigated and the results show that this specialty type of steel can have yield strengths up to 140 ksi, tensile strengths up to 160 ksi, and maintain a long service life (2007). These qualities make MMFX Steel® very advantageous for

bridge deck applications, especially where corrosion is a concern. However, a very careful design must be developed to insure ductile behavior in elements because of the increased yield strength (Kahl S. , 2007). Currently MMFX Technologies manufactures a 100 and 120 ksi steel rebar for use in virtually any application where traditional reinforcement would be used. MMFX has received building standards and approvals from the American Society of Testing Materials (ASTM), the Federal Highway Administration (FHWA), the American Concrete Institute (ACI), the American Association of State Highway and Transportation Officials (AASHTO), 26 State Departments of Transportation across the United States, and the International Commercial Code – Evaluation Service (ICC-ES) (MMFX Technologies Corporation, 2014).

### **2.5.2 UHPC Waffle Deck**

The first two deck systems studied in this project are ultra-high performance concrete waffle decks with either carbon fiber reinforced polymer rods or high strength steel bars acting as reinforcement. There are currently UHPC waffle bridge decks in use around the United States, but it is not a common deck system. The Federal Highway Administration’s Highways for LIFE program funded an innovative project that developed a full-depth precast, UHPC waffle deck panel and its connections. The deck was constructed as a replacement for an existing bridge in Wapello County, Iowa. According to the design guide for this bridge system, a UHPC waffle deck system consists of precast UHPC waffle panels with shear pockets, transverse panel-to-panel connections, longitudinal panel-to-girder connections, some type of overlay to improve rideability if desired, and in situ UHPC material to fill the connections and shear pockets (Aaleti, Petersen, & Sritharan, 2013). This configuration is shown in Figure 2.21. According to Aaleti, et al., the longitudinal ribs help distribute the wheel load to the adjacent panels and the reinforcement needed to support the wheel loads is provided in both directions with the longitudinal and transverse ribs (2013). There are multiple advantages associated with using ultra-high performance concrete waffle deck panels. For decks with the same thickness, UHPC waffle slabs have the same or higher capacity and are 30 to 40 percent lighter than solid precast full-depth panels made of normal strength concrete (Aaleti, Petersen, & Sritharan, 2013). The author states that the lower weight of the UHPC panels can increase the span length, increase the girder spacing, improve bridge ratings when used for replacement projects, and reduce seismic, substructure and foundation loads compared to decks constructed using solid precast panels (2013).

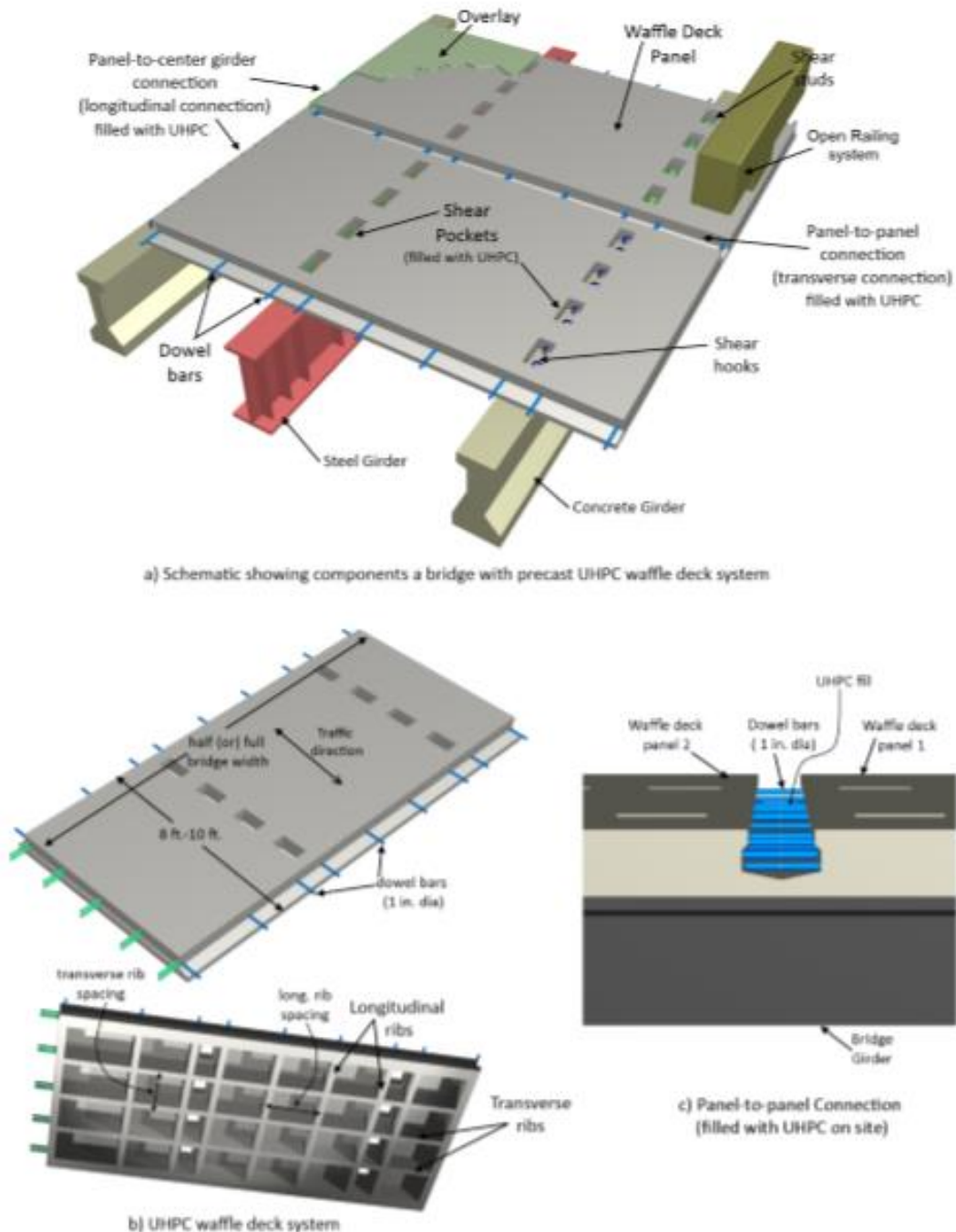


Figure 2.22 FHWA's UHPC Waffle Deck System

Aaleti et al. created a set of design specifications for UHPC waffle deck systems based on test results and research. They surveyed the Departments of Transportation for Alabama, Florida, Georgia, Illinois, Indiana, Iowa, Kentucky, Nebraska, New Jersey, New York, Ohio, Oklahoma, Virginia and Wisconsin to determine typical bridge deck dimensions. According to the survey, the typical spacing for precast pre-stressed girders varied between 6 and 12 feet, with the most common spacing at 8 feet. Based on this survey information, the authors limited the maximum girder spacing in their design guidelines to 10 feet so that the waffle deck panels are optimized

for common bridge designs. The top flange width of the girders determines the spacing between the support ribs and the location of the maximum negative bending moment in the panel. DOT surveys were again utilized and a conservative top flange width was assumed at 12 inches (Aaleti, Petersen, & Sritharan, 2013). Aaleti et al.'s report describes the reasoning and methodology behind their decisions for all of the dimensions and spacing. The dimensions from their design guide are listed below.

- Maximum girder spacing = 10 feet
- Girder top flange width = 12 inches
- Deck panel thickness = 8 inches
- Flat plate thickness (connects the ribs at the top of the bridge surface) = 2.5 inches
- Transverse and longitudinal rib width = 3 inches at the bottom and 4 inches at the top
- Maximum allowable rib spacing = 36 inches
- Shear pocket spacing and dimensions are dependent upon arrangement and spacing of the shear connectors. A minimum opening of 4 inches by 8 inches is recommended to accommodate easy pouring of UHPC to fill in around connections.

For the Wapello County bridge replacement project, much of the design criteria emanated from AASHTO LRFD bridge design specifications. Minimal longitudinal and transverse reinforcement was used in each deck, and no shear reinforcement was used in the decks. Size constraints, for transportation purposes, were specified to be no greater 25 feet long and 8 feet wide.

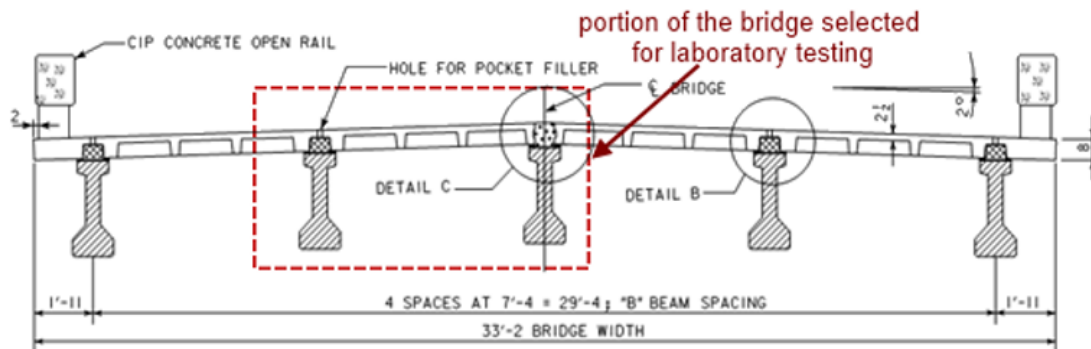


Figure 2.23 Details of the Replacement Bridge with a UHPC Waffle Deck System

Three types of connections were used for the waffle deck: shear pocket connections, longitudinal connections, and transverse connections (Aaleti, Petersen, & Sritharan, 2013). The shear pocket connection, shown in Figure 2.24, is formed between the girder and the waffle deck. The shear pockets in the waffle deck are filled with UHPC and have a shear hook that extends from the girder into the pocket (The Implementation of Full Depth UHPC Waffle Bridge Deck Panel, 2015).

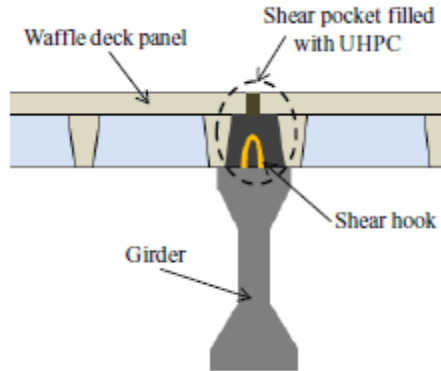


Figure 2.24 Shear Pocket Connection

The longitudinal connection, shown in Figure 2.25, is formed between the central girder and the waffle deck. The dowel bars from the panels and the shear hook are tied together with additional reinforcement along the girder length and the gap between the panels is filled with UHPC (The Implementation of Full Depth UHPC Waffle Bridge Deck Panel, 2015).

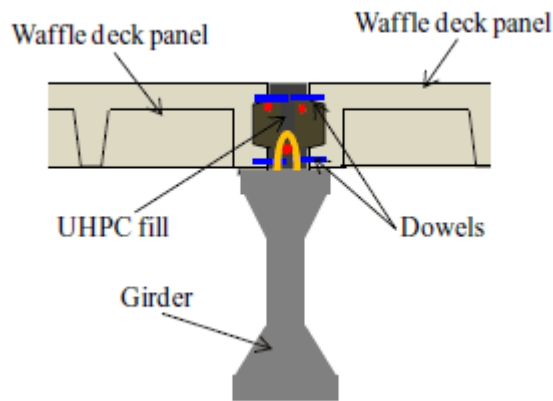


Figure 2.25 Longitudinal Connection

The transverse connection, shown in Figure 2.26, is formed between the waffle deck panels. The dowel bars from the panels are tied together with additional transverse reinforcement and the gap between the panels is filled with ultra-high performance concrete (The Implementation of Full Depth UHPC Waffle Bridge Deck Panel, 2015).

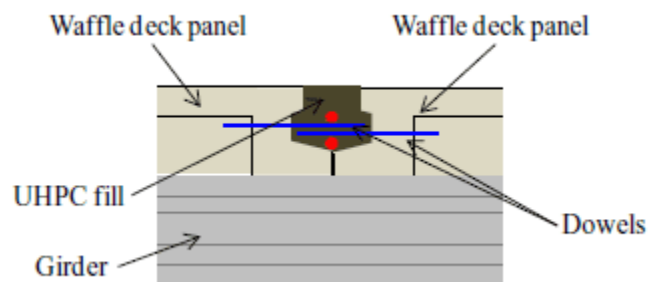


Figure 2.26 Transverse Connection

Before the UHPC waffle deck was constructed in the field, testing was performed at Iowa State University. The purpose of the testing was to examine the overall performance of the waffle deck under loads similar to what would be experienced in the field, including structural performance and the performance of critical connections. The six tests performed were a panel service test, a joint service test, a joint fatigue test, a joint ultimate test, a panel fatigue test, and a panel ultimate test (The Implementation of Full Depth UHPC Waffle Bridge Deck Panel, 2015). The results of these tests showed that the UHPC waffle deck bridge system met or exceeded all of the AASHTO requirements. Based on the study, it was determined that the proposed waffle deck could be constructed in Wapello County as long as the connection reinforcement was the same or better than those provided during the test and the moment demands on the slab were kept below those that occurred during the testing (The Implementation of Full Depth UHPC Waffle Bridge Deck Panel, 2015). The Wapello County bridge was constructed in 2011 and field tested in 2012. Although the maximum strain measured in the waffle panel adjacent to the abutment was slightly more than the cracking strain of UHPC, the maximum strain at midspan showed that the deck was behaving elastically with respect to the applied loads from traffic and the maximum deck deflection was well below the allowable AASHTO deflection requirements, meaning that the bridge system was performing as expected (Aaleti, Petersen, & Sritharan, 2013).

#### **2.5.2.1 FRP Reinforcement**

The Wapello County UHPC waffle deck system used steel for the reinforcing material. Although conventional steel is the most prevalent source of reinforcement, it has a tendency to corrode in certain environments. An alternative reinforcement material is fiber reinforced polymer (FRP) or glass fiber reinforced polymer (GFRP). This material has been successfully utilized as a reinforcement member in a Utah bridge and has seen very good performance that is comparable to a steel reinforced deck (Holden, Pantelides, & Reaveley, 2014). FRP has many advantages as a structural material for bridge decks including its resistance to corrosion, excellent strength-to-weight ratio which lends itself to a lightweight deck application, high tensile strength, high fatigue resistance, and low susceptibility to chloride corrosion (Sahirman, Creese, & Setyawati, 2003). Other advantages include environmental durability, speed of installation, and the potential for an increased load rating for bridges due to the reduced dead load (Liu, Sotelino, Rodriguez-Vera, Lombardi, & Machado, 2011). However, similar to ultra-high performance concrete, fiber reinforced polymer is not a widely used material for bridge deck construction. Sahirman, Creese, and Setyawati believe that this is likely caused by a lack of design standards and experience, as well as the high initial costs associated with the material (2003). Another issue is that there is not a great deal of research pertaining to precast concrete bridge decks with FRP reinforcement, so there is no long-term data for creep, fatigue, and long-term loading effects (Holden, Pantelides, & Reaveley, 2014).

Some research has been performed on fiber reinforced polymer – reinforced concrete bridge systems. One case is the Beaver Creek Bridge on U.S. Route 6 in Utah. The bridge deck was designed based on specifications from the American Concrete Institute (ACI) and the controlling factor for the design was limiting the crack width and deflection. According to Pantelides et al., the low modulus of elasticity for GFRP can lead to wider crack widths than traditional steel reinforcement (2012). Though the allowable crack width regulations are not required to be as strict with GFRP because of its resistance to corrosion, wider cracks can lead to a reduction in

shear capacity. Pantelides et al. state that in order to overcome the material limitations, several design adjustments were made, such as reducing the bar spacing in the transverse direction from 8 inches to 4 inches (2012). The deck thickness was also increased from 8.75 inches to 9.25 inches and the girder spacing was decreased from 9 feet-4 inches to 7 feet-7 inches (Pantelides, Holden, & Ries, 2012). The Beaver Creek Bridge was used as a test subject for health monitoring precast concrete bridges with glass fiber reinforced polymer reinforcing bars. The panels were monitored through the construction process and for another two years after construction completion. According to Pantelides et al., some of the results of the monitoring conclude that

- The maximum tensile strain in the GFRP was equal to 0.8% of the ultimate strain, which is consistent with strain values reported in other similar bridge deck systems.
- Post-tensioning added to the continuity of the bridge deck and much of the shear load was able to transfer to adjacent panels due to the increased shear transfer of the grouted shear pockets.
- During static load tests, the deflection was found to be 0.007 inches, 93% smaller than the design deflection of 0.101 inches. However, the test loads were only 40% of the design loads and the deflections were 7% of the AASHTO limit. When monitored during traffic, relative deflections were observed up to 0.15 inches.
- Live load deflections of the pre-stressed girders were found to be significantly smaller than AASHTO allowable deflection specifications.
- The adjustments made to the bridge deck design to replace the steel reinforcement with GFRP bars were successful in preventing the deck from cracking or experiencing large service deflections.

It was assumed that replacing the steel reinforcement with glass fiber reinforced polymer bars would significantly increase the lifespan of the bridge deck. A cost analysis was performed based on this assumption. The initial cost comparison showed that the glass fiber reinforced polymer deck cost 35% more initially than the steel reinforced deck. However, the design life for the steel reinforced concrete bridge was 45 years and the design life for the GFRP reinforced deck is 100 years based on studies investigating the durability of GFRP bars. The extended lifespan of the GFRP reinforced deck allows it to be more competitive with the conventional steel reinforced deck, which would need at least one replacement to reach an age of 100 years (Pantelides, Holden, & Ries, 2012).

#### **2.5.2.2 HSS Reinforcement**

Another alternative to conventional steel reinforcement is high strength steel (HSS). Several states have already tested bridge deck systems using high strength steel reinforcement bars. High strength steel is given the American Society of Testing Materials (ASTM) designation A1035, also known as MMFX after the company that manufactures the rebar, MMFX Technologies Corporation. The first state Department of Transportation to use MMFX was Iowa on the eastbound IA 520 bridge over South Beaver Creek. Iowa's DOT wanted to test the corrosion resistance of the MMFX against epoxy-coated rebar in the westbound deck. The initial corrosion readings showed the epoxy-coated deck had approximately six times as much corrosion current as the MMFX deck, but the corrosion currents stabilized as the concrete cured (Kahl S. , 2007). The Iowa DOT used accelerated laboratory testing to speed up the corrosion process and after 40

weeks of intense corrosion exposure, neither the MMFX reinforcement nor the undamaged epoxy coated reinforcement showed any signs of corrosion. It was determined that 40 weeks was not a long enough period of time to predict the life expectancy of the materials without further testing (Kahl S. , 2007).

The Florida Department of Transportation performed flexural testing on concrete panels with #6 MMFX rebar and Grade 60 reinforcement. The testing determined that the ductile behavior of the two materials is identical until the Grade 60 reinforcement fails (Kahl S. , 2007). However the two materials respond differently in terms of lapping. According to Kahl, lap splices that are adequate for yielding Grade 60 reinforcement will not yield MMFX reinforcement (2007).

The Virginia Transportation Research Council compared the chloride corrosion resistance of MMFX to stainless and uncoated reinforcement. The results showed that the MMFX corroded after 244 to 247 days compared to the uncoated bars that corroded after 90 to 95 days (Kahl S. , 2007). The report continues to state that the corrosion rate of the MMFX was still much less than that of the uncoated bars and that MMFX or stainless steel reinforcing bars should be used for urban and heavily traveled bridges (Kahl S. , 2007).

The Utah Department of Transportation wanted to gain experience with MMFX for a bridge that was in-service. UDOT replaced the conventional rebar in the US-6/White River Bridge with MMFX (Barr & Wixom, 2009). According to Barr and Wixom, the members of the construction crew were interviewed about their experience installing the MMFX. They stated that not only was there no additional labor associated with the placement of the MMFX compared to epoxy coated reinforcement, it was actually a safer material to use because it was not slippery, even when wet from rain (2009). UDOT's conclusions after completion of the projects are:

- The research that has been conducted on the corrosive properties of MMFX so far have shown that MMFX demonstrates approximately four times more corrosion resistance than mild steel reinforcement.
- MMFX has been found to corrode at a much lower rate than mild reinforcement, though some studies have shown that the rate of corrosion increases over time.
- Most of the stainless steel specimens tested performed better than the MMFX, but stainless steel is much more expensive.
- Not enough long-term tests have been performed to accurately determine the life-cycle costs of MMFX (Barr & Wixom, 2009).

Based on these conclusions, UDOT made some recommendations for future MMFX usage in the state, including that MMFX should be considered for critical concrete bridge decks that will be exposed to large amounts of traffic and salting, that UDOT should continue to monitor the corrosion potential of the White River Bridge, and that UDOT should not use different types of steel for the top and bottom mats until more research is performed to ensure that cracking does not occur (Barr & Wixom, 2009).

A laboratory study was performed at North Carolina State University to evaluate the behavior of a standard concrete bridge slab reinforced with MMFX. Three full-scale bridge decks with a span-to-depth ratio of 12.5 were tested to determine the structural performance of MMFX

compared to Grade 60 steel reinforcement (Seliem, Lucifer, Rizkalla, & Zia, 2006). The three bridge decks were identical except for the type of reinforcement used. The first two decks used the same reinforcement ratio, but one was reinforced with MMFX and the other with Grade 60 steel; the third deck was reinforced with MMFX but the reinforcement ratio was only two-thirds of the ratio in the first two decks (Seliem, Lucifer, Rizkalla, & Zia, 2006). Seliem et al. listed the conclusions of the study in their report entitled *Behavior of Bridge Decks Reinforced with MMFX Steel*. Seliem et al.'s conclusions are:

- The ultimate load carrying capacity for the three bridge decks tested was 8-10 times the service load required by the 1998 AASHTO Design Specifications.
- The primary failure mode in all three bridges was punching shear.
- Punching failure resulted in a sudden decrease of the load carrying capacity.
- Flexural failure led to a much more gradual decrease of load carrying capacity.
- The MMFX bridge deck that had the same reinforcement ratio as the Grade 60 deck exhibited the same deflection as the Grade 60 deck. However, the MMFX bridge deck had a higher load carrying capacity than the Grade 60 bridge deck.
- The MMFX bridge deck that had a reinforcement ratio two-thirds as high as the other bridge decks developed the same ultimate load carrying capacity and deflection as the Grade 60 deck, as expected of the higher strength of MMFX.
- Bent MMFX bars behave similar to straight bars. However, bending the bars severely impacts the ductility and reduces the ultimate strength by 6% and the ultimate strain by 70% (Seliem, Lucifer, Rizkalla, & Zia, 2006).

The overall conclusions drawn about this material is that although expensive, it has excellent corrosion resistive properties and a higher strength capacity than Grade 60 steel. There have not been enough long-term studies to determine how the corrosion resistance will hold up over time, but the manufacturer claims that the MMFX steel rebar has a 100-year service life. Although this material is no more difficult to install than traditional reinforcing bars, MMFX steel is best suited for heavily traveled, urban roadways where a large amount of de-icing agents are used.

### **2.5.3 Hybrid Full-Depth UHPC-FRP Deck System**

The third deck systems studied in this project is a hybrid full-depth ultra-high performance concrete – fiber reinforced polymer deck system, which is similar to available lightweight fiber reinforced polymer sandwich decks with embedded structural foam cores. The hybrid system consists of fiber reinforced polymer shear and tension reinforcement, an ultra-high performance concrete compression top flange, and a polyurethane foam core.

As previously stated, fiber reinforced polymer has multiple advantageous properties that make it a promising material for bridge deck systems. Several all-FRP bridge decks were constructed and studied in the United States (Keller, Schaumann, & Vallée, 2006). According to Keller et al., the decks were shown to increase the allowable live loads and construction details could be simplified compared to reinforced concrete decks (2006). These decks were mostly pultruded, which is a manufacturing process for producing continuous lengths of reinforced polymer structural elements with constant cross-sections (The Pultrusion Process, 2015). The process involves pulling the raw materials through a heated steel forming die using a continuous pulling device (The Pultrusion Process, 2015). Various concerns have been noted with existing FRP

bridge decks including leakage of joints, delamination of the wearing surface and fiber reinforced polymer, inadequate stiffness, and a lack of methods for identifying damage in service (Liu, Sotelino, Rodriguez-Vera, Lombardi, & Machado, 2011). Other weaknesses include the limitation of the maximum transverse span between girders to 9.8 feet, or 3 meters, meaning that multi-girder systems are needed which is not cost efficient for longer spans, and low stiffness in the main girder direction when compared to reinforced concrete, which reduces the capacity of the deck (Keller, Schaumann, & Vallée, 2006). Keller et al. suggests that one way to overcome the material weaknesses is to use fiber reinforced polymer composites with traditional materials, such as concrete (2006).

Several countries have already researched this possibility. In China, the Miyun bridge was built in 1982 and was the first road traffic bridge constructed with a hybrid of FRP and concrete (Keller, Schaumann, & Vallée, 2006). The bridge is comprised of six honeycomb sandwich FRP box girders and a ~4 inch (10 centimeter) thick reinforced concrete slab. Keller et al. studied a hybrid bridge sandwich structure that was comprised of fiber reinforced polymer composites for the tension layer, lightweight concrete for the core material, and ultra-high performance concrete for the compression layer in their paper entitled “Flexural Behavior of a Hybrid FRP and Lightweight Concrete Sandwich Bridge Deck” (2006). The FRP layer in their proposed bridge deck consisted of a ~0.2 inch (5 millimeter) glass fiber reinforced polymer (GFRP) sheet with T-upstands that not only serve as the formwork but also provide the composite action between the GFRP sheet and the lightweight concrete layer. The thin ultra-high performance fiber reinforced concrete layer is poured on top of the lightweight concrete layer (Keller, Schaumann, & Vallée, 2006). To test the feasibility of this design, Keller et al. performed flexural experiments on eight hybrid beams with dimensions ~11.8 feet (3600 millimeters) x ~15.75 inches (400 millimeters) x ~7.87 inches (200 millimeters).

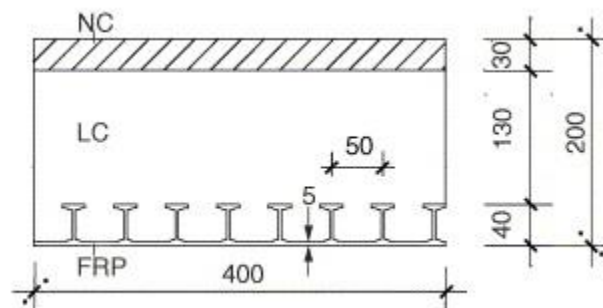


Figure 2.27 Cross-Section of Hybrid Beams Used in Experiments by Keller et al.

There were two parameters included in the tests: the fiber reinforced polymer/ lightweight concrete interface when unbonded and epoxy bonded and the type of lightweight concrete used, either low density or high density (Keller, Schaumann, & Vallée, 2006). The conclusions from Keller et al.’s experiment are as follows:

- Changing the interface of FRP and lightweight concrete from unbonded to epoxy bonded increased ultimate load by 104%, but also changed failure mode to brittle.

- Increasing the lightweight concrete's density by 44% also increased the ultimate load by 81% on average. The effects were much more noticeable for the unbonded beams than for the bonded beams.
- Manufacturing the beams was fast and simple. The beams were constructed without intermediate curing within 30 minutes, which makes the fabrication very economical from a time standpoint.
- Tests showed feasibility of the hybrid ultra-high performance fiber reinforced concrete bridge deck (Keller, Schaumann, & Vallée, 2006).

Other hybrid fiber reinforced polymer deck systems have been researched by various entities. For example, tests by Alagusundaramoorthy et al. compared four different FRP panels by the criteria of the Ohio Department of Transportation (ODOT). Four types of FRP panels were tested and compared to a baseline reinforced concrete panel. The reinforced concrete panel along with the four FRP decks is shown in Figure 2.28.

The first FRP deck panel tested was manufactured by Creative Pultrusions and consisted of double trapezoidal and hexagonal pultruded components bonded and interlocked to form the deck panel [See Figure 2.28b]. The second panel tested was concrete reinforced with glass fiber reinforced polymer reinforcement bars and cast over pultruded GFRP tubular sections [See Figure 2.28c]. The third panel tested consisted of cell foam wrapped with fiberglass fabric [See Figure 2.28d], manufactured using the process called the Seeman composite resin infusion molding process (SCRIMP), which is a resin transfer molding process that uses a vacuum to pull liquid resin into a dry lay-up and is used for making composite parts (An Overview of the SCRIMP Technology, 2001). Lastly, a hand layup FRP fiberglass deck panel was tested with a corrugated core sandwich system shown in Figure 2.28e. These panels were tested both as single and double spans.

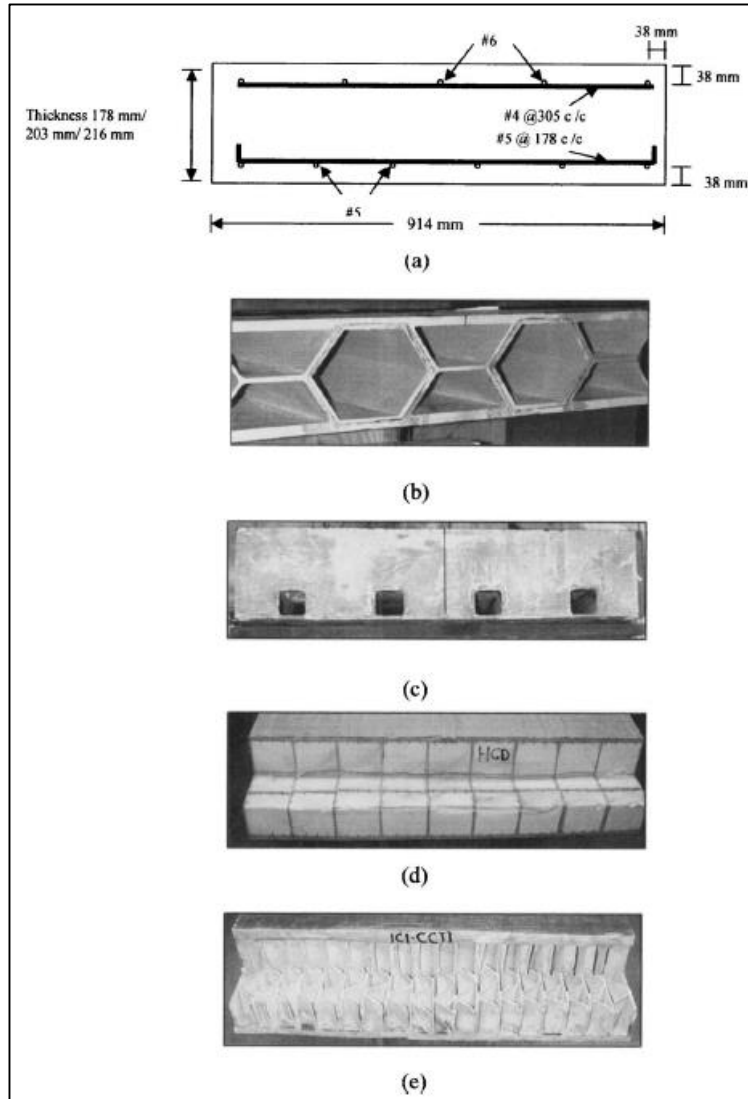


Figure 2.28 ODOT Sample Deck Tests: (a) Reinforced Concrete (b) Creative Pultrusions (c) Composite Deck Solutions (d) Hardcore Composites (e) Infrastructure Composites International

These panels were tested versus Ohio Department of Transportation (ODOT) flexural and shear capacity criteria which consisted of the following:

1. Flexural:

- Maximum allowable strain is limited to 20% of ultimate strain under live, impact, and dead service load.
- Maximum allowable dead load strain is 10% of ultimate strain.
- Maximum factored load (where a factored load =  $1.3 \cdot [1.67 \cdot (LL + IL) + DL]$ ) must be less than 50% of ultimate load capacity of FRP.
- Maximum factored load must be less than 100% for hybrid FRP/concrete deck panels.

2. Shear:

- Shear capacity must be equal or greater than corresponding reinforced conventional deck panel.
  - Maximum allowable shear at factored load must be less than 45% of the ultimate shear load for non-hybrid FRP decks.
  - Maximum allowable shear for a factored load cannot be less than 100% of the ultimate shear for hybrid FRP/concrete decks.
3. Deflection criteria based on ODOT standards for typical reinforced concrete:
- Maximum allowable deflection for single span decks vary from  $L/596$  to  $L/762$ .
  - Maximum allowable deflections for double span decks vary from  $L/851$  to  $L/1097$ .

Important conclusions from these tests applicable to this study include the following:

- All single and double span decks satisfy ODOT requirements for shear.
- Both the single and double span Pultruded decks satisfied ODOT flexural and deflection requirements.
- Both the single and double span FRP/concrete decks satisfied ODOT flexural and deflection requirements.
- Both the single and double span SCRIMP decks satisfied flexural requirements, but the single span exceeded deflection criteria.
- The hand layup decks satisfied flexural and deflection requirements but did not satisfy the ultimate load being less than 50% of ultimate load.
- While the safety factor against failure is 3 to 8 on these tests, ultimate failure of the specimens contained some degree of debonding of the deck and a sudden ultimate failure (Alagusundaramoorthy, Harik, & Choo, 2006).

Research on hybrid fiber reinforced polymer – concrete deck systems has been performed worldwide as a cost-effective solution to the high initial cost of fiber reinforced polymer bridge deck systems. Along with cost-effectiveness, the hybrid FRP-concrete bridge deck systems are intended to be durable and structurally sufficient due to the combination of the properties of both materials (Aref & Alnahhal, Hybrid FRP-Concrete Bridge Deck Systems Project No.: C-02-07, 2009). Much of the research has returned positive results, which confirms that the hybrid deck systems have a great potential for success in the field. Amjad Aref and Gordon Wren performed an investigation on the long term and ultimate behavior of a hybrid FRP-concrete system, which included creep and fatigue testing to understand the long term behavior of the composite system and destructive testing to understand the failure mode and capacity of the system (Aref & Wren, Hybrid FRP-Concrete Bridge Deck Systems Final Report II: Long Term Performance of Hybrid FRP-Concrete Bridge Deck System, 2009). The conclusions of the tests were that the hybrid composite deck system showed excellent long term structural performance, with the ultimate capacity of the hybrid FRP-concrete deck exceeding design expectations (Aref & Wren, Hybrid FRP-Concrete Bridge Deck Systems Final Report II: Long Term Performance of Hybrid FRP-Concrete Bridge Deck System, 2009).

## **2.6 Summary and Conclusions**

The purpose of this literature review is to provide information that will aid in the design, development, and implementation of a prefabricated bridge deck for use in accelerated bridge

construction. This literature review covers the current state of bridges in the United States and problems that the bridge decks are facing related to early-age cracking, accelerated bridge construction systems, technologies, and examples of bridges within the United States and internationally that were constructed using ABC methods, Department of Transportation surveys for AASHTO Region 2, a synthesis of data collected from the National Bridge Inventory on the number of structurally deficient and functionally obsolete bridges in the United States, and information about three high-performance materials and deck systems using those materials.

Accelerated bridge construction is a collection of techniques that are very useful when trying to avoid lengthy traffic disruptions. ABC primarily consists of prefabricated bridge elements that are built off-site or adjacent to the structure and then moved into place. This cuts down the time that construction crews are on the jobsite, which improves safety and efficiency. Concrete construction is no longer weather dependent because the concrete can be cast and cured in warehouses, which also allows for better quality control checks. The biggest factors working against the implementation of accelerated bridge construction nationwide are the higher initial costs and the risks associated with engineering each individual project. However, on high-profile projects where lengthy traffic delays would be detrimental, the time saved from using accelerated bridge construction methods will often offset the increased material and labor costs. A manual for accelerated bridge construction has been developed that standardizes design and construction practices for some bridge systems that should help eliminate the risk of custom engineering. Overall, accelerated bridge construction is an excellent tool that can lessen the impact of construction on the motoring public, create a safer environment for construction crews, and reduce the impact of weather on concrete construction.

The Departments of Transportation for AASHTO Region 2 (Alabama, Arkansas, Florida, Georgia, Kentucky, Louisiana, Mississippi, North Carolina, South Carolina, Tennessee, Virginia, and West Virginia) were surveyed to determine typical bridge geometries, girder systems, girder spacing, and whether or not the states had used high-performance materials, accelerated bridge construction, or prefabricated deck panels. The conclusions showed that many of the DOTs prefer pre-stressed girders. Although the use of high-performance materials like ultra-high performance concrete, high strength steel, and fiber reinforced polymer is limited, several states are implementing the materials both in test projects and construction projects in the field. Most of the states surveyed have some experience or plan to gain experience with accelerated bridge construction techniques including precast deck panels, emergency repairs, and lateral slide elements.

The National Bridge Inventory collects data for the United States bridge system, including the number of structurally deficient and functionally obsolete bridges. The Inventory shows that in AASHTO Region 2, 9.1% of the bridges are considered structurally deficient and a significant portion of the deficiencies are occurring in bridge decks.

Three systems are studied in this report: an ultra-high performance concrete waffle deck with fiber reinforced polymer reinforcing bars, an ultra-high performance concrete waffle deck with high strength steel reinforcing bars, and a hybrid full-depth ultra-high performance concrete deck system with FRP reinforcement. Literature was not available for systems identical to those studied in this report, so similar systems were reviewed. Based on the information gathered, all

three systems will have high initial costs, but those costs will be offset in certain situations. For example, high strength steel is an excellent reinforcing material for locations where de-icing agents are necessary in the winter or where salt is prevalent. However, southern states where winters are not as harsh and where salt deposits from the ocean are not an issue will not receive the full benefits from this material. Other factors will help offset costs, such as the ability to select smaller members because of the increased strength of all three materials compared to conventional construction materials.

Although the three high-performance materials studied in this report have high initial costs, they also have strong benefits. In the correct situation and as long as the design is able to meet the necessary specifications, any of these systems would perform well and give the owner a durable, high strength bridge system that should outlast conventional bridges.

# Chapter-3

---

## Hybrid UHPC-FRP Deck System

### 3.1 Introduction

Fiber reinforced polymer (FRP) composite materials have been under research for several decades and have shown great potential as alternative construction materials, especially in the field of repair and rehabilitation of existing bridges, and to some extent in new bridge construction. FRP composites applications in the bridge industry have been accelerated in recent decades because of their superior properties, such as high strength, long-term durability, fatigue resistance, and good corrosion resistance. Moreover, FRPs are a good choice for mass production of structural shapes because of their light weight, which allows rapid installation of FRP modular decks on bridges. The prefabricated FRP bridge deck weighs approximately 80% less than a concrete deck. The lightweight FRP deck could be especially beneficial for movable bridges, in which spans have to be lifted for the passage of vessels. In addition, a light structure is always convenient to transport and install, which enables shorter construction periods and lower construction costs.

A new lightweight hybrid UHPC-FRP deck system has been fabricated in the University of Central Florida structural lab by using vacuum-assisted resin transfer molding (VARTM) infusion and tested to examine its applicability in the new bridge construction field. This composite deck can work also as an integral wearing surface, so no additional layer is needed during the replacement or the construction. UHPC-FRP hybrid system tends to be a very good alternative due to its extremely light weight. The self-weight of the new UHPC-FRP composite has been found to be in the range of 12-14 psf comparing to the 20-25 psf for the 1T1S deck. It is known that UHPC has very high compression strength, while FRP has very high tension strength. Theoretically, therefore, a deck system with UHPC cast as the upper layer for compression resistance, CFRP distributed on the bottom layer for tension resistance, and GFRP as shear reinforcement, as shown in Figure 3.1, is optimal. In this chapter, the fabrication, testing and the results of this new hybrid system will be presented.

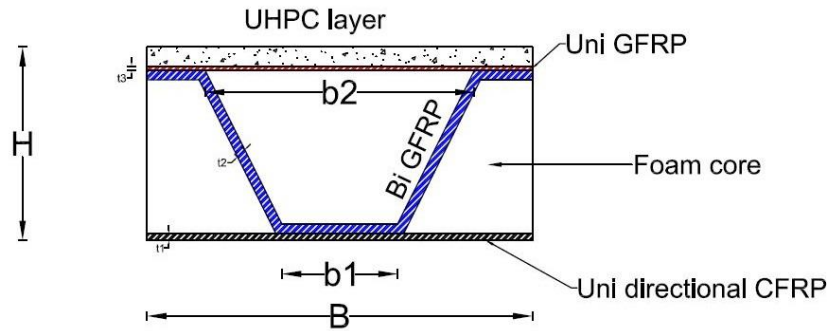


Figure 3.1 Details of the New Hybrid Deck

### 3.2 Literature Review

Previously, different FRP deck systems and their connections has been studied to characterize the static and dynamic performance. Connections of FRP decks were studied by Keller and Gurtler (2005), Righman et al. (2004), and Davalos et al. (2011). Material constituents and mechanical properties were investigated by Davalos et al. (2001) and Alagusundaramoorthy et al. (2006). Deflection and deformation, ultimate capacity, and failure mode were studied by Wu et al. (2003), Kumar et al. (2004), and Davalos and Chen (2005). Creep and fatigue in FRP decks were investigated by Scott et al. (1995), Cole et al. (2006), Alnahhal et al. (2006), and Wu et al. (2004).

Five different deck panels that made of FRP webbed cores was fabricated and evaluated by Robinson et al. (2008) and compared with an existing aluminum deck that previously tested as one option of the composite army bridge. Each deck has different core configuration and is composed of either glass/carbon web, and 3/8 in. carbon face sheet. Three of the five cores were fabricated using machine process while the other two were fabricated using hand wrapping. Their goal was to develop a system which its one bending shear strength is greater than 740 psi and the compressive strength exceed 1340 psi. Therefore, only a three point bending and compression tests were performed. Also, the buckling load of the web is also studied by using beam on elastic foundation theory. They found that four of their cores met and exceed the shear and compressive requirements. Their results showed that there is a got a good agreement between the experimental and finite element model. Also, they found that using FRP webbed cores can increase the mechanical properties with up to 35% weight saving comparing to existing aluminum deck.

Williams et al. (2003) studied the performance and behavior of filament-wound GFRP bridge deck. Different decks were constructed using different number of triangular filament wound glass tubes and a GFRP plates were bonded to the bottom and top of the tubes to form one modular unit. They fabricated their deck in two generations. In the first generation, there decks were tested and based on the results they modified the design and fabrication in the second generation to enhance the deck performance. The performance of the deck was examined based on the capacity, strain, deflection at service load, and the mode of failure. The failure mode in the first generation was the delamination and buckling of the top plate. Different mode of failure has been observed in the second generation such as top plate and tube buckling, slippage of the tube, and bottom plate delamination. Also, an analytical model within the elastic range was

presented to predict the behavior of the GFRP decks. They showed that the GFRP deck is able to support an HS30 design truck load and the deflection met a preset limit of  $L/360$ .

Chakraborty et al. (2011) studied the performance of outside filament-wound hybrid FRP-concrete beams. Their beam was made of concrete block, GFRP pultruded hollow section, and CFRP laminate all wrapped together using filament winding. Three different types of concrete were studied in their experiment: normal concrete, high strength concrete and steel fiber high strength concrete. The CFRP laminate was used in the bottom to provide the required stiffness for the section. The use of the filament-wound laminate has two advantages. First, to provide some confinement to the beam. Second, to enhance the shear strength of the pultruded section. It was mentioned that the wrapping eliminated the risk of the premature failure that resulting from the debonding between the concrete block and the pultruded profile. Also, it enhances the stiffness and load capacity of the beam.

Alagusundaramoorthy et al. (2006) tested and evaluated four commercial FRP deck that were available commercially and compared them with the test results of reinforced concrete deck panels. The force deformation response of 16 FRP composite deck and four conventional reinforced concrete decks were evaluated under effect of AASHTO MS22.5 wheel load until failure. The results of all tested panels were compared with shear, flexural, and deflection criteria for Ohio department of transportation specifications. Also, flexural and shear rigidities were calculated for the deck depending on the experimental results in order to use it in the modeling of the First Salem bridge in Ohio. All deck panels met and satisfied the Ohio performance criteria and the factor of safety against failure ranged from 3 to 8.

Tuwair et al. (2015) manufactured and tested an innovative sandwich panel system under monotonic and fatigue loading. This system consists of GFRP facing layers separated by a polyurethane foam core with a trapezoidal shape. Their investigation mainly focused on the new system utilizing a new thermoset polyurethane resin that has longer pot life which is perfect for VARTM process. In addition to the static and dynamic flexural strength, they test the material characterization like tensile and compressive coupons. The results showed that the polyurethane resin exhibited a superior performance in both monotonic and fatigue test. Also, an excellent bond between the components of the system was noticed because of the corrugated shear layers that used to connect the top and bottom facing layers. They used the first-order shear deformation theory to estimate the specimen's deformation and it is be found to have a good agreement with experimental results.

Over 40 FRP bridge decks have been installed on existing or new bridges in the U.S. during the past decades. These bridges mainly are located in California, Florida, Delaware, Iowa, Kansas, Idaho, Illinois, Maryland, Missouri, New York, Ohio, Oregon, Pennsylvania, Virginia, North Carolina, South Carolina, West Virginia, and Wisconsin. Several commercial FRP deck systems are available in U.S. Some of them are adhesively bonded pultrusions manufactured such as DuraSpan deck from Martin Marietta Composites, Superdeck from Creative Pultrusions, Teckdeck from fiber reinforced system, EZspan deck and ZellComp deck. Also, there are sandwich constructed deck which they are fabricated using either hand/automated lay-up or VARTM process such as Kansas Structural Composites deck, Hardcore composite, TYCOR deck from 3TEX, and Structural Composite deck which still under investigation. Due to

proprietary design and manufacturing methods of FRP decks, their design guidelines and specifications are often performance-based. A list of some bridges that were constructed using FRP decks in U.S. is shown in Table 3.1. From this table, a significant increase in the use of this type of decks is noted in the construction or rehabilitation of bridges over the past few years.

Table 3.1 Sample of FRP Bridges in the U.S.

No.	Bridge	State	Deck Type	Year
1	Hanover Bridge	WV	Kansas Composites deck	2001
2	Cats Creek Bridge	OH	DuraSpan deck	2002
3	County Road 153	NY	Hardcore composite	2002
4	Katty Truss Bridge	WV	Superdeck	2002
5	Goat Farm Bridge	WV	Kansas Composites deck	2003
6	Chief Joseph Dam Bridge	WA	DuraSpan deck	2003
7	Tangier Island	VA	ZellComp deck	2006
8	Belle Glade	FL	ZellComp deck	2009
9	Redstone Arsenal	AL	ZellComp deck	2010
10	Rocks Village	MA	Composites Advantage	2014

### 3.3 Hybrid UHPC-FRP Deck

#### 3.3.1 Material Properties

The carbon fiber cloth that used in this project is FG-CF121250U, 12oz - 12k unidirectional from iLSTREET Composites and it is fully compatible with polyester resin, epoxy resin, and vinyl ester resin. The unidirectional GFRP that was placed under the UHPC plate is JBMTG-13-U-50 from JAMESTOWN Distributors, while the bidirectional GFRP that was used for the web shear reinforcement is 18 oz. E-Glass Fiberglass Cloth from U.S. composites. A chopped mat was used with the bi-directional glass fiber in the web to build the thickness and enhance resin transfer. Chopped mat is a randomly oriented long fiberglass strands that are linked together with a styrene-soluble binder that works like glue connecting the fibers. This mat allows the resin to flow easily through the glass fiber and provide more stiffness to the attached laminates. The laminate mechanical properties are summarized in Table 3.2.

Table 3.2 Material Properties from Coupon Tests

FRP type	Modulus (ksi)	Poisson's ratio
Carbon	7615	0.2
Bidirectional glass	2000	0.25
Unidirectional glass	3547.5	0.18

The matrix that used in this research was #1110 Vinyl Ester resin from Fibre Glast Development Corporation. It has desirable properties like affordable cost, good corrosion resistance, good tensile strength, fast curing time, and the most important one low viscosity of 275 cps, which makes it ideal choice for resin infusion applications. According to the manufacturer, this resin has a pot life of 15-30 min, tensile strength of 12,000 psi and modulus of elasticity of  $5.4 \times 10^5$  psi based on the ASTM D638 tests.

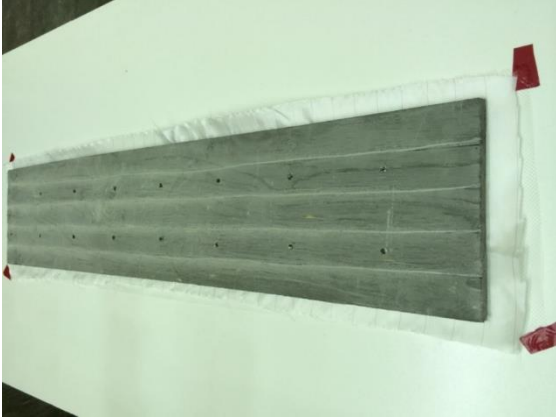
### 3.3.2 Specimen Preparation and Test Setup

The hybrid or composite system is infused with low viscosity resin using VARTM infusion system to get a high quality system with better adhesion and fiber volume content than would be achieved using typical wet layup. The method is typically suitable for manufacturing of carbon and glass fiber composites and it is commonly used by professional manufacturers for the production of any fiber body panels such as boats and motor manufacturers. In this method dry fabric is placed in the mold, and then applies in a special configuration the bagging materials (such as peel ply, infusion mesh and bagging film) before being subjected to vacuum pressure using a composites vacuum pump. Once the specimen is prepared, it will be fully sealed so the air can be evacuated from the bag, resin is drawn through the part and is then fully cured under vacuum.

Two sets of deck have been constructed with different geometry. Six UHPC plates were cast for the hybrid system in the first set with total length of 48 in. Five of these UHPC plates have a thickness of 0.5 in, whereas the sixth plate has 0.75 in. During the casting, several holes with dimensions of 0.25 in  $\times$  0.25 in.  $\times$  0.25 in were made in the plates to enhance the bond and the shear transfer between the UHPC and fibers. Also, after casting, several longitudinal and transverse canals were drilled in the plates in order to allow the resin to flow and improve the bond between the UHPC plate and top GFRP layers. The construction stages of the hybrid deck are shown in Figure 3.2. One layer of chopped mat only was used with one specimen that has UHPC plate thickness equal to 0.5 in. to see if this mat enhanced the resin transfer and the performance of the system. According to the findings of this stage, a decision was made to use multiple layers of chopped mat in the second set of decks. In the second set of the decks, five plates were cast with 34 in. total length and 0.5 in. thickness.

The first set was infused as one system including the UHPC plate while in the second set the infusion process was done in two stages. The first stage included preparing and infusing the foam core with web FRP reinforcement to ensure that the resin would be transferred and impregnate all the FRPs along the total length. Then after two days, the product of the first stage was bagged and infused with the UHPC, top GFRP and bottom CFRP to get the final deck.

The first set of hybrid specimens had a 48 in. overall length and 43.5 in. center-to-center spacing between the supporting steel girder as shown in Figure 3.3. All specimens were loaded at mid-span with an AASHTO prescribed footprint of 20 x 10 in. for an HS20 wheel using neoprene pad with a steel plate on top and the longer side along the span (see Figure 3.5). The instrumentation plan and loading arrangement are shown in Figure 3.6. Four strain gages were attached to the bottom CFRP layer on the tension side. One strain gauge was attached to the top UHPC plate on the compression side. Two string pots were used at the center of each specimens to record the maximum deflection. After preparing the setup, the decks were tested using a loading rate of 0.03 in/min.



(a) Laying the Peel Ply, Infusin Mesh, and UHPC Plate



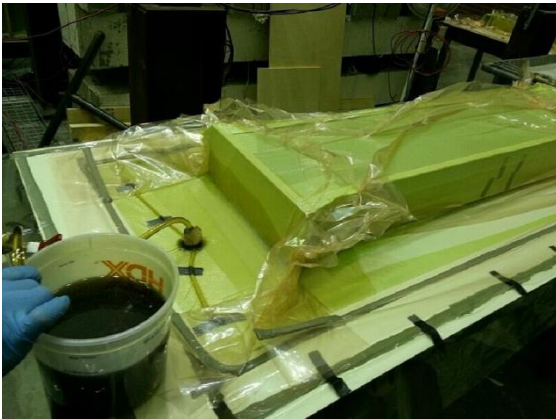
(b) Putting the Side Mold and Laying the Top Glass Fiber Sheets



(c) Installing Foam and Laying Shear Fiber



(d) Laying Carbon Fiber Sheets

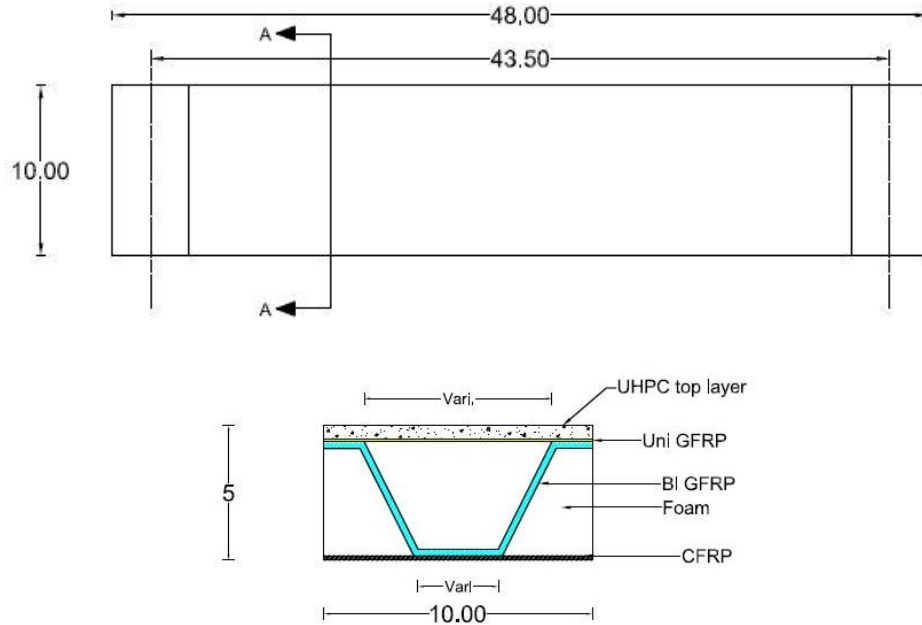


(e) VARTM Process



(f) Final Deck after Demolding

Figure 3.2 Construction Stages of Hybrid System



### Section A-A

Figure 3.3 Details of First Set of Decks

The second set of the specimens have a 34 in. total length with 30 in. center-to-center spacing between the two supports as shown in Figure 3.4. These specimens were tested using four point load configuration. All specimens were tested using Universal Testing Machine (UTM) with a loading rate equal to 0.03 in/min. The test setup of the hybrid sections (UHPC-FRP) are shown in Figure 3.7. Three strain gages were attached to the bottom CFRP and one strain gage was attached to the top UHPC plate. Linear variable differential transformer (LVDT) was used to record the displacement at the mid-span. Also, LVDT are placed at the two supports to calculate the relative displacement. The instrumentation plan of this system is shown in Figure 3.8. This set of specimens was manufactured and tested in two groups. The first group includes specimens 7, 8, and 9. The second group includes specimens 10 and 11.

The first specimen in the first set experienced premature bearing failure resulted in the rotation of the actuator. The reason for this failure may be that some eccentricity at low load level existed with concentrated load reaction from support. So, the web at end wall failed due to compression. The bearing capacity was increased for the remaining specimens of the first set of deck by excavating the foam within the first 4.5 in. of each end of the specimens (which are placed on the supports) and filling the voids with grout, as shown in Figure 3.9.

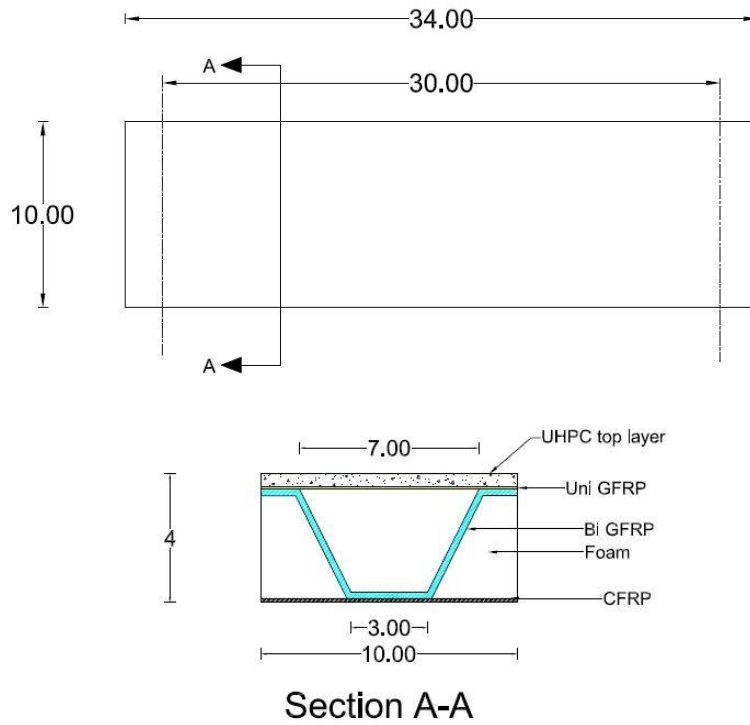


Figure 3.4 Details of the Second Set of Decks



Figure 3.5 Test Setup for the First Set

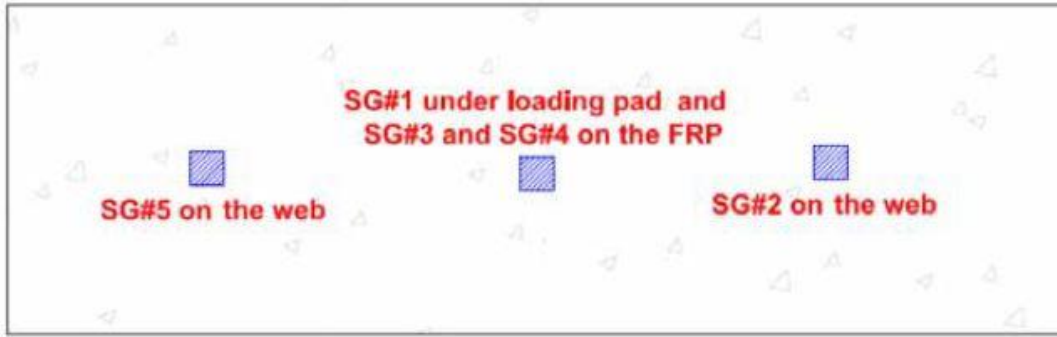


Figure 3.6 Instrumentation Plan for the First Set



Figure 3.7 Test Setup for the Second Set

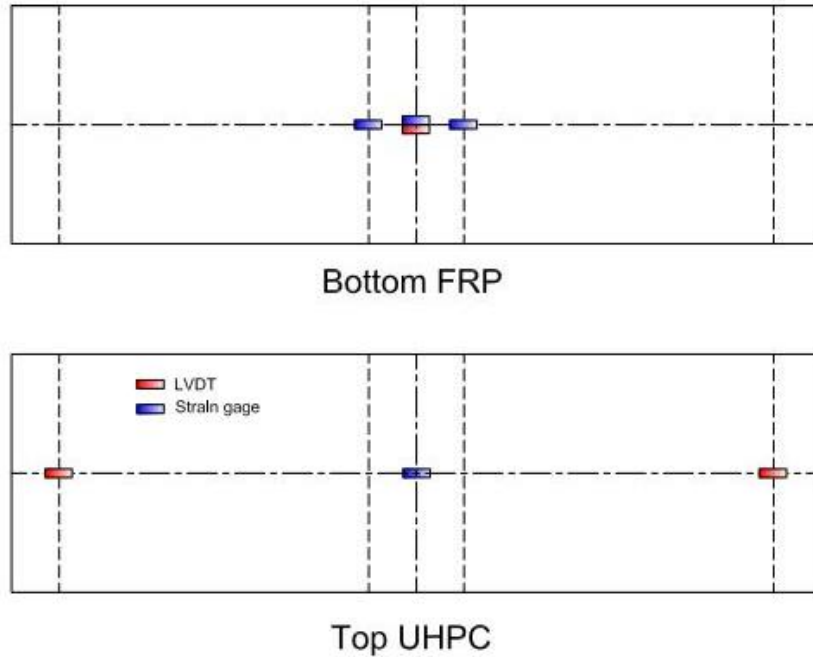


Figure 3.8 Instrumentation Plan for the Second Set

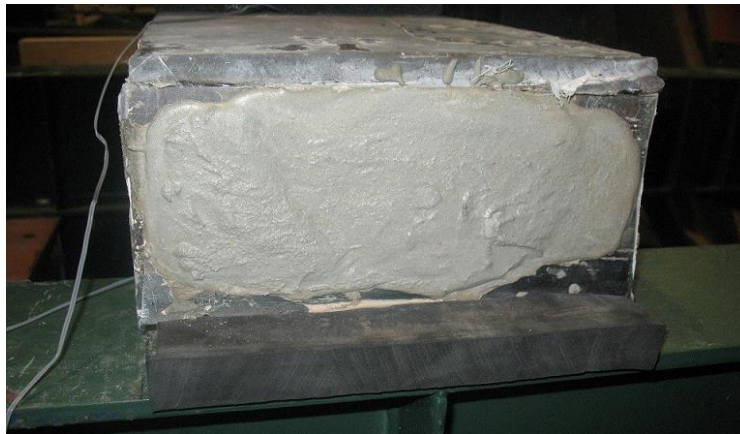


Figure 3.9 End of the Specimen after Grouting

### 3.3 Experimental Results

#### 3.3.1 First Set Specimens

Figure 3.10 shows the load deflection responses for all specimens at the mid span. From observing the result of this tests, it can be seen that chopped mat in the diagonal GFRP webs has a significant effect on the behavior of the system. It is shown that the ultimate load for specimen #6 is 14.37 kips, while the ultimate load for the other specimen that have the same UHPC plate thickness ranged between 6.05 and 8.7 kips. The deflection at the peak load for specimen #6 is 0.48 in., while it is more for the other specimens at their peak load.

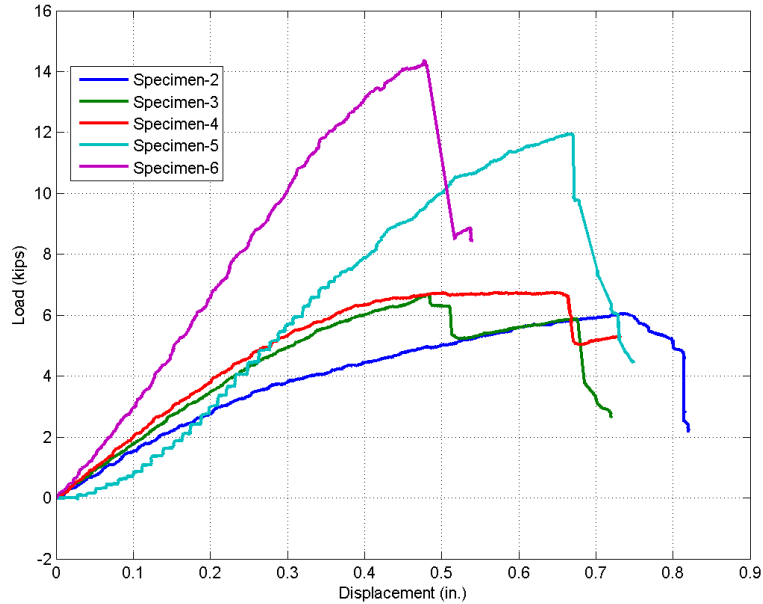


Figure 3.10 Load-Displacement Responses for the First Set

Another reason for this difference in the results is due to resin transfer inside the deck. After the test, all the specimens were cut to investigate the quality of the infusion. As shown in Figure 3.11, all the fibers in web area (shear reinforcement) were completely dry, and resin only transferred through short distance from the edge. The exception was for specimen no. 6 where the resin transferred all the way to end due to the advantage of the chopped mat. This issue prevented load transfer from the UHPC plate to the other parts. The mode of failure as shown in Figure 3.12 was local failure due to the crushing of UHPC at the end of the loading pad or at the end of the grouting due to high shear force. Also, Figure 3.13 shows that the interface between the UHPC and top FRP was sufficient to ensure the composite action between the two materials but the debonding failure happened between the FRP and side foam core as shown in Figure 3.14.



Figure 3.11 The FRP Cloth after Demolding



Figure 3.12 Failure Mode near the End of the Grouted Region



Figure 3.13 The Bond between the UHPC and Top FRP



Figure 3.14 The Failure Mode near the End of the Grouted Region

Figure 3.15 and Figure 3.16 show the load-strain curve for all the specimens at UHPC plate (at the top of the specimen) and at the CFRP layer (at the bottom of the specimen). From the strain results, it can be noted that the strain at UHPC plate at the mid span is much lower than the crushing strain of the concrete ( $\epsilon_{cr} = 0.0032$ ), and the strain in bottom FRP layer is lower than the yielding strain of the carbon laminate, so the failure will be most likely interface failure or the buckling of the web.

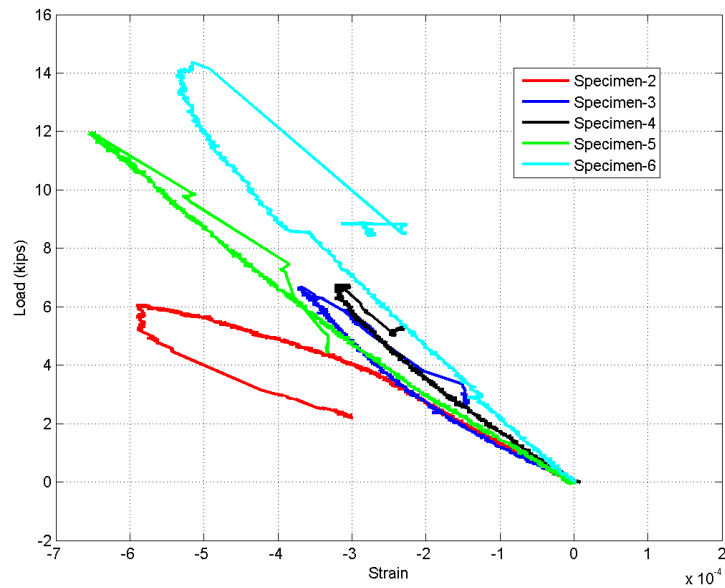


Figure 3.15 Strain at Top UHPC Plate for the First Set

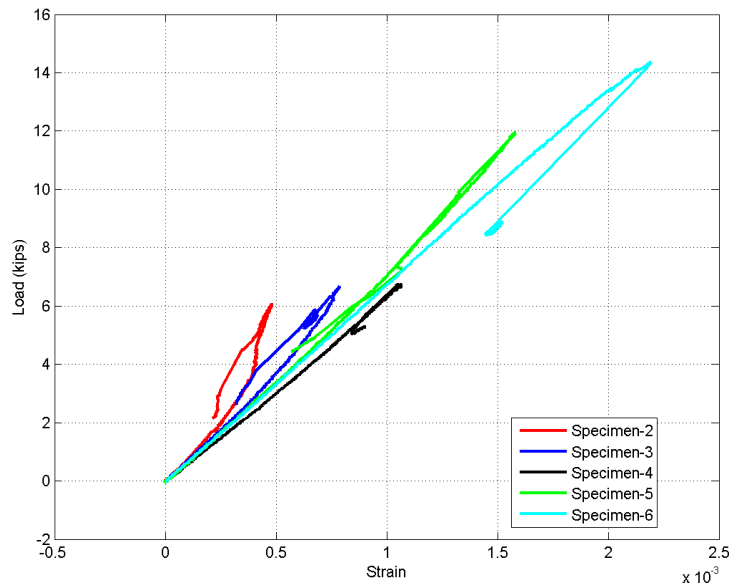


Figure 3.16 Strain at Bottom FRP for the First Set

### 3.3.2 Second Set Specimens

The load-deflection curves for the second set of the lightweight system are shown in Figure 3.17. As mentioned before, this test was prepared and tested in two groups to enhance the performance of the deck. From this figure, it can be seen that both specimen no. 7 and no. 9 had a sudden drop in the load due to the initiation of the debonding at the supports. After this drop, the load began to increase again with the propagating the debonding prior to the final failure when the UHPC top plate was fully delaminated. Specimen no. 8 showed a linear behavior throughout the loading history. The maximum load was achieved with specimen no. 8 and it was around 15 kips with a

0.27 in. corresponding displacement. Also, it was observed that in this specimen the delamination occurred at the support and then propagated along the length of the specimen.

Depending on the results of the first group and the interface test, a decision was made to increase the interface strength in the second group. After several trials with the interface test to increase the bond strength between the UHPC and top GFRP, the UCF team has decided to increase the numbers of grooves along the specimens as shown in Figure 3.18 to provide better bond strength and increase the strength of the deck. It can be seen from Figure 3.17 that there is a significant increase in the strength of specimen no.10 and a slight improvement for specimen no.11. From the figure, it can be seen that specimen no. 10 exhibit a linear behavior until the first drop around load level 17.2 kips which is due to the initiation of the interface delamination at the support. After that the load started to increase until reached the peak load which is around 19.0 kips. The delamination propagated toward the mid of span, and a UHPC crushing was observed under the loading points at the end of the test.

The load versus strain curves for the second set of deck at the top UHPC plate and bottom CFRP layer are shown in Figure 3.19 and Figure 3.20 respectively. From these figures, the strain results of this sets decks below the crushing strain of the UHPC and the value governing the material strength of the CFRP. The maximum compressive strains in the UHPC plate 0.0023, which is equal to about 72% of the crushing strain of the concrete ( $\epsilon_{cr} = 0.0032$ ). The tensile strains at the maximum at bottom CFRP layer at the peak load for the all decks were 0.0026, 0.0023, 0.00255, 0.0022, and 0.0016 respectively, which are more less than the ultimate strain of CFRP material ( $\epsilon_u = 0.01$ ).

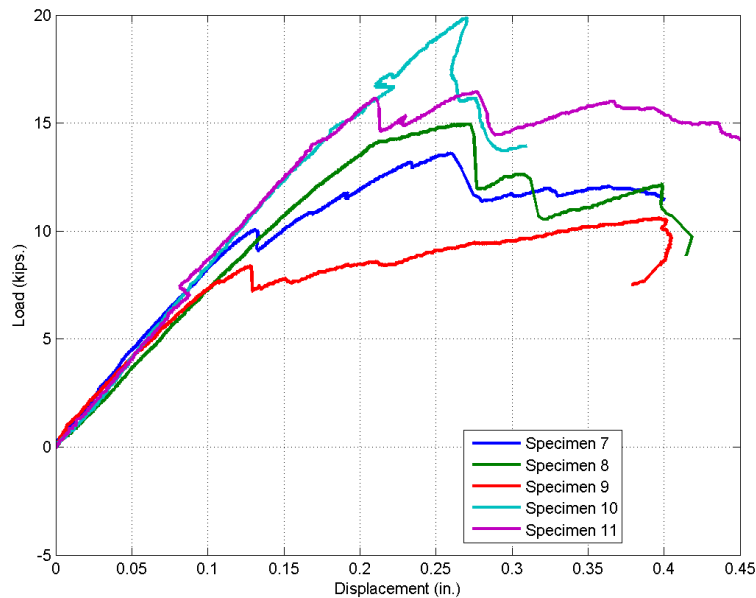


Figure 3.17 Load-Displacement Responses for the Second Set

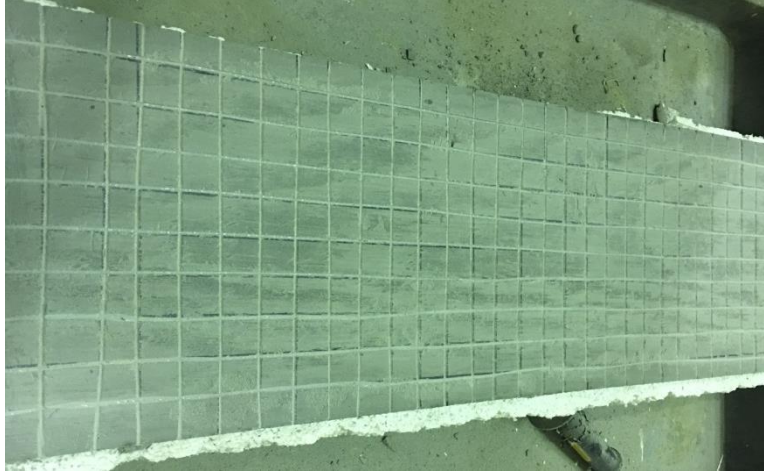


Figure 3.18 Number of Grooves in the Second Group of the Second Set

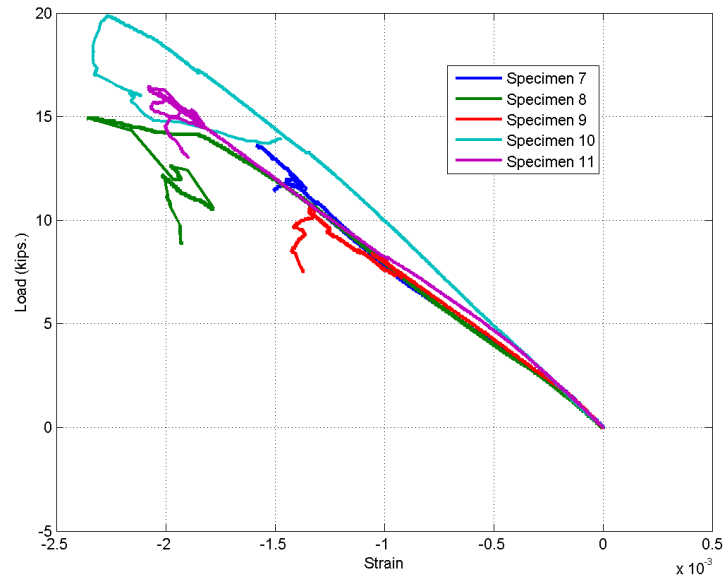


Figure 3.19 Strain at Top UHPC Plate for the Second Set

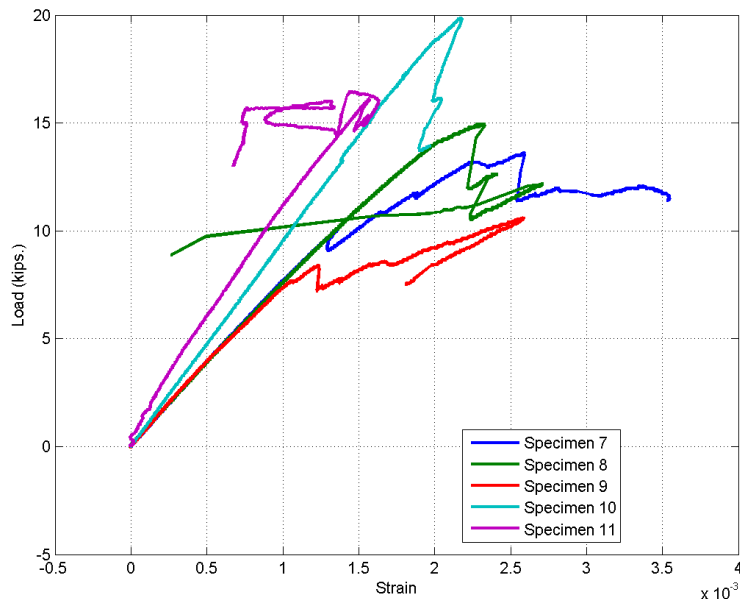


Figure 3.20 Strain at Bottom FRP for the Second Set

### 3.3.3 Comparison of Test Results

In order to compare the outcomes of the two sets of specimens, the results are normalized and plotted together as shown in Figure 3.21 and Figure 3.22, respectively. The specimens 2 to 6 represent the results of the first set of the hybrid specimens while the specimens 7, 8 and 9 represents the second set of the hybrid specimens. In Figure 3.21, the moment at the mid span of the deck are scaled to the nominal moment of each deck from equilibrium analysis and plotted versus the scaled displacement, where the mid-span displacement was divided by the half length of the deck. Figure 3.22 represents the scaled load versus the scaled displacement for all hybrid specimens as well as the load for the 1T1S deck. Each load for each specimen was scaled to the demand load for each deck. As known, the demand load for the 1T1S is 16 kips, and since the hybrid specimen width (10 in.) is less than the width of the 1T1S (15 in.), the demand load for the hybrid deck was reduced by the ratio of the hybrid width/1T1S width.

Test results of the two sets showed that the strain at maximum load in both the UHPC and the bottom CFRP layer didn't reach the crushing strain and FRP ultimate strain respectively. So the failure mode in most cases was most likely being either at the interface or through buckling of the web. To enhance the bond between the UHPC and top fibers, the number of grooves increased in the group two of the second set in the longitudinal and transverse direction over that used previously to provide better bond. The results showed that specimen's no. 10 and 11 have better global behavior and better bond strength over the rest of the specimens in the first and second set. The bond strength between the UHPC and the top uni-GFRP plays a significant role in performance of the hybrid deck and control the behavior of the system. Different types of connections may need to be considered to improve the bond between UHPC and FRP including mechanical connection, FRP connectors, resin beads, or more grooves in UHPC.

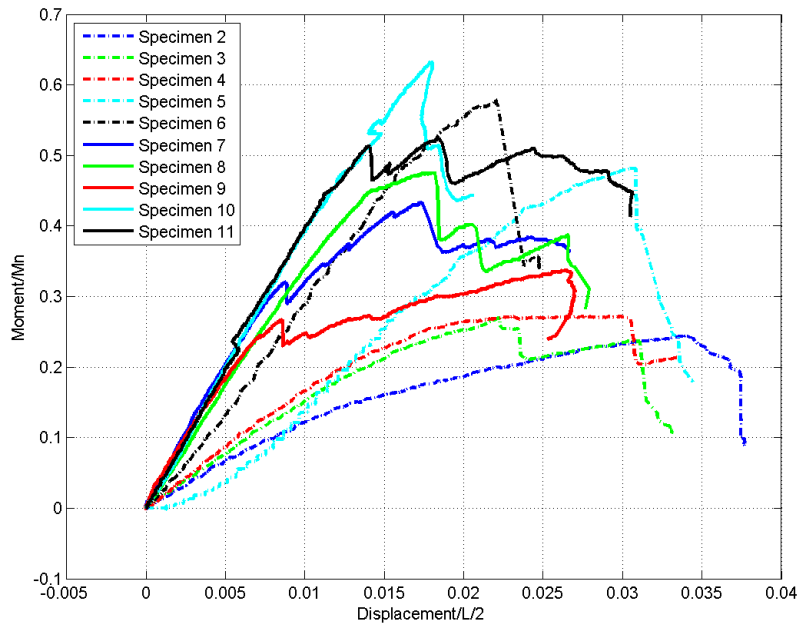


Figure 3.21 Scaled Moment - Scaled Displacement for the First and Second Set

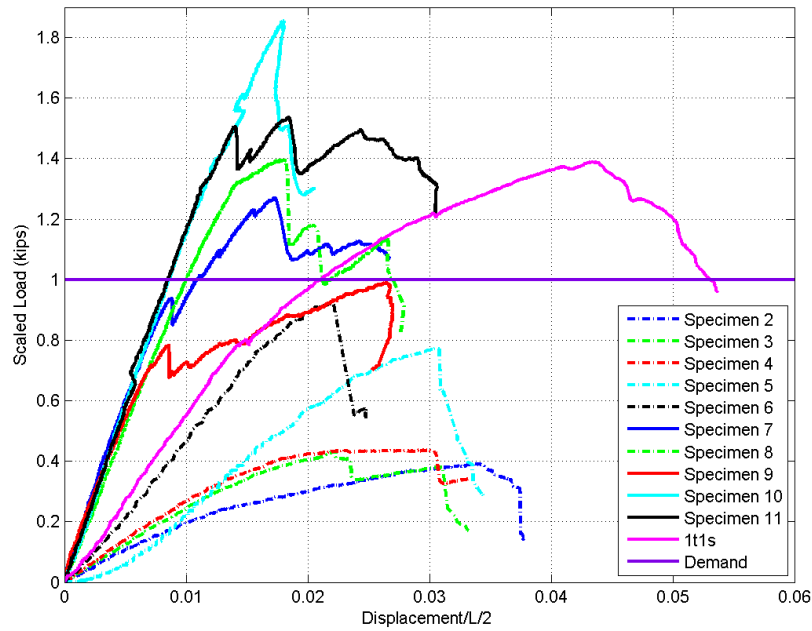


Figure 3.22 Scaled Load - Scaled Displacement for the First and Second Set

### **3.4 Bonding of FRP Laminates to UHPC**

#### **3.4.1 Background**

The use of fiber reinforced polymer (FRP) composites in the repair and strengthening of different reinforced concrete structural elements has become very commonplace and extensively used nowadays. A reinforced concrete element is a combination of two or more materials with different properties acting together to resist the external loads. The performance of these elements depends mainly on the load transfer between the constituent materials. The interfacial bond between an FRP sheet and concrete substrate is the key factor for the ultimate load-carrying capacity of FRP-strengthened reinforced concrete structures (typically on the tensile face). Bond behavior dictates the transfer length of the FRP and the debonding mode failure. Determination of the bond characteristics of composite fibers to the concrete is important for design purposes since the debonding load capacity is fundamental for safe and economic design.

Several test setups have been used to determine and evaluate the bond properties between the concrete and continuous fiber sheets. Some test setups that have been used in the bond test between FRP laminates and concrete are shown in Figure 3.23. The most common tests and widely used are single lap shear and double lap shear tests, as shown in Figure 3.23(a) and (b), respectively. The stress fields within the specimen in the single lap shear test match few applications in actual construction because the concrete near the loading tip in this type of test will be in compression while the FRP will be in tension state. This issue can be avoided by using double lap shear test where the concrete near the loading tip will have the same state of stress as the FRP laminate.

In this section, double and single lap shear test were performed to study the bond properties between ultra-high performance concrete (UHPC) and uniaxial carbon/glass fiber reinforced polymer composites (CFRP/GFRP) with vinyl ester matrices. This double lap shear test was done using two different sizes of concrete block with CFRP and GFRP. On the other hand, single lap test was performed using one size concrete block with two layers of GFRP.

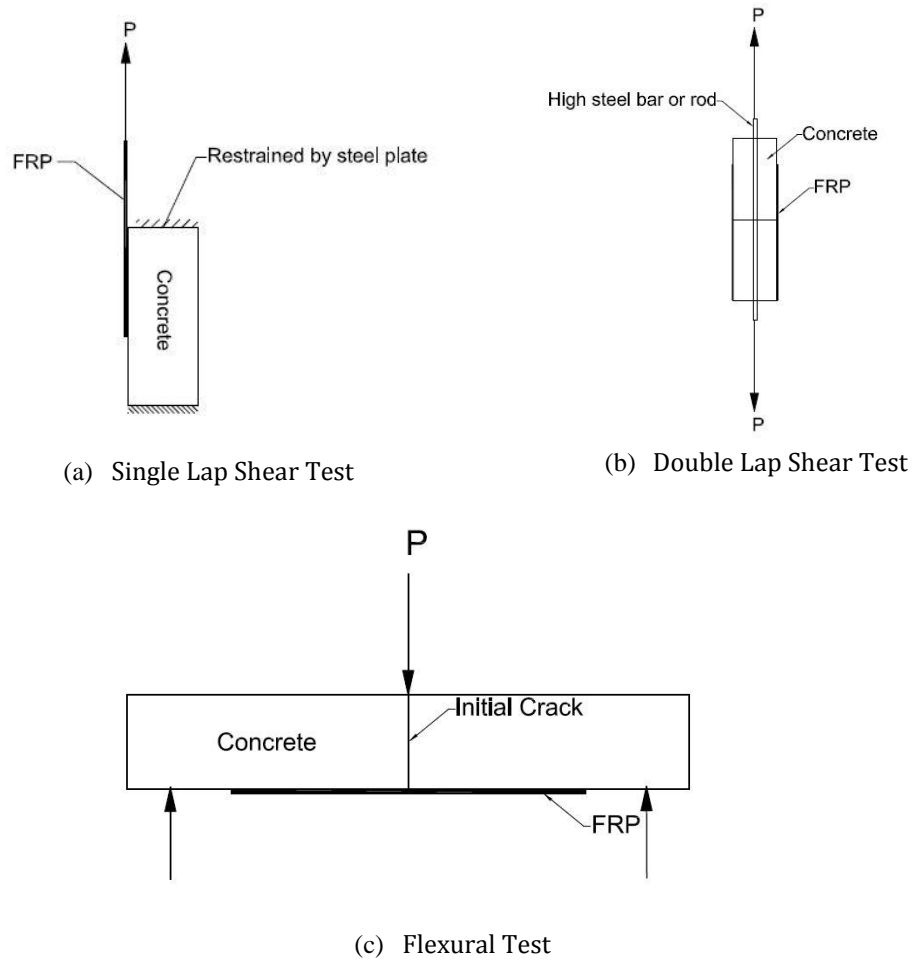


Figure 3.23 Different Test Setup for FRP Bond

### 3.4.2 Literature Review

Many studies have been done over the years to understand the mechanism of bond and stress transfer between FRP and concrete, and the factors that affect the delamination of different types of FRP from concrete. Some of these factors include; compressive strength of concrete, surface preparation, type of fiber sheet, and method of bonding.

Chajes et al. (1996) used a single-lap shear test specimen to study and evaluate the effect of the surface preparation, adhesive type, and the strength of concrete on the average bond strength. Also, another set of tests was conducted to study the force transfer mechanism from the composite material plates into concrete. Two failure mechanisms were observed: cohesive-type failure and direct concrete shearing beneath the concrete surface, depending on the type of adhesive. Their results showed that the concrete surface preparation can influence the ultimate bond strength and the concrete should be mechanically abraded or sand blasted to achieve the best possible bond. They concluded also that there is an effective bond development length for a joint beyond which no additional increase can be gained in the failure load. Also, if the governing failure mode of the joint is the shearing of the concrete, the ultimate bond strength will be proportional to the square root of concrete compressive strength.

Yoshizawa et al. (1996) studied the effect of different type of concrete surface preparation on the bond of CFRP sheets. A concrete prism with CFRP sheets applied to two opposite sides was used in the study. The specimen was tested in tension, causing direct shear to be placed on the CFRP sheets. Water jet or sand blasting was used to prepare the concrete surface of the specimens. It was found that the water jet had more effect and doubled the capacity of the specimen comparing to the sandblasting. The bonded length of the CFRP sheet was determined to have little effect on the ultimate load of the specimen.

Horiguchi and Saeki (1997) conducted a study on the effect of the concrete compressive strength and the test method on the bond of CFRP sheets. Shear test, flexural test, and direct tensile tests were employed and investigated in the study. It was found that the tensile test produced the largest average bond strength, followed by the bending test, and the lowest average bond strengths have been found in the shear test. Shearing of the concrete, delamination, and rupture of the FRP were the three failure modes that observed in this study. They observed that the failure occurred in the concrete when the concrete compressive strength was low, less than 3600 psi. On the other hand, when the concrete compressive strength was high or when the shear-type test was conducted, the delamination failure occurred. FRP fracture was observed in the bending tests with higher strength of concrete. Bond strength increased as the concrete compressive strength increased and the CFRP bonded length of had minimal effect on the ultimate load.

Nakaba et al. (2001) studied the bond behavior between FRP laminates and concrete. Also, a numerical model was proposed to represent the local bond stress versus the slippage based on Popovics's formula. A double lap shear bond test was performed to obtain the local bond stress slip relationship. Different factors have been considered to address their effects on the bond behavior between the laminated and the concrete such as; laminate stiffness, concrete strength and influence of putty thickness, which it is a thickened epoxy paste that used to smooth surface discontinuities and filling the voids. A total of 36 specimens was tested with different concrete/mortar-fiber combination. They concluded that the maximum load increases as the stiffness of the FRP increases. Also, they verified that the putty thickness has no effect and the increase in its thickness did not mean an increase in the maximum load. Also the type of FRP has no effect on the maximum local bond stress. However, the maximum local bond stress increases as the concrete compressive stress increases. Their analytical results showed good agreement with the bond strength and strain distribution obtained from the experiment.

Elmahdy et al. (2007) studied the bonding of CFRP and Steel Reinforced Polymer SRP to ultra-high performance concrete using double lap shear test configuration. For half of the specimens, the epoxy was applied before casting the UHPC, so that bonding to wet concrete could be assessed. For the remaining half specimens, they attached the CFRP/SRP to the hardened concrete. Also, they used several cover types to study the difference in the surface finishing. The specimens were covered with either regular duct type, plastic sheet, or woven glass cloths. They concluded, in wet bonding, the epoxy was more effective in CFRP than SRP. The wet bonding in CFRP reached almost 77% of the bond strength of the bond in the case of the sand blasted dry bonding, whereas in SRP case, the wet bonding reached only 57% of the sand blasted dry bond value.

### 3.4.3 Specimen Preparation

#### 3.4.3.1 Double Lap Shear Test

Nine UHPC specimens were prepared with two different sizes. The dimensions of the first group were  $4 \times 4 \times 20$  in. The dimensions of the second group were  $2.5 \times 2.5 \times 20$  in. The first batch included three big specimens and three small specimens. The second batch included three small specimens. Each specimen is comprised of two blocks separated by 0.2 in. thick plywood as shown in Figure 3.24. One high strength threaded rods were embedded in each block for each specimen through the center of the cross section to allow the specimens to be gripped during the pull-out test. The diameter of the threaded rod was 1 in. for the  $4 \times 4$  in. section and  $\frac{1}{2}$  in. for the  $2.5 \times 2.5$  in. section. To prevent the slippage of the rod during the test, three high-strength nuts were put on each rod in each side of the specimens as shown in Figure 3.25.



Figure 3.24 Specimen Preparation Showing the Plywood Position



Figure 3.1 Installation and Distribution of High Strength Nuts

Three of the six total small specimens and two of the three big specimens were tested with two layers of unidirectional GFRP. The remaining specimens were tested with one layer of

unidirectional carbon fiber. The testing matrix and the identification of each specimen are clarified in Table 3.3 and Figure 3.26.

Table 3.1 Test Matrix

<b>Fiber</b>	<b>Glass</b>		<b>Carbon</b>	
Specimen's Size	Small	Big	Small	Big
No. of Tested Specimens	3	2	2	1

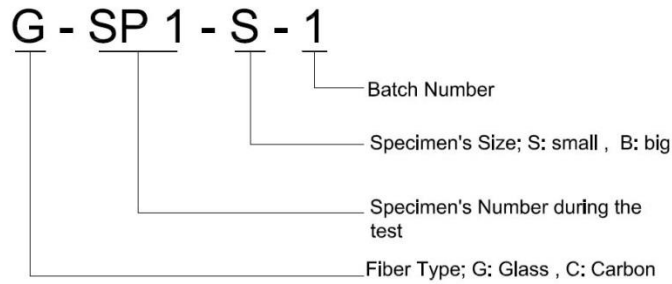


Figure 3.2 Specimen's Identification

The application of FRP layers to the UHPC surface was done using a vacuum bagging process. This process includes using a flexible and transparent film to enclose and compact the wet laminate under atmospheric pressure as shown in Figure 3.27. A vacuum and pump are used to extract the air from the bag and compress the part by using atmospheric pressure to promote cure under pressure. The benefit of using vacuum bagging over the lay-up methods is that the final product will have a lower void contents and higher fiber content laminates. Also, lower void contents can be achieved than with wet lay-up. Here, the process was done using 36'' × 54'', 20 mil thick vinyl vacuum bag with 280 lb tear strength resistance. Also, continuous duty diaphragm type with 1 CFM was used. After completing the bagging process, the fibers on both sides are trimmed to a final FRP layer width of 2''. The bond length was 5'' on one side while in the other side all the length was bonded to ensure that the debonding will happen on the desired side. The final dimensions and the bonded length are shown in Figure 3.28.



Figure 3.27 The Carbon Specimens under Atmosphere Pressure

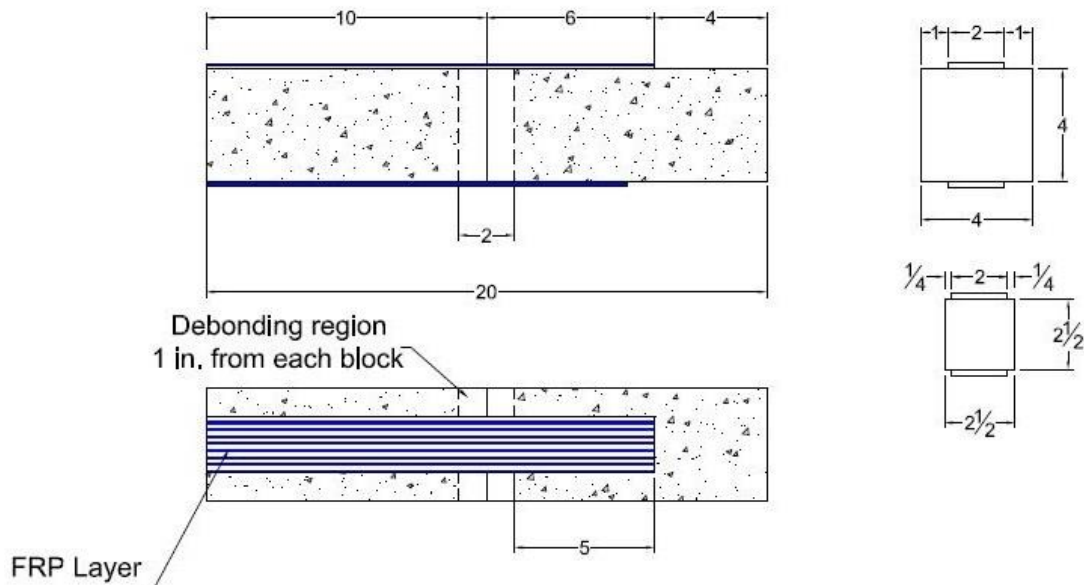


Figure 3.28 Details of bonding Length

### 3.4.3.2 Single Lap Shear Test

Six UHPC specimens with dimensions of  $4 \times 4 \times 10$  in. were prepared in this type of test. All of these specimens were tested with two layers of unidirectional GFRP. The bonded length was selected to be 5" to match the one that has been used in double lap shear test. The 1" unbonded length of FRP was introduced using duct tape at the loaded end to prevent the possibility of any transverse shear failure of the concrete that could happen at the edge closest to the loaded end as shown in Figure 3.29. Two different configurations were used to enhance the bond strength

between the UHPC and GFRP. Three of the six specimens were prepared by drilling a mesh of grooves. The other three specimens were prepared by inserting two plastic bolts to connect the FRP to UHPC. The details of these two configurations are shown in Figure 3.30 and Figure 3.31, respectively. Similar to double lap shear test, the application of FRP layers to the UHPC surface was done using a vacuum bagging process. After completing the bagging process, the fibers were trimmed to have a final FRP layer width of 2". Two beveled-edge end tabs made of Natural G10 FR4 Fiberglass Epoxy sheets were used at the end of the FRP laminate to prevent the slippage of FRP during the test.

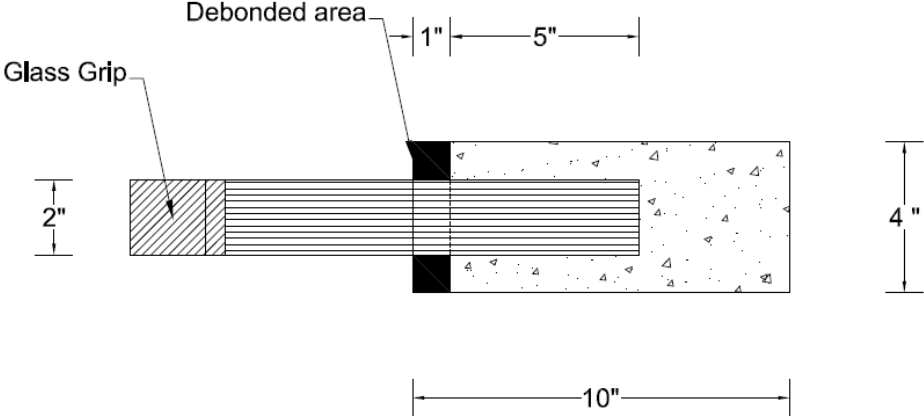


Figure 3.29 Details of bonding length in single lap test

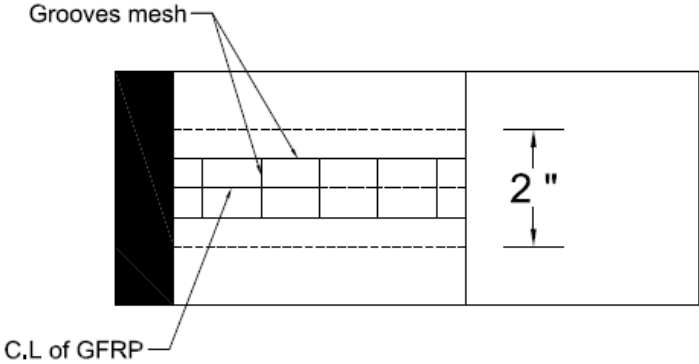


Figure 3.30 Details of grooves mesh

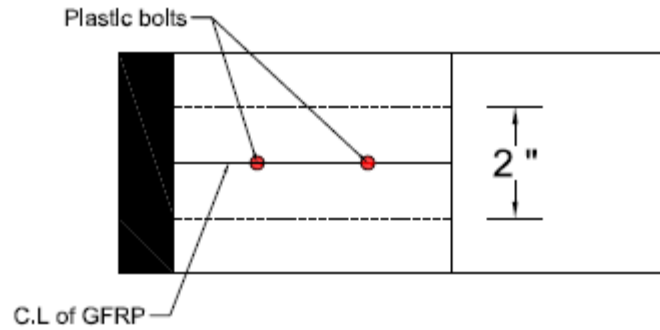


Figure 3.31 Location of plastic bolts

### 3.4.4 Test Setup and Measurement

#### 3.4.4.1 Double Lap Test

All specimens were tested using a Universal Testing Machine (UTM) and subjected to pure tensile load that should cause a direct shear on the adhesive. Total displacement from the machine and strain gage reading from six strain gages in each specimen were recorded to process the data. Since it is difficult to avoid the moment caused by the eccentricity between the top and bottom grips during the test, the maximum load is not equally distributed between the two laminates. Therefore, one of the six strain gages was attached to the opposite face in order to calibrate the maximum load later as shown in Figure 3.32. The top end was designed to be stationary during the test, and the load was applied to the bottom end as shown in Figure 3.33.

Displacement control was adopted in the test with the initial loading rate of 0.05 mm/min, and it was found so slow and take around 100 min to complete the first test. Later the rate was increased for other specimens 10 times to be 0.5 mm/min and test time was around 10 min for each one. To obtain the tensile properties, which include ultimate strength and elastic modulus; laminates were prepared employing one layer of CFRP and GFRP.

#### 3.4.4.2 Single Lap Test

Similar to double test, all specimens were tested using a Universal Testing Machine (UTM) and subjected to pure tensile load under displacement control with loading rate of 0.4 in./min. Total displacement from the machine and strain gage reading from five strain gages in each specimen were recorded to process the data. Two thick steel plates at the top and bottom of UHPC block with four high strength threaded steel rod were used to support and attach the UHPC block to UTM platform. The top platform of UTM was designed to be stationary during the test, and the load was applied by moving the bottom platform downward with the applied loading rate to the bottom end. The details of the test configurations and the distribution of strain gages are shown in Figure 3.34.

Tensile coupons were made and prepared with dimensions of 12" long and 1" wide. Beveled-edge end tabs made of Natural G10 FR4 Fiberglass Epoxy sheets provided by ePlastics Inc. were used with dimensions of (2 long  $\times$  1 wide  $\times$  0,125 thick) in following ASTM D3039. The details of coupon test are shown in Figure 3.35.

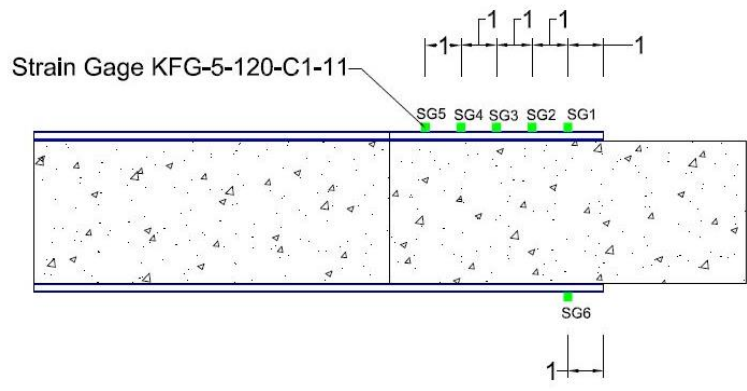


Figure 3.32 Strain Gage Distribution



Figure 3.33 Double Lap Specimen Arrangement during the Test

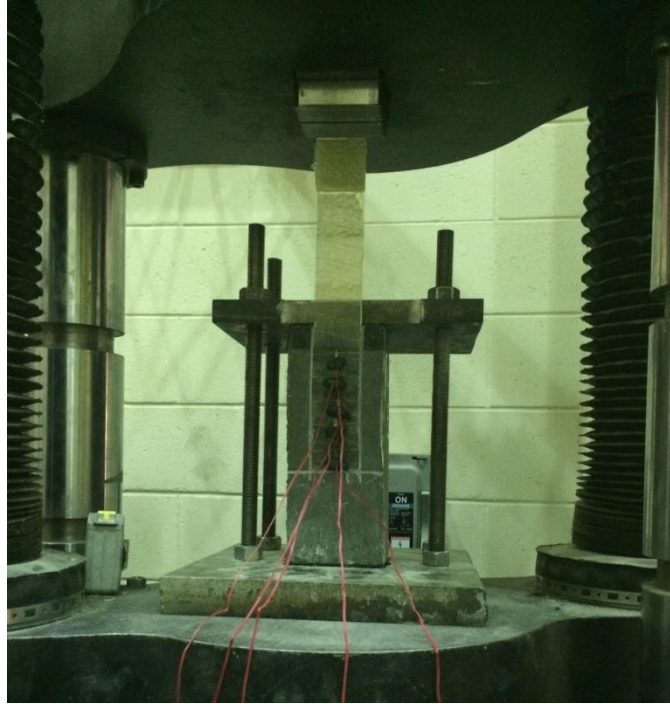


Figure 3.34 Single Lap Specimen Arrangement during the Test



Figure 3.35 FRP Coupons

### 3.4.5 Test Results

All specimens were testing under tensile force until debonding failure occurred. The maximum load, displacement at maximum load from the UTM, and failure mode for all the specimens are summarized in Table 3.4 and Table 3.5, respectively. The failure mode of some specimens is shown in Figure 3.36 and Figure 3.37, respectively. During the test, one small specimen from double lap test was lost unintentionally from the GFRP group. Table 3.6 summarized the fiber tensile properties that were obtained from the coupon tests. The maximum tensile strength for the carbon fiber was 77.3 ksi, and for the unidirectional GFRP was 37.8 ksi.

The data from five strain gages was collected to create strain profiles for all specimens in both tests. The strain versus the strain gage distance from the center of the specimen was plotted for different load levels for double lap test as shown in Figure 3.38 to Figure 3.45. In single lap test, the strain versus the strain gage distance measured from the loaded edge of the specimen was plotted for different load levels as shown in Figure 3.46 to Figure 3.51. In the first test, it is evident that the debonding occurred in most of the cases on the strain gages side. In the cases that the failure took place in the one gage side, it can be seen from the plots that debonding also occurred on the side with the gages, but debonding propagated faster on the one gage side. As mentioned, this is due to the unequal sharing of load between the two bonded laminates.

Table 3.4 Test Results for Double Lap Test

Specimens ID	Maximum Load (kips)	Displacement (in)	Failure Mode
G-SP1-S-1	2.7879	0.2142	Bond failure on gages face
G-SP2-S-2	2.7262	0.2063	Bond failure on one gage face
G-SP3-S-2	2.8744	0.2041	Bond failure on gages face
C-SP4-S-1	3.8183	0.2828	Bond failure with carbon fiber rupture on unloaded block (one gage face)
C-SP5-S-1	3.5840	0.2306	Bond failure on gages face
G-SP7-B-1	3.1167	0.2289	Bond failure on one gage face
G-SP8-B-1	2.7303	0.1943	Bond failure on gages face
C-SP9-B-1	4.3335	0.2393	Bond failure with carbon fiber rupture on unloaded block (gages face)

Table 3.5 Test Results for Single Lap Test

Specimens ID	Maximum Load (kips)	Displacement (in)	Failure Mode
Grid-SP1	1.734	0.174	Full debonding
Grid-SP2	2.088	0.256	Full debonding
Grid-SP3	2.355	0.3105	Full debonding
Bolt-SP1	1.975	Displacement reading was lost during the test	debonding with shear failure of the bolt
Bolt-SP2	2.400	0.3062	Full debonding – bolt didn't fail
Bolt-SP3	2.270	0.1947	Full debonding – bolt didn't fail

Table 3.6 Fiber Properties from Coupon Tests

Type of Fibers	Tensile Strength ksi	Modulus of Elasticity ksi
Carbon	77.3	7615
Glass	37.8	3547.5



(a) G-SP3-S-2



(b) C-SP4-S-1



(c) G-SP2-S-2



(d) G-SP8-B-1

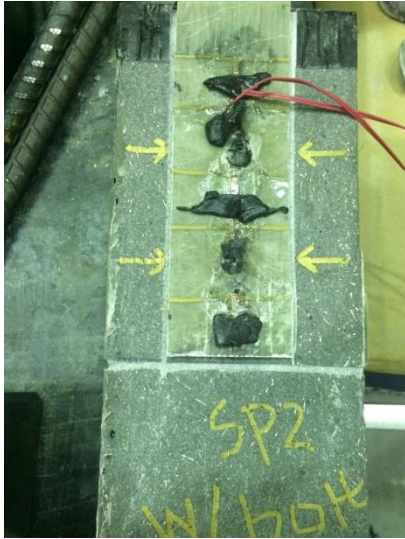
Figure 3.36 Failure Modes of Specimens in Double Lap Test



a) Bolt-SP1



b) Grid-SP1



c) Bolt-SP2



d) Grid – SP2

Figure 3.37 Failure Modes of Specimens in Single Lap Test

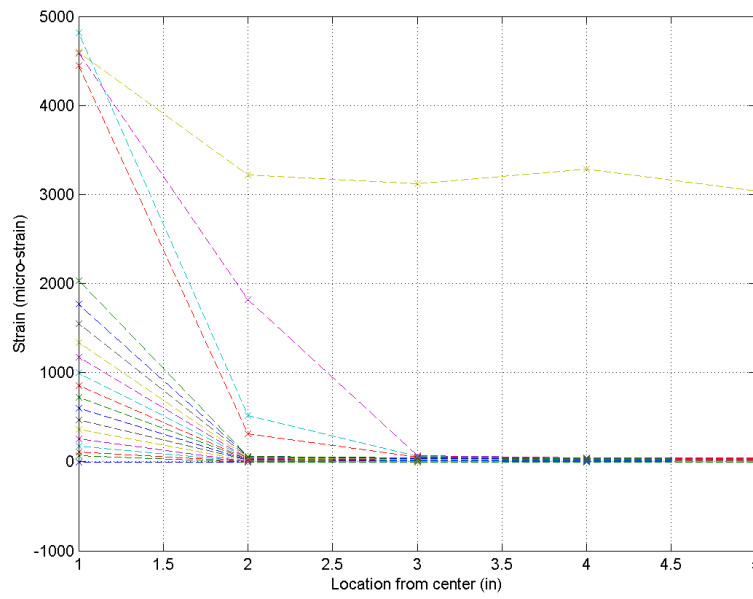


Figure 3.38 Strain Profile for G-SP1-S-1

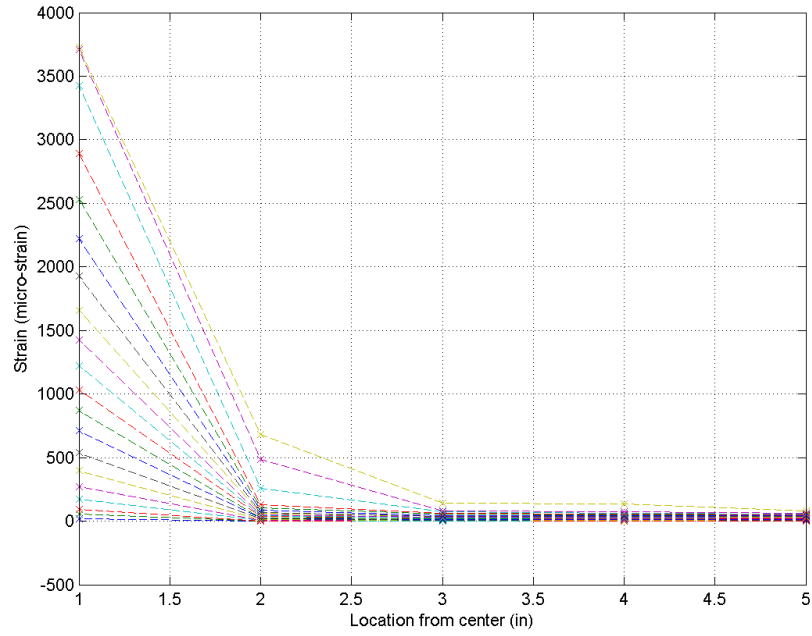


Figure 3.39 Strain Profile for G-SP2-S-2

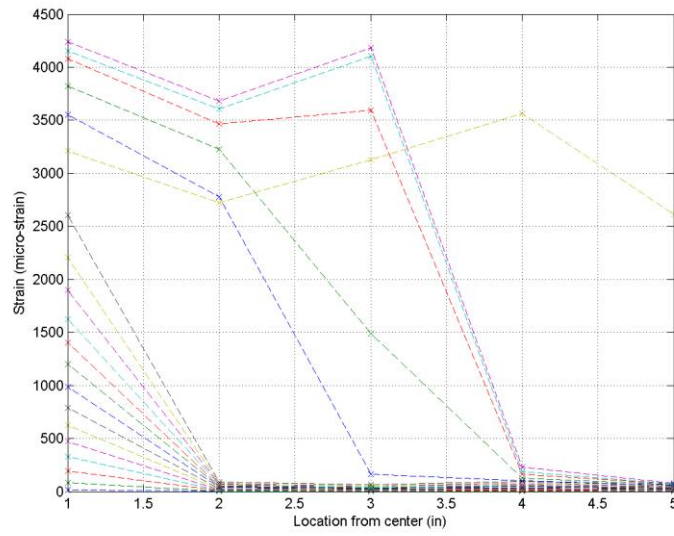


Figure 3.40 Strain Profile for G-SP2-S-2

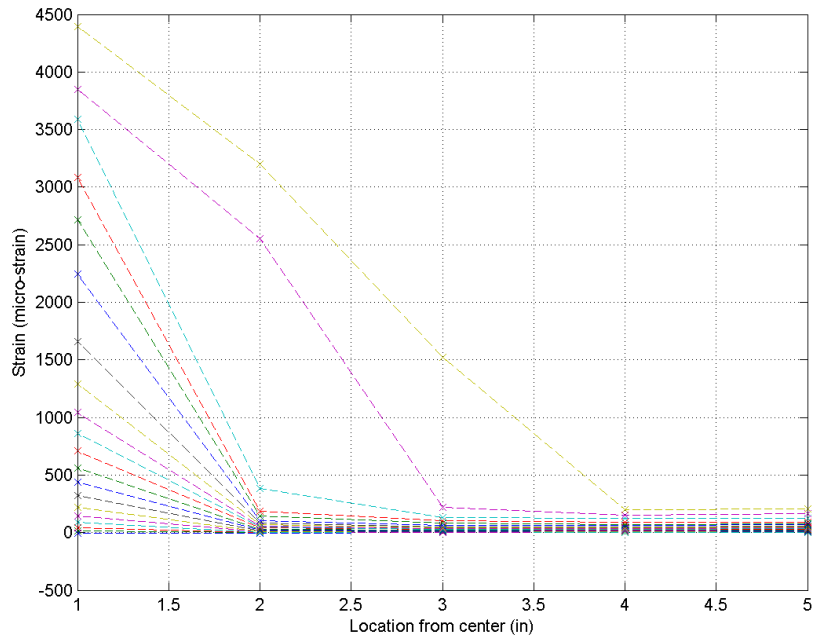


Figure 3.41 Strain Profile for C-SP4-S-1

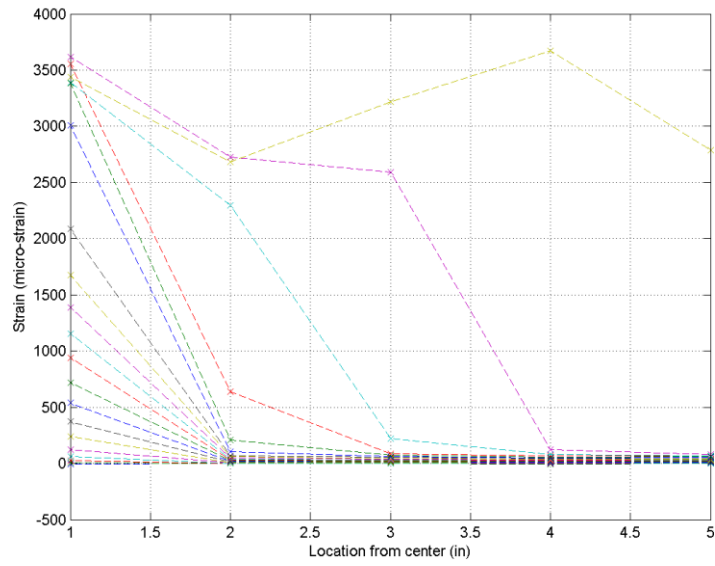


Figure 3.42 Strain Profile for C-SP4-S-1

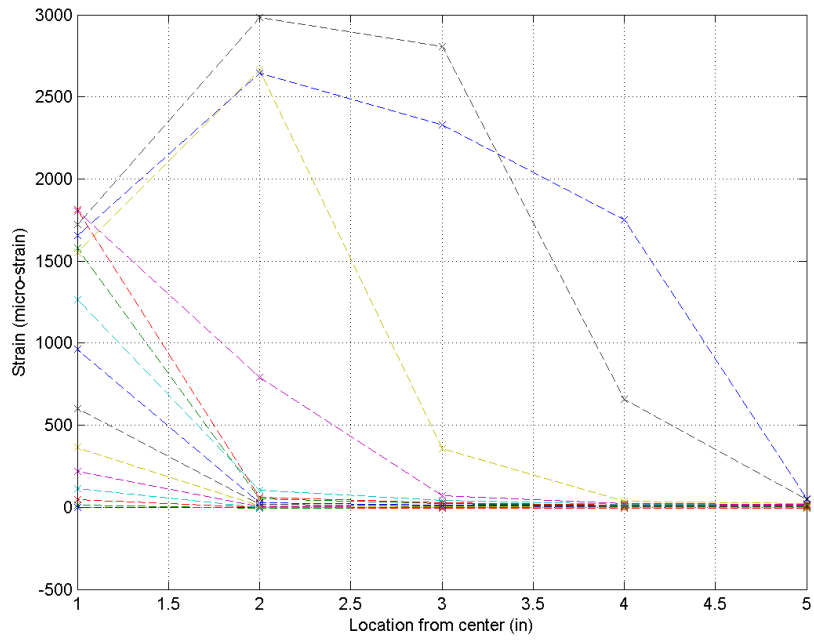


Figure 3.43 Strain Profile for C-SP5-S-1

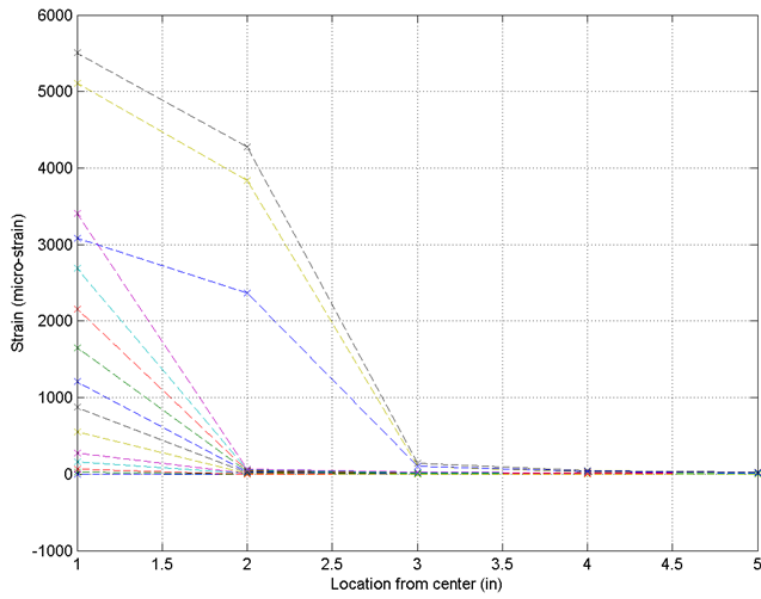


Figure 3.44 Strain Profile for G-SP7-B-1

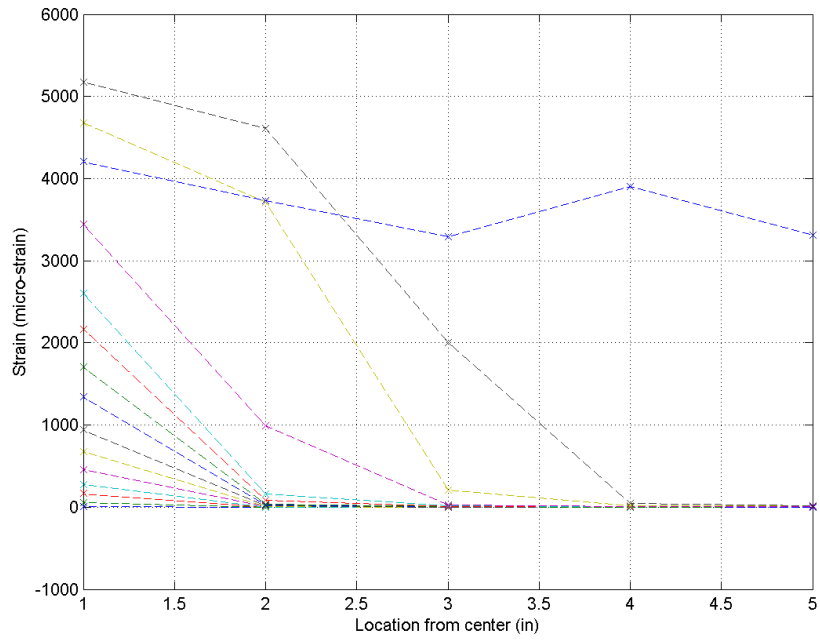


Figure 3.45 Strain Profile for G-SP8-B-1

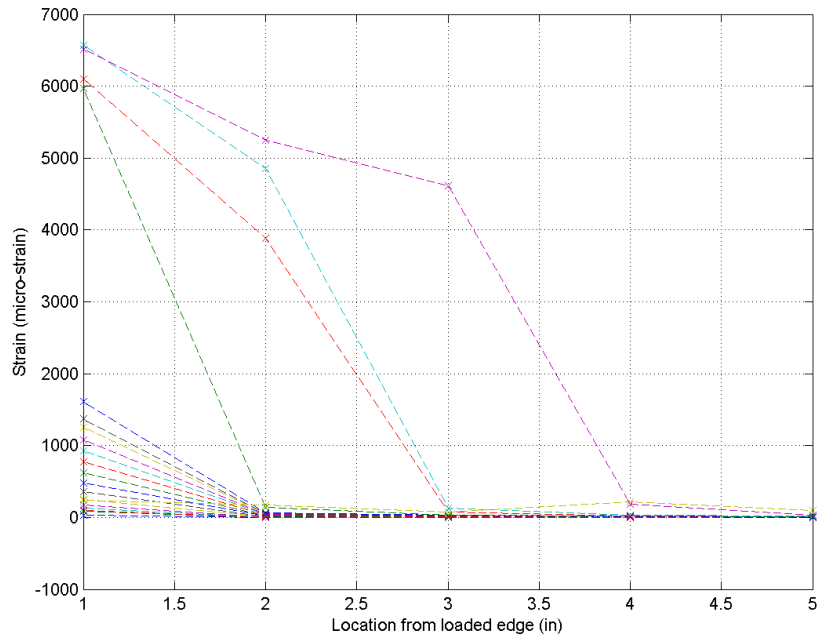


Figure 3.46 Strain Profile for Grid-SP1

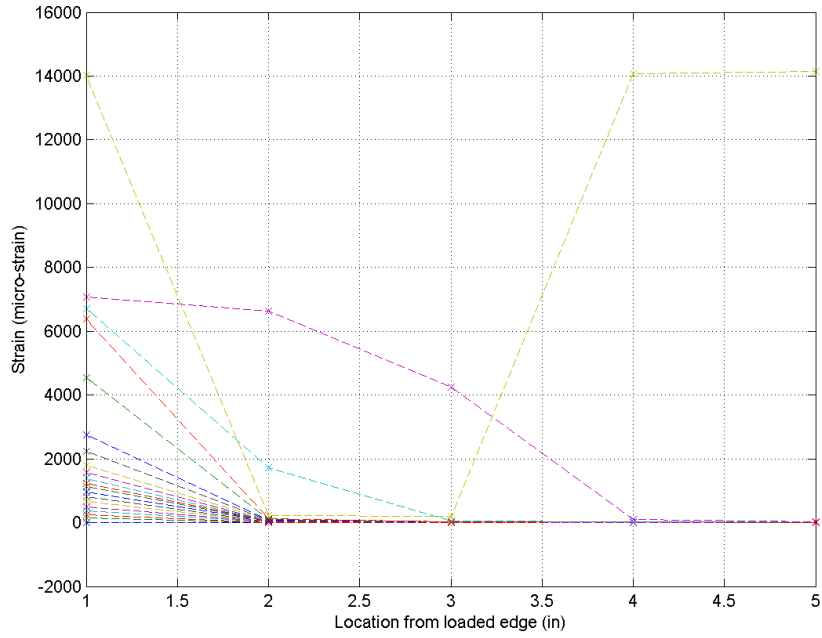


Figure 3.47 Strain Profile for Grid-SP2

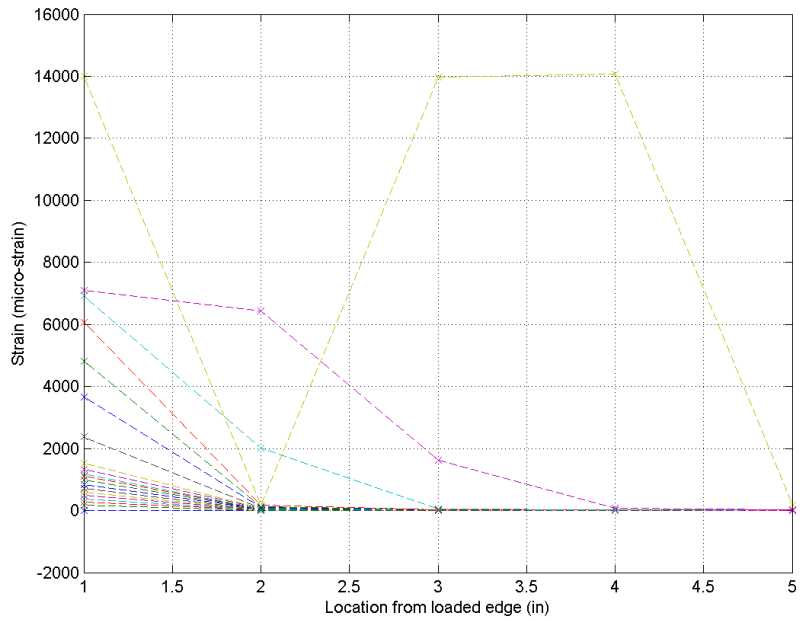


Figure 3.48 Strain Profile for Grid-SP3

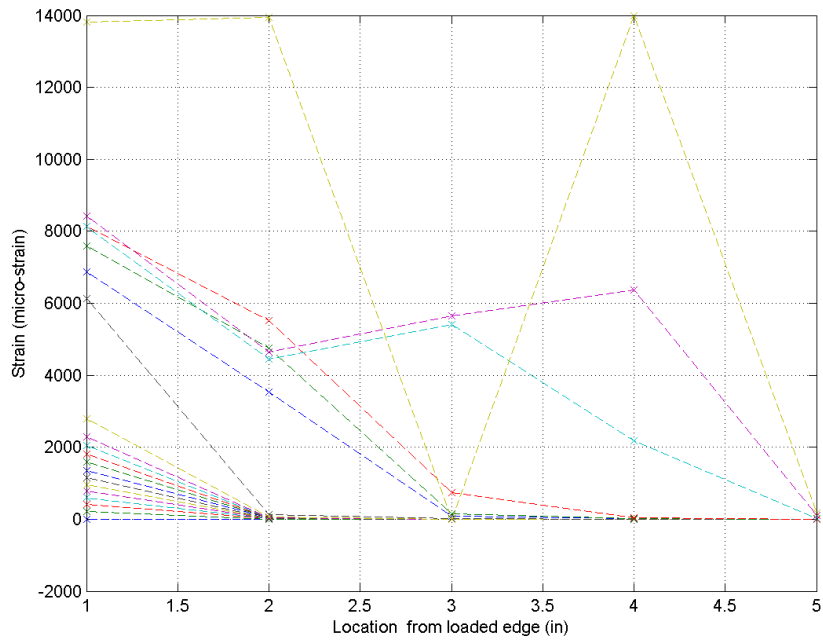


Figure 3.49 Strain Profile for Bolt-SP1

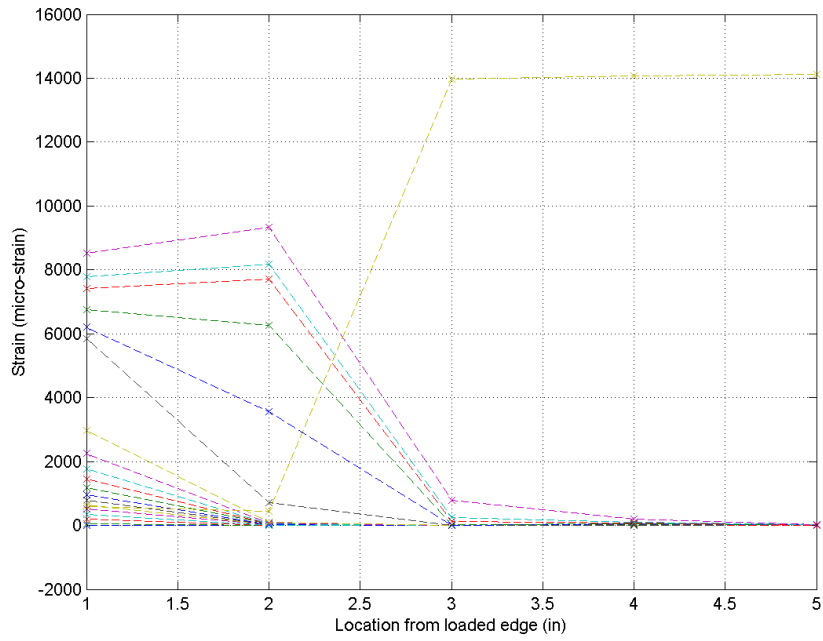


Figure 3.50 Strain Profile for Bolt-SP2

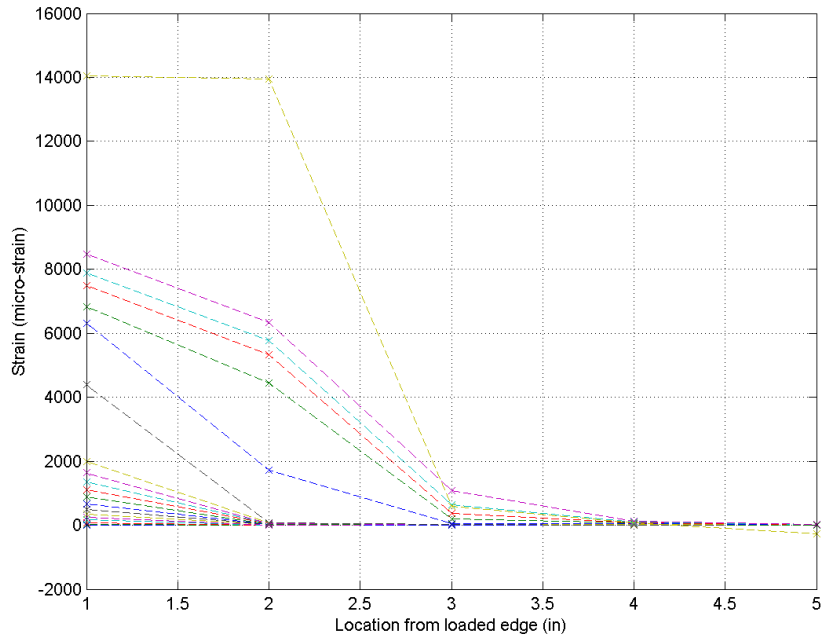


Figure 3.51 Strain Profile for Bolt-SP3

### 3.5 Conclusions

In the double lap test, all the bond failures happened at the loaded block and strain gages attached, except for two specimens from the carbon group where the debonding happened at the unloaded block with rupture of carbon fibers. The different edge length or the boundaries between the small and big specimens has no effect on the peak load. For GFRP specimens, it can be seen that maximum load is in the range of 2.7-2.8 kips except for one specimens where it exceeded 3 kips. There is a noticeable increase in CFRP specimen's results comparing to GFRP specimens. All specimens achieved the debonding failure in the micro thickness in cohesive layer. Due to the setup of this test, the debonding should be occurred and propagated equally on both sides of the specimen. Due to the fact that the eccentricity between the bottom and top machine's grips during the test is difficult to be avoided, the moment was developed and the load was not equally distributed between the two opposite side. Therefore, the debonding propagated faster on side and failure took place in one side rather than both sides. It can be shown that there is no significant difference between the two configurations of interface in the single lap test. From the results shown in Table 3.4, the results of specimens with bolts or gird mesh have almost the same peak value. So, increasing the number of gird lines in the bonded area might help to increase the peak load. The peak load values that have been achieved in double lap are greater than the values in single lap test due to the fact that the load in the double lap shear test is resisted by two sides.

# Chapter-4

---

## Waffle UHPC Deck System

### 4.1 Introduction

Movable bridges often include open grid steel deck for its light weight and ease of installation. However, inherent problems with these decks include poor rideability, susceptibility to fatigue, and high noise levels and maintenance cost (Mirmiran et al., 2009, 2012). A new generation of lightweight decks with solid riding surface are sought to address these issues, while staying within the weight limit of 21 psf for a movable bridge with a stringer spacing of 4 ft. (Saleem, 2011). With applications well beyond movable bridges, such lightweight decks are expected to include advanced construction materials, e.g., ultra-high performance concrete (UHPC), high-strength steel (HSS), and carbon fiber reinforced polymer (CFRP).

UHPC, first developed in France in the 1990's (Keierleber, 2007), consists of high-strength cementitious materials, steel fibers, ground quartz, and super plasticizer (Habel, 2006, Graybeal, 2007). UHPC has less permeability, creep and shrinkage as compared to conventional concrete (Graybeal, 2006), while it also features compressive strengths above 21 Ksi, elastic moduli over 66720 Ksi, usable tensile strengths in excess of 0.7 Ksi, and high durability and damage tolerance (Graybeal, 2005, Ahlborn, 2008). UHPC is also shown as a suitable pavement overlay (Graybeal, 2003), and has recently been applied in several bridges in the US, Canada, Europe and Asia (Blais et al., 1999, Hajar et al., 2003, and Graybeal, 2011).

HSS rebars offer another advanced option in bridge construction (El-Hacha et al., 2006), with almost 25% higher yield strength, six times more corrosion resistance and two times slower corrosion rate than conventional steel. These exceptional properties can lead to less reinforcement, longer service life and lower life-cycle costs (Kahl, 2007).

Fiber reinforced polymer (FRP) is another advanced material with high strength-to-weight ratio and excellent corrosion resistance. An FRP deck weighs 80% less than a comparable reinforced concrete deck (Mu et al., 2006). Chen and El-Hacha (2011) proposed a hybrid UHPC-FRP beam, made up of a pultruded glass FRP hollow box section with a cast-in-place UHPC layer on top and a carbon FRP sheet bonded along its soffit. Saleem (2011) conducted experiments on a hollow core UHPC deck made with pultruded carbon FRP tubes. Both systems showed potential for combining the excellent properties of FRP and UHPC. Frostlechner (2012) studied flexural behavior of a thin-walled UHPC-GFRP hollow rectangular section, and subsequently made a strong case for combining UHPC with FRP shapes or FRP reinforcement to fully utilize the benefits of the two advanced materials.

The purpose of this study was to develop a new generation of ultra-lightweight super shallow solid deck systems to replace open grid steel decks on movable bridges and as well serve as a viable alternative in bridge deck replacements across the country. The study has led to a lightweight low-profile asymmetric waffle deck made with advanced materials. The asymmetry comes from the arrangement of primary and secondary ribs, respectively perpendicular and parallel to the direction of traffic. The waffle deck is made with ultrahigh performance concrete (UHPC) reinforced with either high-strength steel (HSS) or carbon fiber reinforced polymer (CFRP) reinforcement. It was further envisioned that the ultra-high strength of UHPC is best matched with the high strength of HSS or CFRP reinforcement for an efficient system and the ductile behavior of UHPC can help mask the linear elastic response of CFRP reinforcement and result in an overall ductile system. The issues of consideration from the design and constructability perspectives have included strength and stiffness, bond and development length for the reinforcement, punching shear and panel action. A series of experiments were conducted to help address these issues. Moreover, several ancillary tests were carried out with the purpose of finding a proper anchorage system for CFRP bars. Additionally full-size panels were made for testing under heavy vehicle simulator (HVS) at the accelerated pavement testing (APT) facility in Gainesville. Detailed finite element analyses were also carried out to help guide the design of this new generation of bridge decks. The research has confirmed the superior performance of the new deck system and its feasibility resulted in numbers of publication.

Saleem et al. (Saleem, 2011 and 2012) developed a novel bridge deck system, utilizing UHPC in the form of a low-profile solid waffle slab reinforced with HSS rebars, and an asymmetric arrangement of primary and secondary ribs, respectively perpendicular and parallel to traffic. The feasibility of the proposed system was shown through a number of experiments with single and multiple ribs, and in simple or two-span configurations. Although the weight of each panel was reasonably low as 32.37 psf, the total weight of the deck system including haunches and accessories turned out to exceed the weight limits for existing movable bridges. Therefore, the main objective of the first part of the study was to improve the proposed UHPC-HSS deck system by reducing its weight below 21 psf, while still meeting the strength and ductility demands.

The second part of the study expands the work of Aaleti et al. (2011) and Heimann (2013) on UHPC waffle deck with mild steel reinforcement and the work of Saleem et al. (2011) on low-profile UHPC waffle deck with HSS reinforcement, by (a) significantly reducing the depth and weight of the panels, and (b) replacing the steel reinforcement with carbon FRP (CFRP) bars. It is believed that not only the ultra-high strength of UHPC is best matched with the high strength of CFRP reinforcement for an efficient system, but more importantly, the ductile behavior of UHPC can help mask the linear elastic response of CFRP reinforcement and result in an overall ductile system. This is the first time that UHPC and CFRP reinforcement are combined in an ultra-lightweight super shallow waffle deck for bridge applications. The issues of consideration from the design and constructability perspectives include strength and stiffness, bond and development length for the reinforcement, punching shear and panel action. A series of experiments are conducted to help address these issues for the development of this new type of bridge deck.

## 4.2 Assessment of UHPC-HSS Deck System

### 4.2.1 Experimental Work

As depicted through a three-dimensional perspective in Figure 4.1, the proposed waffle deck consists of a very thin slab with primary ribs perpendicular to the direction of traffic, and shallower and less frequent secondary ribs in the direction of traffic. In order to study the behavior of the deck, two groups of specimens were investigated; single-rib and multi-rib specimens. The experiments also aimed at finding the optimal depth of the panels.

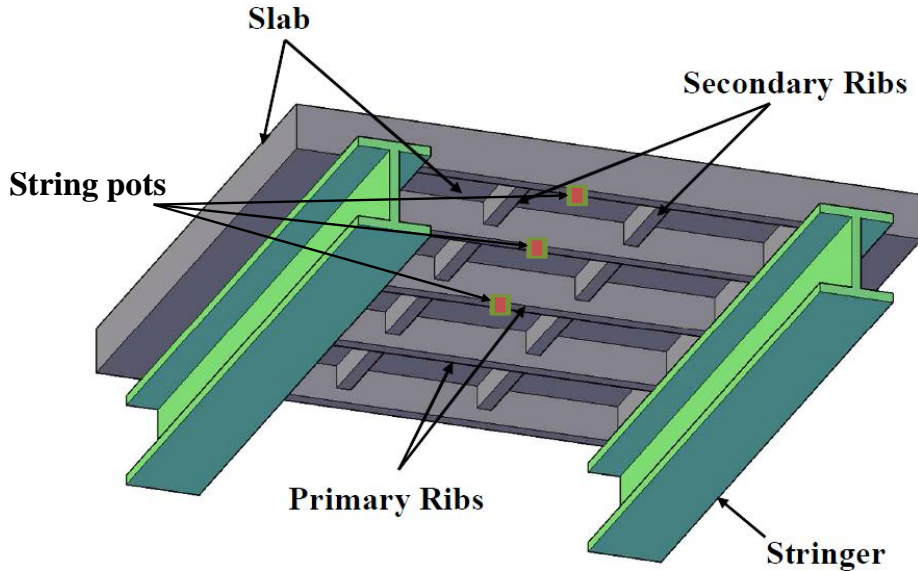


Figure 4.1 Schematics of the Proposed UHPC Waffle Deck System

### 4.2.2 Test Matrix

Table 4.1 presents the test matrix for two groups of UHPC-HSS deck specimens tested in two consecutive phases. The specimen names in the table include number of primary ribs (1 or 4), number of spans (1 or 2), overall depth (5, 4½, or 4 in.), and the duplicate number in the case of identical specimens. In Phase 1, both section geometry and reinforcement were modified from those tested by Saleem (2011), which are also shown as Phase 0 for comparison. The overall section depth, slab thickness, and the width of the primary rib were each reduced by ½ in., while the spacing of the primary ribs was increased by 3 in. The reinforcement was also reduced from No.4 to No.3 in the slab and from No.7 to No.5 in the rib. Two identical 4½ in. deep single-rib simple-span specimens were tested in this phase (Figure 4.2).

The specimens in Phase 1 weighed 0.15 psf or 33% less than those of Saleem (2011). The weight was calculated using a unit weight of 150 lb/ft<sup>3</sup> for UHPC, and includes a 4½ in. wide solid block to support the deck on each stringer. Test results, as will be presented later, still showed excess capacity over demand. Hence, the section was further optimized in Phase 2, reducing its

depth by another ½ in. (Figure 4.2) and lowering its weight to only 20.26 psf. In this phase, one single-rib simple-span specimen was tested, along with a single-rib two-span specimen and a multi-rib simple-span specimen (Figures 4.2 and 4.3). The two-span and multi-rib specimens were utilized to investigate the continuity behavior of the deck, its punching shear behavior, and load distribution among the ribs.

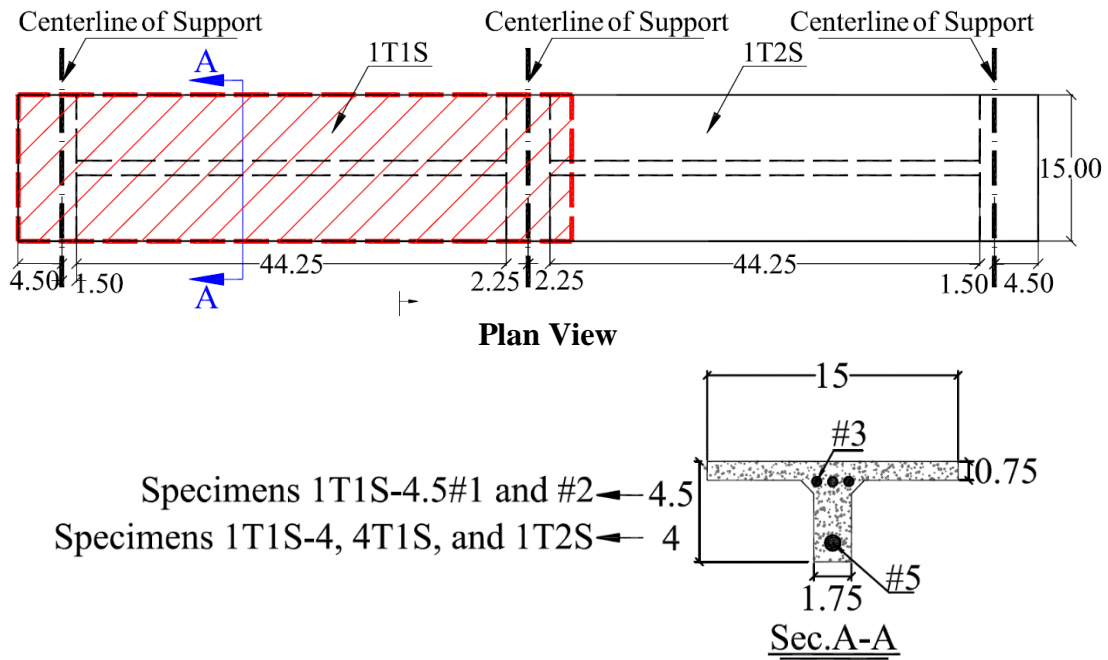
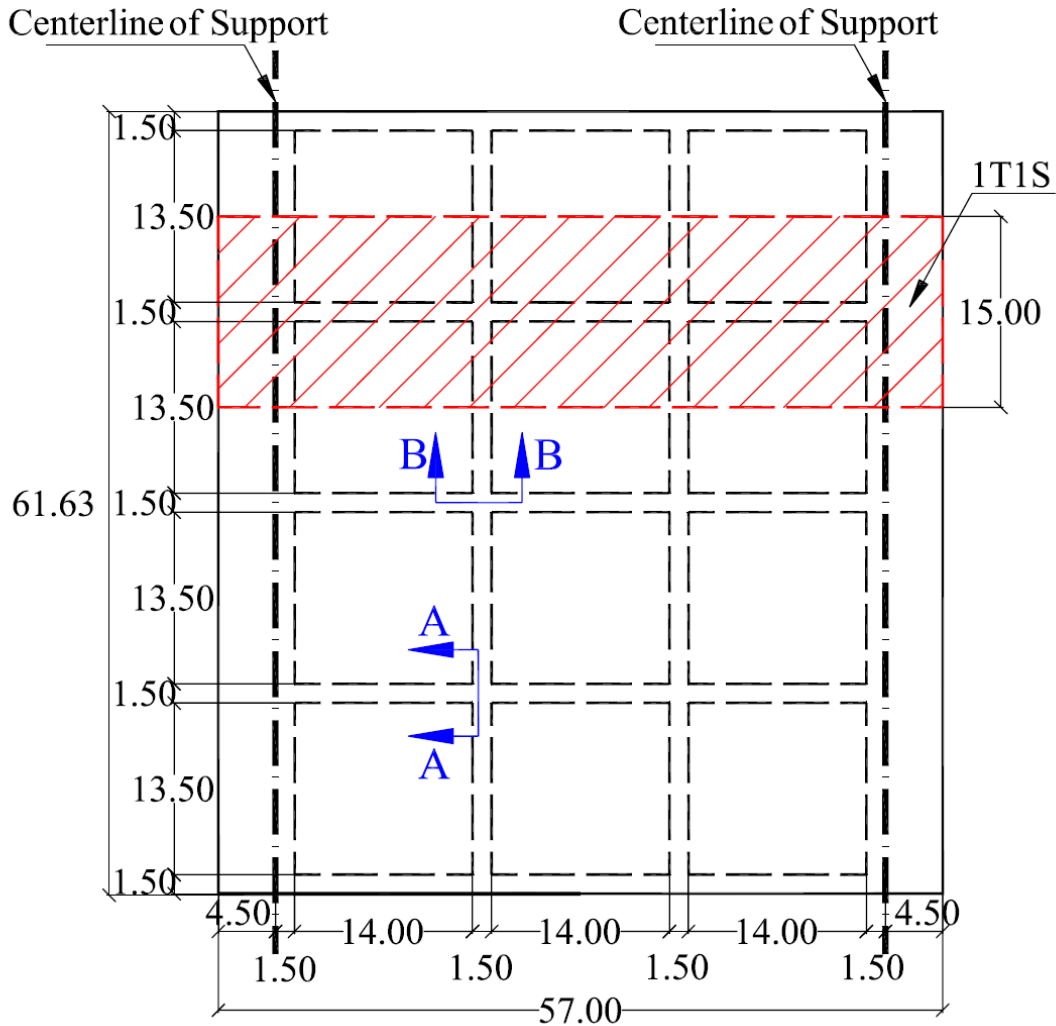


Figure 4.2 Schematics of Single-Rib, Simple-Span, or Two-Span Specimens

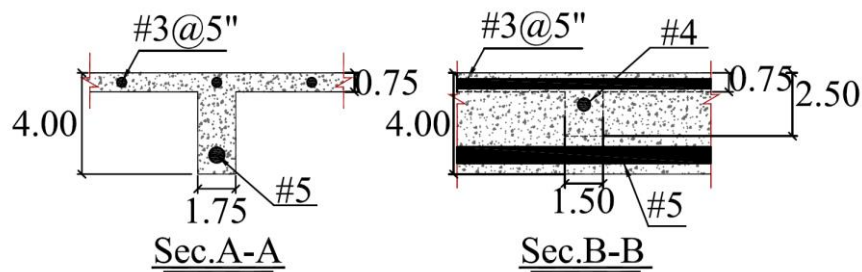
Table 4.1 Test Matrix

Phase	Specimen Name	Overall Depth (in.)	Rib Spacing (in.)	Slab Thickness (in.)	Unit Weight (psf)	28-Day UHPC Compressive Strength (ksi)	Flexural Reinforcement	
							Slab	Primary Rib
0*	1T1S-5#1	5	12	1¼	32.37	18	No. 4	No. 7
	1T1S-5#2					27		
	4T1S-5					26		
	1T2S-5					22		
1	1T1S-4½#1	4½	15	¾	21.72	24	No. 3	No. 5
	1T1S-4½#2					24		
2	1T1S-4	4	15	¾	20.26	27	No. 3	No. 5
	4T1S					27		
	1T2S					25		

\* Taken from Saleem (2011).



**Plan View**



\*All measurements are in inch.

Figure 4.3 Schematics of Multi-Rib Simple-Span Specimen

#### 4.2.3 Specimen Preparation and Material Properties

Formwork was made using Styrofoam and timber (Figure 4.4). HSS rebars made by HSS Technologies of Irvine, CA, were used as primary reinforcement with yield strength of 100 ksi, as reported by the manufacturer. Rebars in primary ribs were all anchored using 180° hook at

both ends. Transverse ribs included a No. 4 rebar. Only multi-rib specimen featured transverse ribs to help with load distribution among its ribs, and to assess the punching shear behavior of the deck. A clear cover of  $\frac{1}{2}$  in. was maintained for all rebars.

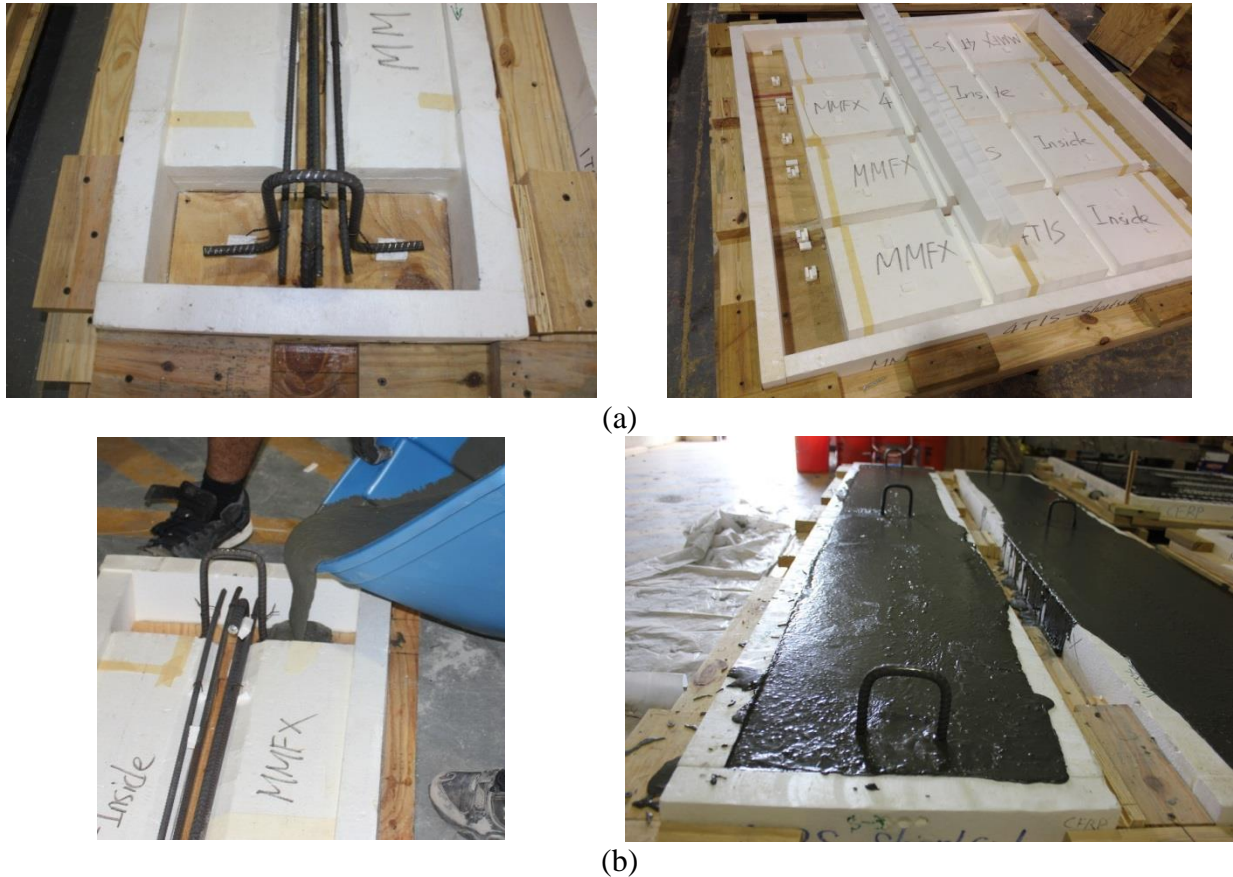


Figure 4.4 Specimen Preparation: (a) Formwork, and (b) Casting

Ductal<sup>®</sup>, a commercially available UHPC product, made by Lafarge North America, was used in this study. It is composed of premix powder (cement, silica fume, ground quartz and sand), water, superplasticizer, and 2% metallic fibers by volume. The fibers were  $\frac{1}{2}$  in. long with a tensile strength of 406 ksi. Six different batches of UHPC were mixed for casting the specimens (Figure 4.4). All specimens were air cured in the laboratory for a period of 28 days. Two companion 4 in.  $\times$  8 in. cylinders were used to measure the average 28-day compressive strength of each batch, as reported in Table 4.1.

#### 4.2.4 Test Setup and Instrumentation

A 10 in.  $\times$  20 in. steel plate was used to simulate the prescribed dual tire wheel load of an HS20 truck. The simple-span specimens were subjected to a single load at mid-span (Figures 4.5a and 4.7a), whereas the two-span specimen was under two equal loads applied simultaneously in the middle of both spans (Figure 4.10a). At the conclusion of its flexure test, the multi-rib specimen was further tested using the same load patch to determine the punching shear capacity of its thin slab (Figure 4.9a). Several strain gauges were used to monitor responses of HSS rebars and UHPC at critical points. String pots were used to measure deflections at strategic locations.

Loading was applied using a 230-kip capacity hydraulic actuator, at an average rate of 0.03 in./min. The data were recorded at a frequency of 1 Hz, and tests were stopped at 30% load drop, unless preceded by a clear sign of failure due to significant deflection, which may make the specimens unbalanced.

#### **4.2.5 Test Results and Discussion**

Table 4.2 presents a summary of test results. Also shown in the table are the required live load demands calculated using the equivalent strip method and the deck slab design table for each group of specimens based on the specimen width, load factors, multiple presence factors, dynamic load allowance, and the loading configuration. The table shows the over-capacity for each specimen as well as over-capacity per unit weight of the deck panel. The optimized specimens have comparable over-capacity per unit weight as those of Saleem (2011), demonstrating the effectiveness of the new design. The table also shows measured deflections for each specimen at the levels of service and ultimate loads. The ratio of these two deflection levels indirectly suggests a reasonable ductility for each deck specimen.

Figure 4.5 shows the test setup, failure mode, and load-deflection responses of single-rib simple-span specimens. Failure was initiated by minor web shear cracks near supports. Minor flexural cracks were also present near mid-span, but did not seem to have an impact on the failure. As the load increased, shear cracks propagated towards the slab near the loading plate. These cracks gradually widened, leading to eventual failure and a significant load drop, much the same as those observed by Saleem (2011). Figure 4.5c shows the load-deflection responses of the three specimens tested in this study, as well as the two deeper specimens tested by Saleem (2011). Deflections are averages of three recorded values (D1-D3) at mid-span, as shown in the figure inset. The ultimate and service demand loads are also shown, as described earlier. Given its smaller section and reduced reinforcement, while the capacity of Specimen 1T1S-4 is about half of those tested by Saleem (2011), it is still twice its expected demand.

Table 4.2 Summary of the Test

Phase	Specimen Name	Service Load Deflection (in.)	Ultimate Deflection (in.)	Ultimate Load (kip)	Demand Load (kip)	Capacity/Demand	Capacity/Demand per Unit Weight
0*	1T1S-5#1	0.06	0.98	40.02	8.21	4.9	0.15
	1T1S-5#2	0.1	0.98	46.99		5.7	0.18
	4T1S-5	0.19	0.79	84.98	34.17	2.5	0.08
	1T2S-5	0.9	1.26	55.08	12.52	4.4	0.14
1	1T1S-4½#1	0.1	0.83	27.65	10.25	2.7	0.12
	1T1S-4½#2	0.14	0.87	24.73		2.4	0.11
2	1T1S-4	0.15	0.91	22.71		2.2	0.11
	4T1S	0.18	0.87	51.48	42.04	1.2	0.06
	1T2S	0.07	0.87	44.96	15.65	2.9	0.14

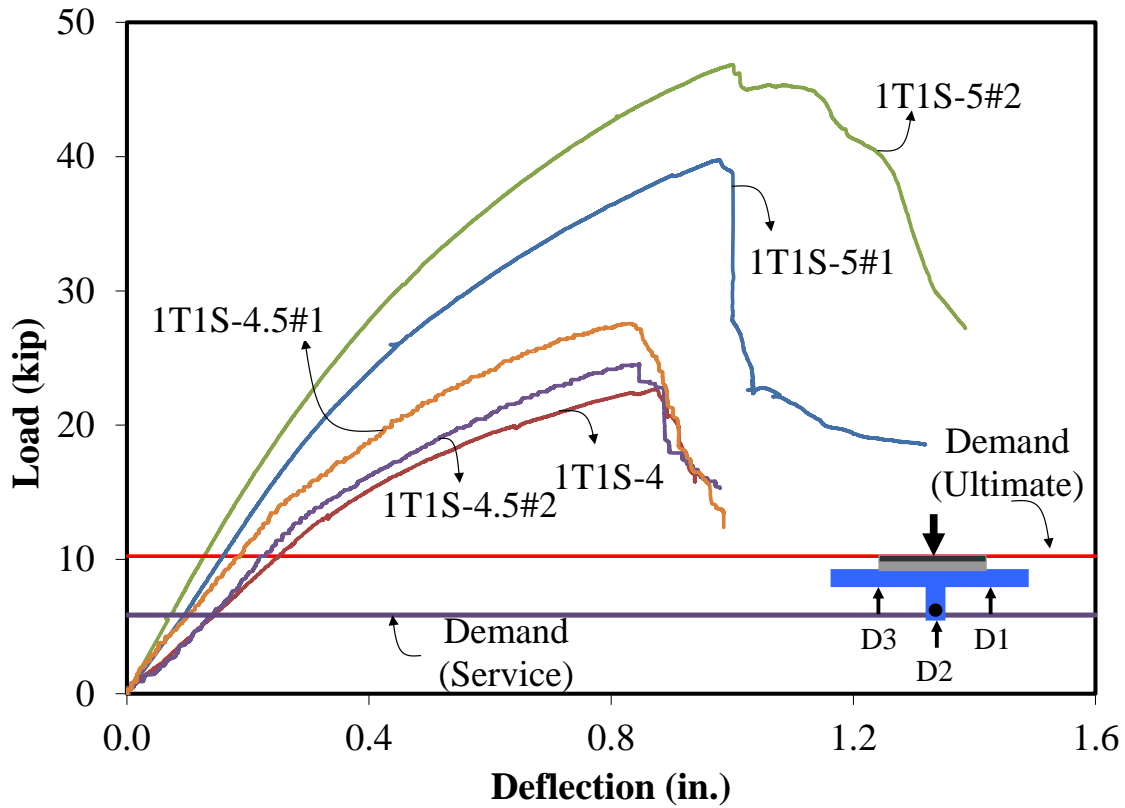
\* Taken from Saleem (2011)



(a)



(b)



(c)

Figure 4.5 Flexure Tests of Specimens 1T1S: (a) Test Setup, (b) Failure Mode, and (c) Load-Deflection Responses (Note: Curves 1T1S-5#1 and #2 from Saleem 2011)

Figure 4.6 shows load-strain responses for Specimens 1T1S-4.5#1 and 1T1S-4, based on strain gauges attached at the mid-span to the rebar in the primary rib. Although yielding of rebar in both specimens occurs at a level much higher than the service load demand, it may generally be construed as a good indication of a fairly ductile behavior. It should be noted that in the face of dominant shear cracks, Xia et al. have demonstrated that the ductile behavior of these decks is more representative of the fiber pull-out mechanism in UHPC and the dowel action of the HSS bars rather than traditional yielding of steel reinforcement.

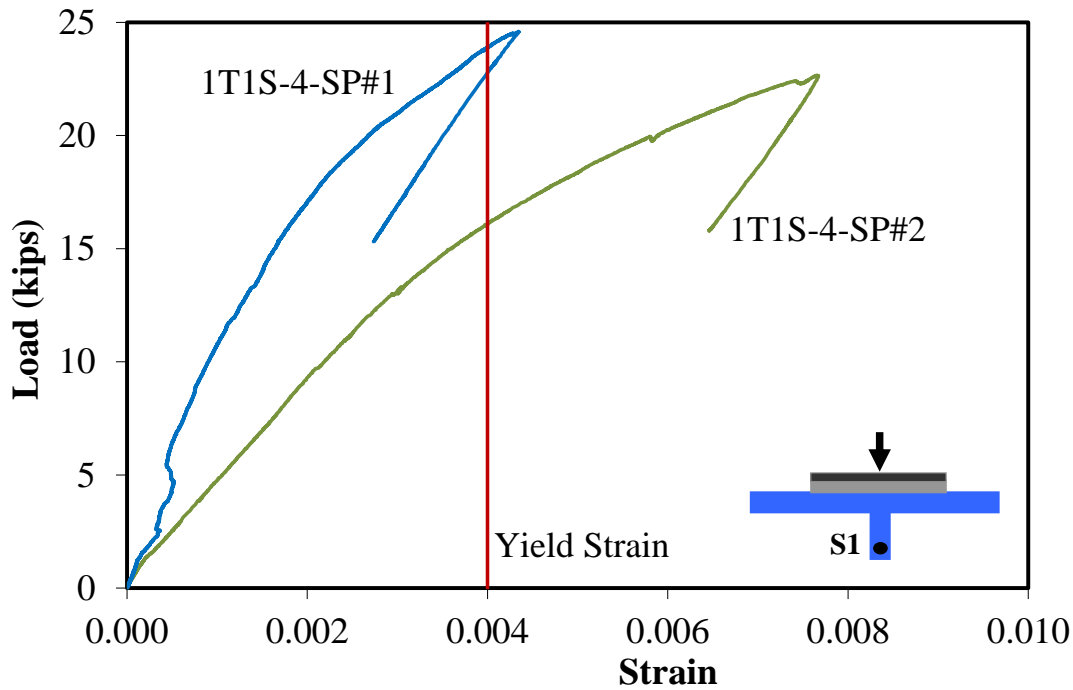


Figure 4.6 Load-Strain Response of Rebars in Specimens 1T1S

#### 4.2.5.1 Panel Action

Figure 4.7 shows the test setup, failure mode and load-deflection responses of the multi-rib simple-span specimen. Deflections are three recorded values (D1-D3) at mid-span, as shown in the figure inset. The failure mode was generally similar to that of single-rib simple-span specimens, in that it initiated with diagonal shear cracks near the supports, albeit mainly in the interior ribs. With the increase of the load, shear cracks grew both in width and length, especially in the center rib, leading to the failure accompanied by a considerable load drop.

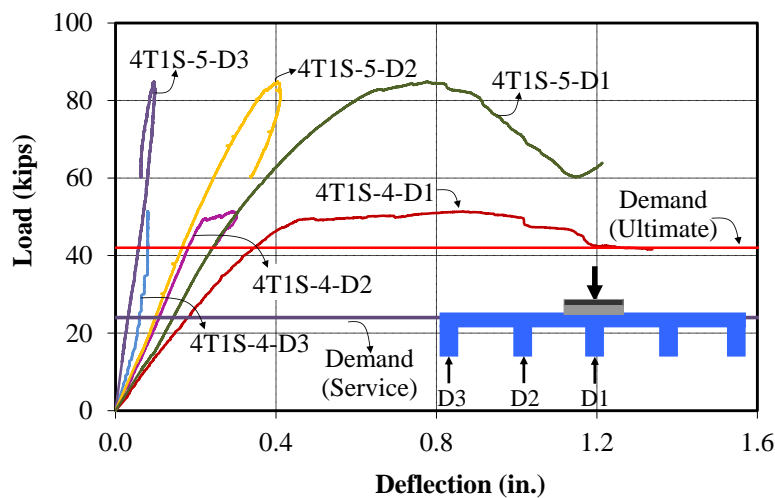
As shown in Figure 4.7c, Specimen 4T1S showed an almost linear response up to about twice the service load deflection, while exhibiting a plastic behavior thereafter until failure. In comparison to the single-rib specimens (Figure 4.5c), the presence of multiple ribs helped increase the ductility of the proposed deck panel significantly through a considerable plastic deformation. This confirms earlier findings that failure of the proposed UHPC-HSS deck panel system is clearly ductile, despite the presence of dominant shear cracks.

For comparison, Figure 6c also includes the load-deflection response curves for the deeper specimen tested by Saleem (2011). Although specimen 4T1S-4 has a 20% shallower section and

28% less reinforcement, while its capacity is about 60% of Specimen 4T1S-5, it still exceeds its expected demand by at least 22%.

Load distribution among the ribs may be calculated based on mid-span deflections of each rib or mid-span strains in HSS bar in each rib. Using either approach, the load distribution among the ribs is found as 33% for the center rib and 22% and 11% for the next two ribs. These factors are quite similar to those reported by Saleem et al. (2011).

Figure 4.8 shows load-strain responses for Specimen 4T1S based on the strain gauges attached to the rebars in each of the primary ribs at the mid-span. The strain gauge in the exterior rib was damaged before reaching the ultimate load. Of the other two, the largest strain occurred in the rebar of the center rib, although it was still below the yield limit. As discussed earlier, one should note the sizeable displacement-based ductility of the deck system (Figure 4.7a); despite the apparent shear failure and the relatively low strain levels in the flexural reinforcement.



(c)

Figure 4.7 Tests of Specimens 4T1S: (a) Test Setup, (b) Failure Mode, and (c) Load-Deflection Responses (Note: Curves 4T1S-127-D1, D2, and D3 from Saleem 2011)

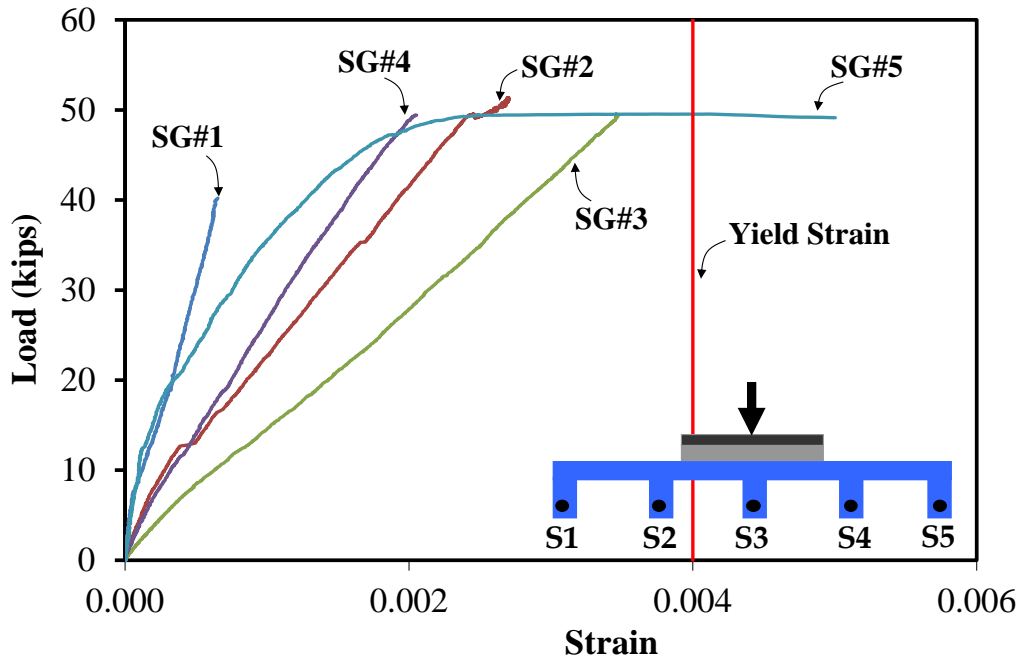


Figure 4.8 Load-Strain Response of Rebars in Specimen 4T1S

#### 4.2.5.2 Punching Shear Behavior

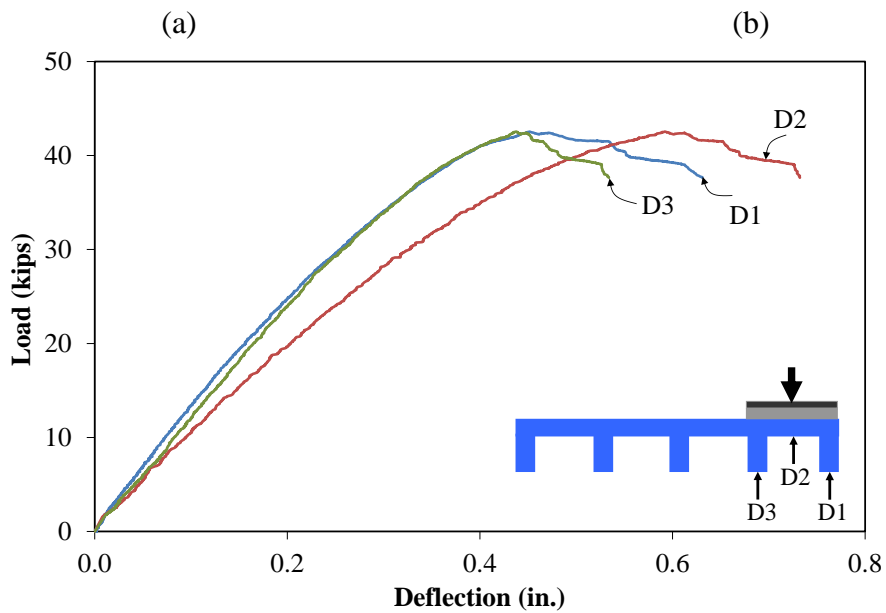
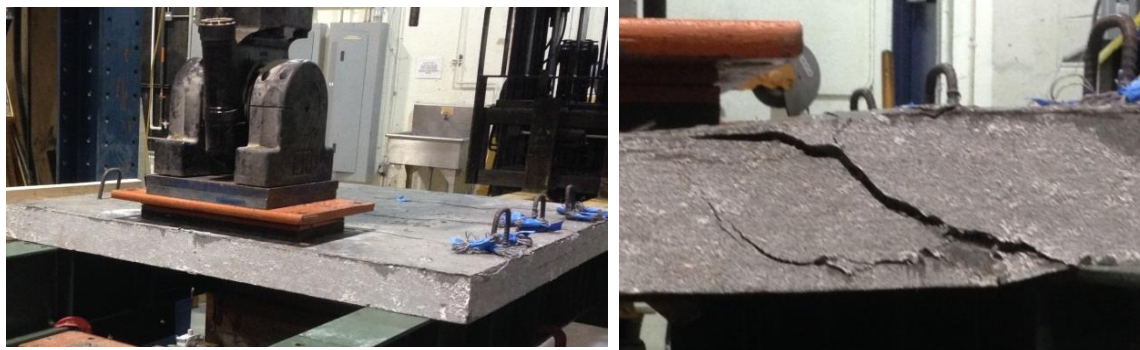
Figure 4.9a shows the reserved punching shear test carried out on an exterior panel of Specimen 4T1S at the conclusion of its flexural test described above. The load was applied using the same loading plate on the slab between the first two ribs. Figure 8b shows the failure governed by major cracks in the primary ribs adjacent to the loading patch. No sign of punching shear, however, was observed on the top of the slab around the loading plate. Figure 8c shows the load-deflection responses. As shown in the figure inset, the deflections (D1-D3) were recorded at mid-span, under the loading patch and the two adjacent ribs. A sizeable deflection of 0.6 in. was measured in the middle of the panel right under the loading patch at the ultimate load of 42.49 kips. The ultimate load was about 17% lower than that observed in the first flexure test of the specimen. Clearly, the asymmetric loading did not allow full contribution of other ribs. The test was stopped after the load dropped to 37.32 kips due to excessive damage in the exterior rib.

Harris and Roberts-Wollmann (2005) proposed a modification to ACI equation for concrete breakout strength to predict the punching shear capacity of thin UHPC slabs

$$V_c = 0.38 f_{ten} \frac{[(3h+a) \times (3h+b)] - (a \times b)}{\sqrt{h}} \quad (2.1)$$

where  $f_{ten}$  = tensile strength of UHPC,  $h$  = thickness of the UHPC slab, and  $a$  and  $b$  = dimensions of the loading plate. Using a tensile strength of 1.1 ksi for a 10 in.  $\times$  20 in. loading plate, the punching shear capacity of the  $\frac{3}{4}$  in. slab is calculated as 6.97 kips, which is substantially lower than its experimentally measured capacity of 42.49 kips. This explains why no sign of punching

shear was observed in the slab, clearly because the spacing of the primary ribs prevents a punching shear failure of the slab, and instead promotes one-way shear failure of primary ribs.



(c)  
 Figure 4.9 Punching Shear Test of Specimen 4T1S: (a) Test Setup, (b) Failure Mode, and (c) Load-Deflection Responses

#### 4.2.5.3 Continuity Effects

The effects of continuity and negative moments were investigated using the single-rib two-span Specimen 1T2S. Figure 4.10 shows the test setup, deflected shape, and the failure mode, where diagonal cracks initiated near an exterior support in one span and propagated to the slab leading to the eventual failure. Minor shear cracks were also present in the other span, while some flexural cracks were observed on top of the slab over the interior support.

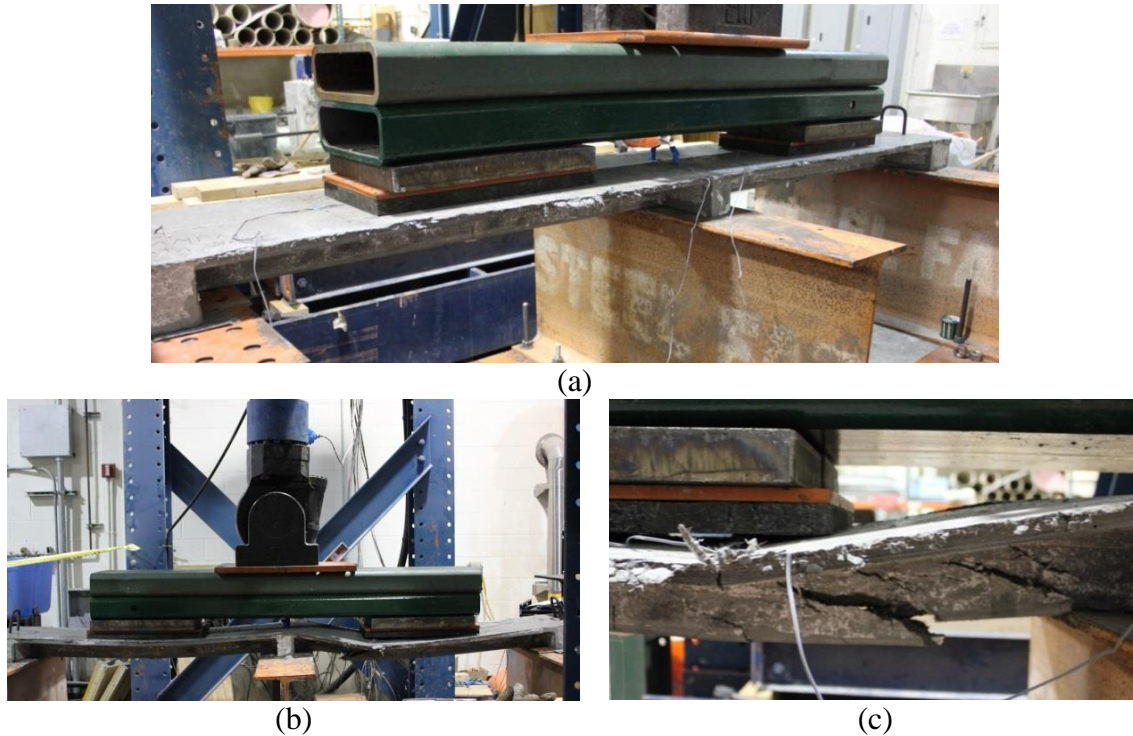


Figure 4.10 Flexure Tests of Specimen 1T2S: (a) Test Setup, (b) Deflected Shape, and (c) Failure Mode

Figure 4.11 shows the load-deflection response for the two measured mid-span displacements. Also shown for comparison are the load-deflection response curves for the deeper specimen tested by Saleem (2011). The comparison shows that although the new design has led to 18% reduction in the ultimate load, the capacity is still close to three times that of the expected demand, while the weight has been reduced by 37%. It is equally important to note the apparent high displacement-based ductility of the deck.

From the perspective of serviceability, the specimen showed a deflection of 0.07 in. at the service demand of 8.92 kips. This corresponds to  $L/697$ , where  $L$  = center to center spacing of stringers, i.e., 4 ft. Noting the continuity effect of typical decks spanning over multiple stringers, one can calculate a correction factor of 0.74 comparing the deflections of two-span and five-span decks under two wheel loads. As such, the corrected deflection of the proposed deck turns out to be  $L/942$ , which clearly meets the deflection limit of  $L/800$ .

Figure 4.12 shows the load-strain response of Specimen 1T2S, based on its measured rebar strains at both mid-spans. Similar to the load-displacement response, the strain in the north span was higher than that at the other span, where the gauge was damaged before reaching the ultimate load. As discussed earlier, the load-deflection behavior of the specimen was very ductile, while the rebar clearly did not reach its yield strain in either span.

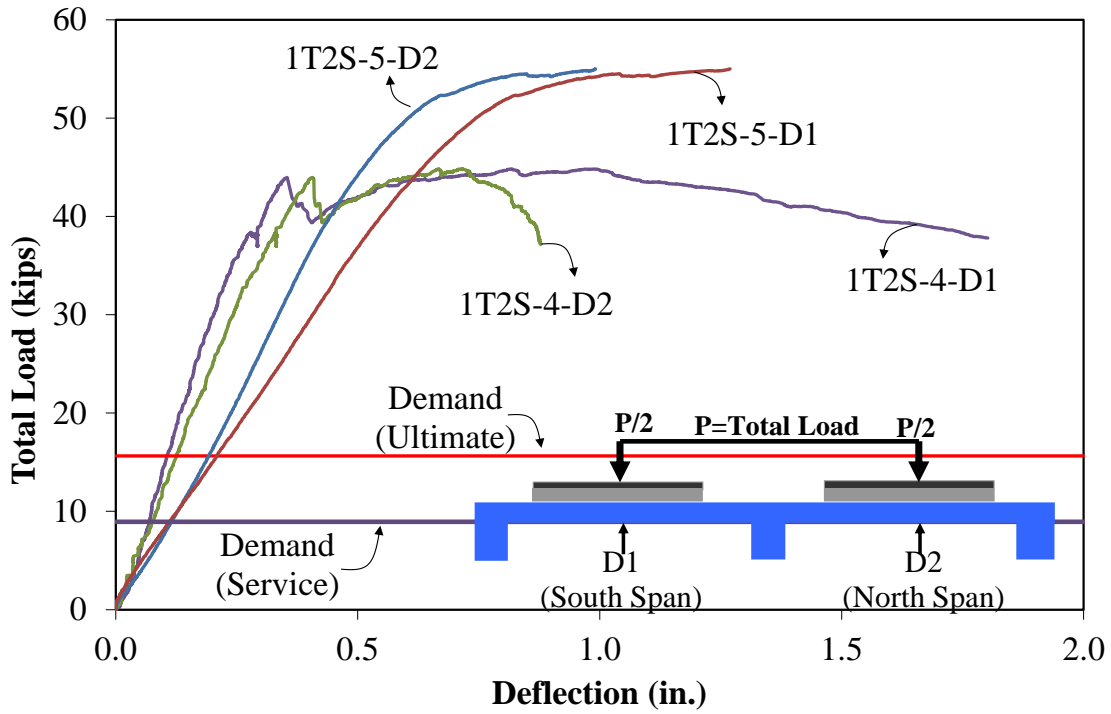


Figure 4.11 Load-Deflection Responses of Specimens 1T2S (Note: Curves 1T2S-127-D1 & D2 from Saleem 2011)

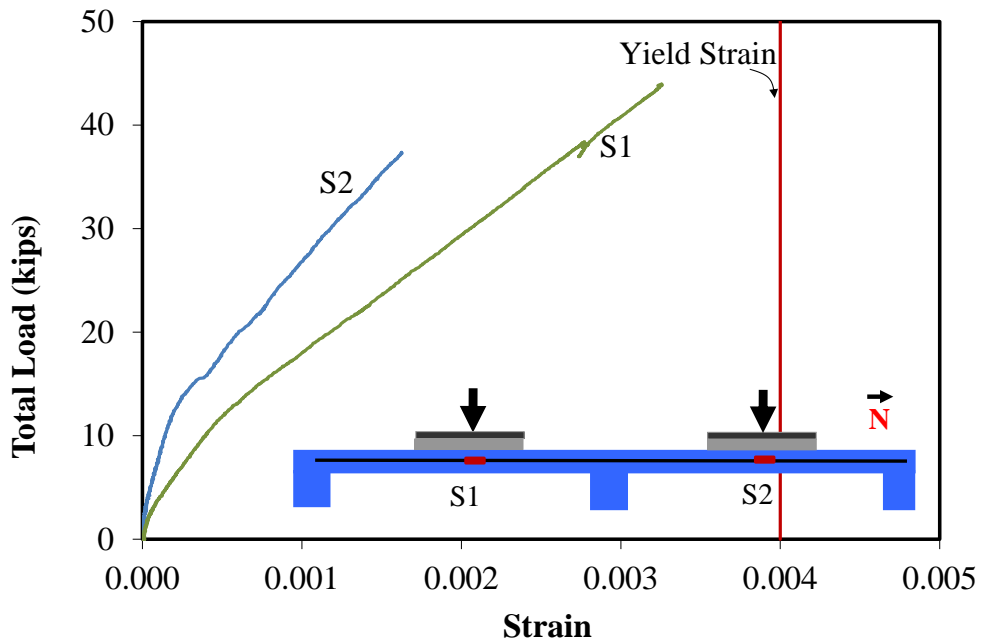


Figure 4.12 Load-Deflection Responses of Specimens 1T2S (Note: Curves 1T2S-127-D1 & D2 from Saleem 2011)

#### **4.2.6 Summary of Findings from UHPC-HSS Deck Tests**

A comprehensive experimental study was carried out to develop an optimized lightweight bridge deck system primarily for movable bridges, while it is expected to have extended applications in other bridge deck replacement and widening projects. The objective of the research was to reduce the weight of a recently developed low-profile asymmetric waffle UHPC slab reinforced with HSS rebars. A weight limit of 21 psf was imposed on the bridge deck with a stringer spacing of 4 ft. In a two-step optimization process, both the size and the reinforcement of the deck were modified, reducing the weight by over 37%. Test results showed that the optimized section can suitably meet the load demand, ductility, and serviceability requirements, while staying within the weight limits for movable bridges. The main conclusions of this study are as follows:

1. The proposed deck system fails in a clearly ductile manner, despite its apparent shear failure and in the absence of consistent yielding in steel reinforcement.
2. The proposed deck system is not susceptible to punching shear of its thin slab, due to the arrangement of the primary and secondary ribs, which promotes one-way shear of the primary ribs instead.

The load distribution for the center rib in the optimized deck is about 33%, very similar to that observed for the original deeper deck

### **4.3 Assessment of UHPC-CFRP Deck System**

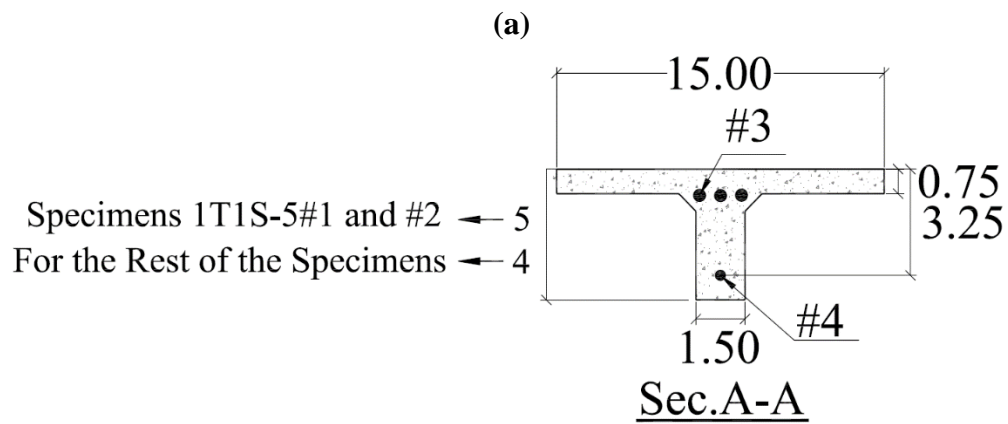
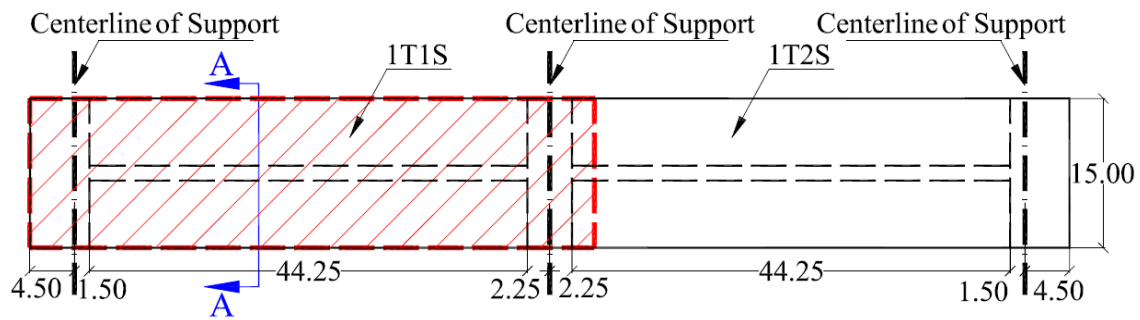
#### **4.3.1 Test Matrix and Specimen Preparation**

Table 4.3 shows the test matrix for this study with two groups of specimens made and tested in two consecutive phases. The specimen names include number of ribs (T), number of spans (S), specimen depth and sample number (if more than one). Group 1 consisted of four single-rib specimens tested in a simple-span configuration, with two identical samples for each of the two depths of 4 and 5 inch (see Figure 4.13). Group 2 included three specimens, all with the same depth of 4 inch, but in three different configurations; single-rib simple-span, single-rib two-span, and multi-rib simple-span (see Figure 4.13). The multi-rib specimen featured  $2\frac{3}{4}$  inch deep transverse ribs to help with load distribution among primary ribs. For comparison, the table also shows three groups of UHPC waffle deck specimens with HSS reinforcement tested in previous studies (Saleem et al. 2011, Mirmiran et al., 2014).

Table 4.3 Test Matrix

Group	Specimen Name	Test Phase	Overall Depth (in.)	Rib Spacing (in.)	Slab Thickness (in.)	Unit Weight (psf)	28-Day UHPC Compressive Strength (ksi)	Flexural Reinforcement	
								Slab	Primary Rib
<b>UHPC-CFRP</b>									
CFRP-1	1T1S-4#1	1	4	15	$\frac{3}{4}$	18.80	24	No. 3	No. 4
	1T1S-4#2	1					24		
	1T1S-5#1	1	5			24			
	1T1S-5#2	1				24			
CFRP-2	1T1S-4#3	2	4	15	$\frac{3}{4}$	18.80	27	No. 3	No. 4
	4T1S-4	2					27		
	1T2S-4	2					26		
<b>UHPC-HSS</b>									
HSS-0 <sup>1</sup>	1T1S-5#1	0	5	12	$1\frac{1}{4}$	32.37	18	No. 4	No. 7
	1T1S-5#2	0					27		
	4T1S-5	0					26		
	1T2S-5	0					22		
HSS-1 <sup>2</sup>	1T1S-4 $\frac{1}{2}$ #1	1	4 $\frac{1}{2}$	15	$\frac{3}{4}$	21.72	24	No. 3	No. 5
	1T1S-4 $\frac{1}{2}$ #2	1					24		
HSS-2 <sup>2</sup>	1T1S-4	2	4	15	$\frac{3}{4}$	20.26	27	No. 3	No. 5
	4T1S	2					27		
	1T2S	2					25		

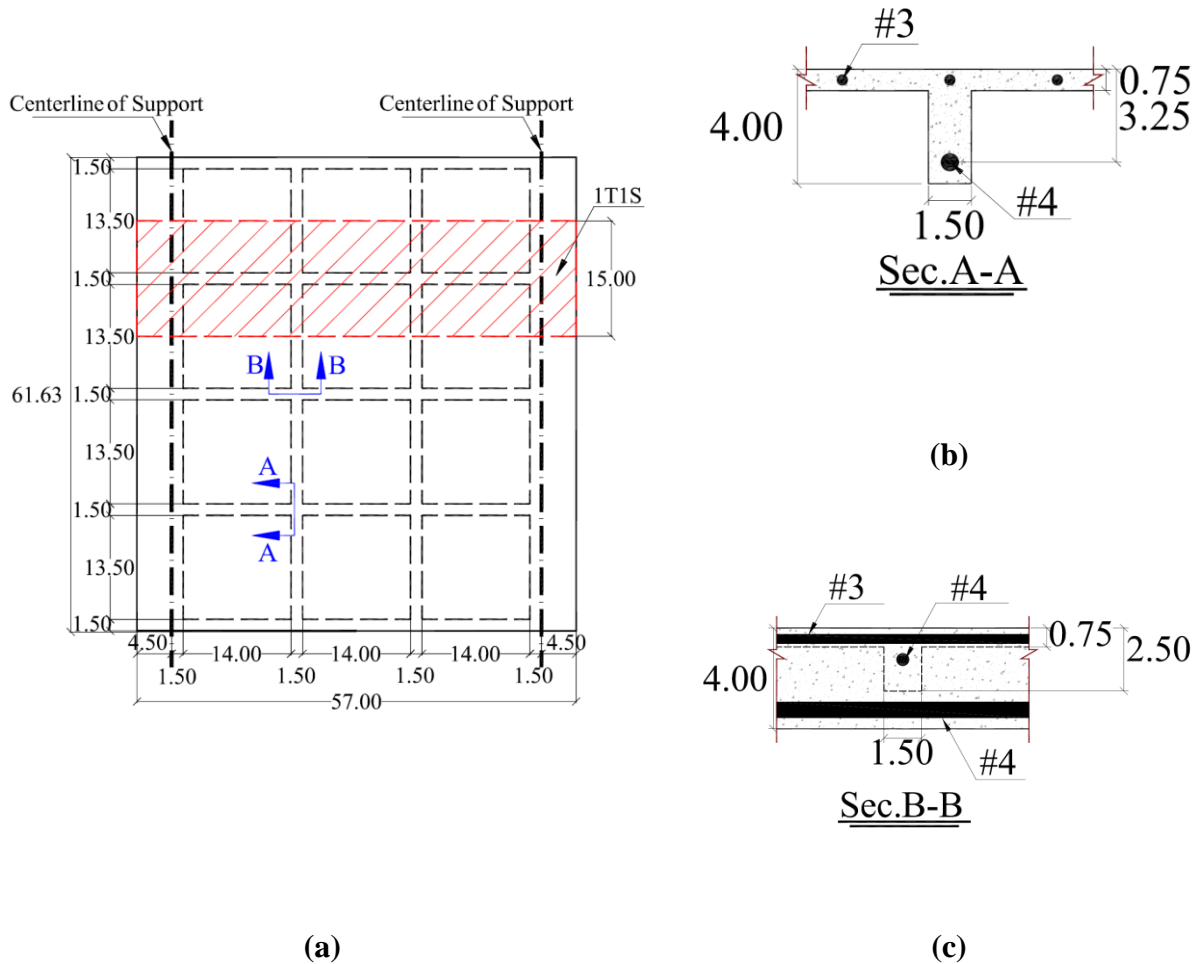
<sup>1</sup> Taken from Saleem et al. (2011).<sup>2</sup> Taken from Mirmiran et al. (2015).



\*All measurements are in inch.

(b)

Figure 4.13 Schematics Single-Rib Specimens in Simple-Span or Two-Span Configurations:  
 (a) Plan View, and (b) Section



\*All measurements are in inch.

Figure 4.14 Schematics of Multi-Rib Simple-Span Specimen: (a) Plan View, and (b) and (c) Sections

Ductal<sup>®</sup>, a commercially available UHPC product, made by Lafarge North America, was used. It is composed of a premix powder (cement, silica fume, ground quartz and sand), water, superplasticizer, and 2% metallic fibers by volume. The fibers were ½ inch long with a tensile strength of 406 ksi. Six different batches of UHPC were mixed for casting the specimens in formwork made of Styrofoam and timber (see Figure 4.15). All specimens were air cured in the laboratory for a period of 28 days. Two companion 4 × 8 inch cylinders were used to measure the average 28-day compressive strength of each batch, as shown in Table 4.3. A C-grid CFRP mesh made by Chomarat of Anderson, SC, was used in the thin slab to improve its load-carrying capacity. The mesh has an elastic modulus of 34083 ksi and an ultimate strain of 0.76%. ASLAN 200 CFRP bars made by Hughes Brothers of Seaward, NE, were used as primary reinforcement with a clear cover of ½ in. Table 4.4 lists the geometric and material properties of CFRP bars.



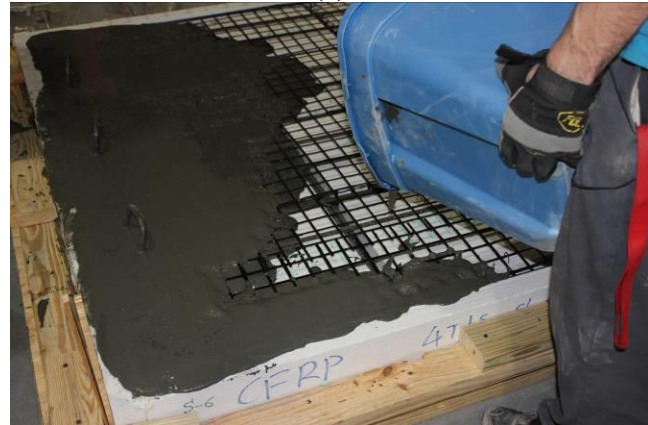
(a)



(c)



(b)



(d)

Figure 4.15 Specimen Preparation: (a) & (b) Formwork, and (c) & (d) Casting

Table 4.4 Geometric and Material Properties of CFRP Bars

Nominal Diameter (in)	Cross-Sectional Area <sup>1</sup> (in. <sup>2</sup> )	Nominal Cross-Sectional Area <sup>2</sup> (in. <sup>2</sup> )	Tensile Strength (ksi)	Modulus of Elasticity (psi 10 <sup>6</sup> )	Ultimate Strain (%)
3	0.121	0.110	315	18	1.75
4	0.201	0.196	300	18	1.67

Note: As reported by the manufacturer.

<sup>1</sup> Cross-sectional area determined by immersion testing, as per ASTM D7205, Section 11.2.5.

<sup>2</sup> Cross-sectional area used in tensile strength calculations.

Figure 4.16 shows the anchorage for the main CFRP bars in the specimens of Group 1 as a series of wrapped unidirectional E-glass fiber fabric (SikaWrap Hex 100G), made by Sika Corp. of Lyndhurst, NJ. The GFRP wrap was impregnated using Sikadur 32 Hi-Mod epoxy resin by the same manufacturer, for a total thickness of  $\frac{3}{4}$ -inch. The end surface of the wrap was then ground to facilitate monitoring of the bar slippage. As seen in Figure 4.16b, the anchorage was found insufficient to prevent the slippage of CFRP bar. Therefore, for specimens of Group 2, a more elaborate anchorage system was adopted from Schesser et al. (2013), consisting of a grout-filled steel tube. The tube was sized according to ASTM Standard D7205M (2011) with a 10-inch length,  $\frac{1}{2}$ -inch outside diameter and  $\frac{1}{4}$ -inch wall thickness. The tube was filled with Bustar, an expansive grout made by Demolition Technologies of Greenville, AL. A wooden frame was made to ensure proper alignment of CFRP bars during the grouting process (Figure 4.17a). A gauge length of  $\frac{3}{4}$ -inch was used for the bars, with at least  $\frac{1}{4}$ -inch of the bar exposed at each end (Figure 4.17b) to help measure slippage. The ancillary tests, as will be described later, showed no bar slippage for this anchorage system.

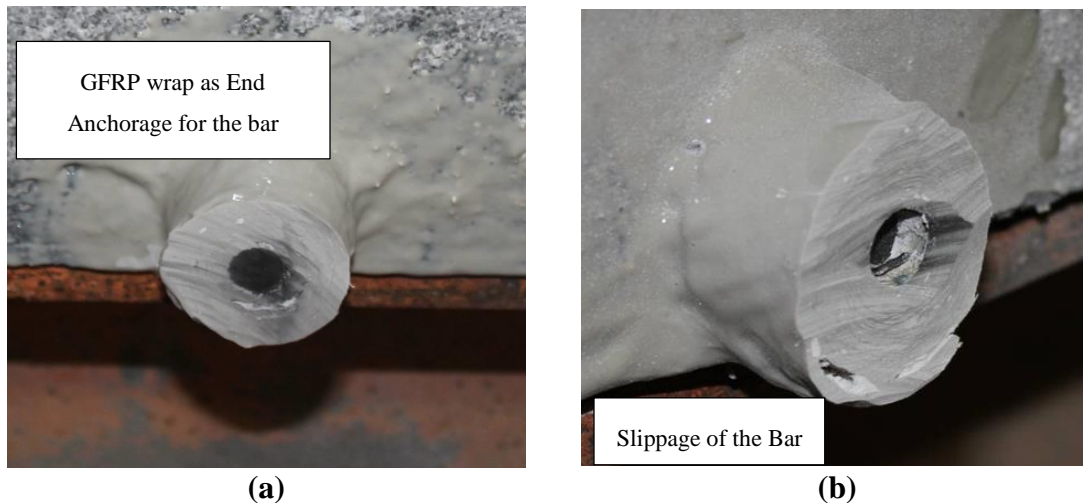


Figure 4.16 Simple End Anchorage System for CFRP Bars in Phase 1: (a) Grinded End, and (b) Slippage of CFRP Bar

The preliminary design of specimens was conducted using a finite element model. The required live load demands, shown in Table 4.5, were calculated using the equivalent strip method and the deck slab design table (AASHTO LRFD 2013) for each group of specimens based on the specimen width, load factors, multiple presence factors, dynamic load allowance, and the loading configuration. It should be noted that a similar approach was used by Aaleti and Sritharan (2014) for the design of their UHPC waffle deck system.

Ancillary tests were conducted to assess the performance of anchorage system in CFRP bars of Group 2. Figure 4.17c shows the self-reacting test frame with two 60 kips hydraulic jacks controlled by a single hydraulic pump. The frame was assembled with three 1 inch thick plates of  $16 \times 24$  inch and four No.7 high-strength steel threaded rods.

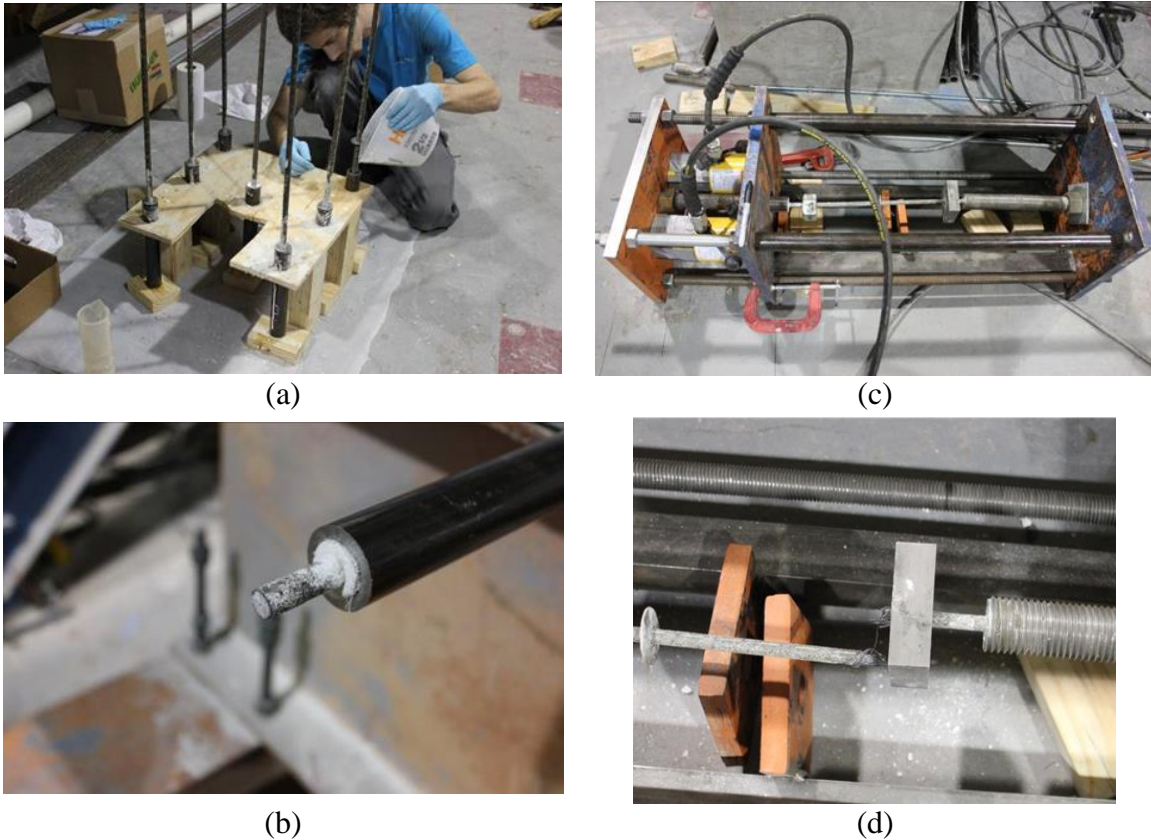


Figure 4.17 Anchorage System for CFRP Bars in Phase 2: (a) Casting of Expansive Grout, (b) Close-up View, (c) Ancillary Test Setup, and (d) Failure of CFRP Bar

### 4.3.2 Test Setup and Instrumentation

Figure 4.18a shows the test setup with one of the 1T1S specimens resting on two W24×76 stringers placed at 4 ft. on center on W12×16 floor beams with 3 ft. spacing. This arrangement was designed to simulate the typical superstructure of a movable bridge. The loading patch of an HS20 truck dual-tire wheel (AASHTO LRFD 2013) was simulated using a 10 × 20 inch steel plate over a neoprene pad. Except for the punching shear test, the loading patch was placed at the center of the span and aligned in the direction of traffic. The simple-span specimens were subjected to a single load at their mid-span (Figures 4.18a and 4.18c), while two equal loads were applied concurrently in the middle of both spans in two-span specimen (Figure 4.18b). At the conclusion of its flexure test, the multi-rib specimen was tested for punching shear in between the first and second ribs with the same loading patch (Figure 4.18d). Several strain gauges were used to monitor responses of CFRP bars and UHPC at critical locations. String pots were also used to measure deflections of the specimen under each rib. Loading was applied using a 230 kips capacity hydraulic actuator, at an average rate of 0.03 mm/min. The data was recorded at a frequency of 1 Hz, and tests were stopped at around 30% load drop, unless preceded by a clear sign of failure.



(a)



(c)



(b)



(d)

Figure 4.18 Setup for Flexure Tests of (a) Specimen 1T1S, (b) Specimen 1T2S, (c) Specimen 4T1S, and (d) Punching Shear Test of Specimen 4T1S

### 4.3.3 Test Results and Discussion

Table 4.5 shows a summary of test results for the two groups of specimens, as well as results from prior experiments on the UHPC waffle decks with HSS reinforcement (Saleem et al. 2011, and Mirmiran et al. 2014). The table shows the required live load demand for each group of specimens, along with capacity/demand ratio and capacity/demand per unit weight of the deck panel for each specimen. All specimens met their respective demand loads. In the following sections, test results are grouped together for discussion of each performance metric.

Table 4.5 Summary of Test Results

Group	Specimen Name	Overall Depth (in.)	Service Load Deflection (in.)	Ultimate Deflection (in.)	Ultimate Load (kip)	Demand Load (kip)	Capacity/Demand	Capacity/Demand per Unit Weight
<b>UHPC-CFRP</b>								
CFRP-1	1T1S-4#1	4	0.54	1.19	16.77	10.25	1.6	0.09
	1T1S-4#2		0.48	1.06	17.15		1.7	0.09
	1T1S-5#1	5	0.37	1.03	21.49		2.1	0.10
	1T1S-5#2		0.35	0.97	19.56		1.9	0.09
CFRP-2	1T1S-4	4	0.45	1.03	18.66	42.04	1.8	0.10
	4T1S-4		0.50	0.83	51.26		1.2	0.06
	1T2S-4		0.19	0.80	26.75		15.65	1.7
<b>UHPC-HSS</b>								
HSS-0 <sup>1</sup>	1T1S-5#1	5	0.06	0.98	40.02	8.21	4.9	0.15
	1T1S-5#2		0.1	0.98	46.99		5.7	0.18
	4T1S-5		0.19	0.79	84.98	34.17	2.5	0.08
	1T2S-5		0.9	1.26	55.08	12.52	4.4	0.14
HSS-1 <sup>2</sup>	1T1S-4½#1	4½	0.1	0.83	27.65	10.25	2.7	0.12
	1T1S-4½#1		0.14	0.87	24.73		2.4	0.11
HSS-2 <sup>2</sup>	1T1S-4	4	0.15	0.91	22.71	42.04	2.2	0.11
	4T1S-4		0.18	0.87	51.48		1.2	0.06
	1T2S-4		0.07	0.87	44.96		15.65	2.9

<sup>1</sup>Taken from Saleem et al. (2011).

<sup>2</sup>Taken from Mirmiran et al. (2015).

#### 4.3.3.1 Anchorage of CFRP Bars

Ancillary tests showed the adequacy of steel tube for the anchorage of CGRP bars, as evident by the rupture of the bar with no slippage (Figure 4.17d). On the other hand, the simple GFRP wraps in specimens of Group 1 did not provide adequate anchorage, leading to premature slippage of the CFRP bars (Figure 4.16b), and affecting the overall deflection (Figure 4.19a) and failure mode of deck specimens. The bar slippage was observed in specimens of Group 1 at about half the ultimate load or 80% of the demand load. Based on data from Table 4.5, the average service-level deflection of Specimens 1T1S-102 in Group 1 was about 15% higher than the similar specimen in Group 2. Also, specimens of Group 1 showed a pronounced shear anchorage failure (Figure 4.19b), as compared to the shear-flexure cracks in similar specimen in Group 2 (Figure 4.19c). The tubular anchorage system effectively increased the stiffness and capacity of the deck, and decreased the corresponding deflection. This behavior was quite similar to that observed for UHPC waffle deck specimens in previous studies with HSS reinforcement that were effectively anchored using 180° hooks (Saleem et al. 2011, and Mirmiran et al., 2014).



(a)



(b)



(c)

Figure 4.19 Flexure Test and Failure Mode of Specimens 1T1S, (a) Deflected Shape of Specimen 1T1S, (b) Close of View of Beam Shear Crack, and (c) Shear Crack at the Edge of the Loading Pad

#### 4.3.3.2 Flexural Behavior

Figure 4.20 shows the load-deflection responses of the two groups of single-rib simple-span specimens (1T1S) with different depths. For comparison, one response curve is shown for a similar 4-inch deep specimen with HSS reinforcement (Mirmiran et al. 2014). The difference in the latter part of the responses for the two identical 5-inch deep specimens may be attributed to the slippage of the bars occurring at two different load levels of 21.60 and 19.11 kips,

respectively, and rather prematurely due to the ineffective wrapping of CFRP bars in Group 1. Although all specimens clearly exceeded the required demand load, both the stiffness and capacity of the specimen with HSS reinforcement are higher than those with CFRP. On the other hand, Table 4.5 shows that UHPC decks with CFRP reinforcement provide a more optimal design solution, given their lower capacity/demand ratio and capacity/demand per unit weight of the deck. Table 4.5 also shows measured deflections for each specimen at the levels of service and ultimate loads. The ratio of these two deflection levels indirectly suggests a reasonable ductility for each deck specimen. Figure 4.21 shows load-strain responses of 1T1S specimens, based on strain gauges attached at the mid-span to the CFRP bar in the primary rib. The figure shows a maximum strain of 0.8%, which is less than half of the rupture strain of CFRP bars. As such, ductile behavior of the specimens is attributed mainly to the dowel action of CFRP bars and the fiber pull-out mechanism in UHPC.

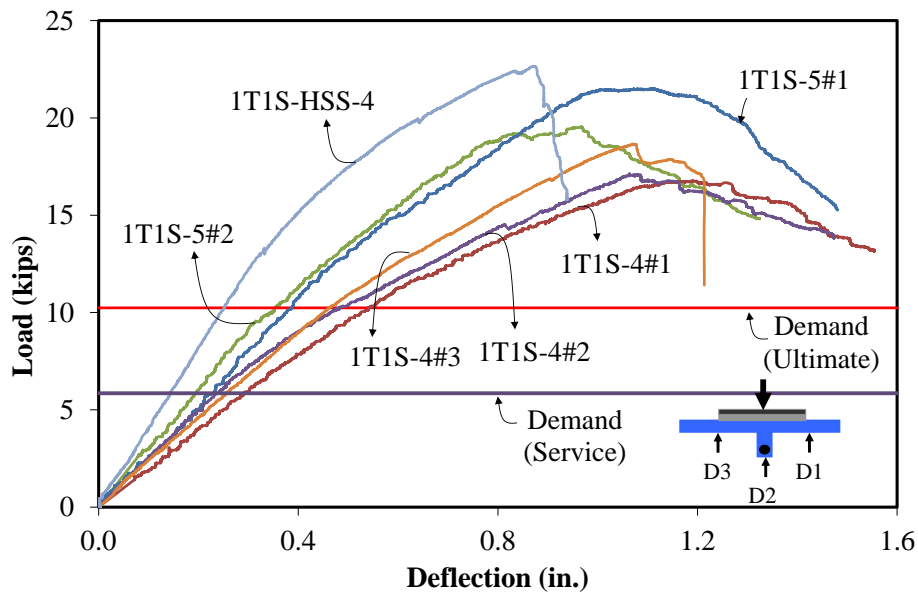


Figure 4.20 Load-Deflection Responses of Specimens 1T1S

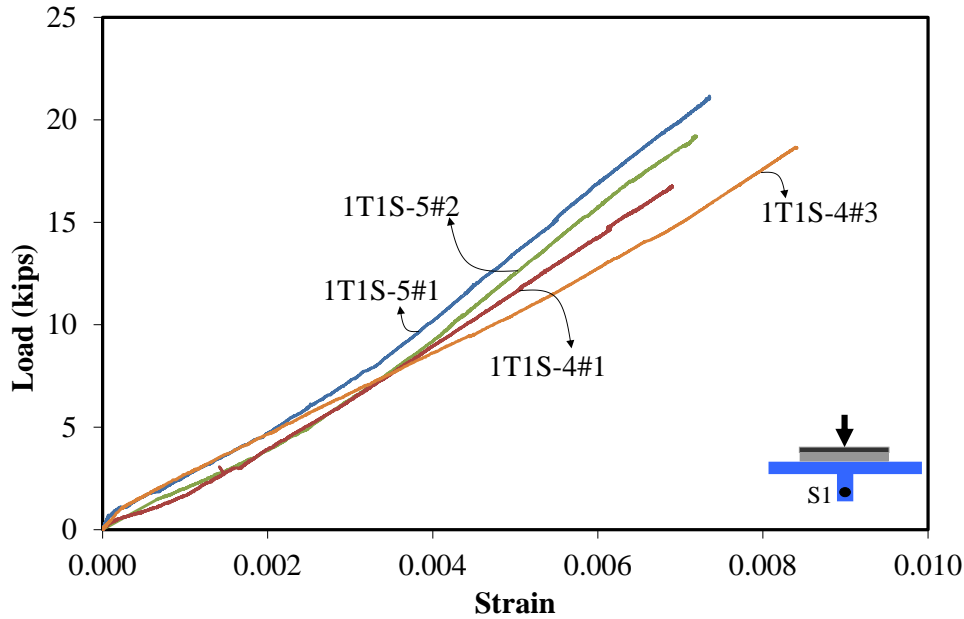


Figure 4.21 Load-Strain Responses of CFRP Bars in Specimens 1T1S

#### 4.3.3.3 Panel Action

Figures 4.22a and 4.22.b show the top and bottom views of the multi-rib simple-span Specimen 4T1S after its flexural test, shown in Figure 4.18c. The failure mode was similar to that observed for single-rib specimens. The cracks appeared in the main ribs under the loading patch, and grew in length and width until failure. Figure 4.22c shows the load-deflection responses under each rib for the same specimen. The failure load at 51.26 kips was about 20% higher than the ultimate demand of 41.81 kips. The ductility and plastic deformation, on the other hand, were considerably larger than that observed for the single-rib specimens. The reason for higher load capacity may be attributed to the presence of additional ribs and their participation in carrying the load through panel action.

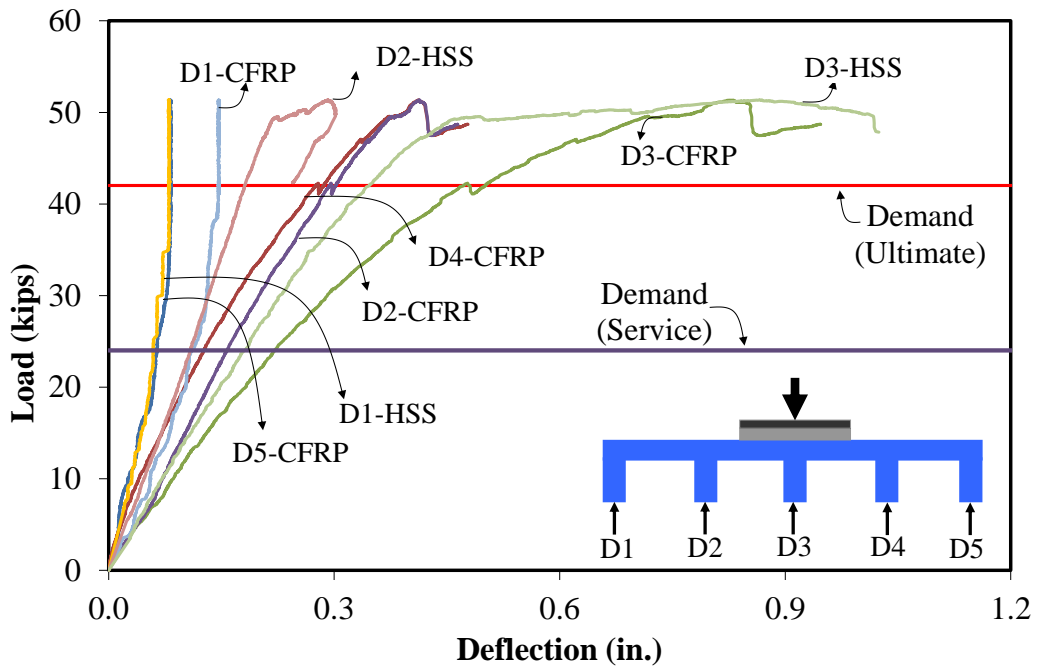
For comparison, Figure 4.22c also shows the response curves under each rib for a similar 4 inch deep multi-rib specimen with HSS reinforcement (Mirmiran et al. 2014). It is clear both from the figure and Table 4.5 that the capacity of the multi-rib specimen is the same with either type of HSS or CFRP reinforcement, while the CFRP-reinforced panel seems more flexible. Load distribution among the ribs may be calculated based on mid-span deflections of each rib or mid-span strains in the bar in each rib. Using either approach, the load distribution among the ribs is found as 33% for the center rib and 22% and 11% for the next two ribs. These factors are quite similar to those for UHPC-HSS specimens (Saleem et al. 2011 and Mirmiran et al. 2014).

Figure 4.23 shows load-strain responses of the multi-rib specimen, based on strain gauges attached at the mid-span to the CFRP bar in each rib. The figure shows a maximum strain of 0.6% in the center rib, higher than that observed in single-rib specimens, but still about half of the rupture strain of CFRP bars. Again, the apparent ductile behavior of the specimen may be attributed to the dowel action of CFRP bars and the fiber pull-out mechanism in UHPC. It is clear from both deflection and strain responses in Figures 4.22c and 4.23 that side ribs lose their effectiveness beyond service loads.



(a)

(b)



(c)

Figure 4.22 Failure Modes in Specimen 4T1S: (a) Top View, (b) Bottom View, (c) Load-Deflection Responses under Each Rib of Specimen 4T1S

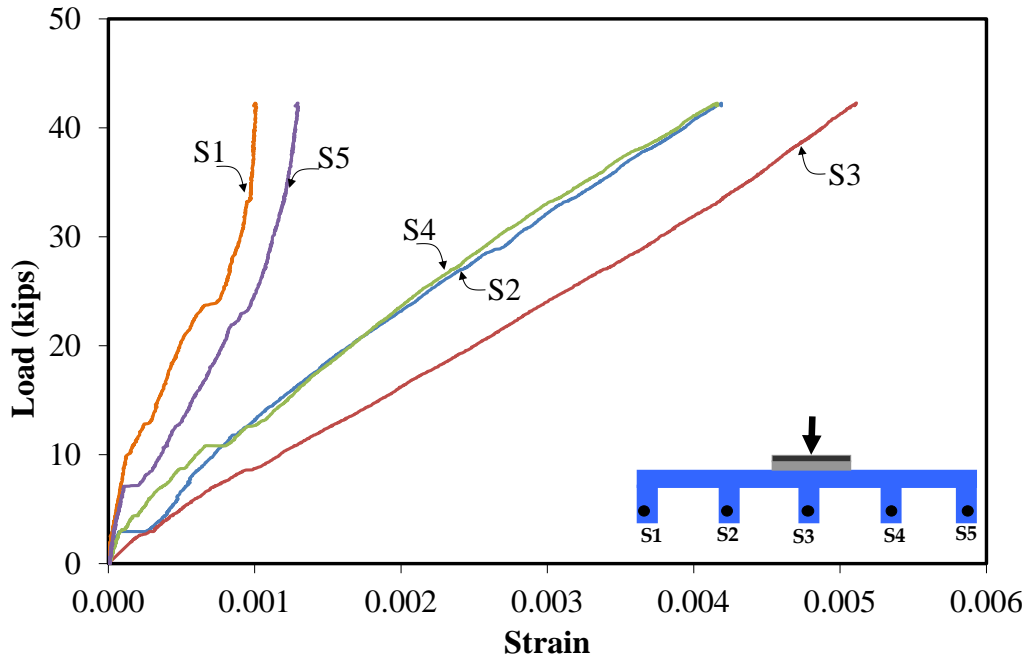


Figure 4.23 Load-Strain Responses of CFRP Bars in Each Rib of Specimen 4T1S

#### 4.3.3.4 Punching Shear

Figure 4.24 shows the punching test and failure mode for Specimen 4T1S at the conclusion of its flexure test, where only the center rib was damaged. The failure was marked by major shear cracks forming in the two ribs adjacent to the loading patch, with no sign of punching. The load-deflection responses under each rib are shown in Figure 4.25, with the maximum deflection occurring right under the loading patch in between the two loaded ribs. It should be noted that the capacity of the specimen under the asymmetric punching was 32.15 kip, which is only 60% of its capacity under symmetric flexural loading (51.25 kip), primarily because of lack of contribution from adjacent ribs that were either damaged or away from the loading patch. Figure 4.25 also shows the response curves of a similar 4-inch-deep multi-rib specimen with HSS reinforcement (Mirmiran et al., 2014), with clearly higher stiffness and capacity, as compared to UHPC-CFRP deck.

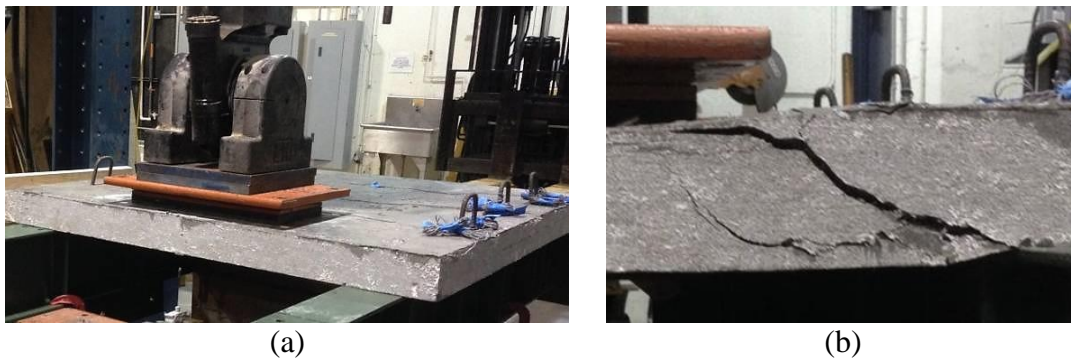


Figure 4.24 Punching Shear Test and Failure Mode in Specimens 4T1S

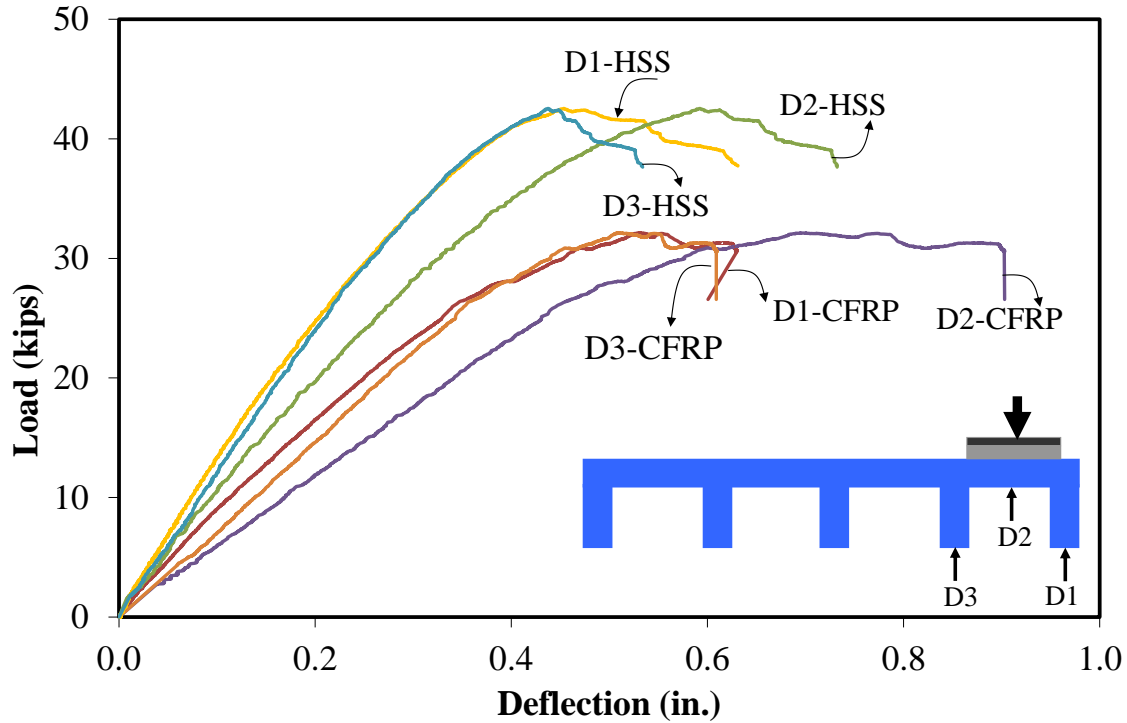


Figure 4.25 Load-Deflection Responses of Specimen 4T1S in Punching Shear

#### 4.3.3.5 Continuity Effect

The behavior of the deck system in negative moment region was investigated by testing a single-rib two-span specimen, as shown in Figure 4.26. Shear in the main ribs near the support was seemingly the predominant mode of failure, similar to that observed in simple-span specimens. The shear cracks initiated in the web in one span and moved towards the top slab. Figure 4.27 shows the load-deflection responses of the specimen along with those of a similar specimen with HSS reinforcement tested in previous studies earlier by Mirmiran et al. (2014). At 26.75 kips, the capacity of the specimen with CFRP reinforcement was 70% higher than the required demand of 15.65 kips, although only 60% of the capacity of similar specimen with HSS reinforcement (i.e., 44.96 kips). Both types of reinforcement resulted in a ductile response for the deck. It is also noteworthy that the capacity of Specimen 1T2S was 26.75 kips or 43% higher than that of Specimen 1T1S at 18.66 kips, which may be attributed to the continuity effect. Figure 3.18 shows the load-strain responses of CFRP bar at the middle of both spans. The maximum strain is about 1/3 of the rupture strain of CFRP bar.

Table 4.5 lists the deflection of Specimen 1T2S at the level of service load as 0.19 inch, which corresponds to  $L/254$ , where  $L$  = center to center spacing of stringers, which was 4 ft. Considering a modification factor of 0.74 comparing the deflections of two-span and five-span decks under two wheel loads, the modified deflection becomes  $L/343$ , which is about twice the deflection limit of  $L/800$  (AASHTO LRFD 2013). It should be noted that continuity effect remains constant beyond five spans. It is also noteworthy that UHPC deck with HSS reinforcement has a modified deflection of  $L/914$ .

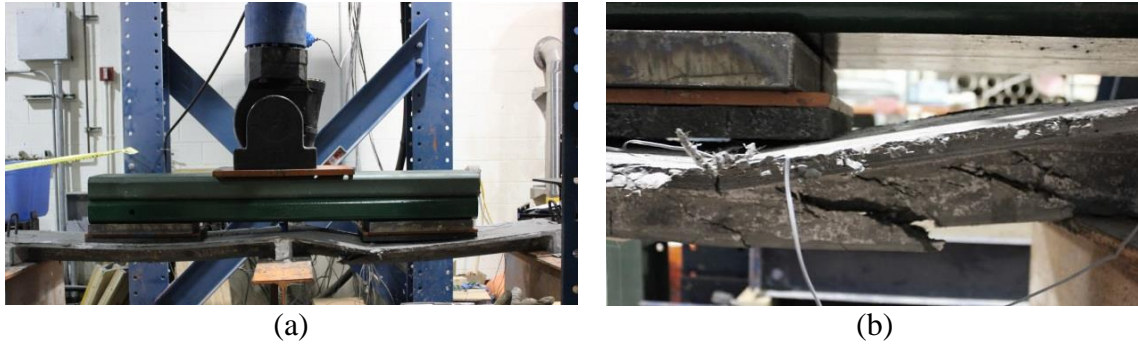


Figure 4.26 Failure Mode of Specimen 1T2S: (a) Deflected Shape, and (b) Shear Crack

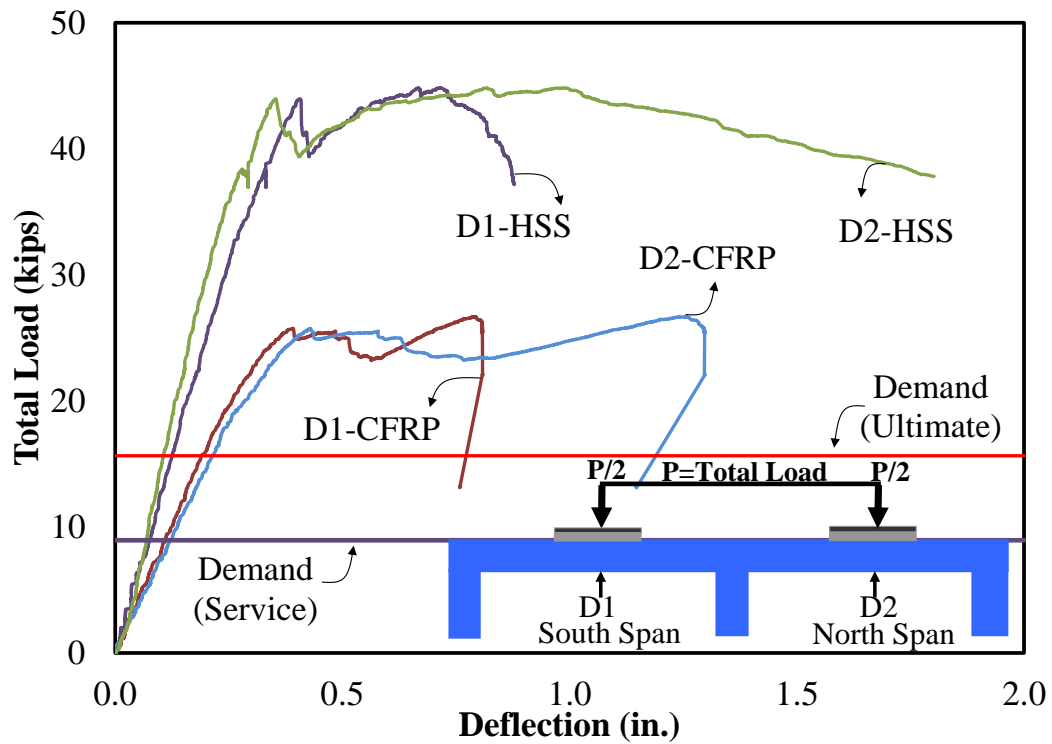


Figure 4.27 Load-Deflection Responses of Specimens 1T2S

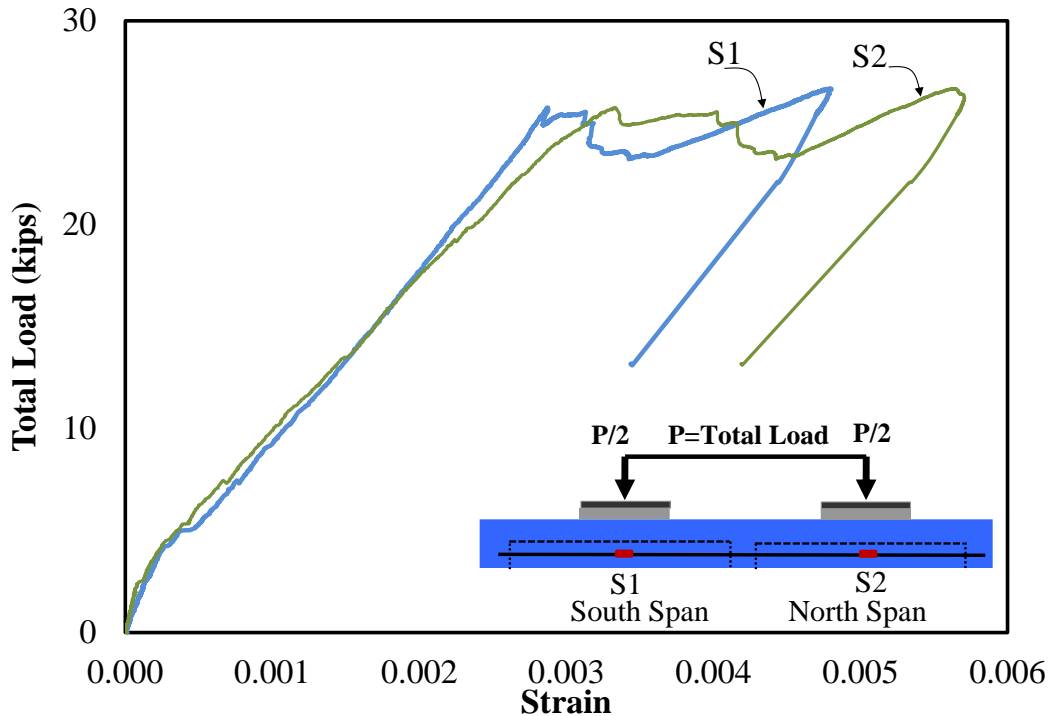


Figure 4.28 Load-Strain Responses of CFRP Bar in Specimen 1T2S

#### 4.3.4 Summary of Findings from UHPC-CFRP Deck Tests

An innovative deck system is proposed for accelerated bridge construction, using ultra high performance concrete (UHPC) in the form of an ultra-lightweight super-shallow waffle slab reinforced with carbon fiber reinforced polymer (CFRP) bars. The novel combination of the two advanced materials leads to a deck panel with only 4 inch overall depth and only 18.80 psf self-weight, while still meeting the load demands for a 4 ft. typical stringer spacing. In this study, seven specimens with two different overall depths, with single or multiple ribs, and in simple or two-span configuration were tested in two consecutive phases. The following conclusions can be drawn from this study:

- The experiments confirmed the feasibility of the proposed deck system, and its comparable performance to a similar deck using high-strength steel reinforcement.
- The proposed deck is not susceptible to punching shear of its thin slab, due to the arrangement of the primary and secondary ribs, which promotes one-way shear of the primary ribs instead.
- The proposed deck system fails in a ductile manner, despite its apparent shear failure and in the absence of yielding of the reinforcement. The ductility stems from dowel action of CFRP bars and the fiber pull-out of UHPC.
- Load distribution among the ribs, whether calculated based on deflections or strains, are quite similar to those for UHPC-HSS specimens. The load distribution for the center rib is 33%, with the next two adjacent ribs at 22% and 11%, respectively.

#### **4.4 Accelerated Pavement Testing**

Based on static testing conducted in the lab, the UHPC waffle deck system has shown great promise as a viable alternative to open grid steel decks. In order to evaluate the long-term performance of the UHPC deck panels under field conditions, it was decided to test the system at the Accelerated Pavement Testing (APT) facility in Gainesville under the Heavy Vehicle Simulator (HVS). It is proposed that four lightweight bridge deck panels and their connections to each other and the stringers be tested under the dynamic impact of wheel load as described in the following.

##### **4.4.1 Preparatory Lab Tests**

Due to the geometry and configuration of the testing pit, the depth of the deck section needed to be 5 inch, which is different from the optimized depth of 4 inch as described in previous chapters. In order to have a better understanding of the behavior of the section with 5-inch depth under HVS loading, six laboratory specimens were built for the purpose of sizing through static tests with single and multiple ribs in simple and double span configurations. The results of recent tests were then compared to those of previous tests, as described in the following sections.

Table 4.6 shows the test matrix for this study. The specimen names include number of ribs (T), number of spans (S), specimen depth and sample number (if more than one). All specimens have the same depth of 5 inch, but in three different configurations, single-rib simple-span, single-rib two-span, and multi-rib simple-span (see Figures 4.2, 4.3, 4.13, and 4.14). The multi-rib specimen featured 2¾-inch-deep transverse ribs to help with load distribution among primary ribs. For comparison, the table also shows all UHPC waffle deck specimens with HSS and CFRP reinforcement tested in all previous studies (Saleem et al. 2011, Mirmiran et al., 2015). The test setup and instrumentation is similar to earlier sections.

Table 4.7 shows a summary of test results for the current studies along with the results from prior experiments on the UHPC waffle decks with HSS and CFRP reinforcement (Saleem et al. 2011, and Mirmiran et al., 2015). The table shows the required live load demand for each group of specimens, along with capacity/demand ratio and capacity/demand per unit weight of the deck panel for each specimen. In the following sections, test results for each group of specimens are presented.

Table 4.6 Test Matrix

Group	Specimen Name	Test Phase	Overall Depth (in.)	Rib Spacing (in.)	Slab Thickness (in.)	Unit Weight (psf)	28-Day UHPC Compressive Strength (ksi)	Flexural Reinforcement	
								Slab	Primary Rib
<b>UHPC-CFRP</b>									
CFRP-3	1T1S-5	3	5	15	¾	24.22	24	No. 3	No. 6
	4T1S-5	3	5	15	¾		25	No. 3	No. 6
	1T2S-5	3	5	15	¾		24	No. 3	No. 6
<b>UHPC-HSS</b>									
HSS-3	1T1S-5	3	5	15	¾	26.13	22	No. 3	No. 6
	4T1S-5	3	5	15	¾		23	No. 3	No. 6
	1T2S-5	3	5	15	¾		22	No. 3	No. 6
<b>UHPC-CFRP</b>									
CFRP-1 <sup>2</sup>	1T1S-4#1	1	4	15	¾	18.80	24	No. 3	No. 4
	1T1S-4#2	1					24		
	1T1S-5#1	1	5				24		
	1T1S-5#2	1					24		
CFRP-2 <sup>2</sup>	1T1S-4#3	2	4	15	¾	18.80	27	No. 3	No. 5
	4T1S-4	2					27		
	1T2S-4	2					26		
<b>UHPC-HSS</b>									
HSS-0 <sup>1</sup>	1T1S-5#1	0	5	12	1¼	32.37	18	No. 4	No. 7
	1T1S-5#2	0					27		
	4T1S-5	0					26		
	1T2S-5	0					22		
HSS-1 <sup>2</sup>	1T1S-4½#1	1	4½	15	¾	21.72	24	No. 3	No. 5
	1T1S-4½#2	1					24		
HSS-2 <sup>2</sup>	1T1S-4	2	4	15	¾	20.26	27	No. 3	No. 5
	4T1S	2					27		
	1T2S	2					25		

<sup>1</sup> Taken from Saleem et al. (2011).<sup>2</sup> Taken from Mirmiran et al. (2015).

Table 4.7 Summary of Test Results

Group	Specimen Name	Graph Labels	Overall Depth (in.)	Service Load Deflection (in.)	Ultimate Deflection (in.)	Ultimate Load (kip)	Demand Load (kip)	Capacity/Demand	Capacity/Demand per Unit Weight	
<b>UHPC-CFRP</b>										
CFRP-3	1T1S-5	CFRP-5#3	5	0.23	1.76	21.80	8.14	2.68	0.11	
	4T1S-5	CFRP-5#3		0.64	2.71	48.48		52.13	0.93	0.04
	1T2S-5	CFRP-5#3		0.12	1.24	38.45		17.45	2.20	0.09
<b>UHPC-HSS</b>										
HSS-3	1T1S-5	HSS-5#3	5	0.076	1.71	23.07	8.14	2.83	0.11	
	4T1S-5	HSS-5#3		0.21	0.93	55.59		52.13	1.07	0.04
	1T2S-5	HSS-5#3		0.084	1.20	35.45		17.45	2.03	0.08
<b>UHPC-CFRP</b>										
CFRP-1 <sup>2</sup>	1T1S-4#1	CFRP-4#1	4	0.54	1.19	16.77	10.25	1.6	0.09	
	1T1S-4#2	CFRP-4#2		0.48	1.06	17.15		1.7	0.09	
	1T1S-5#1	CFRP-5#1	5	0.37	1.03	21.49		2.1	0.10	
	1T1S-5#2	CFRP-5#2		0.35	0.97	19.56		1.9	0.09	
CFRP-2 <sup>2</sup>	1T1S-4	CFRP-4#3	4	0.45	1.03	18.66	42.04	1.8	0.10	
	4T1S-4	CFRP-4#3		0.50	0.83	51.26		1.2	0.06	
	1T2S-4	CFRP-4#3		0.19	0.80	26.75		15.65	1.7	0.09
<b>UHPC-HSS</b>										
HSS-0 <sup>1</sup>	1T1S-5#1	HSS-5#1	5	0.06	0.98	40.02	8.21	4.9	0.15	
	1T1S-5#2	HSS-5#2		0.1	0.98	46.99		5.7	0.18	
	4T1S-5	HSS-5#1		0.19	0.79	84.98		34.17	2.5	0.08
	1T2S-5	HSS-5#1		0.9	1.26	55.08		12.52	4.4	0.14
HSS-1 <sup>2</sup>	1T1S-4½#1	HSS-4½#1	4½	0.1	0.83	27.65	10.25	2.7	0.12	
	1T1S-4½#1	HSS-4½#2		0.14	0.87	24.73		2.4	0.11	
HSS-2 <sup>2</sup>	1T1S-4	HSS-4	4	0.15	0.91	22.71	42.04	2.2	0.11	
	4T1S-4	HSS-4		0.18	0.87	51.48		1.2	0.06	
	1T2S-4	HSS-4		0.07	0.87	44.96		15.65	2.9	0.14

Similar to earlier sections, the flexural behavior of Specimens 1T1S was assessed. Figures 4.29 and 4.30 show the test setup, failure mode, and load-deflection responses of single-rib simple-span specimens for UHPC-HSS and UHPC-CFRP, respectively. Similar to previous experiments, failure was initiated by minor web shear cracks near supports. Minor flexural cracks were also present near mid-span without having any impact on the overall failure. Shear cracks gradually widened as testing progressed, eventually leading to a load drop and failure of the deck panel.

Figure 4.31 shows the load-deflection responses of the single-rib simple-span specimens for both HSS and CFRP reinforcement compared to all previous specimens of the current research projects. The load capacity is normalized to the corresponding ultimate demand load for each specimen according to the data presented in Table 4.7. As seen in the figure, in all of the specimens, the capacity exceeded the ultimate demand load. The 5-inch deep specimens seem to be more flexible as compared to their counterparts in previous phases. This may be attributed to the larger clear span of 5-ft., in contrast to the 4-ft. span in previous phases. Although the overall depth was also changed proportionally, not all thicknesses were sized for the larger span.



Figure 4.29 Flexure Test and Failure Mode of Specimens 1T1S-HSS, (a) Deflected Shape of Specimen 1T1S, and (b) Beam Shear Crack



Figure 4.30 Flexure Test and Failure Mode of Specimens 1T1S-CFRP, (a) Deflected Shape of Specimen 1T1S, and (b) Beam Shear Crack

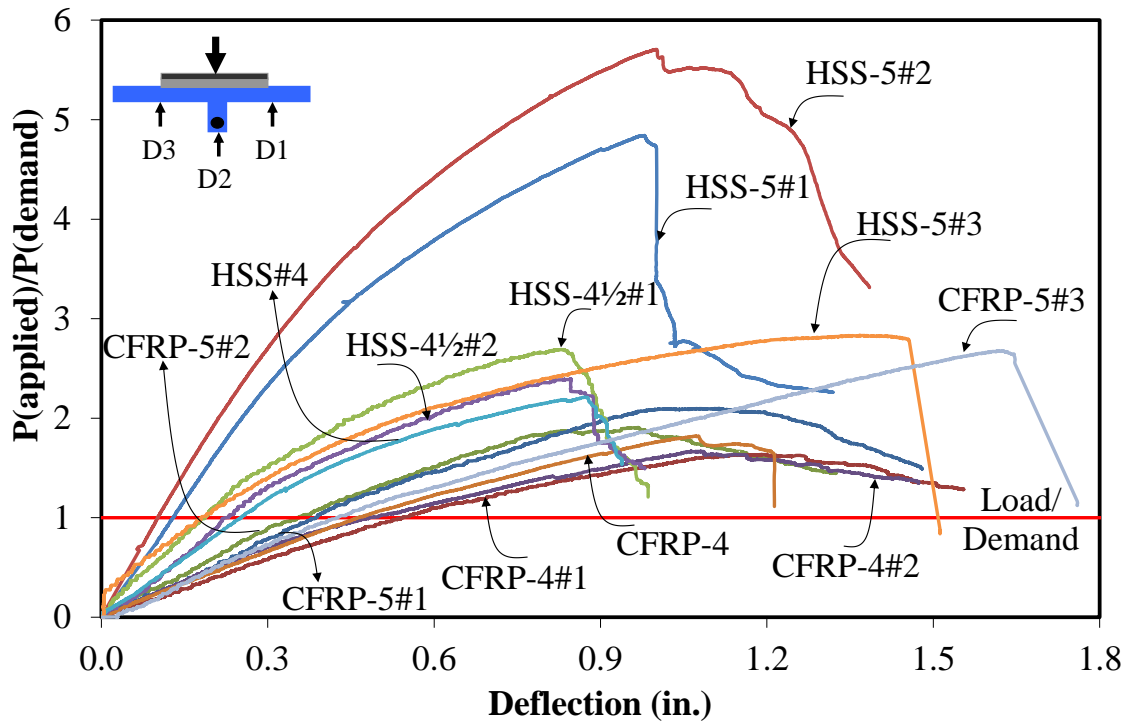


Figure 4.31 Load-Deflection Responses of all Specimens 1T1S

Figures 4.32 and 4.33 show the load-strain responses for all specimens 1T1S with HSS reinforcement and CFRP reinforcement, respectively. As expected, there is great similarity between the results of this phase and those of previous phases.

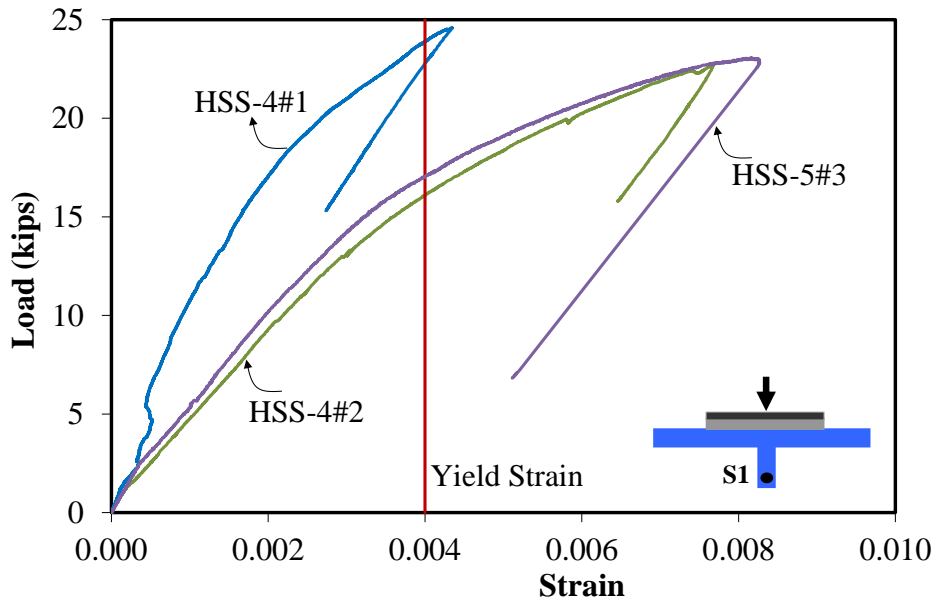


Figure 4.32 Strain Responses of HSS Bars in Specimens 1T1S

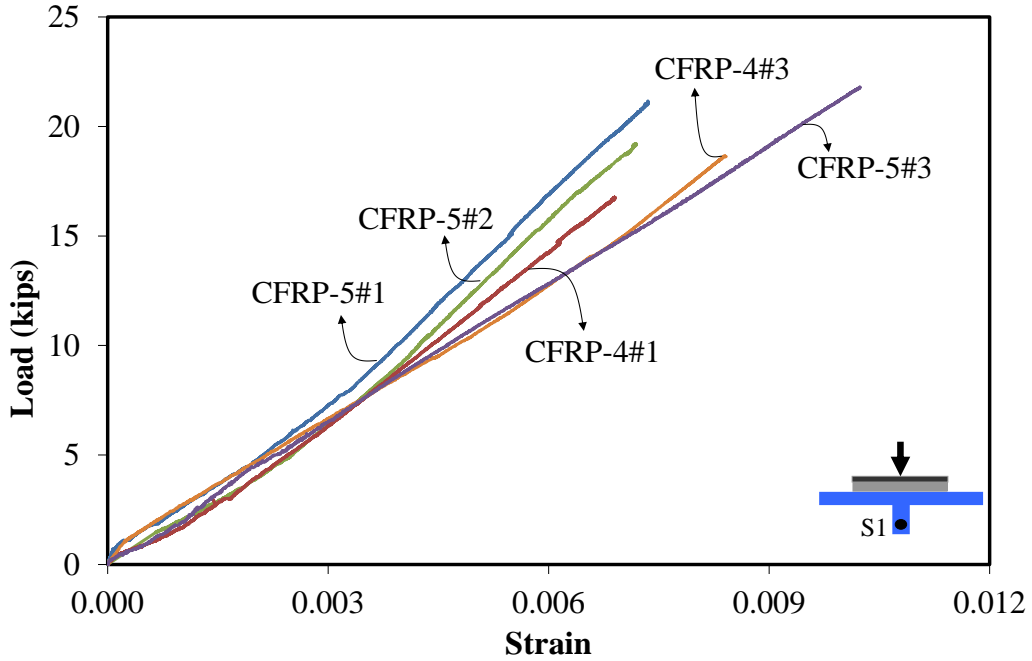


Figure 4.33 Strain Responses of CFRP Bars in Specimens 1T1S

Performance of Specimens 4T1S was evaluated similar to earlier sections. Figure 4.34 shows the top and bottom views of the multi-rib simple-span Specimen 4T1S after its flexural test for Specimen 4T1S-HSS. Test results for Specimen 4T1S-CFRP are illustrated in Figure 4.35. The failure mode was similar to that observed for single-rib specimens of this phase and the previous multi-ribs simple-span specimens.



(a)



(b)



Figure 4.34 Flexure Test and Failure Mode of Specimens 4T1S-HSS, (a) Test Setup, (b) Beam Shear Crack, (c) Cracks on the Slab, and (d) Cracks on the Top Slab

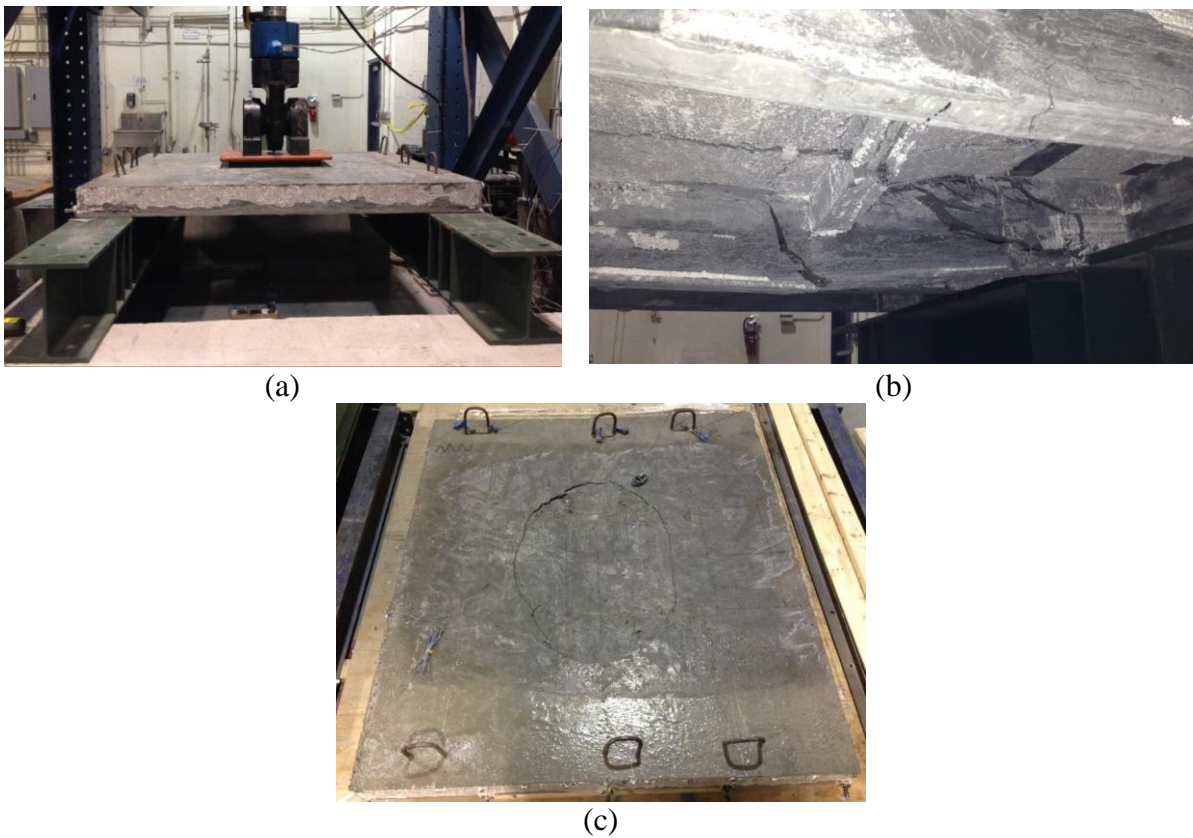


Figure 4.35 Flexure Test and Failure Mode of Specimens 4T1S-CFRP, (a) Test Setup, (b) Beam Shear Crack, and (c) Cracks on the Top of the Slab

For comparison, Figure 4.36 shows the response curves under each rib for current Specimens 4T1S with both types of reinforcement (i.e., either HSS or CFRP) along with all previous specimens in a normalized load capacity basis. The panel with CFRP bars seems to be more flexible, as expected. Also, the 5 inch deep panel with CFRP bars did not meet the ultimate

demand load criteria. Only the load-deflection response of the middle rib (D3) is shown in the figure for all specimens to avoid cluttering the graph.

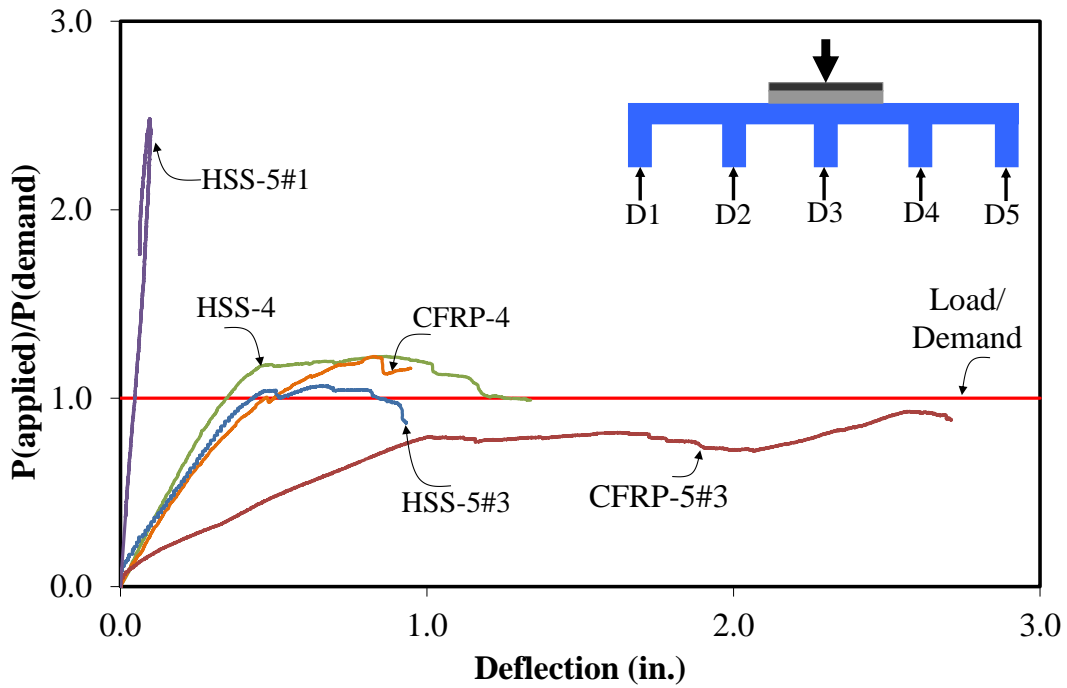


Figure 4.36 Load-Deflection Responses of all Specimens 4T1S

Figure 4.37 shows load-strain responses for all Specimens 4T1S with HSS reinforcement based on strain gauges attached at the mid-span to the rebar in the primary rib. The results are considerably similar to previous phases. Similar results are shown for all Specimens 4T1S with CFRP reinforcement in Figure 4.38.

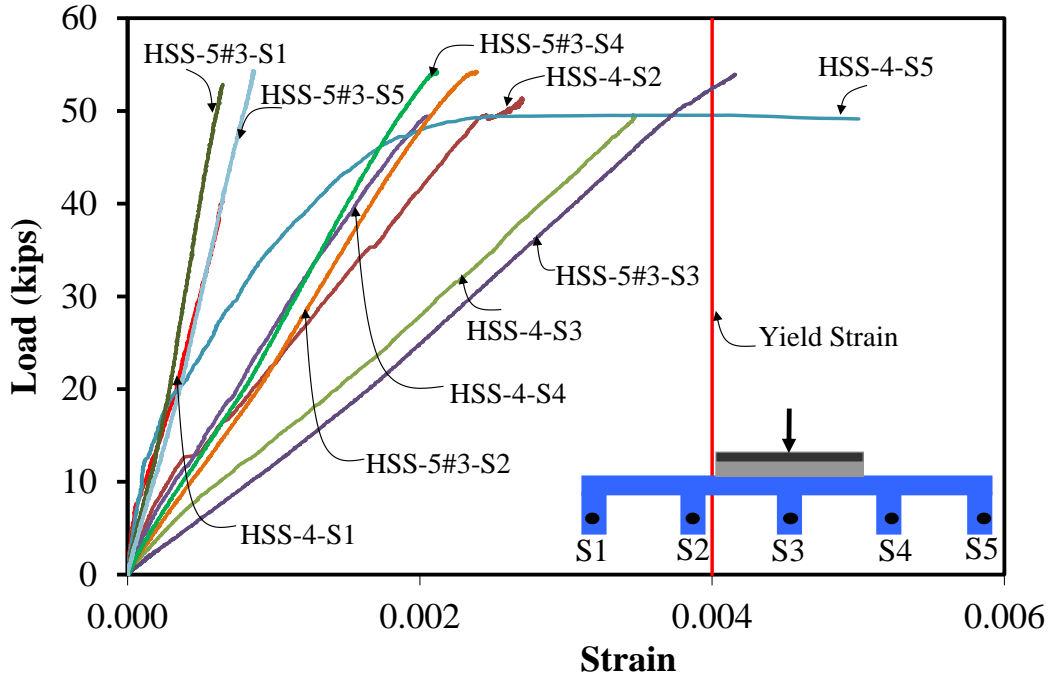


Figure 4.37 Load-Strain Responses of all Specimens 4T1S-HSS

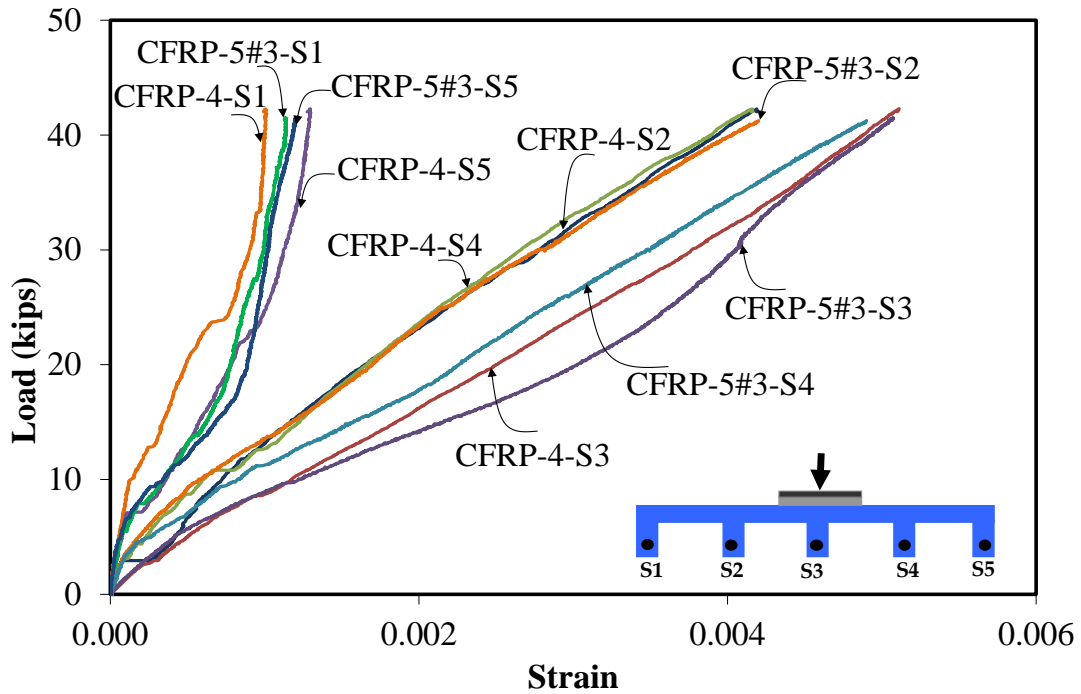


Figure 4.38 Load-Strain Responses of all Specimens 4T1S-CFRP

Figure 4.39 shows punching shear test on exterior panel of Specimen 4T1S-HSS. The load-deflection response of the punching shear test is presented in Figure 4.40. Similar studies have been carried out on Specimen 4T1S-CFRP. The corresponding results are shown in Figures 4.41 and 4.42.

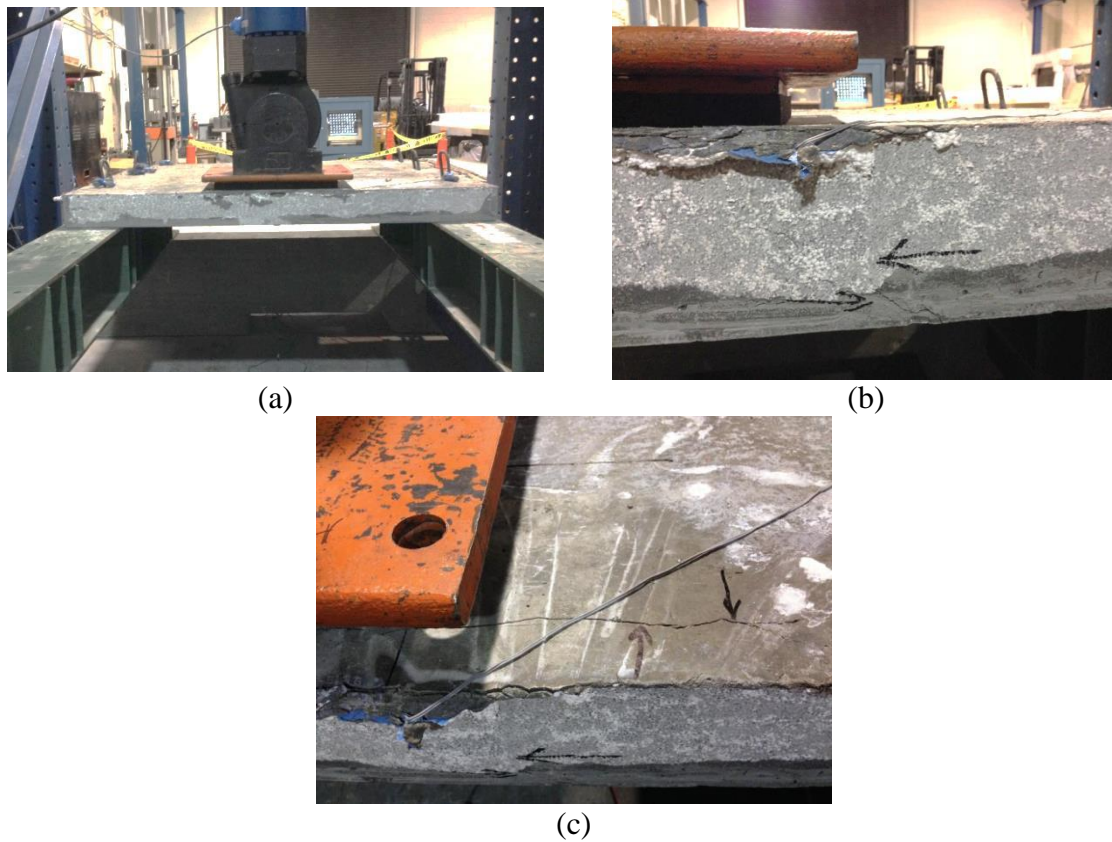


Figure 4.39 Punching Shear Test of Specimen 4T1S: (a) Test Setup, (b) Beam Shear Crack, and (c) Cracks on the Top of the Slab

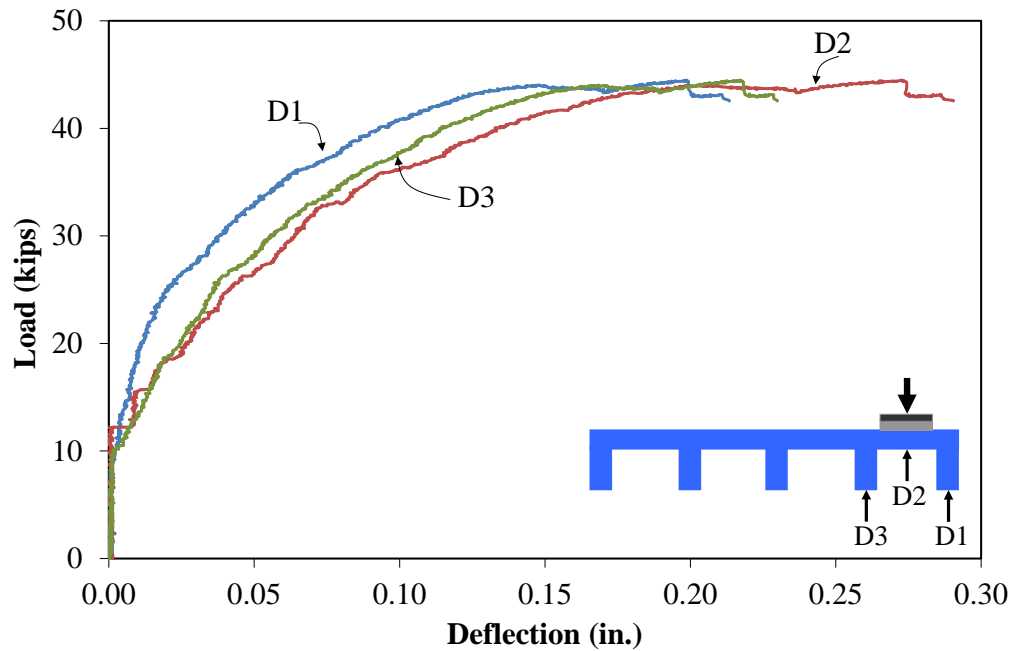
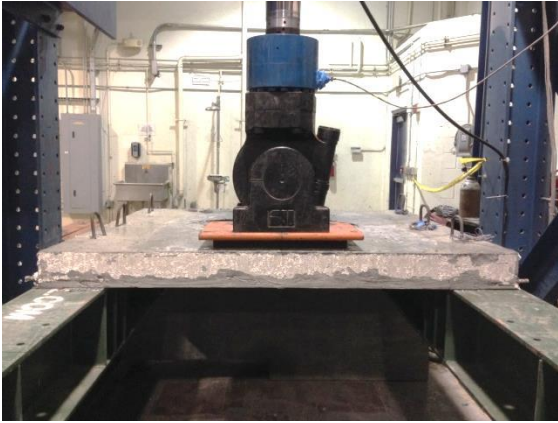


Figure 4.40 Load-Deflection Responses of Specimen 4T1S-HSS



(a)



(b)



(c)

Figure 4.41 Punching Shear Test of Specimen 4T1S: (a) Test Setup, (b) Beam Shear Crack, and (c) Cracks on the Top of the Slab

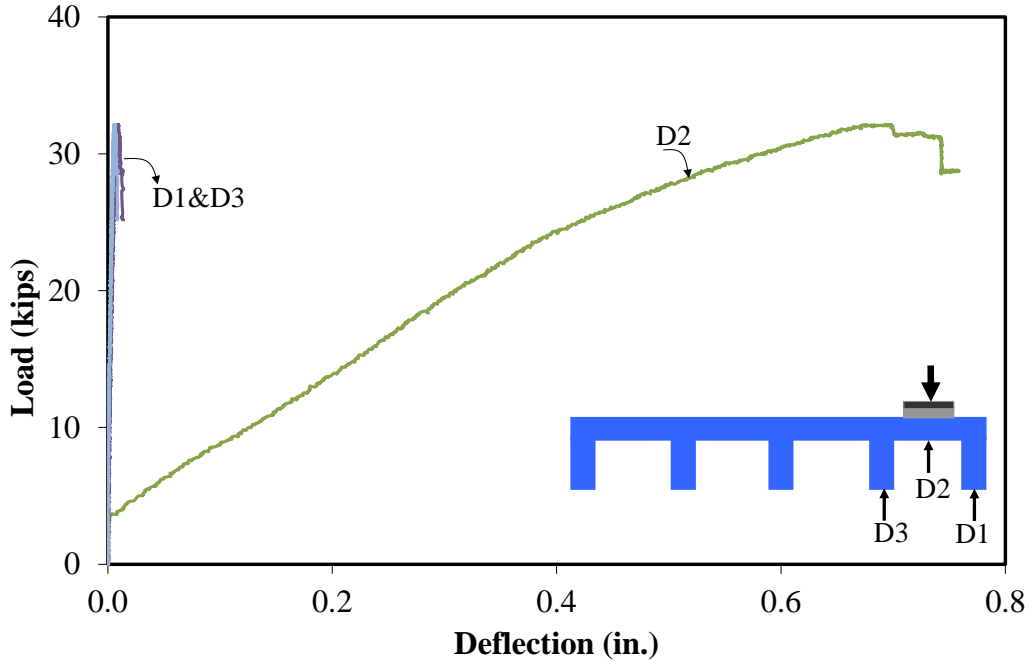


Figure 4.42 Load-Deflection Responses of Specimen 4T1S-CFRP

The effects of continuity and negative moments were investigated using the single-rib two-span Specimen 1T2S. Figures 4.43 and 4.44 show the test setup, deflected shape and the failure mode, where diagonal cracks initiated near an exterior support in one span, and propagated to the slab leading to the eventual failure for Specimens 1T2S-HSS and 1T2S-CFRP. Minor shear cracks were also present in the other span, while some flexural cracks were observed on top of the slab over the interior support. Major flexural cracks on interior support at the face of the northern span of the specimens occurred (see Figure 4.44.d).



(a)



Figure 4.43 Flexure Tests of Specimen 1T2S-HSS: (a) Test Setup, (b) Deflected Shape, and (c) Failure Mode

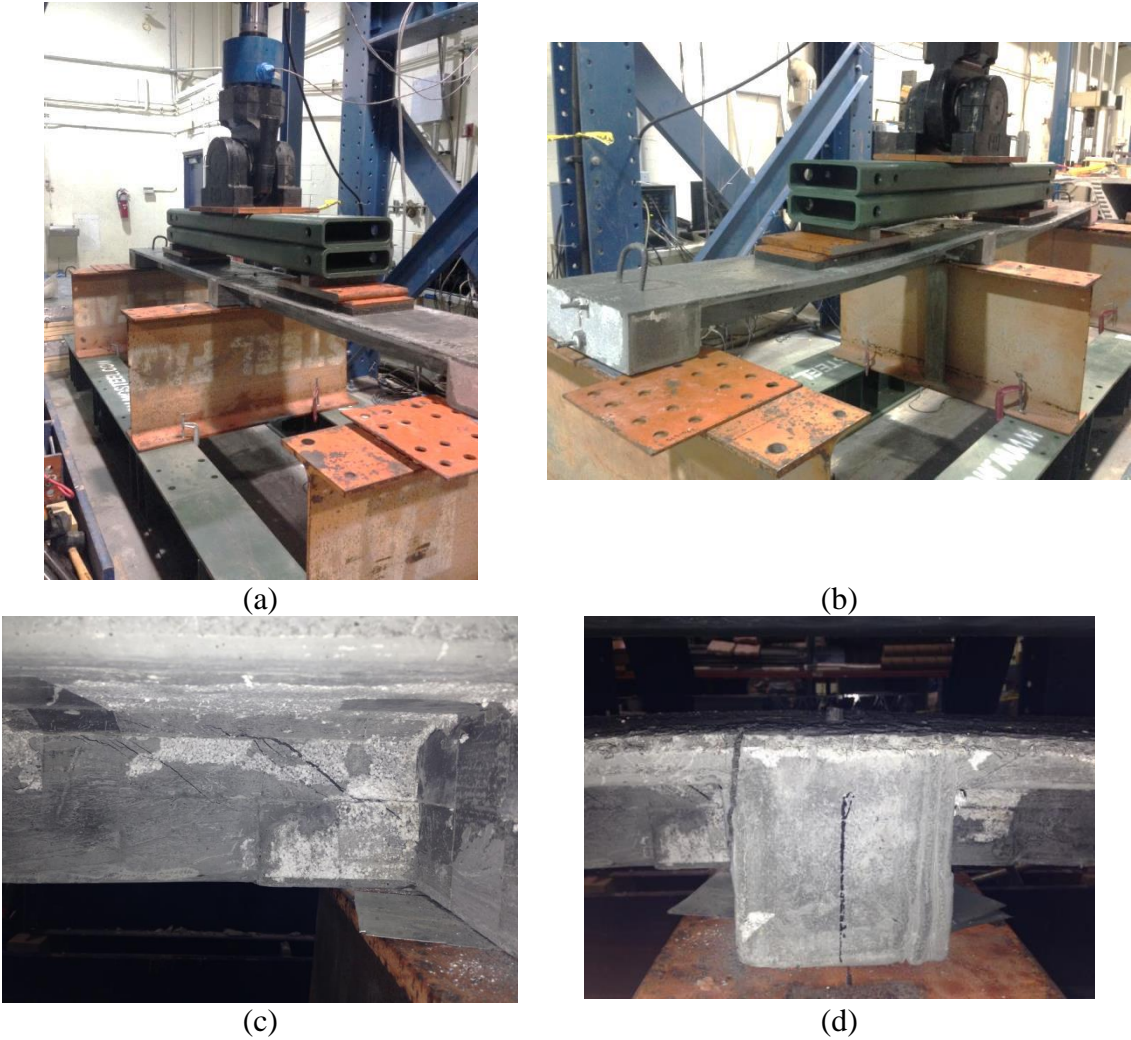


Figure 4.44 Flexure Tests of Specimen 1T2S-CFRP: (a) Test Setup, (b) Deflected Shape, (c) Failure Mode (Beam Shear Crack), and (d) Flexural Crack on the Interior Support

For comparison, Figure 4.45 shows the two mid-spans response curves for current Specimens 4T1S with both types of reinforcement along with all previous specimens. The responses are normalized based on load capacity. All specimens meet the ultimate demand load capacity. The figure clearly shows that the ultimate capacity of the current 5-inch-deep specimens with both types of reinforcement is similar while the UHPC-CFRP specimen seemed to be more flexible.

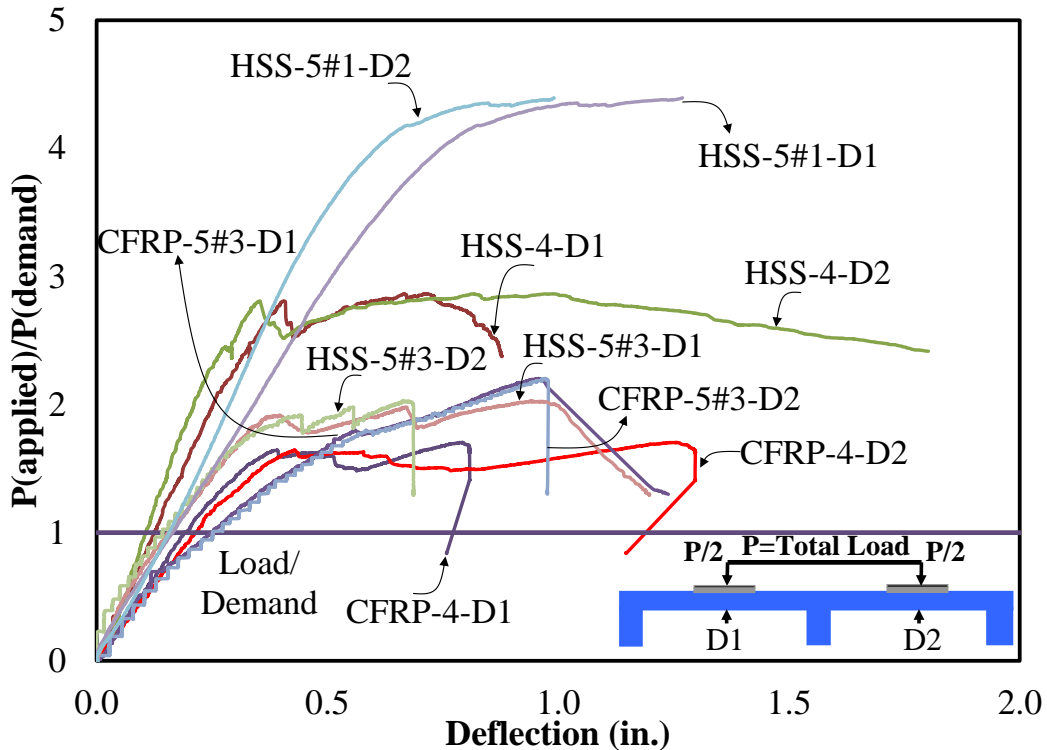


Figure 4.45 Load-Strain Responses of All Specimens 1T2S

Figure 4.46 shows load-strain responses for all Specimens 1T2S with HSS reinforcement based on strain gauges attached at the mid-span to the rebar in the middle of the primary ribs. Contrary to previous specimens with HSS reinforcement, the main bar in the span with maximum deflection yielded.

Figure 4.47 shows load-strain responses for all Specimens 1T2S with CFRP reinforcement based on strain gauges attached at the mid-span to the rebar in the middle rib.

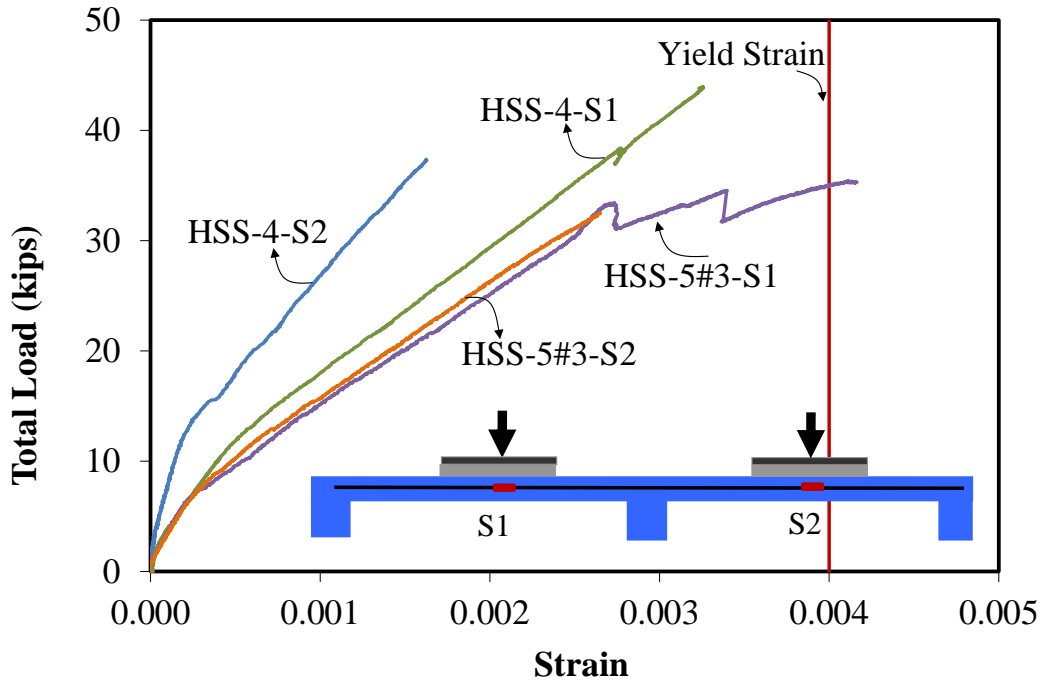


Figure 4.46 Load-Strain Responses of All Specimens 1T2S-HSS

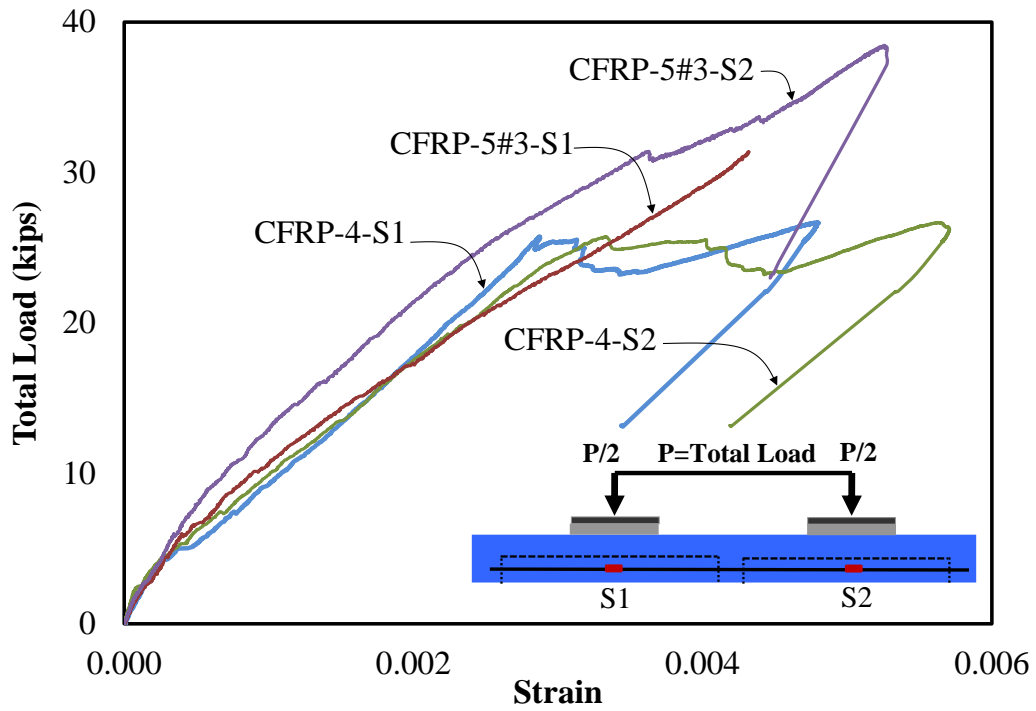


Figure 4.47 Load-Strain Responses of All Specimens 1T2S-CFRP

#### 4.4.2 Heavy Vehicle Simulator Tests

According to Figures 4.34 (c), 4.35 (c), and 4.36 (c) the punching shear cracks occurred on the slab for both Specimens 4T1S-HSS and 4T1S-CFRP. Also, according to Figure 4.36, Specimen 4T1S-CFRP did not meet the ultimate demand load criteria. Therefore, for the final slabs which will be tested under HVS, the thickness of the slab and the amount of reinforcement were both increased.

In the following pages, the overall testing diagram and the arrangement of the four deck panels are shown along with the schematic details of each deck system. Figure 4.48 shows the test setup and layout plan of the waffle decks. As seen in this figure, the bridge deck consists of four deck panels sitting on two support beams of W10×39. All panels have a depth of 5 in. and a transverse length of 6 ft., with center-to-center spacing of the stringers as 5 ft. and a panel width of 5 ft. in the direction of traffic. The dimensions and components of the panels are illustrated in Figures 4.49 to 4.56.

Figure 4.57 shows the connections between the panels containing three different types of details based on the type of the reinforcement of each panel. Figure 4.58 shows the loading plan. As seen in the figure, a 16-kip wheel (based on HS-20 truck loading) will be applied to the decks. Figure 4.59 shows the location of the block-outs, representing the connections between waffle deck panels and the supporting stringers. The loading path of the wheel is shown in Figure 4.60.

The instrumentation plans are shown in Figures 4.61 and 4.62. As seen in Figure 4.61, three types of string pots were planned to measure the deflections at critical locations, including mid-span deflections, relative deflections of the panels, and global deflection of the bridge, as well as transverse deflections. The locations of strain gauges are shown in Figure 4.62. The strain gauges were placed at the mid-span of the bar in the middle rib, where maximum positive moments were intended to occur, and locations under top and bottom flanges of the supporting stringers at mid-span.

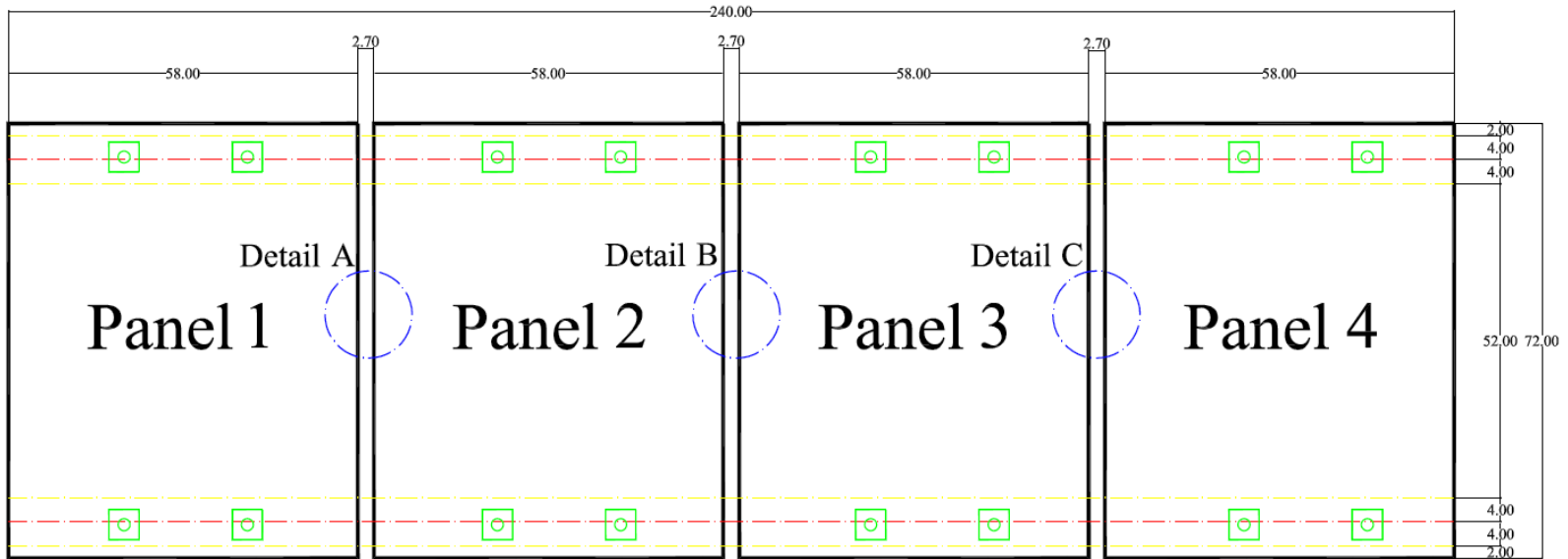


Figure 4.48 Panels Layout

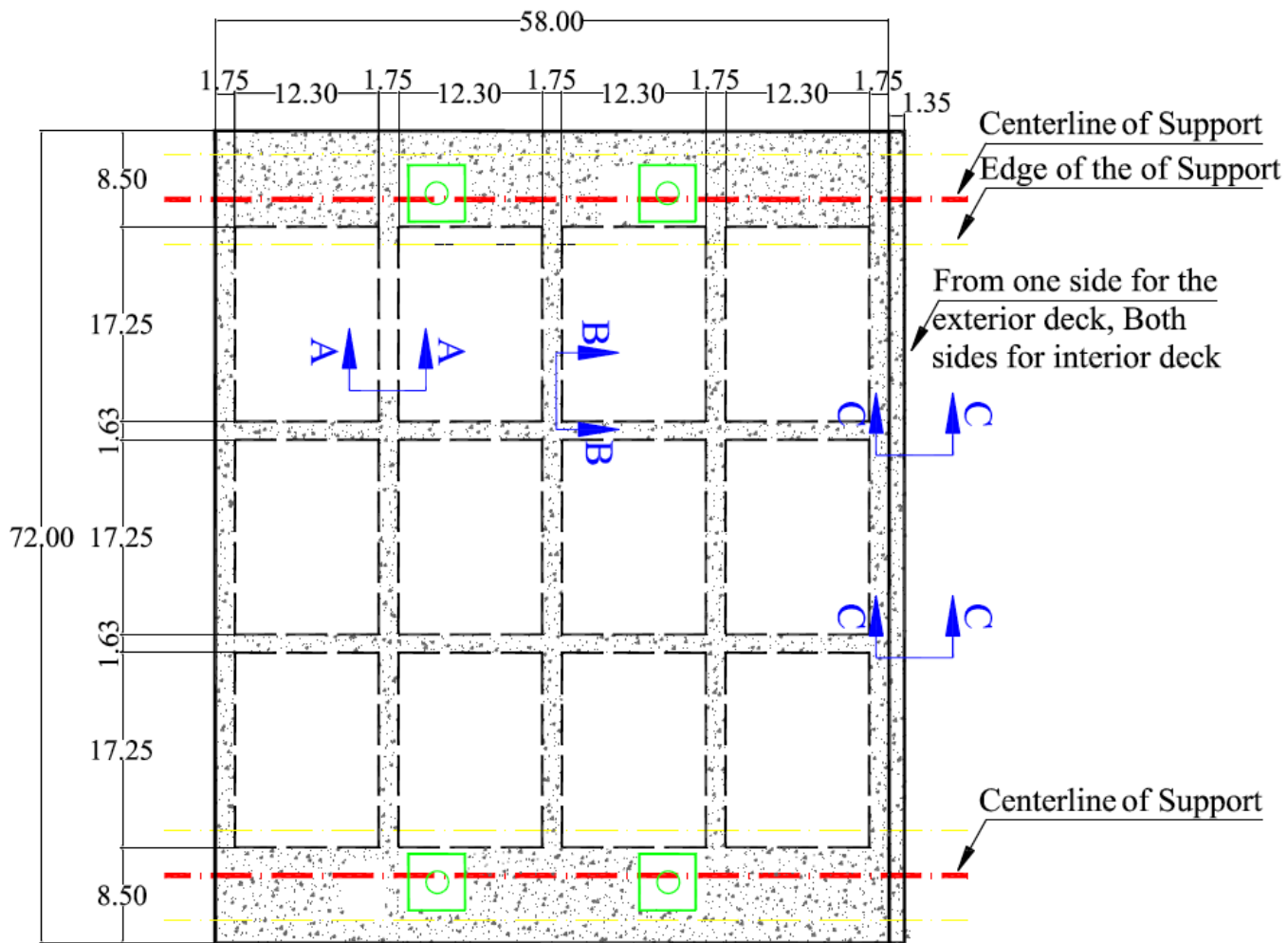


Figure 4.49 Panel 1 (UHPC-HSS)

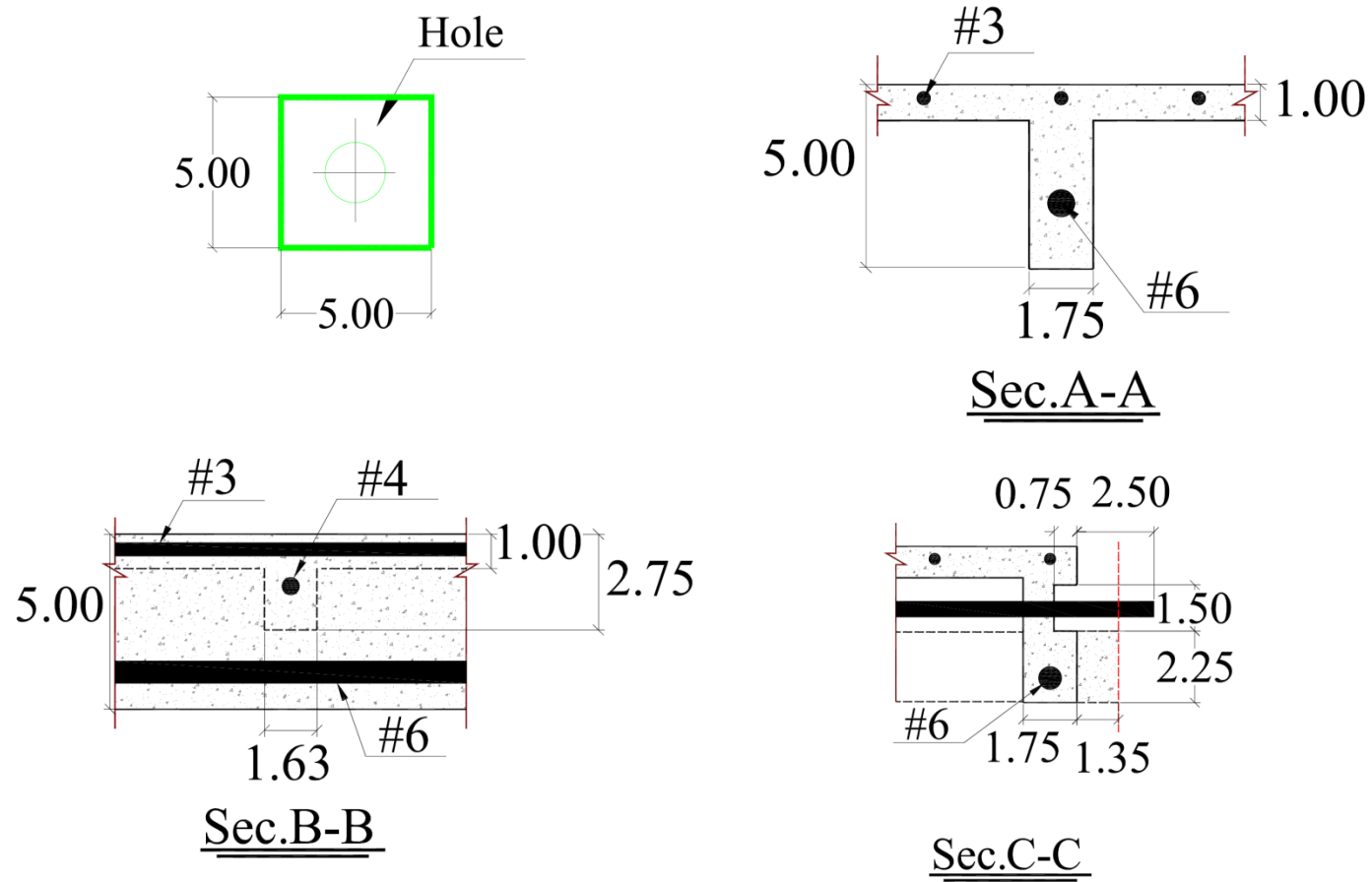


Figure 4.50 Detail of Panel 1 (UHPC-HSS)

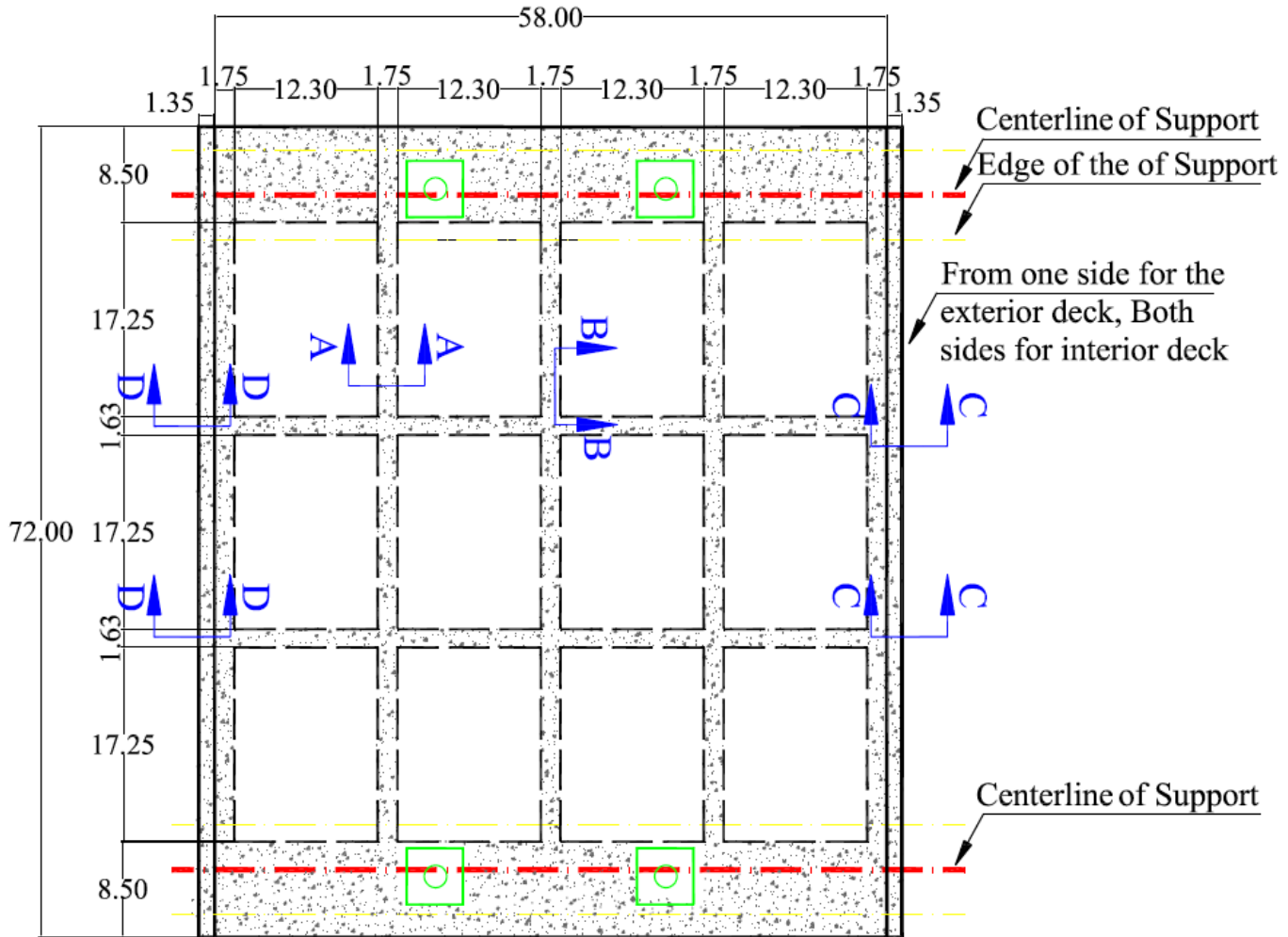


Figure 4.51 Panel 2 (UHPC-HSS)

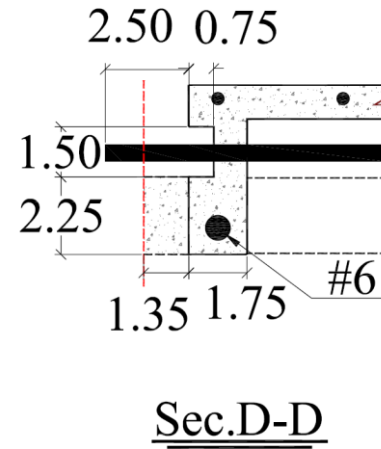
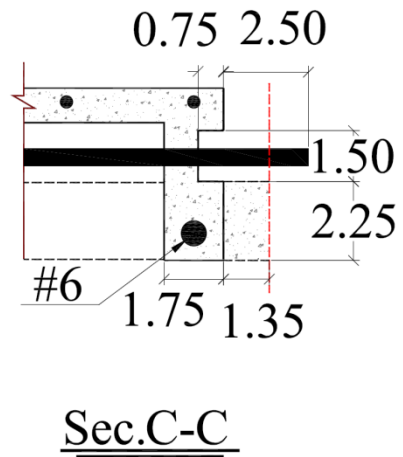
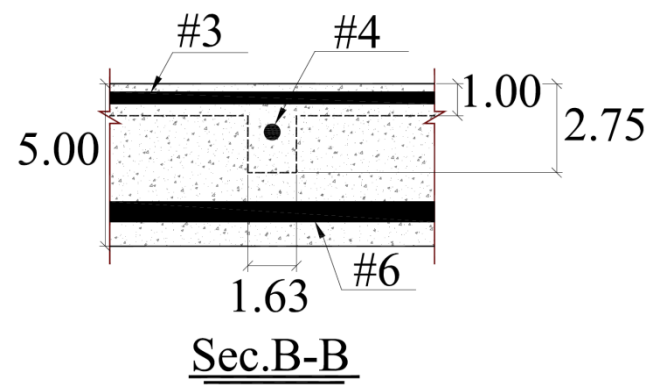
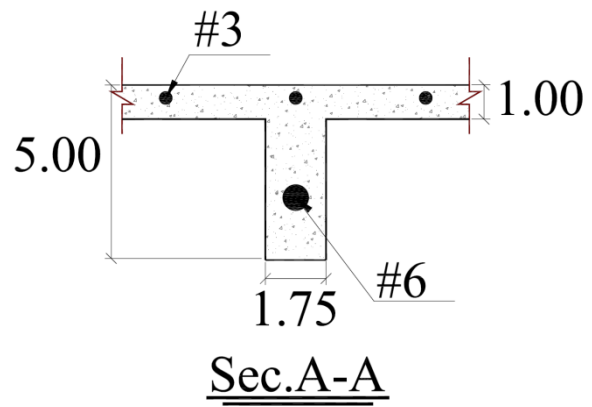


Figure 4.52 Detail of Panel 2 (UHPC-HSS)

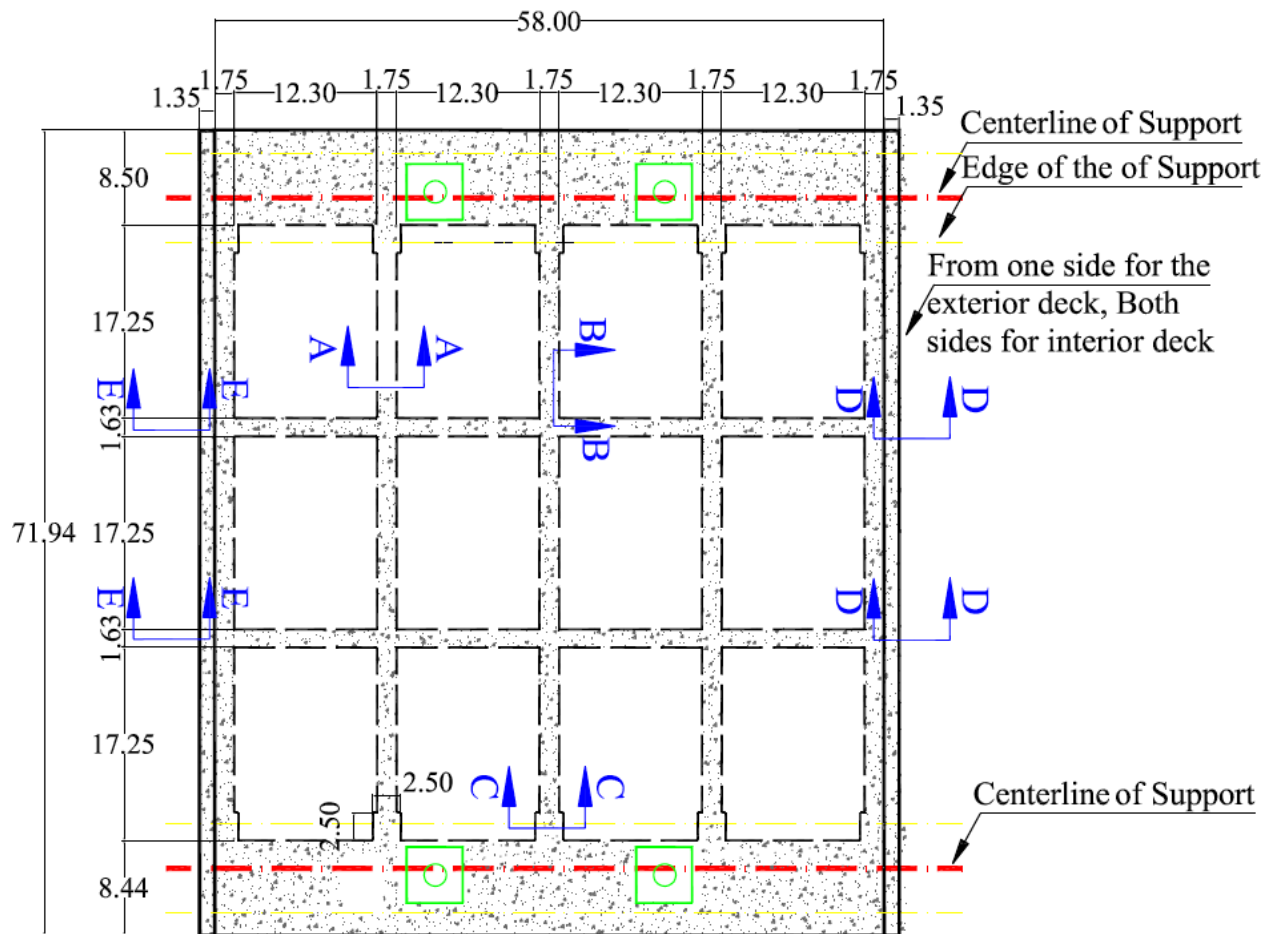


Figure 4.53 Panel 3 (UHPC-CFRP)

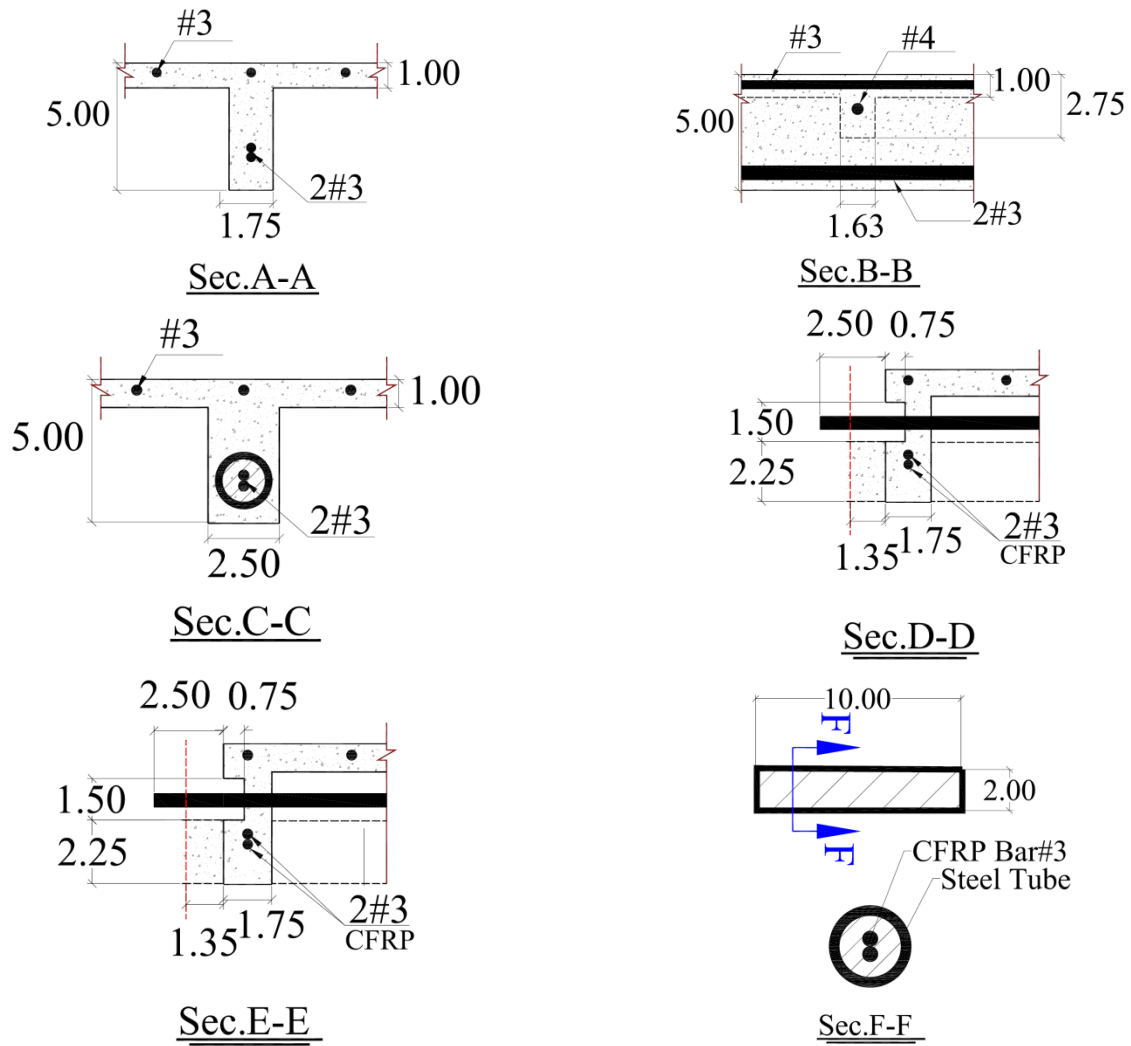


Figure 4.54 Detail of Panel 3 (UHPC-CFRP)

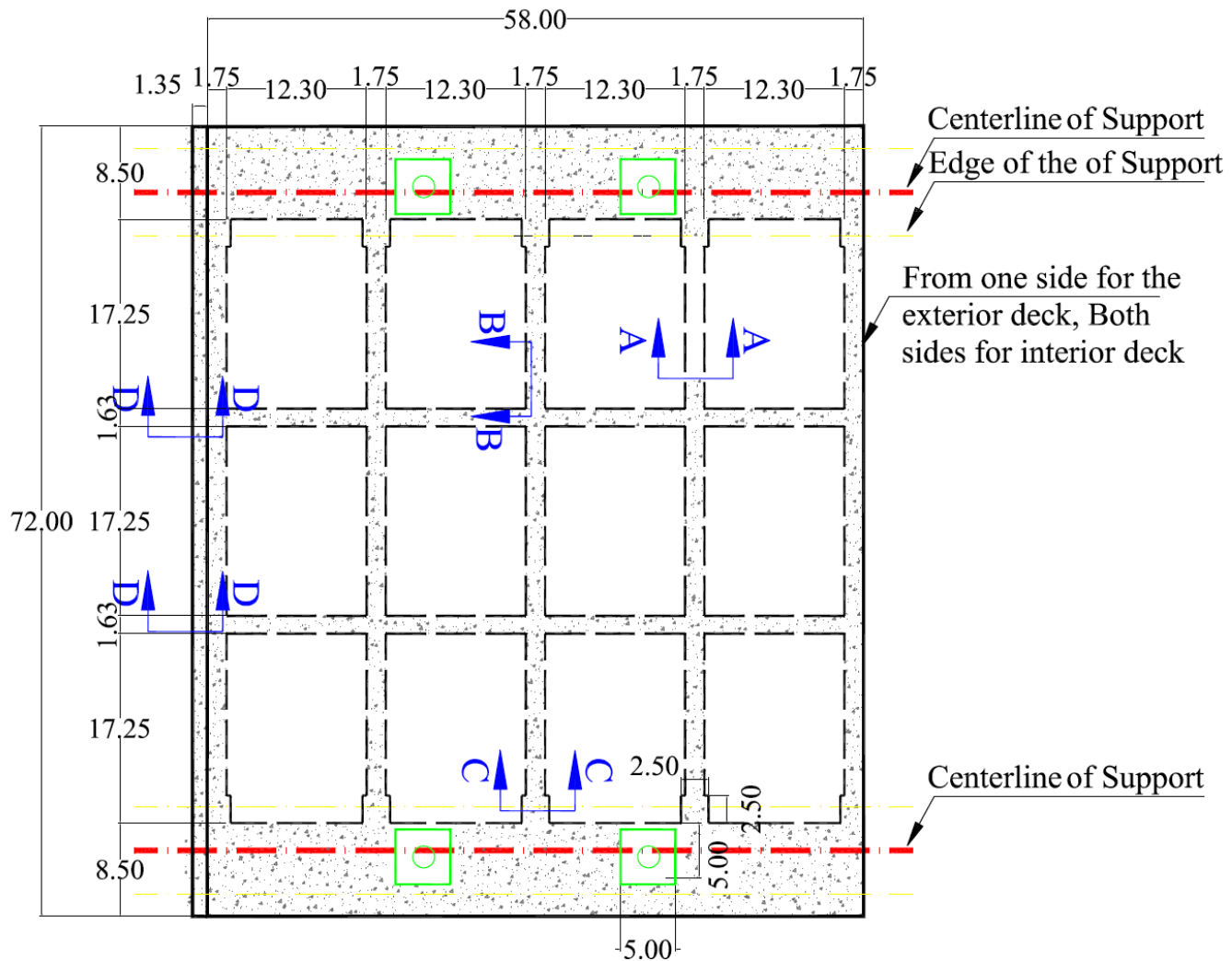


Figure 4.55 Panel 4 (UHPC-CFRP)

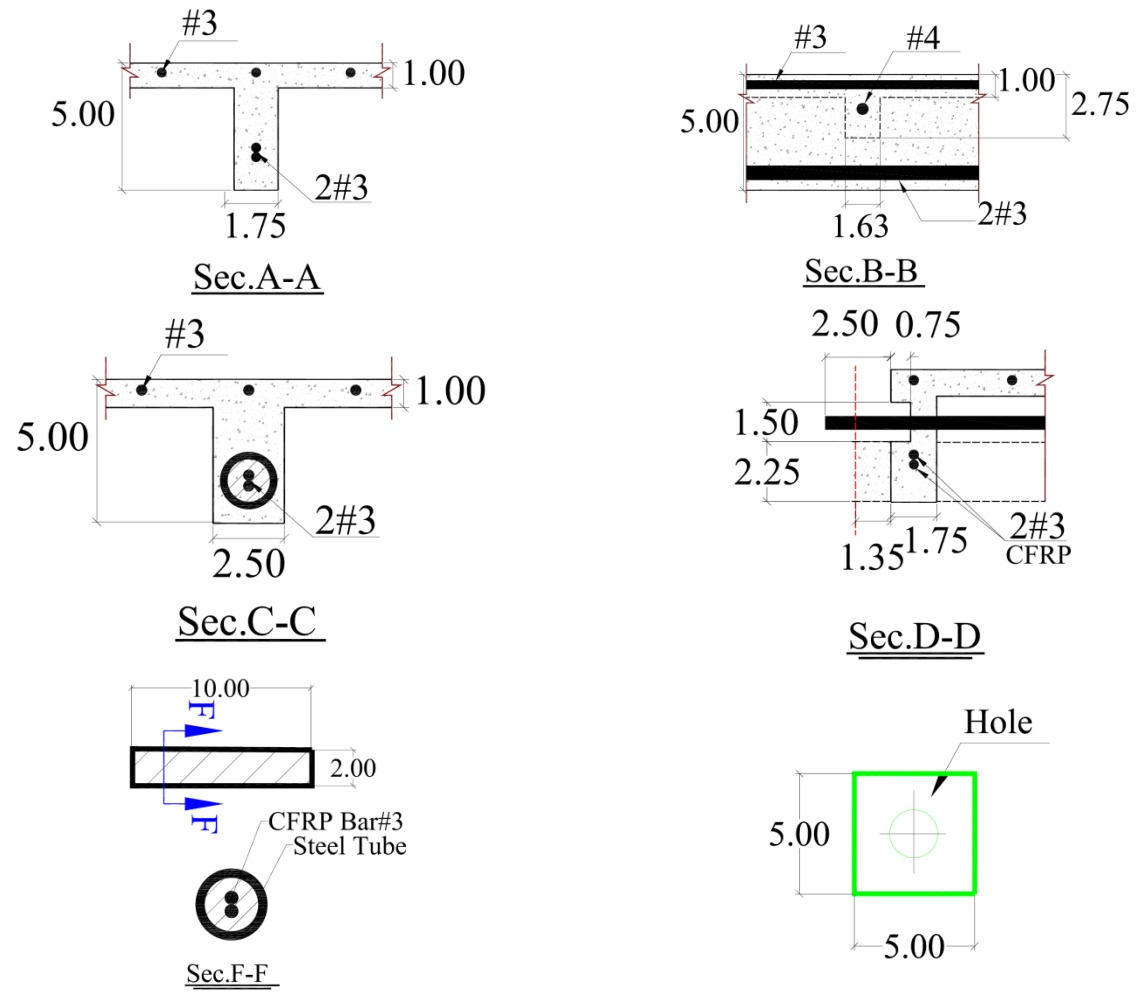
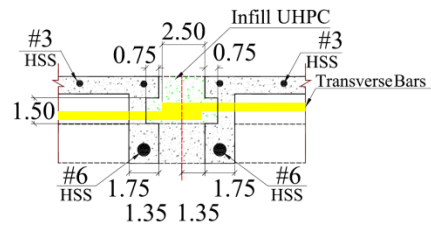
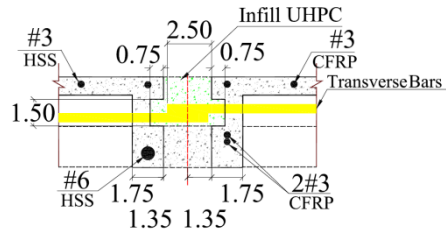
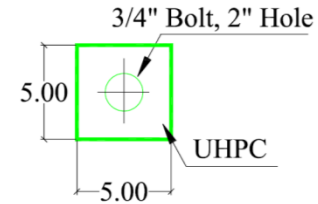


Figure 4.56 Detail of Panel 4 (UHPC-CFRP)



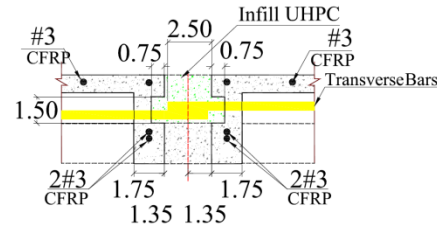
Detail A

UHPC-HSS to UHPC-HSS Connection



Detail B

UHPC-HSS to UHPC-CFRP Connection



Detail C

UHPC-CFRP to UHPC-CFRP Connection

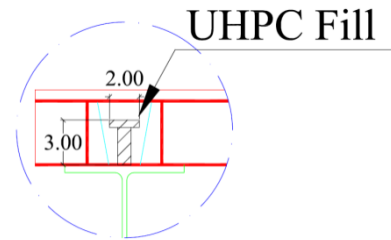
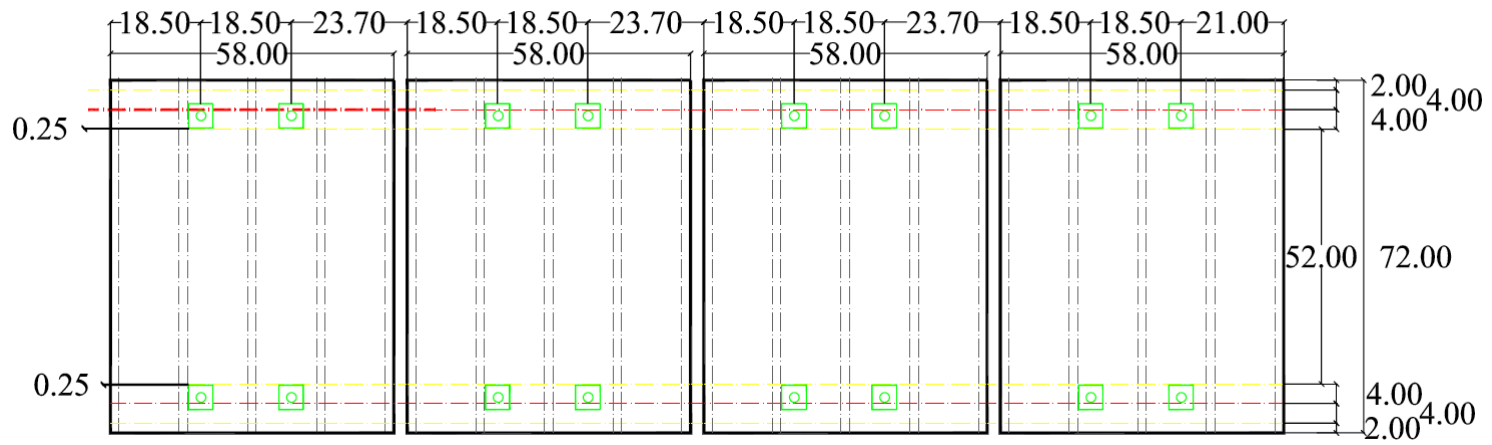
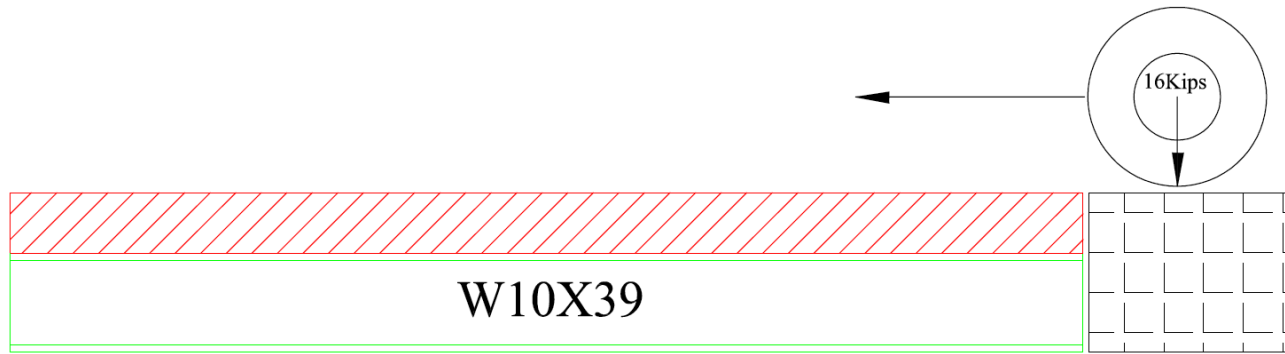


Figure 4.57 Detail of Connections



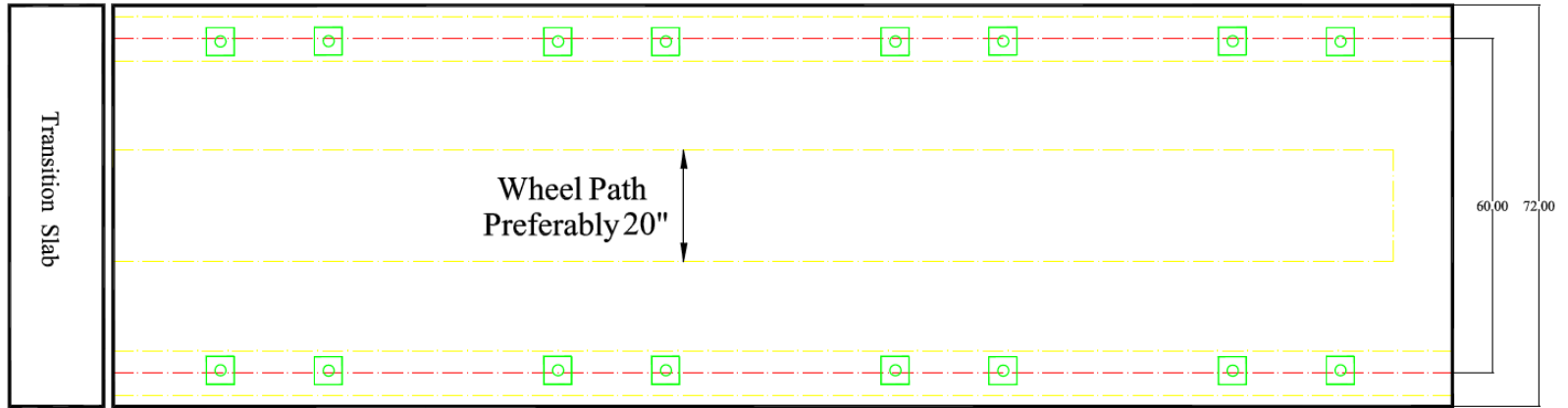


Figure 4.60 Wheel Path Dimensions

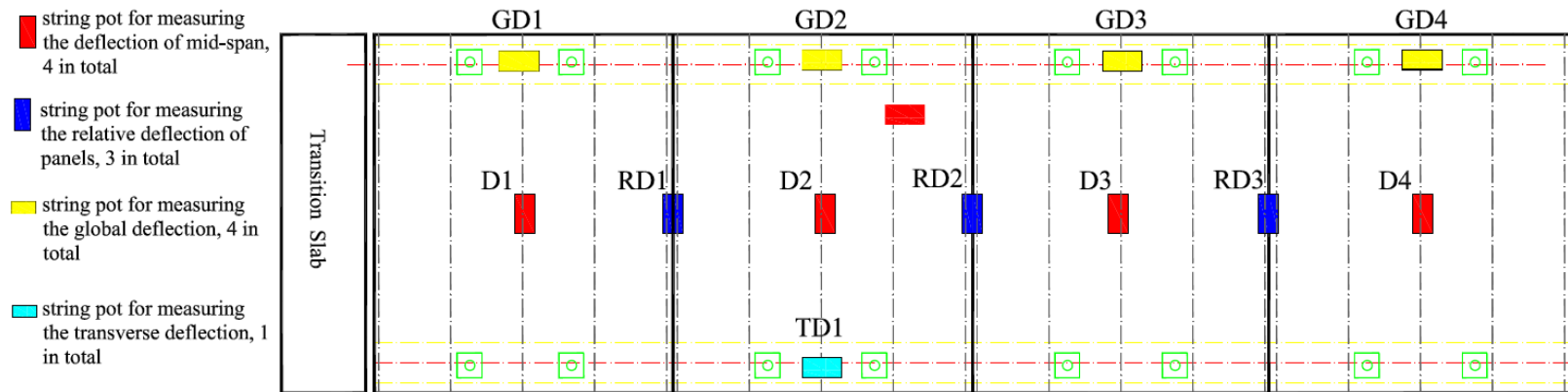
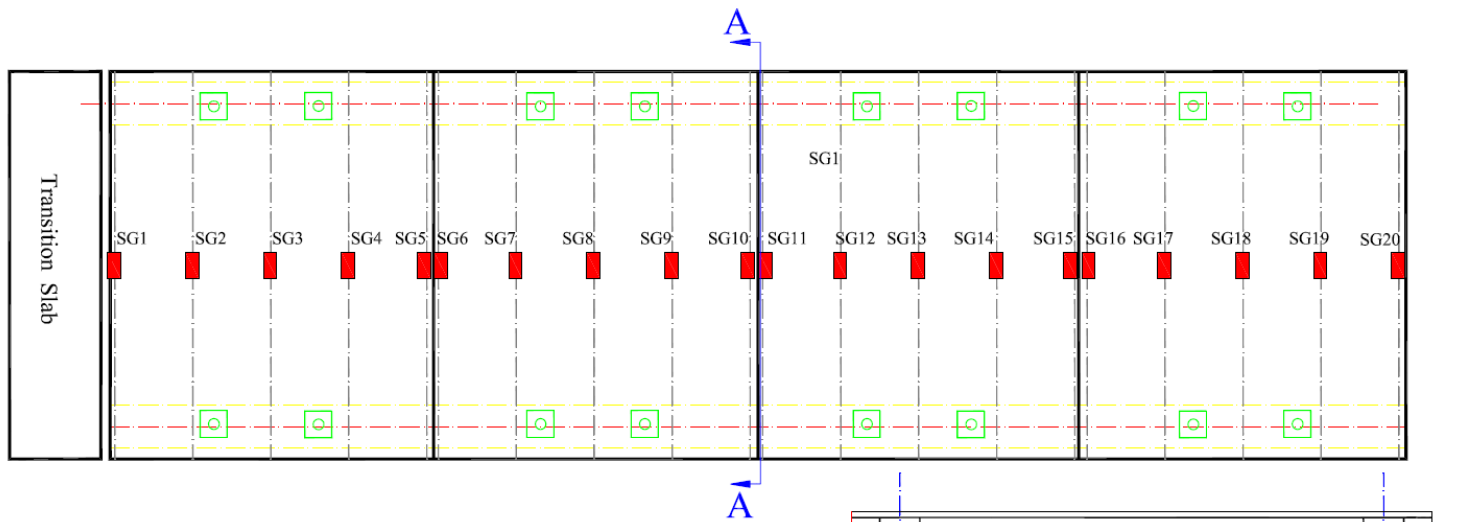
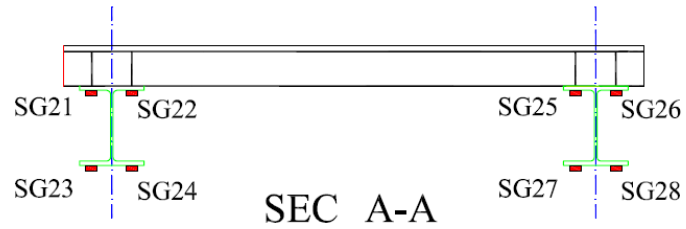


Figure 4.61 Instrumentation Plan (String Pots)



Strain Gauge for HSS rebars (TML)  
 Type: YEFLA-5-5L  
 Lot No. Y510611  
 Gauge length: 5 mm  
 Gauge factor: 2.14 +/- 2 %  
 Gauge resistance: 121 +/- 0.5 ohm  
 Temp. compensation: -  
 Transverse sensitivity: -0.1 %  
 Lead wire: 10/0.12 5m

Strain Gauge for CFRP bars (TML)  
 Type: PFL-30-11-5L  
 Lot No. A703611  
 Gauge length: 30 mm  
 Gauge factor: 2.11 +/- 1 %  
 Gauge resistance: 120 +/- 0.5 ohm  
 Temp. compensation: 11e-6 degree C  
 Transverse sensitivity: -0.6 %  
 Lead wire: 10/0.12 5m



\*Thermocouples may be installed as previous tests.

■ Strain gauge on longitudinal bar (20 in total)

In case of limitation for having 16 strain gauges in total, please eliminate SG1, SG2, SG4, SG5, SG16, SG17, SG19, SG20, SG21, SG23, SG26, and SG28.

Figure 4.62 Instrumentation Plan (Strain Gauge)

Figure 4.63 shows the strain responses of HSS bars vs. number of truck passages. According to the test results, the maximum strain recorded was 0.0012 which was significantly smaller than the yield strain of HSS bar, as 0.004. The strain responses of CFRP bars vs. number of truck passages are illustrated in Figure 3.64.

Figure 4.65 represents the Deflection of Panels vs. the Number of Truck Passages. The maximum deflection recorded for UHPC-HSS panels was 0.018 in. and for UHPC-CFRP panels was 0.021. Comparing to the prior APT test (3<sup>rd</sup> phase of testing) results the deflections of the panels under APT was fairly lower. This phenomenon could be considered as a result of three reasons. First of all, there is an increase in the thickness of the slab from ¾ in. to 1 in. Secondly, the connections between the panels enhanced the overall performance of the bridge deck by benefiting the better load distribution as compared to a single panel deck. Finally, the blockouts which used to connect the bridge deck to the stringers made the supports slightly fixed comparing to the pinned-pinned supports in the previous phases.

Relative deflections between the panels were recorded to assess the performance of the connections. The results are presented in Figure 4.66. The maximum relative deflection was recorded as 0.0011 in. which is 1/220000 of the total length of the deck. Therefore, it could be considered as negligible.

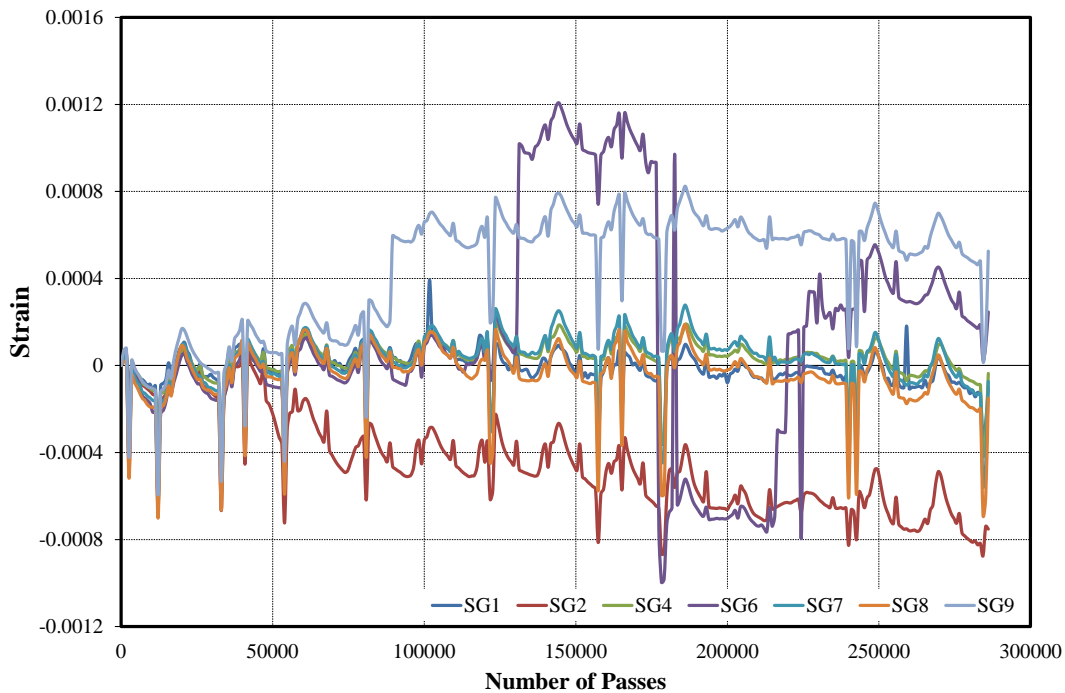


Figure 4.63 Strain Responses of HSS Bars vs. the Number of Truck Passages

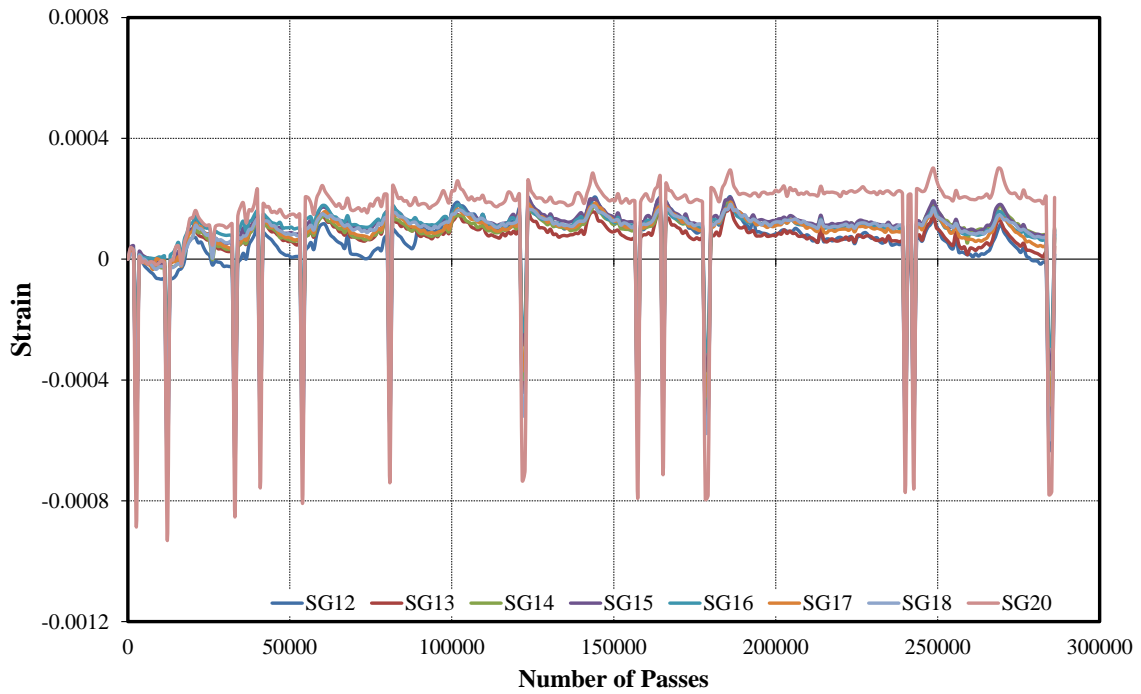


Figure 4.64 Strain Responses of CFRP Bars vs. the Number of Truck Passages

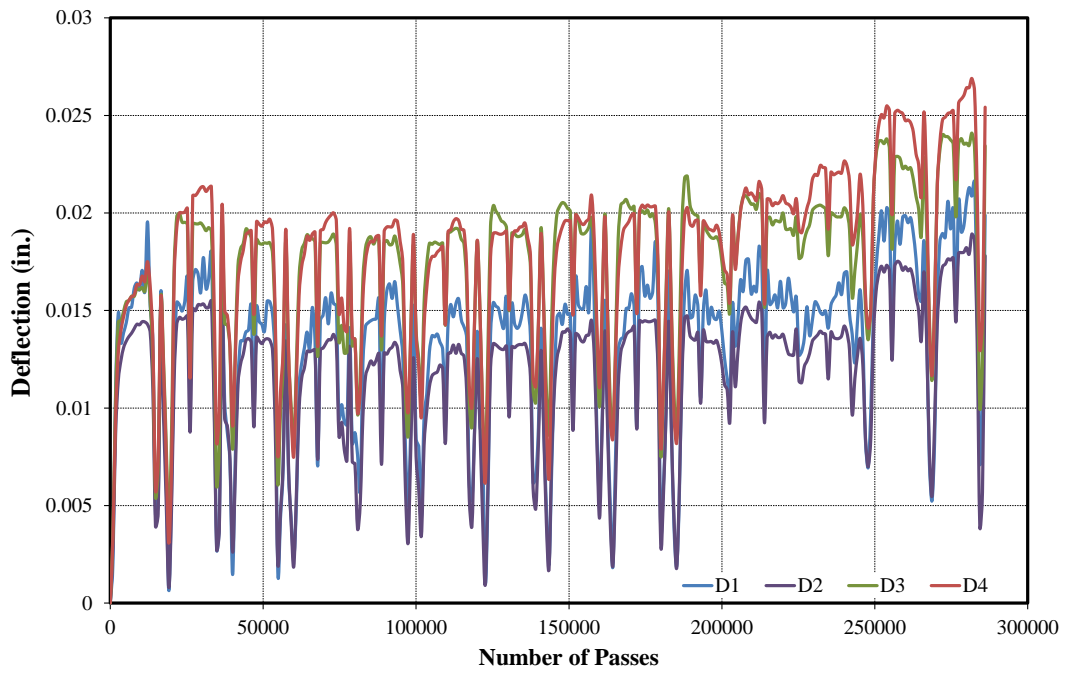


Figure 4.65 Deflections of Panels vs. the Number of Truck Passages

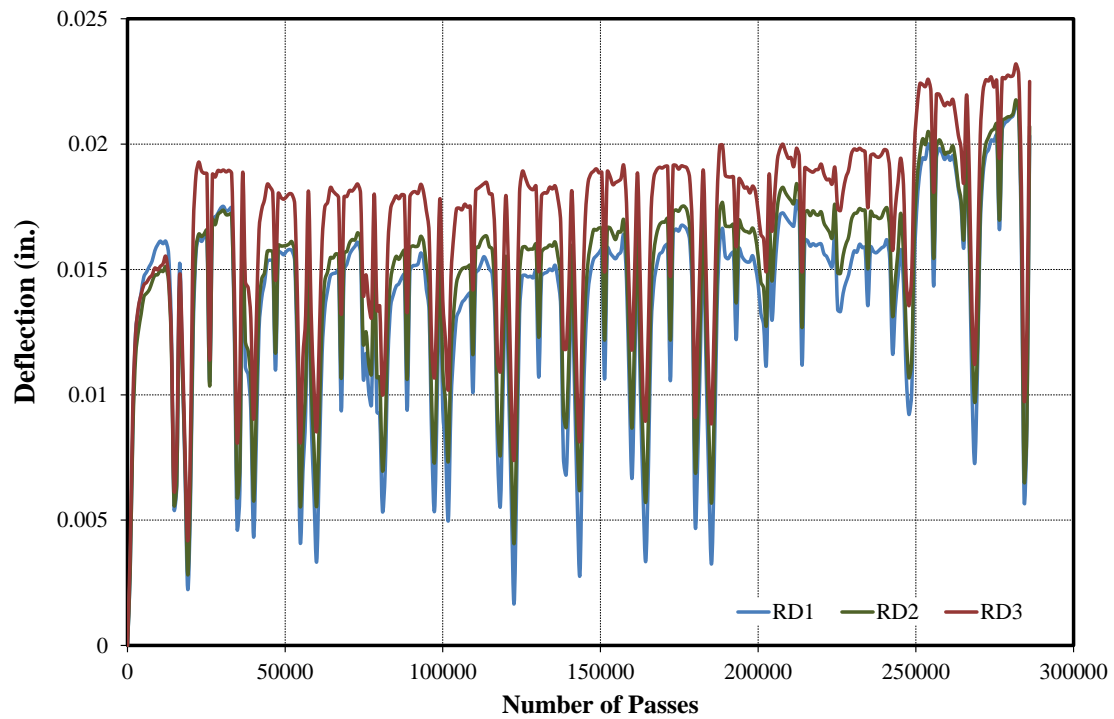


Figure 4.66 Relative Deflections of Panels vs. the Number of Truck Passages

Figure 4.67 shows the deck after the test. As seen in the Figure 4.67 (b), some minor cracks were observed on the connection parts. Also, Figure 4.67 (c) presents the cracks formed on the top of the panel 2 (UHPC-HSS Panel) followed by a close up view of the cracks in Figure 4.67 (d). The average crack width measured was 0.015-0.02 inch.



(a)



(b)



(c)



(d)

Figure 4.67 Deck Status after the APT, (a) Deck Overview, (b) Cracks on the Connection Parts, (c) Cracks on the top of Panel 2 (d) Close up view of the Cracks on Panel 2

#### 4.4 Finite Element Modeling

The numerical simulations were performed using the general-purpose finite element software package ABAQUS. This study includes the finite element analysis of three UHPC waffle deck specimens in T-section shape with single or multiple units in single or double span configurations. The dimensions of the specimens and the boundary conditions are exactly the same as the corresponding experimental tests in order to provide appropriate comparison between the finite element modeling outputs and experimental tests' results. A displacement control method was utilized for analyzing procedure. A 10×20” loading pad was modeled representing the HS 20 truck tire footprint. The displacement was assumed uniformly applied to the loading pad. Enhanced hexahedral 3D stress element with secondary order of accuracy was used to model the UHPC material. The element deletion option is on meaning that that the element will be removed from the stiffness matrix if it failed. In order to model the reinforcement, 3-node two-dimensional truss element type was used.

Compressive strength of the each specimen was modeled based on the compressive test results on 4 by 8 cylinders corresponding to each specimen. The compressive strength tests were carried out 28 days after the casting day.

The stress-strain recommended by Aaleti was used in the modeling with a difference in peak stress value for the UHPC (value of stress at point A in Figure 4.68). The peak stress value was taken from the experimental tests results.

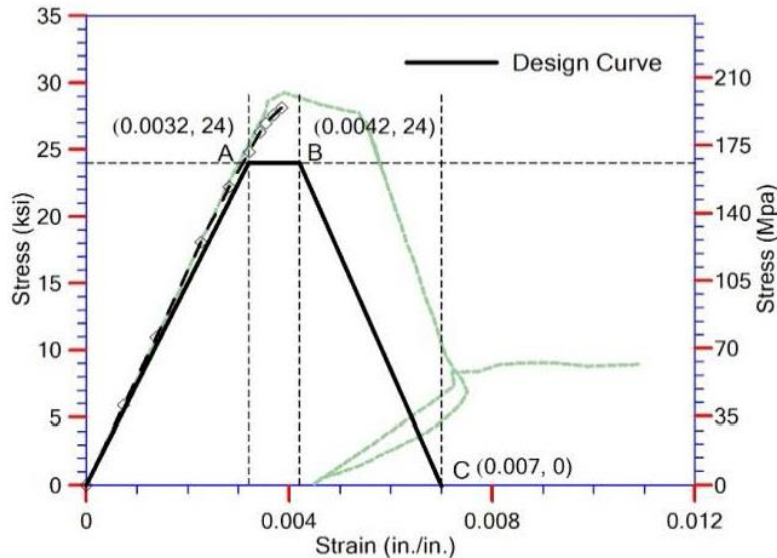


Figure 4.68 Stress-Strain Behavior of UHPC

Different experimental methods were investigated to evaluate the tensile behavior of UHPC, including the flexural prism test, dog-bone test, split cylinder test and direct tension test (Graybeal, 2006). According to this study, the cracking tensile strength of UHPC is recommended as 1.3 ksi for steam-cured and 0.9 ksi for and untreated curing. Graybeal (2006) recommended the cracking tensile strength of UHPC to be taken as 0.9 -1.2 ksi. In this study, the value of 1.0 ksi was used in the finite modeling.

Graybeal (2007) recommended a formula for calculating the modulus elasticity of UHPC:

$$E(\text{psi}) = 46,200 \sqrt{f'_c} \text{ (psi)}$$

According to this formula, different modulus of elasticity was used for different specimens according to the corresponding test results; however the values were relatively close to each other. Some investigation was carried out on Poisson ratio of UHPC (Ahlborn, 2008). The Poisson ratio was taken as 0.2 in the finite element modeling.

Figure 4.69 presents the stress-strain curve for HSS which is taken from the manufacturer data sheet.

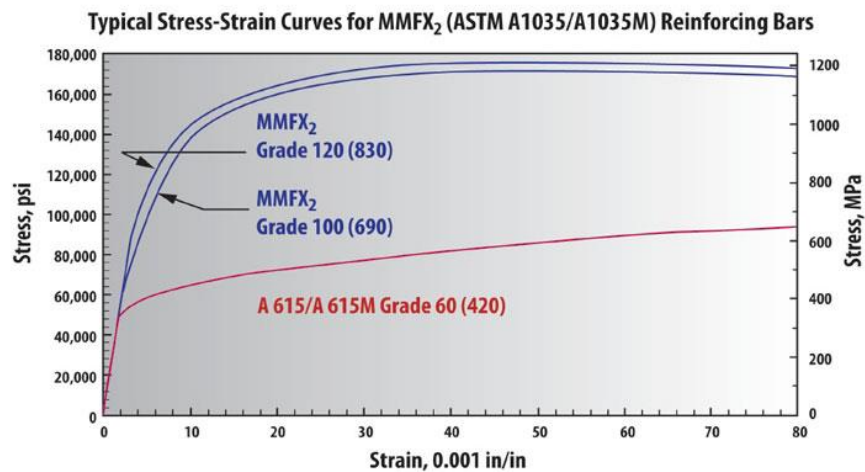


Figure 4.69 Stress-Strain Behavior of HSS (MMFX)

Figure 4.70 shows the geometry and mesh of the Specimen 1T1S. The boundary condition is presented in Figure 4.71. As seen in the figure, the boundary conditions on the support are modeled by constraining the lines on both ends. In one side three degrees of displacement are constrained to model a pin support; on the other side two degrees are constrained to model a roller support.

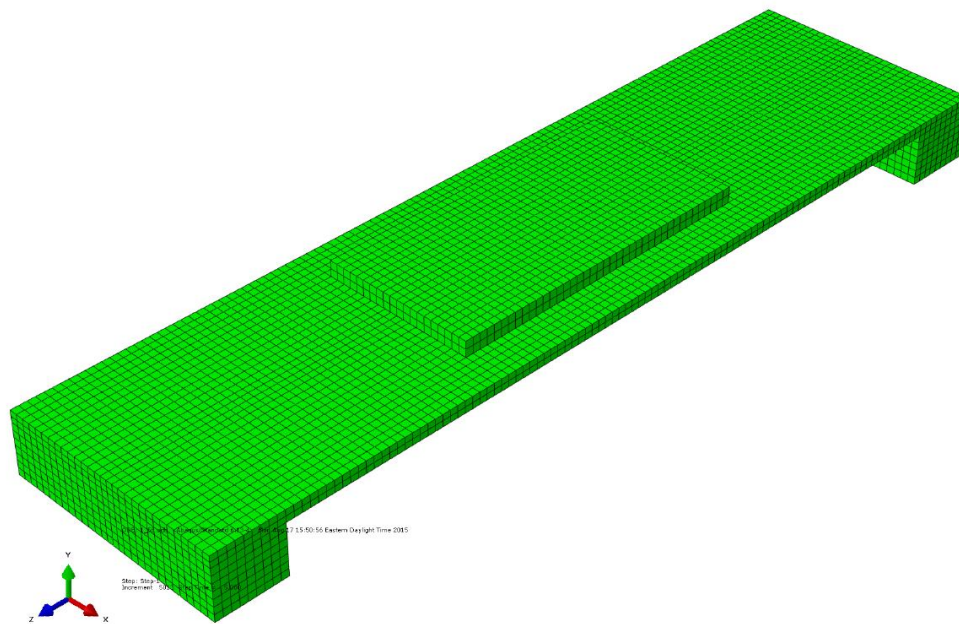


Figure 4.70 Geometry and Mesh of Specimen 1T1S-HSS

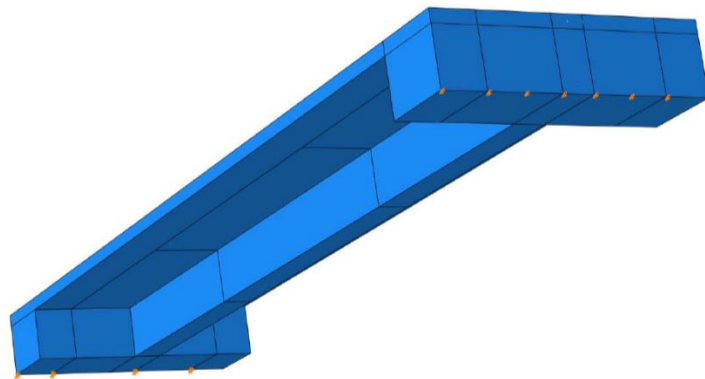


Figure 4.71 Boundary Conditions of Specimen 1T1S-HSS

Figure 4.72 shows the deflected model as compared to the tested specimen. As seen in the figure, the failure mode is the beam shear crack next to the supports which determined the good consistency in the modes of failure between the FE model and the tested specimen. The load-deflection response of the specimen is shown in Figure 4.73 which is compared to the corresponding experimental test.

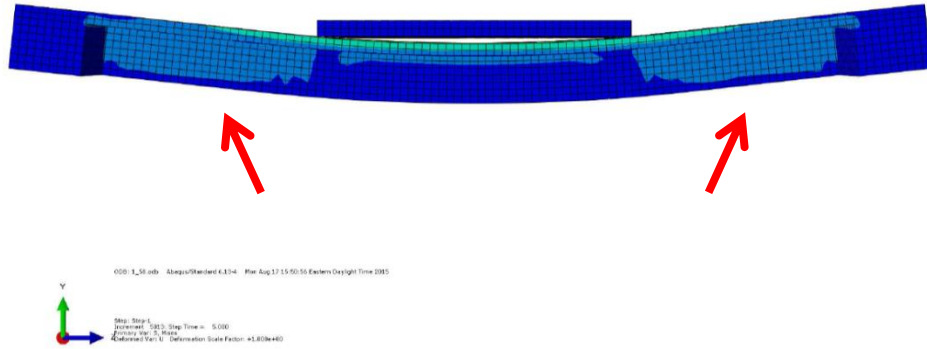


Figure 4.72 Failure Modes and Deflected shape of the Specimen 1T1S-HSS, (a) FE Modeling, and (b) Failure Mode in Experimental Test

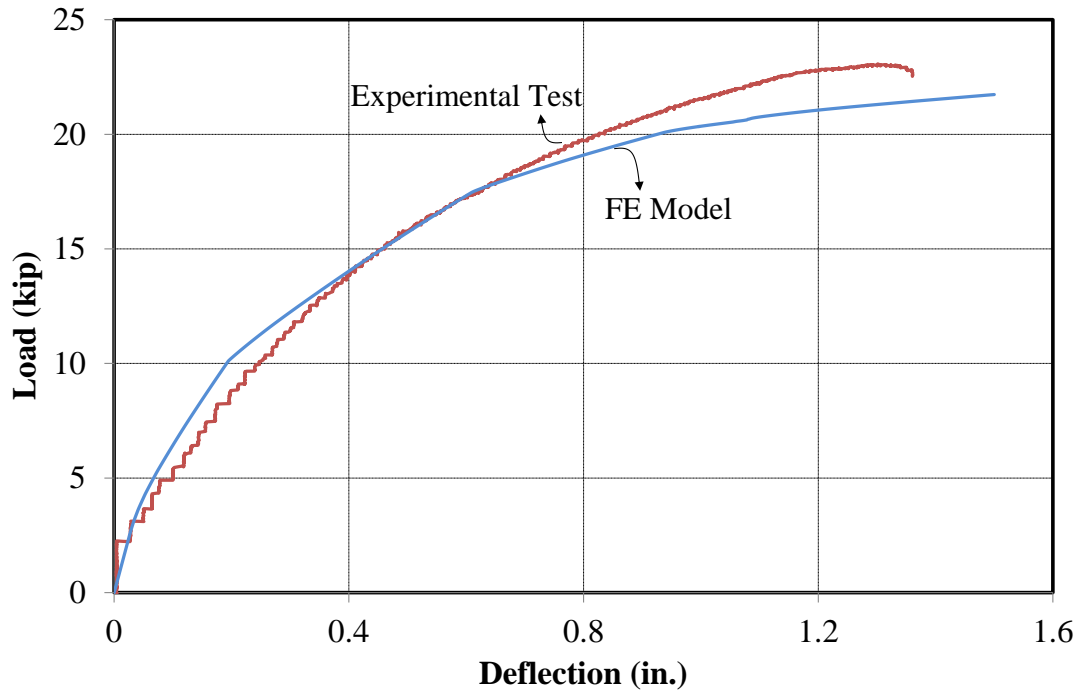


Figure 4.73 Load-Deflection Response of Model 1T1S-HSS

It can be noticed that the finite element results showed a good agreement with the tests results although the model underestimate the load capacity for 1.34 kips which may be results from the value for the shear strength made in the model.

The finite element model of Specimen 1T2S-HSS is shown in Figure 4.74.

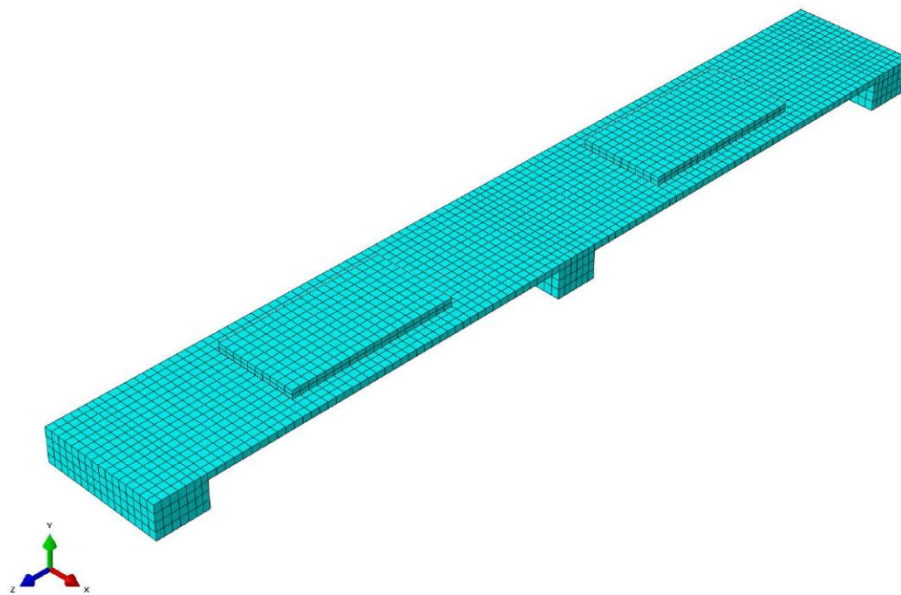
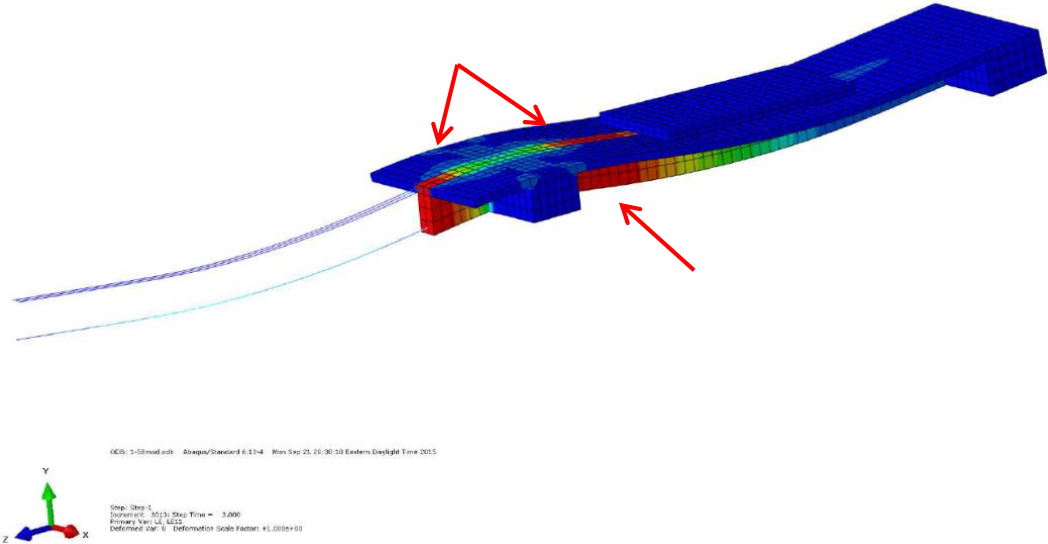


Figure 4.74 Finite Element Model of Specimen 1T2S-HSS

The deflected shape of the specimen along with the failure mode is presented in Figure 4.75. The top view and side view of the model is shown in separate figures in Figure 4.76 and 4.77, respectively. Figure 4.78 which illustrate the load-deflection response of the specimen comparing to its counterpart in the experimental tests.



(a)



(b)

Figure 4.75 Failure Modes and Deflected shape of the Specimen 1T2S-HSS, (a) FE Modeling, and (b) Failure Modes in Experimental Test

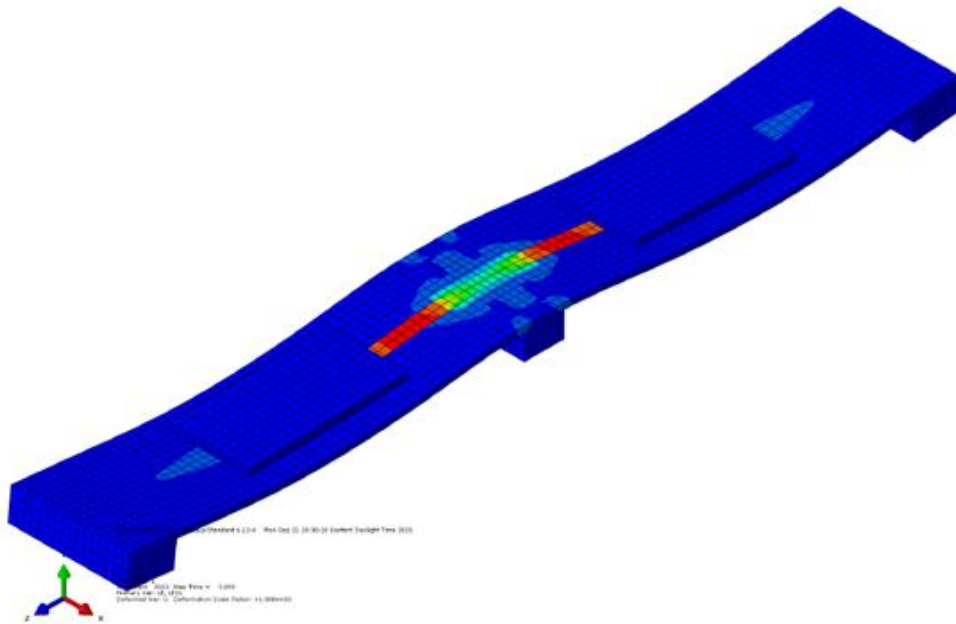


Figure 4.76 Top View of the Deformed Model

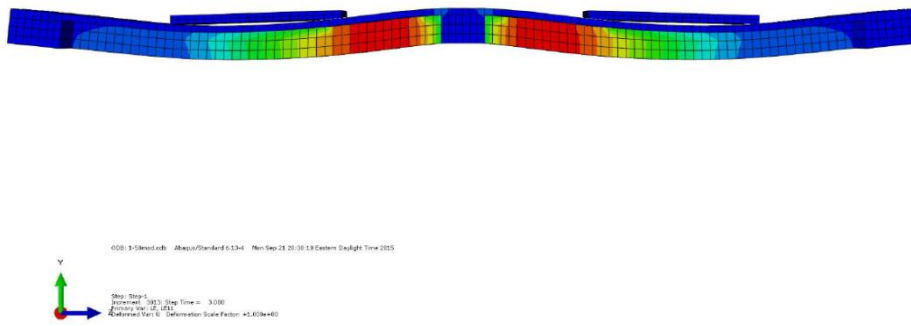


Figure 4.77 Side View of the Deformed Model

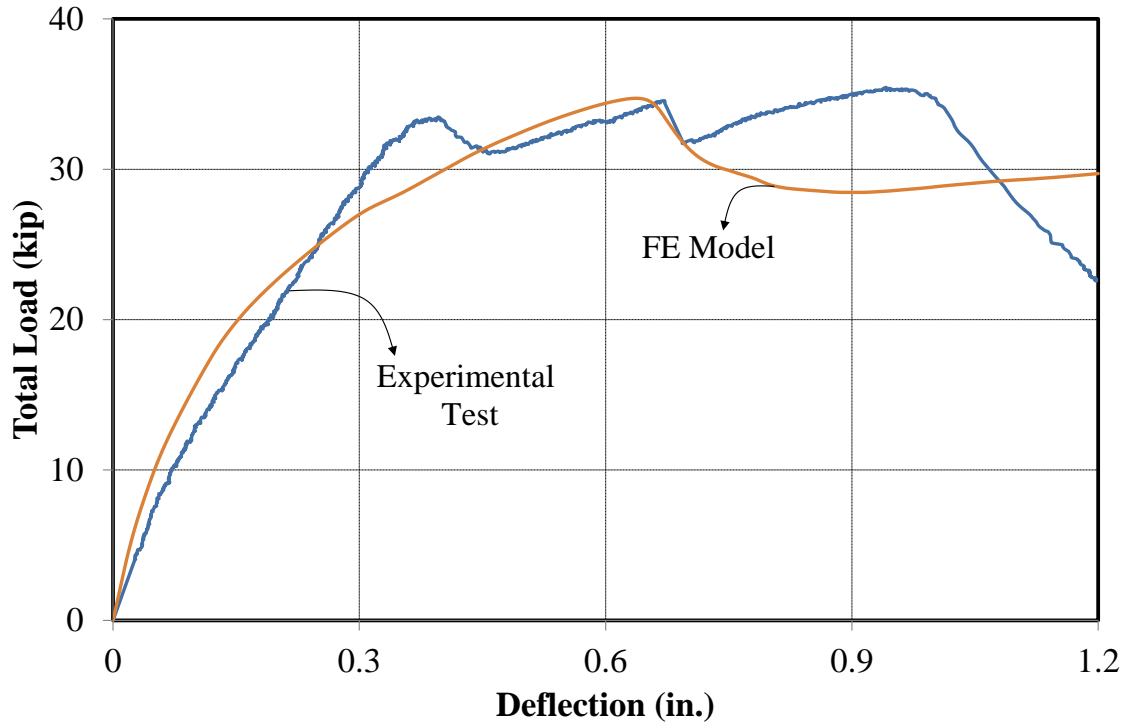
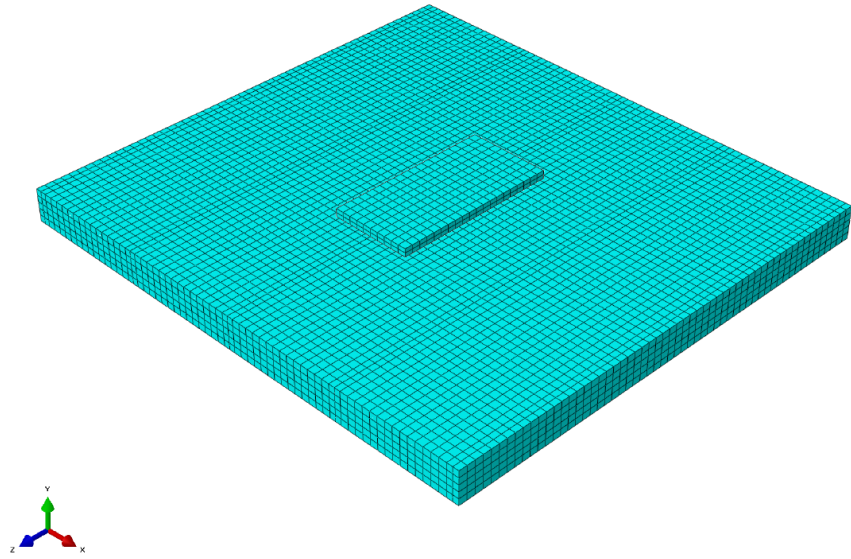


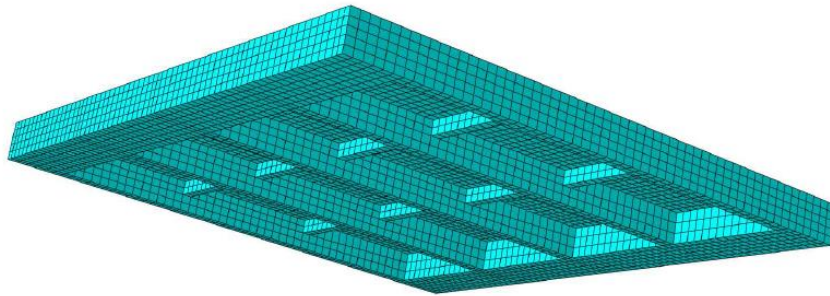
Figure 4.78 Load-Deflection Response of Specimen 1T2S-HSS

Figure 4.78 shows a good agreement between the result of the finite element model and the experimental test. Also, the FE model estimates the maximum load so consistent to the experiments.

The finite element model of Specimen 4T1S-HSS is shown in Figure 4.79 followed by the deflected shape of the specimen along with the failure mode in Figure 4.80. Figure 4.81 shows the failure mode and shear cracks on the main ribs. Similar cracks are detected on the transverse ribs shown in Figure 4.82. In each case, the finite element results are compared to the corresponding experimental specimen.

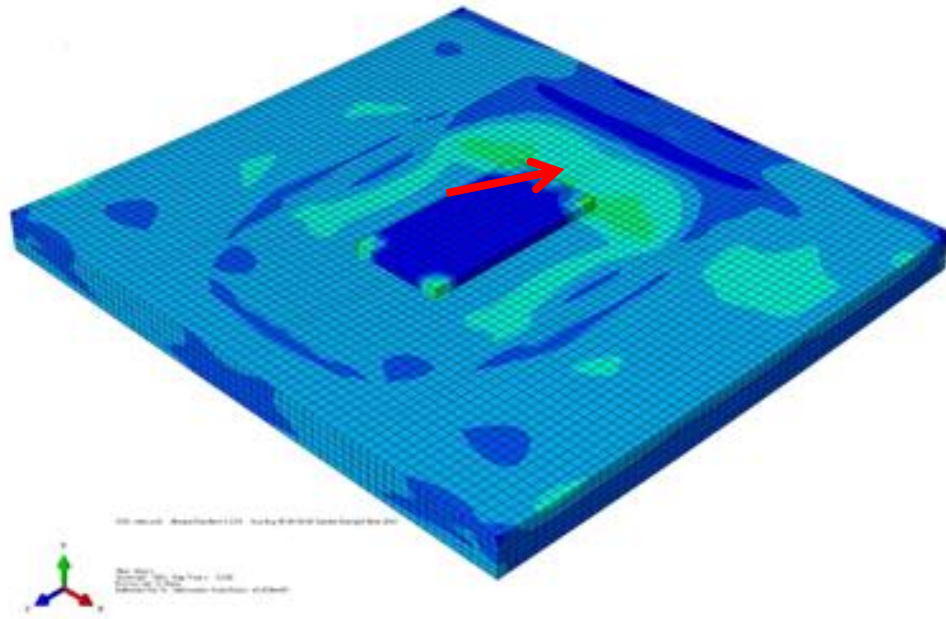


(a)



(b)

Figure 4.79 Finite Element Modeling of Specimen 4T1S-HSS, (a) Geometry and Mesh, and (b) Modeling of the Main and Transverse Ribs

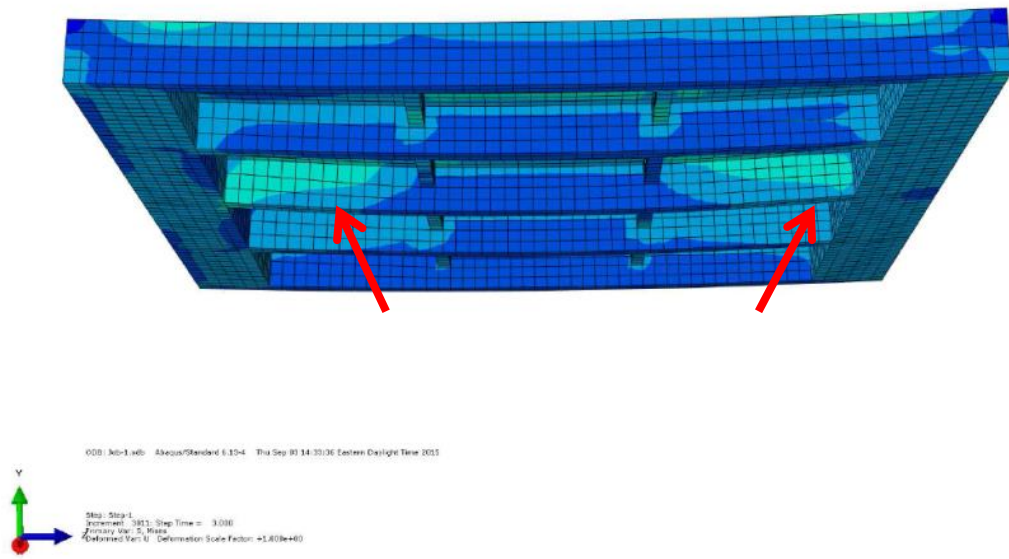


(a)



(b)

Figure 4.80 Failure Modes and Deflected shape of the Specimen 4T1S-HSS, (a) FE Modeling, and (b) Failure Modes in Experimental Test



(a)



(b)

Figure 4.81 Beam Shear Cracks on the Main Ribs, (a) FE Modeling, and (b) Experimental Test



(a)



(b)

Figure 4.82 Beam Shear Cracks on the Transverse Ribs, (a) FE Modeling, and (b) Experimental Test

Figure 4.83 shows the load-deflection response of the finite element modeling of Specimen 4T1S. According to the figure, the finite element model was able to estimate the overall behavior of the experimental specimen.

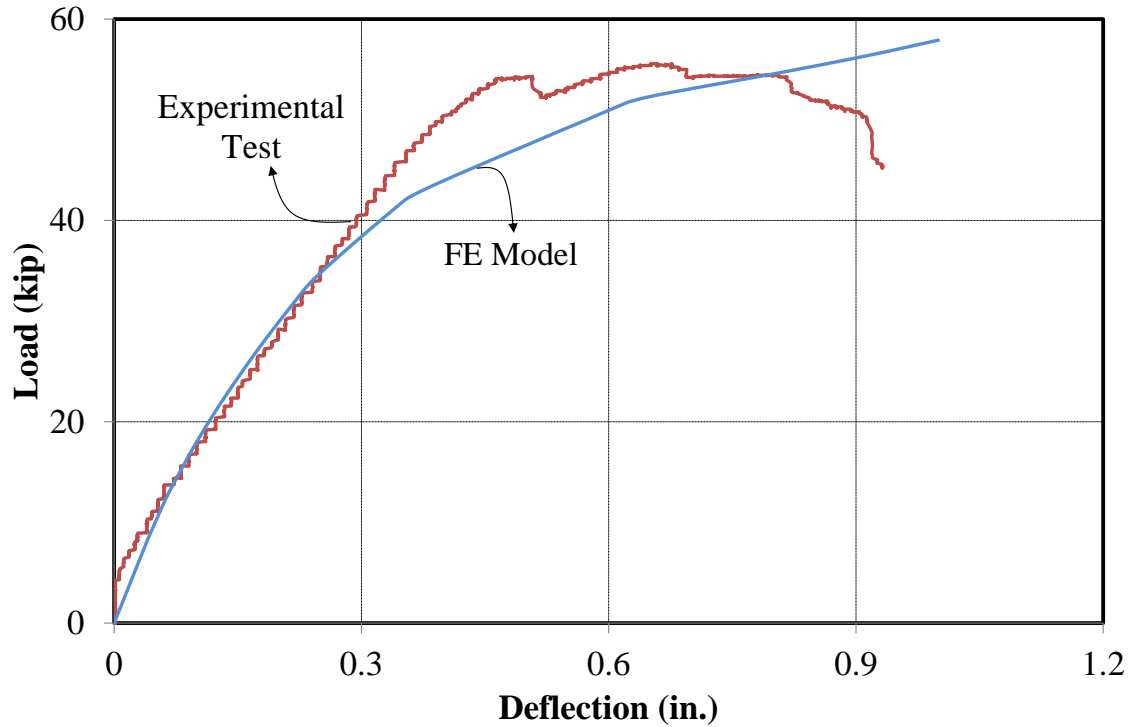
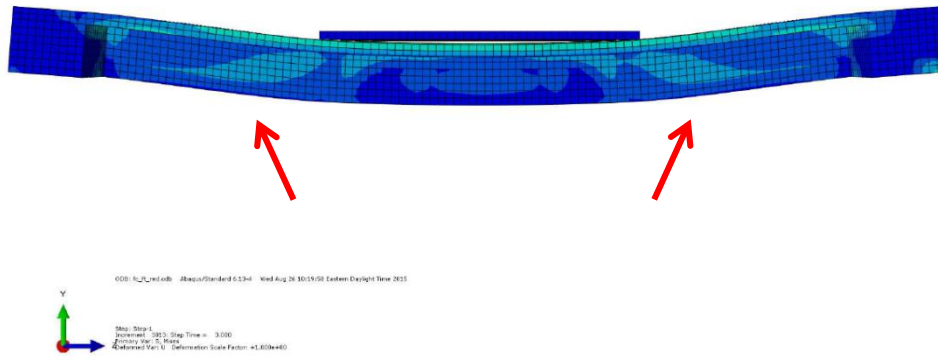
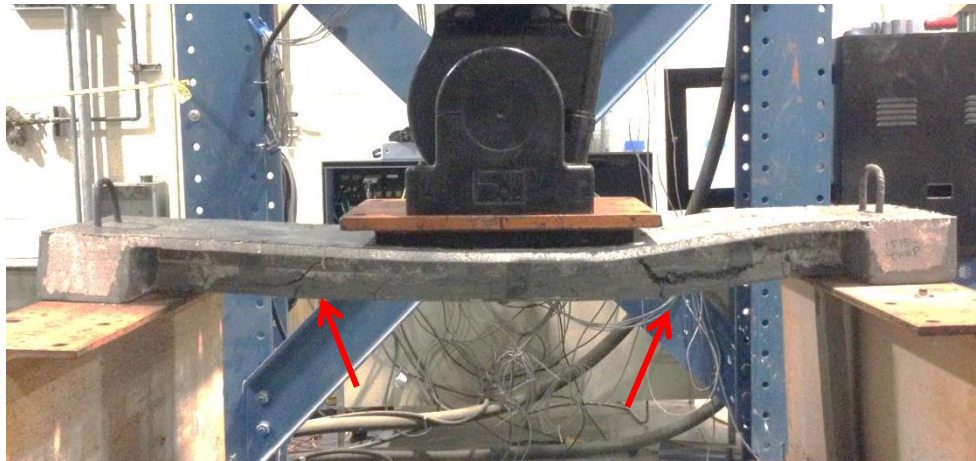


Figure 4.83 Load-Deflection Response of Specimen 4T1S

The Geometry, mesh and boundary conditions of UHPC-CFRP specimens are the same as those for UHPC-HSS specimens. Figure 4.84 shows the deflected model as compared to the tested specimen. As seen in the figure, the failure mode is the beam shear crack next to the supports which determined the good consistency in the modes of failure between the FE model and the tested specimen. The Load-Deflection response of the specimen is shown in Figure 4.85 which is compared to the corresponding experimental test. It can be noticed that the finite element results showed a good agreement with the tests results although the model underestimate the load capacity for 1.75 kips which may be a result for the value for the shear strength in the modeling.



(a)



(b)

Figure 4.84 Failure Modes and Deflected shape of the Specimen 1T1S-CFRP, (a) FE Modeling, and (b) Failure Mode in Experimental Test

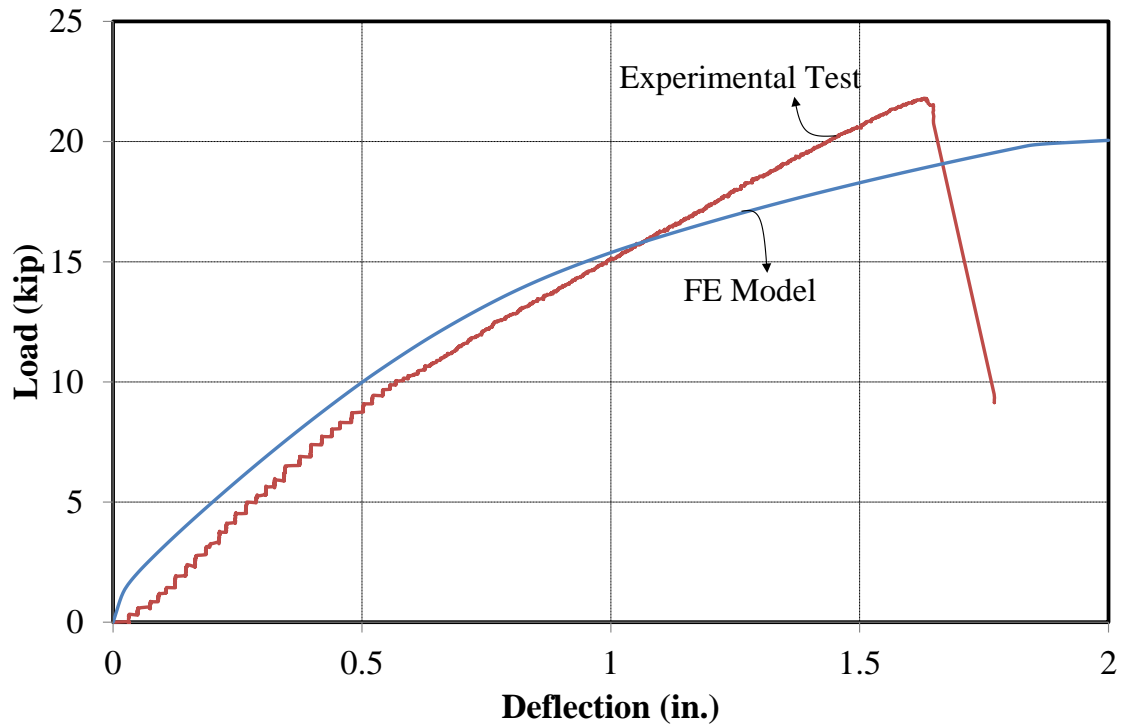


Figure 4.85 Load-Deflection Response of Model 1T1S-CFRP

The finite element model for 1T2S-CFRP specimens is the same as described in earlier sections. The deflected shape of the specimen along with the failure mode is presented in Figure 4.86. The top view and side view of the model is shown in separate figures in Figure 4.87 and 4.88, respectively. Figure 4.89 which illustrate the load-deflection response of the specimen comparing to its counterpart in the experimental tests.

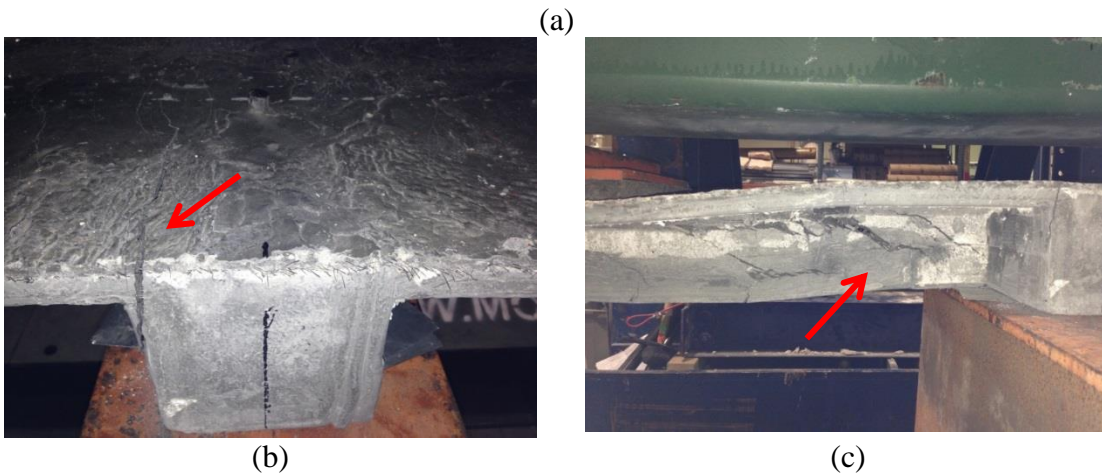
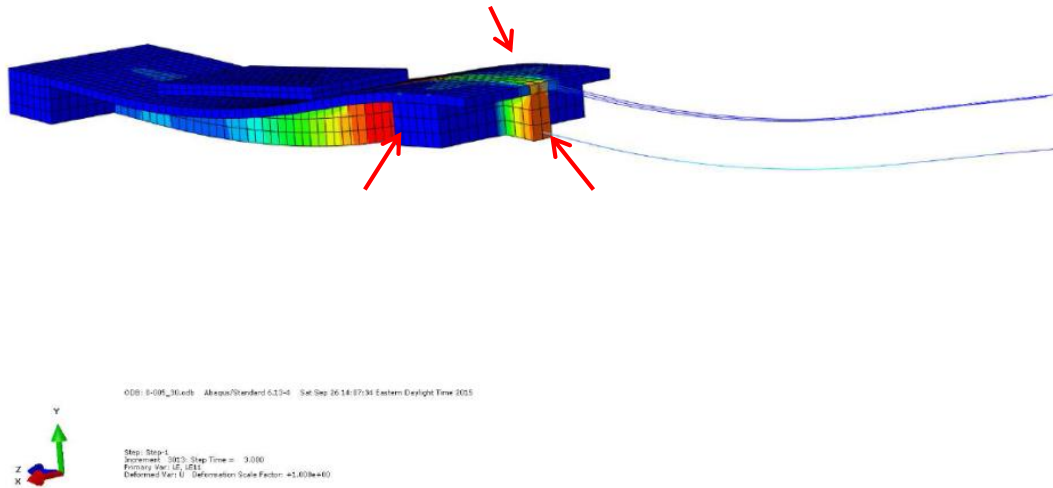


Figure 4.86 Failure Modes and Deflected shape of the Specimen 1T2S-CFRP, (a) FE Modeling, (b) Crack on the Slab, and (c) Shear Cracks on the Web

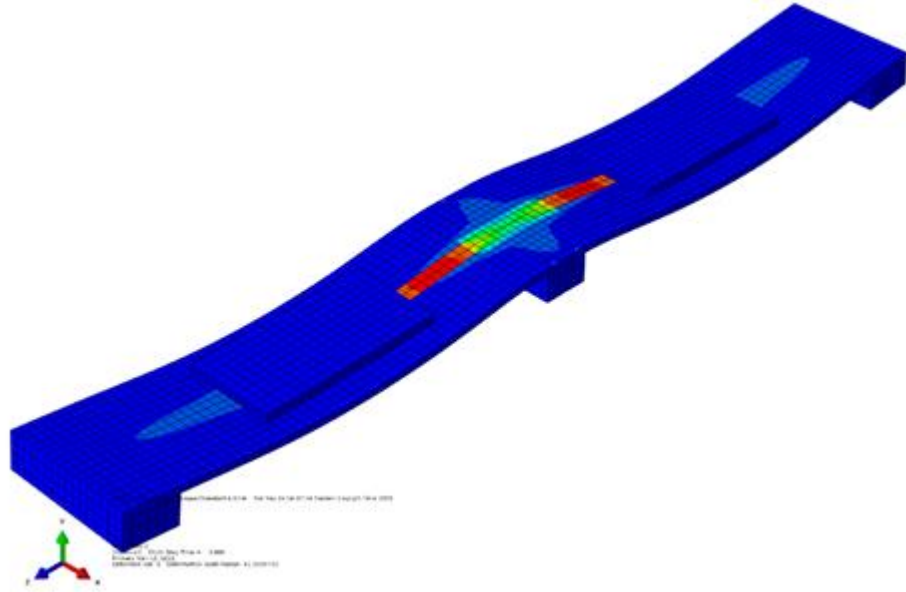


Figure 4.87 Top View of the Deformed Model

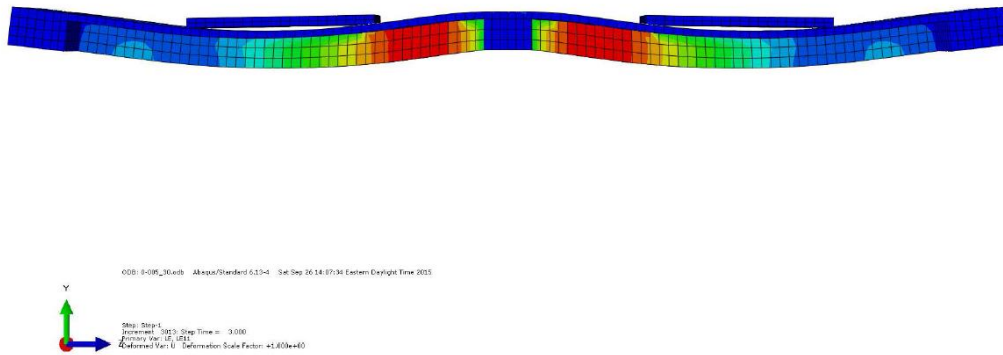


Figure 4.88 Side View of the Deformed Model

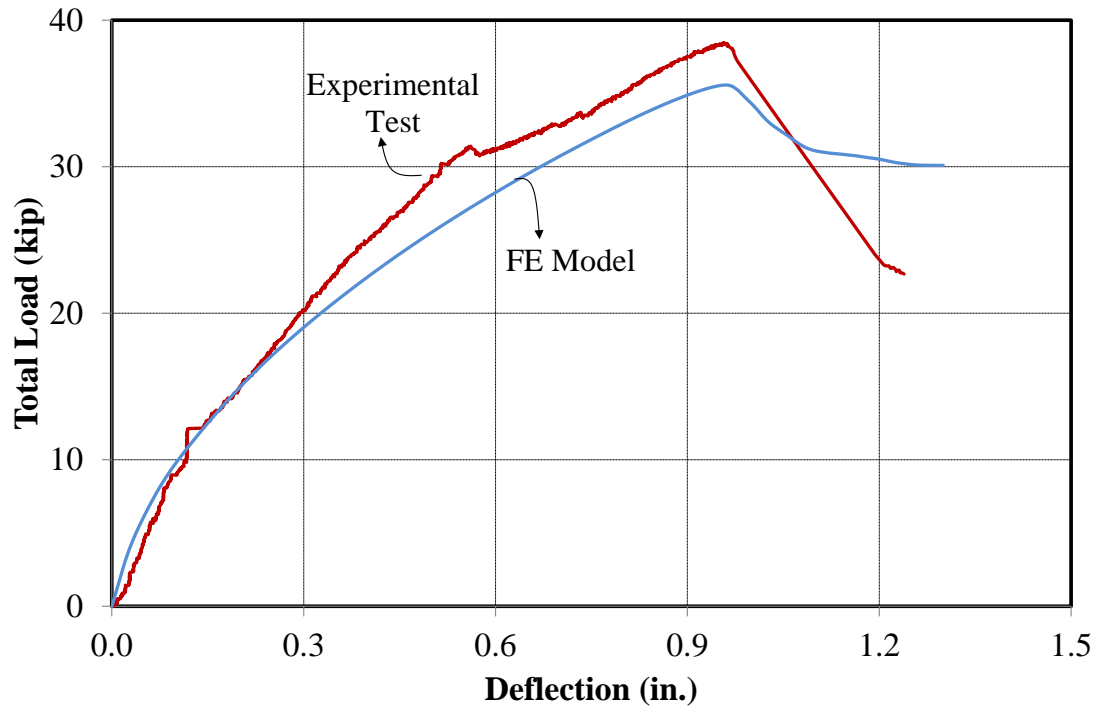
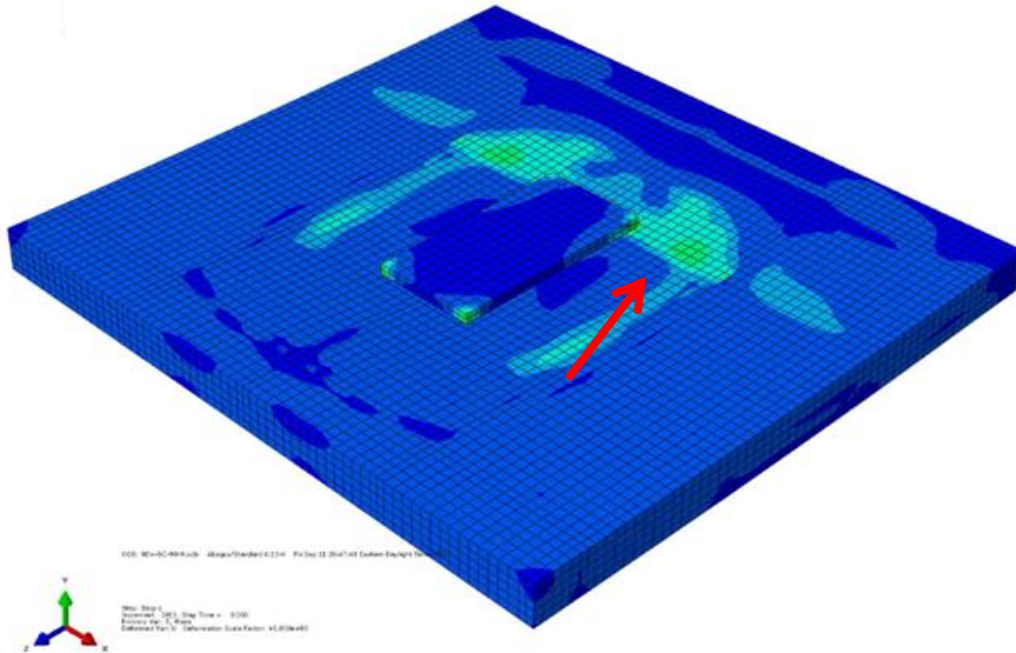


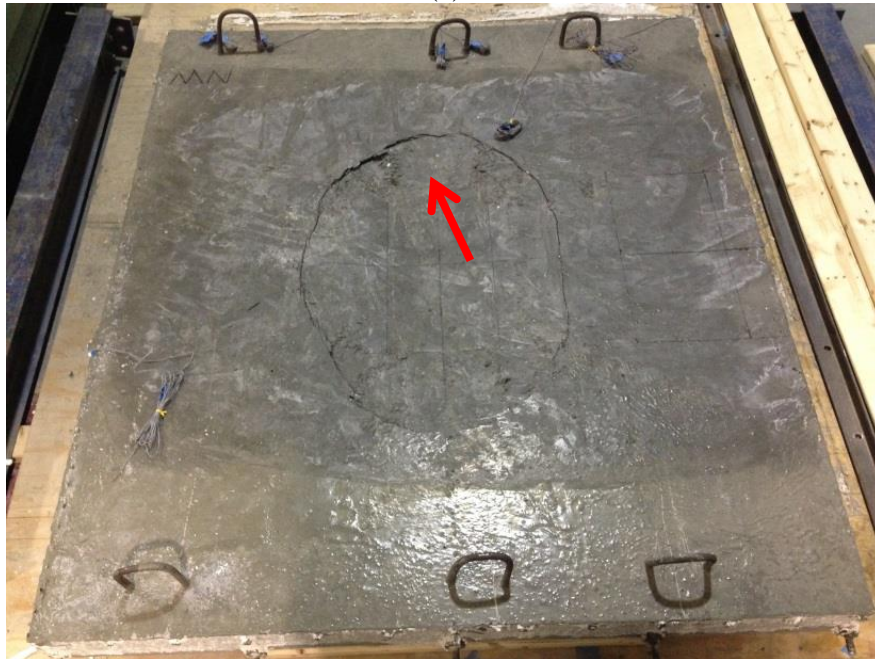
Figure 4.89 Load-Deflection Response of Specimen 1T2S-CFRP

Although the Figure underestimate the maximum load for about 7% , it still shows a good agreement with the result of the experiments.

The finite element model for Specimen 4T1S-CFRP is the same as described in earlier sections. Following the same procedure, Figure 4.90 Shows the failure mode and cracks on the slab. The shear cracks on the main ribs are illustrated in Figure 4.91. Similar cracks are detected on the transverse ribs shown in Figure 4.92. In each case, the finite element results are compared to the corresponding experimental specimen.

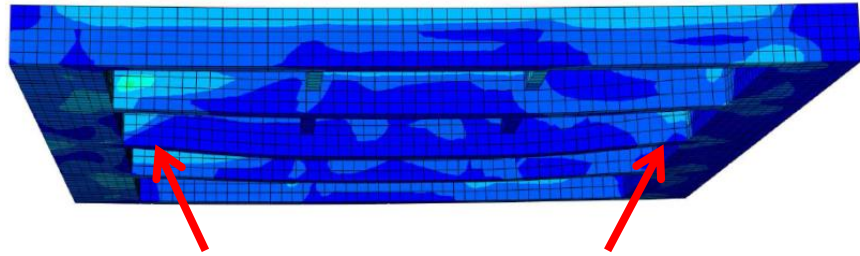


(a)



(b)

Figure 4.90 Failure Modes and Deflected shape of the Specimen 4T1S-CFRP, (a) FE Modeling, and (b) Failure Modes in Experimental Test



008: New-SC-R9-Rad6 - Abaqus/Standard 6.13-4 Fri Sep 11 20:47:48 Eastern Daylight Time 2015

Step: Step-1  
Increment: 385; Step Time = 3.000  
Position: up; 0.0000  
Deformed (Var): 1; Deformation Scale Factor = 1.6000e+03

(a)



(b)

Figure 4.91 Beam Shear Cracks on the Main Ribs, (a) FE Modeling, and (b) Experimental Test

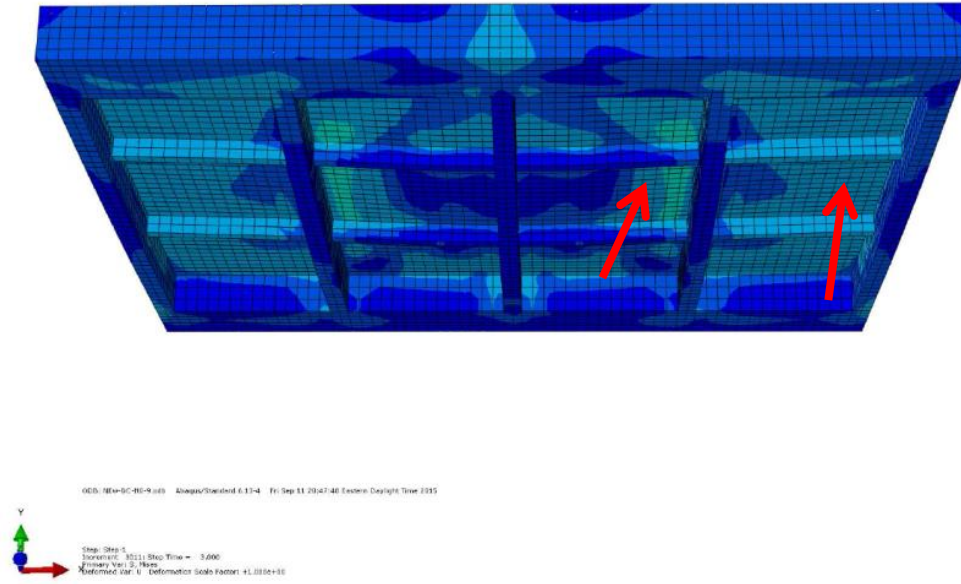


Figure 4.92 Beam Shear Cracks on the Transverse Ribs, (a) FE Modeling, and (b) Experimental Test

Figure 4.93 shows the load-deflection response of the finite element modeling of Specimen 4T1S-CFRP. According to the figure, the finite element model was able to estimate the overall behavior of the experimental specimen.

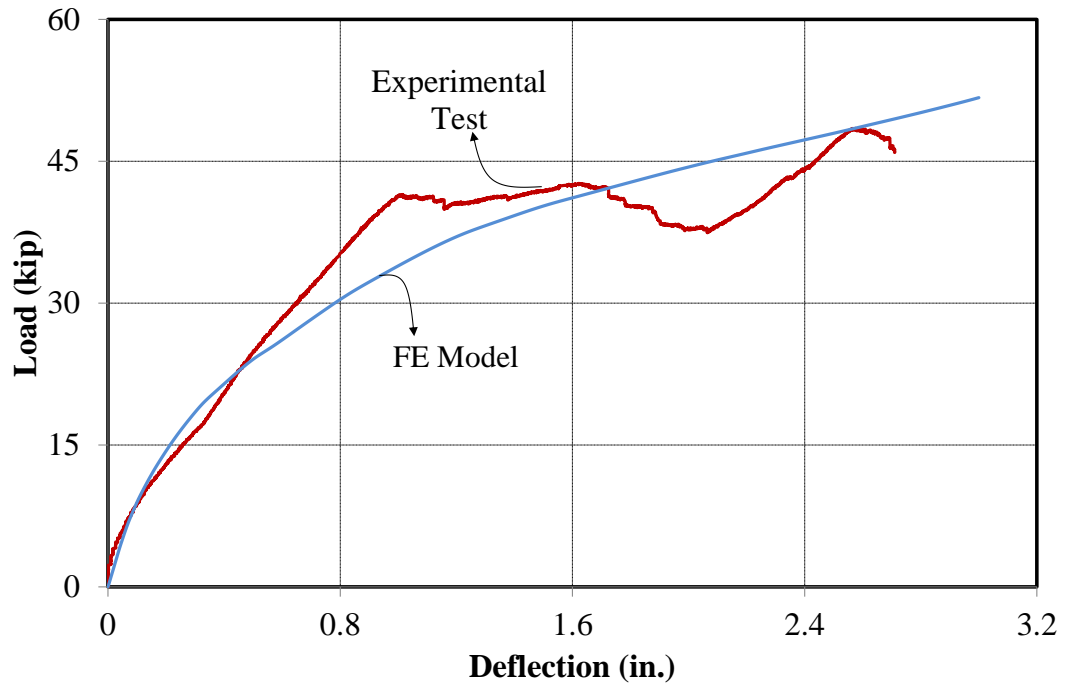


Figure 4.93 Load-Deflection Response of Specimen 4T1S-CFRP

# Chapter-5

---

## *Conclusions and Recommendations*

### **5.1 UHPC-FRP Hybrid Bridge Deck System**

A lightweight UHPC-FRP hybrid system was fabricated using vacuum-VARTM infusion in two phases. Analytical and experimental test results can be summarized as below:

1. Except for the first three specimens, the system satisfied the load and displacement requirements. This substandard performance of the first three specimens was attributed to their fabrication process.
2. The dominant mode of failure was either at the interface of FRP and UHPC, or through buckling of the FRP web.
3. At the end of first phase, all specimens were cut to investigate the quality of the infusion. All fibers in web area were completely dry and resin only transferred through short distance from the edge. The exception was for Specimen No. 6 due to the advantage of the chopped mat. This issue was solved in the second phase of the tests.

As complementary studies, bonding of GFRP and CFRP to UHPC was studied through experimental tests. Tests results led to the following conclusions:

1. The bond failure for the majority of the specimens occurred at the loaded block and strain gauges attached except for two specimens from the carbon group where the debonding happened at the unloaded block with rupture of carbon fibers.
2. The different edge length or the boundaries between the small and large specimens had no effect on the peak load
3. Maximum load at which the failure occurred was greater for carbon fibers as compared to glass fibers.

Although the hybrid UHPC-FRP system seems very promising, the following additional work is needed for improving the bond between the UHPC and top fibers layers:

1. Additional indentations are needed in the UHPC slab to accommodate a better bond with FRP.
2. Different types of connections such as mechanical, FRP connectors, and resin beads need to be considered.

### **5.2 UHPC Waffle Deck System**

The main objective of this research was to develop lightweight solid deck alternatives for movable bridges. The alternatives should meet the AASHTO LRFD loading and serviceability requirements while satisfying 21 psf self-weight requirements. Five different bridge deck systems were considered for this purpose, including UHPC waffle deck with HSS reinforcement, UHPC waffle deck with CFRP reinforcement, UHPC-FRP hybrid deck, and FRP composite

deck. Detailed experimental and analytical evaluation of these systems let to the following conclusions and recommendations.

Detailed component and ancillary tests were carried out to evaluate UHPC waffle deck with HSS reinforcement in three phases. The results let to the following conclusions:

1. The system showed viability to serve as an alternative for light-weight bridge decks. It was shown by the experimental and analytical evaluations that the system meets the load and displacement requirements.
2. The dominant mode of failure was beam shear cracks. The cracks initiated on the web near the supports and propagated toward the slab which eventually resulted in load drop and final failure.
3. The main bar in longitudinal ribs yielded in single-rib simple-span specimens, but not in two-span or multi-rib specimens.
4. No sign of punching shear failure was observed in any of the optimized deck panels for the 4-ft. spacing of the stringers. The punching observed in the panels with 5-ft. span was addressed by increasing the thickness of the flange.
5. In regards to load distribution among primary ribs, the middle rib takes 33% of the load, while each of the adjacent ribs take 22% and 11% of the load.

Similar studies were carried out on UHPC-CFRP bridge deck system in three phases. The results can be summarized as follows:

1. The system showed its capability to work as an alternative for light-weight bridge decks by satisfying load and displacement requirements.
2. The dominant mode of failure for all but the first four specimens was beam shear cracks. The cracks started on the web next to the supports and widened and propagated toward the slab; resulting the eventual failure and significant load drops. In the first four specimens, the anchorage system was with GFRP wrap impregnated in epoxy resin, and did not provide adequate anchorage against bar slippage. As such, shear cracks in those specimens began at the mid-point between supports and edge of loading pad and propagated toward the loading pad.
3. Performance for punching shear was quite similar to the decks with HSS reinforcement.
4. Load distribution among primary ribs was similar to the decks with HSS reinforcement.

The long term behavior of the proposed deck under the dynamic effects of moving wheel load was assessed with Heavy Vehicle Simulator (HVS) in the Accelerated Pavement Testing (APT) facility of the Florida Department of Transportation in Gainesville, FL. The results can be summarized as follows:

1. No sign of severe cracks or any catastrophic failure was observed in APT.
2. Displacement and strain values were fairly lower than the criterion.
3. According to the results, no difference was observed in terms of deflection and strain patterns after the machine setup at day 9 of the test.

# References

---

A Toolkit for Accelerated Bridge Construction. (2015, June). Washington, D.C., United States of America.

Aaleti, S., Petersen, B., & Sritharan, S. (2013). *Design Guide for Precast UHPC Waffle Deck Panel System, including Connections FHWA-HIF-13-032*. Washington, DC: Federal Highway Administration.

Aaleti, S., & Sritharan, S. (2014). Design of ultrahigh-performance concrete waffle deck for accelerated bridge construction. *Transportation Research Record: Journal of the Transportation Research Board*, 2406(1), 12-22.

Aaleti, S., Sritharan, S., Bierwagen, D., & Wipf, T. (2011). Structural Behavior of Waffle Bridge Deck Panels and Connections of Precast Ultra-High-Performance Concrete: Experimental Evaluation. *Transportation Research Record: Journal of the Transportation Research Board*, (2251), 82-92.

AASHTO, LRFD. (2013). Bridge design specifications. *American association of state highway and transportation officials*. Washington, D.C.

*Accelerated Bridge Construction*. (n.d.). Retrieved from U.S. Department of Transportation Federal Highway Administration: <http://www.fhwa.dot.gov/bridge/abc>

Accelerated Bridge Construction. (2012, May 18). Washington, D.C., United States of America.

*Accelerated Construction - Construction Strategies*. (n.d.). Retrieved from FHWA Work Zone: <http://www.ops.fhwa.dot.gov/Wz/construction/accelerated/index.htm>

ACI Committee, American Concrete Institute, & International Organization for Standardization (2011). *Building code requirements for structural concrete (ACI 318-11) and commentary*. American Concrete Institute.

ACI 408-R03. (2003). Bond and development of straight reinforcing bars in tension. *American concrete institute*. Farmington Hills, MI.

Ahlborn, T. M., Peuse, E. J., & Misson, D. L. (2008). Ultra-high-performance-concrete for michigan bridges material performance–phase I.

Ahmad, A. S. (2011). *Bridge Preservation Guide FHWA-HIF-11042*. Federal Highway Administration.

Alagusundaramoorthy, P., Harik, I., & Choo, C. (2006). Structural behavior of FRP composite bridge deck panels. *Journal of Bridge Engineering*, 11(4), 384-393.

Alnahhal, W. I., Chiewanichakorn, M., Aref, A. J., & Alampalli, S. (2006). Temporal thermal behavior and damage simulations of FRP deck. *Journal of Bridge Engineering*, 11(4), 452-464.

*An Overview of the SCRIMP Technology*. (2001). Retrieved from MIT Open Courseware: [http://ocw.mit.edu/courses/mechanical-engineering/2-996-sailing-yacht-design-13-734-fall-2003/study-materials/scrimp\\_overview.pdf](http://ocw.mit.edu/courses/mechanical-engineering/2-996-sailing-yacht-design-13-734-fall-2003/study-materials/scrimp_overview.pdf)

Andres, T. (2014 14-August). Florida Department of Transportation Survey on Prefabricated Bridge Decks. (T. Sanford, Interviewer)

Aref, A. J., & Alnahhal, W. I. (2009). *Hybrid FRP-Concrete Bridge Deck Systems Project No.: C-02-07*. Albany: New York State Department of Transportation.

Aref, A. J., & Wren, G. (2009). *Hybrid FRP-Concrete Bridge Deck Systems Final Report II: Long Term Performance of Hybrid FRP-Concrete Bridge Deck System*. Department of Civil, Structural, and Environmental Engineering University of Buffalo - State University of New York.

ASCE. (2013). Report card for America's infrastructure. *American society of civil engineers*. Reston, VA.

ASTM Standard D7205/D7205M. (2011). Standard test method for tensile properties of fiber reinforced polymer matrix composite bars. *ASTM international*. West Conshohocken, PA.

Attanayake, U., Abudayyeh, O., Cooper, J., Mohammed, A. W., & Aktan, H. (2014). *First Full-Depth Deck-Panel Accelerated Bridge Construction Project in Michigan: Constructability Challenges and Lessons Learned*. American Society of Civil Engineers

Barr, P., & Wixom, K. (2009). *Feasibility of Using High-Strength Steel and MMFX Rebar in Bridge Design*. Salt Lake City: Utah Department of Transportation Research Division.

Beerman, B., & Garcia, R. (2007). *Manual on Use of Self-Propelled Modular Transporters to Remove and Replace Bridges*. Washington, D.C.: Federal Highway Administration.

Bennett, C. (2014, October 7). State Bridge Engineer. (T. Sanford, Interviewer) Georgia Department of Transportation

Black, J. (. (2014 14-August). Alabama Department of Transportation. (T. Sanford, Interviewer)

Blais, P. Y., & Couture, M. (1999). Precast, prestressed pedestrian bridge-world's first reactive powder concrete structure. *Pci journal*, 44, 60-71.

- Carter III, J. W., Pilgrim, T., Hubbard, F. K., Poehnelt, T., & Oliva, M. (2007). Wisconsin's Use of Full-Depth Precast Concrete Deck Panels Keeps Interstate 90 Open to Traffic. *PCI Journal*, 2-16.
- Chajes, M. J., Finch Jr, W. W., Januszka, T. F., & Thomson Jr, T. A. (1996). Bond and force transfer of composite-material plates bonded to concrete. *ACI structural journal*, 93(2).
- Chakraborty, A., Khennane, A., Kayali, O., & Morozov, E. (2011). Performance of outside filament-wound hybrid FRP-concrete beams. *Composites Part B: Engineering*, 42(4), 907-915.
- Chen, D., & El-Hacha, R. (2011). Behaviour of hybrid FRP-UHPC beams in flexure under fatigue loading. *Composite Structures*, 94(1), 253-266.
- Cho, A. (2012, September 24). Balancing The Bridge Message. *Engineering News-Record*, pp. 28-33.
- Cho, A. (2012, September 24). Utah Push For Bridge Innovation. *Engineering News-Record*, pp. 34-35.
- Cho, A., & Parsons, J. (2014, January 27). *ABC Tool Kit Crafter Spreads The Word*. Retrieved from Engineering News-Record: <http://enr.construction.com>
- Cole, T. A., Lopez, M., & Ziehl, P. H. (2006). Fatigue behavior and nondestructive evaluation of full-scale FRP honeycomb bridge specimen. *Journal of Bridge Engineering*, 11(4), 420-429.
- Culmo, M. P. (2011). Accelerated Bridge Construction-Experience in Design, Fabrication and Erection of Prefabricated Bridge Elements and Systems.
- Culmo, M. P. (2009). *Conneciton Details for Prefabricated Bridge Elements and Systems*. Fedearl Highway Administration
- Culmo, M. P. (2014, September). Piece By Piece. *Modern Steel Construction*, pp. 52-55.
- Dejong, S. J., & McDougall, C. (2006). *Fatigue Behavior of MMFX Corrosion-Resistant Reinforcing Steel*. Department of Civil Engineering. Ontario: Queen's University
- Davalos, J. F., Chen, A., & Zou, B. (2010). Stiffness and strength evaluations of a shear connection system for FRP bridge decks to steel girders. *Journal of Composites for Construction*, 15(3), 441-450.
- Davalos, J. F., & Chen, A. (2005). Buckling behavior of honeycomb FRP core with partially restrained loaded edges under out-of-plane compression. *Journal of composite materials*, 39(16), 1465-1485.
- Davalos, J. F., Qiao, P., Xu, X. F., Robinson, J., & Barth, K. E. (2001). Modeling and characterization of fiber-reinforced plastic honeycomb sandwich panels for highway bridge applications. *Composite structures*, 52(3), 441-452.

Ductal® Bridge Solutions: Gaining Acceptance in North America. (2010, July). *Ductal® Solutions: LaFarge Ductal® Newsletter*, pp. 6-7.

Ellis, R. (2014, September 25). Bridge Division Head. (T. Sanford, Interviewer) Arkansas Department of Transportation

Elmahdy, A., El-Hacha, R., & Shrive, N. (2007). Bonding of CFRP and SRP to Ultra-High Performance Concrete. *Proceedings of the First Asia-Pacific Conference on FRP in Structures (APFIS 2007)*.

Fact Sheet 16 - States Across the Country Implement Accelerated Bridge Construction. (2010). Washington, D.C., United States of America. Retrieved from U.S. Department of Transportation.

Farris, J. F. (n.d.). *Sam White Lane Bridge Move [Webinar]*. Retrieved from [ftp.dot.state.tx.us/pub/txdot-info/brg/0611\\_webinar/farris.pdf](ftp.dot.state.tx.us/pub/txdot-info/brg/0611_webinar/farris.pdf)

Fossier, J. P. (2014, August 27). Bridge Design Engineer Administrator. *Louisiana Department of Transportation*. (T. Sanford, Interviewer)

*Friedberg Bridge, Friedberg, Germany*. (2015). Retrieved from Roadtraffic-technology.com: <http://www.roadtraffic-technology.com/projects/friedberg-bridge/>

Garcia, H. M. (2007). *Analysis of an Ultra-High Performance Concrete Two-Way Ribbed Bridge Deck Slab*. Washington, D.C.: Federal Highway Administration

Ghasemi, S., Mirmiran, A., Xiao, Y., & Mackie, K. (2015). Novel UHPC-CFRP Waffle Deck Panel System for Accelerated Bridge Construction. *Journal of Composites for Construction*, 04015042.

Goodrich, B., & Kelly, J. (2015, July). Getting a Handle on Traffic. *Modern Steel Construction*, pp. 50-53.

Graybeal, B. (2012). *Ultra-High Performance Concrete Composite Connections for Precast Concrete Bridge Decks FHWA-HRT-12-042*. McLean: Federal Highway Administration.

Graybeal, B. (2011). *Ultra-High Performance Concrete FHWA-HRT-11-038*. McLean: Federal Highway Administration

Graybeal, B. (2010, November). *Field-Cast UHPC Connections for Modular Bridge Deck Elements FHWA-HRT-11-022*. McLean: Federal Highway Administration.

Graybeal, B. A. (2007). Compressive behavior of ultra-high-performance fiber-reinforced concrete. *ACI Materials Journal*, 104(2).

Graybeal, B. A. (2006). Structural behavior of ultra-high performance concrete prestressed I-girders.

- Graybeal, B. A. (2005). Characterization of the behavior of ultra-high performance concrete.
- Graybeal, B. A., & Hartmann, J. L. (2003). Strength and durability of ultra-high performance concrete. *Concrete Bridge Conference, Portland Cement Association*.
- Habel, K., Viviani, M., Denarié, E., & Brühwiler, E. (2006). Development of the mechanical properties of an ultra-high performance fiber reinforced concrete (UHPFRC). *Cement and Concrete Research*, 36(7), 1362-1370.
- Habal, k., Denarié, E., & Brühwiler, E. (2006). Structural Response of Elements Comining Ultrahigh Performance Fiber-Reinforced Concretes and Reinforced Concrete. *Journal of Sturctural Engineering*, 132(11).
- Hällmark, R., White, H., & Collin, P. (2012 1-August). Prefabricated Bridge Construction Across Europe and America. *Practice Periodical on Structural Design adn Construction* , 17 (3)
- Hajar, Z., Simon, A., Lecointre, D., & Petitjean, J. (2003). Construction of the first road bridges made of ultra-high-performance concrete. *Proceedings, 2003 International Symposium on High Performance Concrete*.
- Hanks, B. (2014 26-August). North Carolina Department of Transporation. (T. Sanford, Interviewer)
- Harris, D. K., & Roberts-Wollmann, C. L. (2005). Characterization of the punching shear capacity of thin ultra-high performance concrete slabs.
- Harris, D. K. (2004). *Characterization of Punching Shear Capacity of Thin UHPC Plates*. Master's Thesis, Virginia Polytechnic institute and State University, Blacksburg.
- Heimann, J. (2013). The implementation of full depth UHPC waffle bridge deck panels. *Publication No. FHWA-HIF-13-031*.
- (2001). *High-Strength Low-Alloy Steels*. Materials Park: ASM International.
- Holden, K. M., Pantelides, C. P., & Reaveley, L. D. (2014). *Bridge Constructed with GFRP-Reinforced Precast Concrete Deck Panels:Case Study*. American Society of Civil Engineers
- Horiguchi, T., & Saeki, N. (1997). Effect of test methods and quality of concrete on bond strength of CFRP sheet. *Non-Metallic (FRP) Reinforcement for Concrete Structures*, 1, 265-270.
- Hughes Brothers. “Carbon fiber reinforced polymers (CFRP) bar - Aslan™ 200 Series.” Seward, NE (2011) [Hughes Brothers](#)

*Implementing an Accelerate Bridge Construction Program in Utah.* (2008, March). Retrieved from U.S. Department of Transportation Federal Highway Association: <http://www.fhwa.dot.gov/publications/focus/08mar/01.cfm>

Kahl, S. (2007). Corrosion Resistant Alloy Steel (MMFX) Reinforcing Bar in Bridge Decks.

Keierleber, B., Phares, B., Bierwagen, D., Couture, I., & Fanous, F. (2007). Design of Buchanan County, Iowa, Bridge Using Ultra High Performance Concrete and PI Girders. *Proceedings of the 2007 Mid-Continent Transportation Research Symposium, Ames, IA.*

Kelleher, B. (n.d.). *MassDOT Uses ABC to Replace Wellesley Bridge in a Weekend.* Retrieved from Boston Society of Civil Engineers Section: <http://www.bsces.org/index.cfm/page/MassDOT-Uses-ABC-to-Replace-Wellesley-Bridge-in-a-Weekend/cdid/11359/pid/10371>

Keller, T., & Gürtler, H. (2005). Composite action and adhesive bond between fiber-reinforced polymer bridge decks and main girders. *Journal of Composites for Construction*, 9(4), 360-368.

Keller, T., Schaumann, E., & Vallée, T. (2006). *Flexural Behavior of a Hybrid FRP and Lightweight Concrete Sandwich Bridge Deck.* Philadelphia: Elsevier Ltd.

Kumar, P., Chandrashekhara, K., & Nanni, A. (2004). Structural performance of a FRP bridge deck. *Construction and Building Materials*, 18(1), 35-47.

Li, L., Ma, Z. J., & Oesterle, R. G. (2010 September/October). Improved Longitudinal Joint Details in Decked Bulb Tees for Accelerated Bridge Construction: Fatigue Evaluation. *Journal of Bridge Engineering*

Lini, C. (2015, January). Higher-Strength Steels. *Modern Steel Construction*, p. 9.

Liu, J., Sotelino, E. D., Rodriguez-Vera, R. E., Lombardi, N. J., & Machado, M. A. (2011). *Fiber Reinforced Polymer Bridge Decks.* West Lafayette: Joint Transportation Research Program, Indiana Department of Transportation and Purdue University.

Lwin, M. M., & Triandafilou, L. N. (2011, January). FHWA's Every Day Counts Initiative. *HPC Bridge Views.*

Mercer, M. S. (2012). *Transverse Sub-Assemblage Testing of the Inverted-T Bridge System.* Blacksburg: Virginia Polytechnic Institute and State University.

Mertz, D., Chajes, M., Gillespie Jr., J., Kurich, D., Sabol, S., Hawkins, H., et al. (2003). *Application of Fiber Reinforced Polymer Composites to the Highway Infrastructure.* Washington: Transportation Research Board

Mirmiran, A., Mackie, K., Saleem, M. A., Xia, J., Zohrevand, P., & Xiao, Y. (2012). Alternatives to Steel Grid Decks-Phase II.

Mirmiran, A., Saleem, M. A., Mackie, K., & Xia, J. (2009). Alternatives to steel grid decks.

MMFX Technologies Corporation. (2014). *MMFX Technologies Corporation: About*. Retrieved 2014 24-August from <http://www.mmfx.com/about/>

Mongi, A. (2014, October 19). Quality Assurance/ Quality Control Unit Leader, Engineer Division. (T. Sanford, Interviewer) West Virginia Department of Transportation

Mu, B., Wu, H., Yan, A., Warnemuende, K., Fu, G., Gibson, R. F., et al. (2006). FEA of complex bridge system with FRP composite deck. *Journal of Composites for Construction*, 10(1), 79-86.

Nakaba, K., Kanakubo, T., Furuta, T., & Yoshizawa, H. (2001). Bond behavior between fiber-reinforced polymer laminates and concrete. *ACI Structural Journal*, 98(3).

National Steel Bridge Alliance 2012 Prize Bridge Awards. (2012, June). *Modern Steel Construction*, pp. 38,42-43,50-51.

Noshiravani, T., & Brühwiler, E. (2013 March-April). Experimental Investigation on Reinforced Ultra-High Performance Fiber-Reinforced Concrete Beams Subjected to Combined Bending and Shear. *American Concrete institute Structural Journal*.

O'Donoghue, A. J., Page, J., & McCord, K. (2011, March 27). *UDOT Makes History with American Fork Bridge Move*. Retrieved from KSL.com: <http://www.ksl.com/index.php?sid=14894131&nid=481>

Olifi, M. (2015). *State of Accelerated Bridge Construction (ABC) in the United States*. Georgia Southern University.

Pantelides, C. P., Holden, K. M., & Ries, J. (2012). *Health Monitoring of Precast Bridge Deck Panels Reinforced with Glass Fiber Reinforced Polymer (GFRP) Bars*. Salt Lake City: University of Utah Department of Civil & Environmental Engineering.

Perry, V. H., & Royce, M. (2010). Innovative Field-Cast UHPC Joints for Precast Bridge Decks (Side-By-Side Deck Bubl-Tees), Village of Lyons, New York Design, Prototyping, Testing and Construction. 3rd fib international congress

Reeve, S. (2010, February 15). *FRP Bridge Decking - 14 Years and Counting*. Retrieved from Materials Today: <http://www.materialstoday.com/composite-applications/features/frp-bridge-decking-14-years-and-counting/>

*Representative Exodermic® Bridge Deck Projects: South Grand Island Bridges, Grand Island NY*. (2015). Retrieved from D.S. Brown Exodermic® Bridge Deck: <http://www.exodermic.com/Projects/>

Righman, J., Barth, K., & Davalos, J. (2004). Development of an efficient connector system for fiber reinforced polymer bridge decks to steel girders. *Journal of Composites for Construction*, 8(4), 279-288.

Risser, B., & Humphreys, S. (2008 10-January). *Concrete Construction*. Retrieved 2014 йил 24-August from [http://www.concreteconstruction.net/concrete-construction/high-strength-reinforcing-steel-next-generation-o\\_1.aspx](http://www.concreteconstruction.net/concrete-construction/high-strength-reinforcing-steel-next-generation-o_1.aspx)

Risser, B., & Humphreys, S. (2008 10-January). *Concrete Construction*. Retrieved 2014 24-August from [http://www.concreteconstruction.net/concrete-construction/high-strength-reinforcing-steel-next-generation-o\\_1.aspx](http://www.concreteconstruction.net/concrete-construction/high-strength-reinforcing-steel-next-generation-o_1.aspx)

Rister, D. (2014, September 8). Bridge Construction Engineer. (T. Sanford, Interviewer) South Carolina Department of Transportation

Rizkalla, S., El-Hacha, R., & Elagroudy, H. (2006). Bond characteristics of high-strength steel reinforcement. *ACI structural journal*, 103(6).

Robinson, M., & Kosmatka, J. (2008). Light-weight fiber-reinforced polymer composite deck panels for extreme applications. *Journal of Composites for Construction*, 12(3), 344-354.

Roddenberry, M., & Servos, J. (2012). *Prefabricated/Precast Bridge Elements and Systems (PBES) for Off-System Bridges*. Tallahassee: Florida Department of Transportation.

Rouse, J., Wipf, T. J., Phares, B. M., Fanous, F., & Berg, O. (2011). *Design, Construction, and Field Testing of an Ultra-High Performance Concrete Pi-Girder Bridge*. Ames: Iowa State University Institute for Transportation.

Rubenstein, J. (2015, January 26). *PennDOT Oks P3 Contract for Replacement of 558 Bridges*. Retrieved from Engineering News-Record: <http://enr.construction.com>

Russel, H. G., & Graybeal, B. A. (2013). *Ultra High Performance Concrete: A State-of-the-Art Report for the Bridge Community*. Washington, D.C.: Federal Highway Administration

Sahirman, S., Creese, R. C., & Setyawati, B. R. (2003). *Evaluation of the Economic Feasibility of Fiber-Reinforced Polymer (FRP) Bridge Decks*. Orlando: ISPA/SCEA International Joint Conference.

Saleem, M. A., Mirmiran, A., Xia, J., & Mackie, K. (2012). Development length of high-strength steel rebar in ultrahigh performance concrete. *Journal of Materials in Civil Engineering*, 25(8), 991-998.

Saleem, M. A. (2011). *Alternatives to steel grid bridge decks*. Florida International University.

Saleem, M. A., Mirmiran, A., Xia, J., & Mackie, K. (2011). Ultra-high-performance concrete bridge deck reinforced with high-strength steel. *ACI Structural Journal*, 108(5).

Salem, O., Basu, B., Miller, R., Randell, J., Swanson, J., & Engel, R. (2006). *Accelerating the Construction of a Highway Bridge in Ohio*. American Society of Civil Engineers

Salem, O., Basu, B., Miller, R., Randell, J., Swanson, J., & Engel, R. (2006). *Accelerating the Construction of a Highway Bridge in Ohio*. American Society of Civil Engineers

Sandefur, K. (2014, August 29). Kentucky Transportation Cabinet. (T. Sanford, Interviewer)

Schesser, D., Yang, Q., Nanni, A., & Giancaspro, J. (2013). Expansive Grout-Based Gripping Systems for Tensile Testing of Large-Diameter Composite Bars. *Journal of Materials in Civil Engineering*, 26(2), 250-258.

Scott, D. W., Lai, J. S., & Zureick, A. (1995). Creep behavior of fiber-reinforced polymeric composites: a review of the technical literature. *Journal of Reinforced Plastics and Composites*, 14(6), 588-617.

Seger, W. (2014, August 29). Tennessee Department of Transportation. (T. Sanford, Interviewer)

Seliem, H., Lucifer, G., Rizkalla, S., & Zia, P. (2006). *Behavior of Bridge Decks Reinforced with MMFX Steel*. Raleigh: Department of Civil Engineering, North Carolina State University.

Shahawy, M. A. (2003). *Prefabricated Bridge Elements and Systems to Limit Traffic Disruption During Construction*. Washington, D.C.: Transportation Research Board.

Shahrooz, B. M., Miller, R. A., Harries, K. A., & Russell, H. G. (2011). *Design of Concrete Structures Using High-Strength Steel Reinforcement*. Washington, D.C.: Transportation Research Board.

Shann, S. V. (2012). Application of ultra high performance concrete (UHPC) as a thin-bonded overlay for concrete bridge decks.

Shutt, C. A. (2010 FALL). Route 31 Bridge Over Canadanigua Outlet. *ASPIRE*, pp. 28-30.

Sivakumar, B. (2012). Accelerated Bridge Construction ABC. *New York Statewide Conference on Local Bridges*. Syracuse.

(2015). *The Implementation of Full Depth UHPC Waffle Bridge Deck Panel*. Washington, D.C.: Federal Highway Administration.

*The Pultrusion Process*. (2015). Retrieved from Strongwell: <http://www.strongwell.com/about/the-pultrusion-process/>

Trejo, D., Aguiñiga, F., Buth, G., Yuan, R. L., James, R. W., & Keating, P. B. (2005). *Fiber-Reinforced Polymer Bars for Reinforcement in Bridge Decks*. College Station: Texas Transportation Institute.

Tuwair, H., Volz, J., ElGawady, M. A., Mohamed, M., Chandrashekhara, K., & Birman, V. (2015). Testing and Evaluation of Polyurethane-Based GFRP Sandwich Bridge Deck Panels with Polyurethane Foam Core. *Journal of Bridge Engineering*, 04015033.

*U.S. 6 Bridge Over Keg Creek*. (n.d.). Retrieved from Iowa Department of Transportation: [www.iowadot.gov/us6kegcreek/projectinfo.html](http://www.iowadot.gov/us6kegcreek/projectinfo.html)

*Unibridge Product Info*. (2012). Retrieved from Unibridge Trading: <http://www.unibridge.fr/product-info/>

Vargas, V. V. (2012). *Bridge Deck Cracking Investigation and Repair*. [unpublished].

Walus, K. (2014 15-August). Virginia Department of Transportation. (T. Sanford, Interviewer)

*Wellesley "Heavy Lift" Project Accelerated Bridge Replacement*. (2015). Retrieved from Massachusetts Department of Transportation: <https://www.massdot.state.ma.us/highway/HighlightedProjects/WellesleyBridge.aspx>

Westerfield, S. (2014 19-August). Mississippi Department of Transportation. (T. Sanford, Interviewer)

Wide Load Shipping. (2013). *wideloadshipping.com*. Retrieved 2014 йил 27-August from <http://wideloadshipping.com/alabama-state-shipping-regulations/>

Williams, B., Shehata, E., & Rizkalla, S. H. (2003). Filament-wound glass fiber reinforced polymer bridge deck modules. *Journal of Composites for Construction*, 7(3), 266-273.

(2015). *WisDOT Bridge Manual*. Madison: Wisconsin Department of Transportation.

Wolf, S. (2015, September 28). About Every Day Counts (EDC). Washington, D.C., United States of Alabama.

Wright, J. R., Rajabipour, F., Laman, J. A., & Radlińska, A. (2013). Causes of Early Age Cracking on Concrete Bridge Deck Expansion Joint Repair Sections. *Advances in Civil Engineering*, 1-10.

Wu, H., Mu, B., & Warnemuende, K. (2003). Failure analysis of FRP sandwich bus panels by finite element method. *Composites Part B: Engineering*, 34(1), 51-58.

Wu, Z., Mirmiran, A., & Swanson, J. (2004). Fatigue behavior of prestressed tubular bridge deck of fiber-reinforced polymer. *Transportation Research Record: Journal of the Transportation Research Board*, (1892), 246-255.

Xi, Y., Shing, B., Abu-Hejleh, N., Asiz, A., Suwito, A., Xie, Z., & Ababneh, A. (2003). *Assessment of the Cracking Problem in Newly Constructed Bridge Decks in Colorado*. Denver: Colorado Department of Transportation.

Xia, J., Mackie, K. R., Saleem, M. A., & Mirmiran, A. (2011). Shear failure analysis on ultra-high performance concrete beams reinforced with high strength steel. *Engineering Structures*, 33(12), 3597-3609.

Yoshizawa, H., Myojo, T., Okoshi, M., Mizukoshi, M., & Kliger, H. S. (1996). Effect of sheet bonding condition on concrete members having externally bonded carbon fiber sheet. *Materials for the New Millennium*. ASCE.

Zhu, P., John Ma, Z., Cao, Q., & French, C. E. (2012). Fatigue Evaluation of Transverse U-Bar Joint Details for Accelerated Bridge Construction. *Journal of Bridge Engineering*, 2012.17:191-200.

Zirlin, J. (2011). *The Implementation of Full Depth UHPC Waffle Bridge Deck Panel*. Federal Highways Administration.